Application of virtual anthropological techniques in the reconstruction and analysis of late Middle and Late Pleistocene hominin crania

Dissertation

der Mathematisch-Naturwissenschaftlichen Fakultät

der Eberhard Karls Universität Tübingen

zur Erlangung des Grades eines

Doktors der Naturwissenschaften

(Dr. rer.nat.)

vorgelegt von

Abel Marinus Bosman

aus Nijmegen / Niederlande

Tübingen

2019

Gedruckt mit Genehmigung der Mathematisch-Naturwissenschaftlichen Fakultät der Eberhard Karls Universität Tübingen.

Tag der mündlichen Qualifikation:	22.11.2019
Dekan:	Prof. Dr. Wolfgang Rosenstiel
1. Berichterstatter:	Dr. Yonatan Sahle Chemere
2. Berichterstatterin:	Prof. Dr. Katerina Harvati

Table of Contents

Abstract

The emergence of anatomical modernity remains one of the least understood processes in the evolution of the *H. sapiens* lineage. This is complicated by the fact that critical geographic areas such as eastern Africa present a fragmentary and sparse fossil record, which is especially true for the late Middle and Late Pleistocene geological time periods. As such, most current discussions on the phenotypic representation of anatomical modernity are centered around case-studies on several well-conserved fossils, while fragmented specimens from lesser known sites are disregarded. Moreover, even though specific anatomical characteristics have been proposed as phylogenetically informative, these are frequently only discussed in qualitative contexts, while the extent of morphological variation demonstrated by inclusive analytical frameworks is often not recognized. This cumulative dissertation aims to resolve some of these issues by addressing the following research questions: "1) What is the taxonomic attribution of the Kabua 1 cranium? 2) Does the morphology of the Cioclovina suprainiac region represent the Neanderthal condition? 3) Are suprainiac depressions in later *Homo* symplesiomorphic?" These research questions are investigated by integrating morphometric analyses of discrete morphological features and neurocranial shape with a set of understudied crania. These specimens are analyzed in a virtual environment in order to systematically investigate the origins and evolution of *H. sapiens*. In doing so, this dissertation stresses the need for holistic qualitative and quantitative methods to address current issues in the field of paleoanthropology. Additionally, this dissertation emphasizes the effectiveness of recently developed technologies and virtual anthropology to bring new light to historic paleoanthropological finds.

The first study describes the virtual reconstruction of the Kabua 1 cranium. This specimen was found in 1959, west of Lake Turkana, Kenya. Due to its fragmentary condition, and uncertain geochronological/archaeological context, its anatomical morphological characteristics and phylogenetic affiliation remain inadequately understood. This study presents an exhaustive description of the fragmentary material as well as a set of six virtual anatomical reconstructions. Through a qualitative investigation of these reconstructions

and several non-metric traits, it is inferred that the Kabua 1 specimen exhibits a globular neurocranium and relatively gracile features, without substantial evidence for the presence of definite plesiomorphic traits. This study thereby tentatively supports a taxonomic designation of anatomically modern *H. sapiens*.

The second study is developed to quantitatively verify the reproducibility of the set of virtual Kabua 1 reconstructions, and assess the tentative taxonomic affiliation put forward in the first study. This is achieved through the application of a suite of geometric morphometric procedures, including fixed and curve semi-landmarks, Generalized Procrustes Analysis, Principal Component Analysis, Linear Discriminant Analysis, and two machine learning models: *k*-Nearest Neighbors and Random Forests. These analyses confirm the hypothesis that Kabua 1 aligns with early and recent *H. sapiens* due to its globular neurocranium. However, Kabua 1 shows a combination of several anatomical characteristics by which it falls close to the margins of neurocranial variation in the *H. sapiens* comparative sample. This cranium possibly exemplifies the extent of phenotypic variation present in the African continent during the Late Pleistocene. Moreover, the results of the machine learning algorithms are found to be consistent with those obtained from exploratory ordination techniques and thus might constitute a valuable complement to standard geometric morphometric analyses.

The third and fourth study focus on the suprainiac fossa; a discrete oval depression on the occipital bone which has been proposed as a distinctive Neanderthal autapomorphy. However, morphologically similar features have also been described for early and anatomically modern *H. sapiens*, and discussions have arisen about the etiology of this trait. Most of these discussions can be summarized under one of three hypotheses: admixture with the Neanderthal lineage, common ancestry, and convergent evolution through biomechanical influences. The third study of this dissertation aims to investigate the admixture scenario. Relevant in this discussion is the Late Pleistocene European calvaria from Cioclovina (Romania), as it has been suggested as a possible Neanderthal/*H. sapiens* hybrid due to the proposed presence of Neanderthal traits, including a defined suprainiac

fossa. A combined qualitative and quantitative framework is applied to evaluate the status of the suprainiac fossa as a Neanderthal autapomorphy and to investigate to what extent these methods can be used to characterize Neanderthal/*H. sapiens* interbreeding. This framework includes an investigation of the occipital superstructures as well as measurements of relative thickness of the internal structures, i.e. the diploic layer, across the occipital bone. In all analyses, Cioclovina aligns with recent *H. sapiens*, which suggests little phenotypic evidence that this specimen exhibits high levels of Neanderthal ancestry.

The fourth study of this dissertation is designed to investigate the common ancestry hypothesis. Two Middle-Late Pleistocene crania from eastern Africa, Eyasi I and ADU-VP-1/3, are analyzed by applying and expanding upon the framework that was described in the previous study. The results demonstrate that the suprainiac morphologies of these individuals are within the range of recent anatomically modern *H. sapiens* suprainiac variation, and do not overlap with the Neanderthal condition. As these fossils date close to currently proposed times of dispersal of anatomically modern humans out of Africa (ADU-VP-1/3) and to the time of appearance of modern human anatomical traits in eastern Africa (Eyasi I), these results imply that a common ancestry scenario for shared external morphological characteristics is unlikely. Moreover, this study questions the reliability of non-metric traits as phylogenetically informative and forewarns against the use of terms such as present and absent when evaluating whether singular anatomical traits can be considered indicative of anatomical modernity.

Zusammenfassung

Die Entstehung der modernen Anatomie bleibt einer der am wenigsten verstandenen Prozesse in der Evolution unserer eigenen Spezies: *Homo sapiens*. In diesem Zusammenhang, wichtige geografische Gebiete, wie zum Beispiel Ostafrika, verfügen nur über vereinzelte und fragmentarische fossile Funde, besonders aus dem geologischen Zeitraum des späten Mittelpleistozän und Jungpleistozän. Wenige gut erhaltene Fossilien bilden die Grundlage für einen Großteil der derzeitigen Forschung über die phänotypischen Merkmale der modernen Anatomie, während fragmentierte Fossilien von weniger bekannten Fundorten kaum berücksichtigt werden. Der Effekt von morphologischer Variation wird oft nicht erkannt, da als phylogenetisch informativ geltende anatomische Merkmale nur in qualitativen Kontexten diskutiert werden. Ziel der hier vorgestellten kumulativen Dissertation ist es zur Lösung einiger dieser Probleme durch stellung der folgende Forschungsfragen: „1) Was ist die vorläufige taxonomisch Zugehörigkeit von der Kabua 1 Schädel? 2) War die Morphologie des Hinterhauptsbeins von Cioclovina das Gleiche wie die Neandertaler-Autapomorphie? 3) Sind die Fossa suprainiaca ein Ergebnis vom gemeinsame Abstammung?“ Die Forschungsfragen werden untersucht mit morphometrische Analysen der Form des Hirnschädels und diskreter morphologischer Merkmale an bisher kaum studierten fossilen Kranien. Diese Fossilien wurden in einer virtuellen Umgebung durch eine Kombination von qualitativen und quantitativen Methoden analysiert, um die Ursprünge und die Evolution des anatomisch modernen *H. sapiens* systematisch zu untersuchen. Dabei zeigte sich die Notwendigkeit ganheitlicher qualitativer und quantiativer Methoden zur Beantwortung von Fragen in der Paläoanthropologie. Darüber hinaus stellen alle vier Teilstudien dieser Dissertaton exzellente Beispiele dar, wie neu entwickelte Technologien und die Virtuellen Anthropologie zu neuen Erkentnissen über Fossilien führen können.

In der ersten Teilstudie wurde das fragmentarische craniale Material von Kabua 1 vollständig beschreiben und sechs virtuellen anatomischen Rekonstruktionen des Schädels analysiert. Kabua 1 wurde 1959 westlich des Turkana-Sees, Kenia, gefunden. Der fragmentarische Charakter und der unsichere geochronologische/archäologische Kontext

des Schädels führten bisher zu einem unzureichenden Verständnis seiner anatomisch-morphologischen Eigenschaften und phylogenetischen Zugehörigkeit. Eine qualitative Untersuchung von nicht-metrischen Merkmalen sowie der sechs virtuellen Schädelrekonstruktionen zeigte, dass der Hirnschädel von Kabua 1 eine globuläre Form und vergleichsweise gracile Merkmale aufweist, während wesentliche Beweise für plesiomorphe Merkmale fehlen. Diese Ergebnisse unterstützen eine vorläufige taxonomische Bezeichnung von Kabua 1 als anatomisch moderner *H. sapiens*.

In der zweiten Teilstudie wurde die Reproduzierbarkeit der virtuellen Rekonstruktionen von Kabua 1 quantitativ getested und anschließend die vorläufige taxonomisch Zugehörigkeit aus der ersten Teilstudie erneut beurteilt. Die Grundlage für diese Analysen bildete eine Reihe vielfältiger statistischer Methoden, bestehend aus Geometric Morphometrics basierend auf dreidimensionalen Koordinaten, Principal Component Analysis, Linear Discriminant Analysis, und Algorithmen des maschinellen Lernens, wie *k*-Nearest Neighbors und Random Forests. Die Ergebnisse bestätigen die Hypothese, dass die Hirnschädelform von Kabua 1 der Hirnschädelform von frühen und rezenten anatomisch modernen *H. sapiens* gleicht. Kabua 1 fällt jedoch aufgrund mehrerer Formmerkmale an den Rand der *H. sapiens* Variation. Dies ist möglicherweise ein Beispiel für das große Ausmaß der morphologischen Variation, die während des Jungpleistozäns, auf dem afrikanischen Kontinent vorhanden war. Ferner stimmen die Ergebnisse der Algorithmen des maschinellen Lernens mit den Ergebnissen der explorativen Ordinationstechniken überein und könnten somit eine wertvolle Ergänzung zu standardmäßig verwendeten Analysen aus dem Bereich der Geometric Morphometrics darstellen.

Die dritte und vierte Teilstudie konzentrieren sich auf die Fossa suprainiaca; eine diskrete ovale Depression am Hinterhauptsbein, die häufig als ausgeprägte Neandertaler-Autapomorphie angesehen wird. Jedoch weisen auch einige frühe und anatomisch moderne *H. sapiens* morphologisch ähnliche Merkmale auf, welche den Ursprung und die Aussagekraft dieses Merkmals in Frage stellen. Die meisten Diskussionen über die Fossa suprainiaca lassen sich einer von drei Hypothesen zuordnen: genetische Beimischung mit

der Neandertaler-Linie, gemeinsame Abstammung, und konvergente Evolution aufgrund biomechanischer Einflüsse. Die Vermischung von Genen als Hypothese zur Erklärung der ähnlichen morhplogischen Merkmale in Neanderthalern und *H. sapiens* wurde in der dritten Teilstudie untersucht. Von besonderem Interesse ist hierfür das Kalvarium aus Cioclovina, Rumänien, aus dem Jungpleistozän, welche aufgrund morphologischer Merkmale möglicherweise einen Neandertaler/*H. sapiens* Hybrid darstellt. Eine Kombination aus qualitativen und quantitativen Methoden wurden angewendet, um den Status der Fossa suprainiaca als Neandertaler-Autapomorphie zu überprüfen und zu evaluieren inwieweit diese Methoden sich zur Charakterisierung der Neandertaler/*H. sapiens*-Vermischung anwenden lassen. Hierfür wurden die allgemeine Morphologie des Hinterhauptsbeins sowie Messungen der relativen Dicke von Lamina externa und interna sowie der Diploe an vorher festgelegten Punkten des Hinterhauptsbeins analysiert. In allen Analysen ähnelt Cioclovina anatomisch modernen *H. sapiens*, was andeutet dass es kaum phänotypische Beweise für eine hohes Ausmaß an Neandertaler Abstammung des Cioclovina Individuums gibt.

Die gemeinsame Abstammung als Hypothese zur Erklärung der ähnlichen morhplogischen Merkmale in Neanderthalern und *H. sapiens* wurde in der vierten Teilstudie untersucht. Aus diesem Grund wurden zwei Schädel aus dem Mittel- bis Jungpleistozän aus Ostafrika, Eyasi I und ADU-VP-1/3, mit den Methoden aus der dritten Teilstudie sowie darauf aufbauenden Methoden analysiert. Die Ergebnisse zeigen, dass beide Individuen oberhalb von Inion eine Morphologie aufweisen, die der Morphologie von anatomisch modernen *H. sapiens* ähneln und sich deutlich von der Morphologie der Neanderthaler unterscheidet. In Kombination mit der Datierung beider Individuen erscheint die gemeinsame Abstammung als Erklärung der ähnlichen morphologischen Merkmale unwahrschreinlich. ADU-VP-1/3 datiert in die Nähe des vermuteten Zeitpunkts für das Out-of-Afrika Event und Eyasi I datiert ähnlich wie der vermutete Zeitpunkt für das Erscheinen moderner anatomischer Merkmale in Ostafrika. Die Ergebnisse stellen die phylogenetische Aussagekraft nicht-metrischer Merkmale in Frage und warnen vor Begriffe wie An- und Abwesenheit einzelner Merkmale als Indikatoren für moderne Anatomie

List of publications for cumulative dissertation

Percentages of own contribution to manuscripts are listed in parentheses (original idea/data collection/data analysis/writing and publication).

Accepted publications

Appendix I (30/100/100/70)

Bosman, A. M., Buck, L. T., Reyes-Centeno, H., Mirazón Lahr, M., Stringer, C., & Harvati, K. (2019). The Kabua 1 cranium: Virtual anatomical reconstructions. In Y. Sahle, H. Reyes-Centeno, & C. Bentz (Eds.), *Modern Human Origins and Dispersal* (pp. 137-170). Tübingen: Kerns Verlag.

Appendix III (50/100/100/80)

Bosman, A. M., & Harvati, K. (2019). A virtual assessment of the proposed suprainiac fossa on the early modern European calvaria from Cioclovina, Romania. *American Journal of Physical Anthropology, 169*(3), 567-574.

Submitted manuscripts

Appendix IV (50/100/100/60)

Bosman, A. M., Reyes-Centeno, H., & Harvati, K. (Date of submission: 24.09.2019).
A virtual assessment of the suprainiac depressions on the Eyasi I and ADU-VP-1/3 crania. Manuscript submitted to the *Journal of Human Evolution*.

Manuscripts ready for submission

Appendix II (60/20/100/70)

Bosman, A. M., Buck, L. T., Reyes-Centeno, H., Mirazón Lahr, M., Stringer, C., & Harvati, K. (To be submitted). A geometric morphometric analysis of the Kabua 1 cranium. Manuscript in preparation for the *American Journal of Physical Anthropology*.

Introduction

"*It is important that we know where we come from, because if you do not know where you come from, then you don't know where you are, and if you don't know where you are, you don't know where you're going. And if you don't know where you're going, you're probably going wrong.*"

Terry Pratchet (2010) – I shall wear midnight. New York: Harper

1. Background

Although our understanding of *H. sapiens* evolution has increased in the last decades, there remain large gaps in our knowledge. Some of the most contentious issues surrounding the *H. sapiens* lineage include the tempo and mode of dispersals across the world (e.g. Bons et al., 2019; Ponce de León et al., 2018; Reyes-Centeno et al., 2014a, 2015) and the interaction with pene-contemporaneous hominin taxa in Africa and Eurasia (e.g. Green et al., 2010; Hammer et al., 2011; Harvati & Roksandic, 2016; Posth et al., 2016, 2017; Trinkaus, 2011). The emergence of anatomical modernity is one of these issues and has recently seen an increase in relevant literature (e.g. Bräuer, 2013; Endicott et al., 2010; Henn et al., 2018; Lahr, 1994; Mirazón Lahr, 2016; Scerri et al., 2018). On one hand, there is a general consensus that, based on recent genetic and fossil evidence, early *H. sapiens* originated in Africa somewhere during the late Middle Pleistocene (MIS 11 – MIS 6) (Campbell et al., 2014; Endicott et al., 2010; Grine, 2016; Nielsen et al., 2017; Reyes-Centeno et al., 2015; Rightmire, 2012; Schlebusch et al., 2017; Stringer, 2016; Tattersall, 2009). Furthermore, the common ancestral population of recent modern humans likely resided in and dispersed out of Africa somewhere during the terminal Middle Pleistocene and Late Pleistocene (MIS 5 – MIS 2) (Campbell et al., 2014; Forster, 2004; Galway-Witham et al., 2019; Gronau et al., 2011; Groucutt et al., 2015; Grün et al., 2005; Hubbe et al., 2010; Lahr & Foley, 1994; Pagani et al., 2016; Reyes-Centeno et al., 2014a, 2015; Rightmire, 2009; Scozzari et al., 2014; Weaver, 2012), although Middle Pleistocene out-of-Africa dispersals of early *H. sapiens* have been proposed (e.g. Harvati et al., 2019; Hershkovitz et al., 2018).

On the other hand, the lack of consensus on what "anatomical modernity" actually entails (e.g. Caspari & Wolpoff, 2013; Day & Stringer, 1982; Lieberman et al., 2002; Mirazón Lahr & Foley, 2016; Pearson, 2008; Sahle et al., 2019a; Stringer & Buck, 2014; Stringer et al., 1984) and the sometimes arbitrary usage of other non-taxonomic terms such as "archaic" *H. sapiens* (Collard & Wood, 2007; Howell, 1999; Schwartz, 2016; Tattersall & Schwartz, 2008) render recognition of associated phenotypes a challenging undertaking (e.g. Mirazón Lahr, 2016), hindering discussions on the phyletic relationships between fossils specimens. Moreover, while there exists a certain "working definition" of anatomically modern

H. sapiens based on a set of morphological traits (Day & Stringer, 1982; Stringer, 2016), there has been debate on the phylogenetic importance of certain *H. sapiens* autapomorphies and whether these emerged in either a mosaic or a punctuated pattern in Africa during the late Middle Pleistocene (e.g. Bräuer, 2008; Hublin et al., 2017; Lacruz et al., 2019; Pearson, 2008; Scerri et al., 2018; Tattersall, 2009). Additionally, the borders between plesiomorphic ("archaic") and autapomorphic ("derived") morphologies have become increasingly blurry due to recent proposals that ancestral variation persisted in the *H. sapiens* lineage into the Late Pleistocene in Africa (e.g. Crevecoeur et al., 2009; Eriksson et al., 2012; Grine, 2016; Grine et al., 2010; Harvati et al., 2011; Mirazón Lahr, 2016) and possibly also in Eurasia (Li et al., 2017; Trinkaus, 2011; Wu et al., 2019). These findings suggest a complex transition to anatomical modernity due to factors such as high levels of population structure, morphological variability and interbreeding (e.g. Crevecoeur et al., 2009; Gunz et al., 2009a; Harvati et al., 2011; Scerri et al., 2018; Schlebusch et al., 2017; Stringer, 2016).

Most of the aforementioned discussions cannot be easily resolved due to the fact that the late Middle Pleistocene and Late Pleistocene fossil records are patchy, especially for crucial areas such as eastern Africa (e.g. Grine, 2016; Mirazón Lahr, 2016; Mirazón Lahr & Foley, 2016; Mounier & Mirazón Lahr, 2019; Stringer, 2016). Adding to this problem, recovered fossils are often fragmented and taphonomically distorted (e.g. Haile-Selassie et al., 2004; Mounier & Mirazón Lahr, 2016, 2019; White, 2003), which further obfuscates our knowledge on intraspecific phenotypic variation during these time periods (e.g. Campbell & Tishkoff, 2010; Gunz et al., 2009a; Rightmire, 2008). As such, it is critical that all possible sources of information are incorporated. This includes re-evaluations of fossil remains part of museum exhibitions or stored in paleontological depots (e.g. Buck & Stringer, 2015; Harvati et al., 2019; Porraz et al., 2015; Tryon et al., 2015). Analyses of existing collections complement additional surveys and excavations, serve as a reference framework in which new results can be contextualized, and underline the importance of long-term management of collected finds (Tryon et al., 2019). As fossil recovery, extensive handling, (multiple) attempts at physical reconstruction, and storage conditions have serious consequences for the conservation of paleoanthropological material (e.g. Le Cabec & Toussaint, 2017),

minimally destructive methods such as medical and industrial CT scanning have become crucial in the study of fossils. These methods prevent further degradation through the act of attaining and subsequently sharing virtual representations of the original material (Abel et al., 2012; Balzeau et al., 2010; Weber, 2015; Zollikofer & Ponce de León, 2005).

In order to fill existing gaps in the fossil record, this cumulative dissertation presents four studies in which traditional analyses of shape and discrete morphological anatomical traits are combined with cutting edge techniques from the field of Virtual Anthropology (VA). In short, VA can be described as a multidisciplinary approach which relies on data, methods, and examples from anthropology, mathematics, computer science, and industrial design to study skeletal/fossil material (Weber & Bookstein, 2011; Zollikofer & Ponce de León, 2005). These unified qualitative and quantitative analyses allow for a finer-grained understanding of the morphology of singular fossil finds as well as a more inclusive integration and contextualization of current studies on anatomically modern traits. In this dissertation, virtual anthropological methods are applied to the shape and specific anatomical traits of the neurocranium, as it has been used to reliably separate plesiomorphic and autapomorphic morphologies within the genus *Homo* (e.g. Gunz et al., 2019; Harvati et al., 2019; Hublin et al., 2017).

The first study included in this dissertation explores the taxonomic affiliation of the Kabua 1 cranium, using virtual anatomical reconstructions, descriptions of discrete anatomical traits, and surface distance maps. In the second study, these virtual reconstructions are investigated through the application of quantitative geometric morphometrics with the aim of testing whether neurocranial shape data can be used to find the most accurate taxonomic attribution for Kabua 1. These methods include a Principal Component Analysis and Linear Discriminant Analysis, as well as two machine learning algorithms. The third study focuses on one discrete anatomical trait, the suprainiac depression. By comparing the internal morphology of the Cioclovina suprainiac area to the Neanderthal condition, it is tested whether this trait could be a phylogenetic expression of admixture between *H. sapiens* and the Neanderthal lineage. This is done through the application of framework in which

qualitative observations are supported by equidistant measurements of relative thickness of the external table, diploic layer, and internal table across the occipital bone. The fourth study uses similar methods as the third, but instead aims to resolve whether two Middle-Late Pleistocene individuals from Africa, Eyasi I and ADU-VP-1/3, possess a suprainiac depression, in order to more broadly discuss the etiology and phylogenetic implications of this trait.

2. Research Strategy

2.1. Objectives

The goal of this cumulative dissertation is **to help fill existing gaps in the fossil record through the analysis of neurocranial shape and distinct morphological traits in a series of understudied fossil crania**. This goal was distilled into the following objectives:

(1) To reconstruct and analyze fragmentary fossil crania from geographic areas proposed to be pivotal in the emergence of anatomically modern *H. sapiens* and its interaction with other, non-*sapiens*, lineages as the former dispersed out of Africa.

(2) To apply virtual techniques in the analysis and validation of the phylogenetic importance of specific morphological characteristics that have been proposed as autapomorphic for recent lineages of the genus *Homo*, and are thus used in the taxonomic attribution of fossil material.

(3) To evaluate and contextualize combined qualitative and quantitative frameworks within current models on the evolution of *H. sapiens* in the late Middle and Late Pleistocene.

2.2. Research Questions

Within the wider scope of this dissertation and its objectives, I focus on the following three research questions.

Appendix I & II: What is the taxonomic affiliation of the Kabua 1 cranium?

In order to contribute to the first objective of this dissertation, this research question pertains to the Kabua 1 cranium, which was found in 1959 in Kenya (Whitworth, 1960, 1965a, 1965b, 1966). This cranium is often disregarded in discussions on human evolution due to its fragmented nature as well as its uncertain geochronological context. The lake bed sediments surrounding the cranium have been proposed to date broadly to the Late Pleistocene by nature of supposedly extinct faunal remains found in close proximity to the hominid material (Whitworth, 1960, 1965a, 1965b). However, based on radiocarbon dates on lacustrine shells from layers above the fossil material, the Kabua assemblages could be as

young as 5500 BP (Whitworth, unpublished documents in Natural History Museum Archives). Lithic artifacts recovered from the surrounding surface include tools which Whitworth (1965a) referred to as Kenya Stillbay, Upper Kenya Capsian, and Sangoan; all allocated to different archaeological time periods spanning from the Middle Pleistocene to the Holocene, thus representing a mixed context. (e.g. Ambrose, 1980; Wilshaw, 2016).
As such, while direct ESR and U-series dating is currently underway, a Late Pleistocene-Holocene age range seems to be the most conservative estimate.

The Kabua 1 cranium has been argued to possess several "archaic" anatomical traits, such as a receding forehead, thick cranial bones, pronounced supraorbital tori, an inflated glabella, and a robust mandible with a chin (Whitworth, 1960, 1966), leading to a physical reconstruction that heavily emphasizes a plesiomorphic neurocranial shape (Rightmire, 1975). However, preliminary investigations by most other scholars suggest that the Kabua 1 cranium is instead representative of anatomically modern *H. sapiens* variation, both in its overall cranial shape and most of its discrete anatomical traits (Bräuer, 1978; Rightmire, 1975; Sawchuk & Willoughby, 2015; Schepartz, 1987). On the other hand, the bony labyrinth of Kabua 1, which is considered a reliable indicator of phylogeny (Bouchneb & Crevecoeur, 2009; Ponce de León et al., 2018; Quam et al., 2016), does present some plesiomorphic affinities, such as a superiorly orientated posterior canal (Reyes-Centeno et al., 2014b). As of yet, a detailed investigation of the taxonomic affiliation of the complete Kabua 1 cranium has not been undertaken due to the presence of taphonomic deformation. Moreover, as the original material was used in a physical reconstruction and fragments have been fixed together with laboratory adhesives (Whitworth, 1966), any analysis of the independent fragments is problematic since the integrity of the fossil material could be compromised. However, an exhaustive assessment of Kabua 1 and its proposed mix of autapomorphic and plesiomorphic features is critical, as this cranium, depending on a currently unknown age, might be an example of the persistence of plesiomorphic morphological traits and complex transition to anatomical modernity in Late Pleistocene Africa (e.g. Eriksson et al., 2012; Grine, 2016).

In order to re-contextualize and re-evaluate the Kabua 1 cranium, its fragments are digitized using non-destructive computed tomography imaging, after which sediment is virtually removed and the fragments are exhaustively analyzed and described (**Appendix I**). The proposed plesiomorphic and autapomorphic features are systematically assessed and compared to our current understanding of anatomical modernity. Subsequently, several anatomical reconstructions are created using virtual anthropological methods (Weber, 2015; Weber & Bookstein, 2011; Weber et al., 1998; Zollikofer & Ponce de León, 2005; see Methodology). To test competing evolutionary hypotheses, each reconstruction is based on one of six distinct reference crania from diverse temporal and geographic contexts. These virtual reconstructions are investigated and compared through qualitative analyses and three-dimensional surface distance maps. The validity and reproducibility of the reconstructions, as well as their implications for the taxonomic affiliation of Kabua 1, are quantitatively evaluated with established geometric morphometrics (GM) and machine learning methods in **Appendix II**.

Appendix III: Does the morphology of the Cioclovina suprainiac region represent the Neanderthal condition?

The suprainiac fossa, a rugose discrete elliptical depression located above inion on the occipital bone, has been proposed as a Neanderthal autapomorphic feature (Hublin, 1978; Santa Luca, 1978). However, morphologically similar structures above inion designated as suprainiac depressions have been reported for *H. sapiens* crania from Middle and Late Pleistocene Africa (e.g. Balzeau & Rougier, 2010; Haile-Selassie et al., 2004; Trinkaus, 2004), Upper Paleolithic Europe (e.g. Caspari, 2005; Frayer, 1992; Kramer et al., 2001; Soficaru et al., 2006, 2007; Trinkaus, 2007), and the Late Pleistocene Levant (Hershkovitz et al., 2015, 2017; Kramer et al., 2001; Smith et al., 2005). There are still many unanswered questions about this trait, such as its etiology and how it should be evaluated in the context of phylogenetic relationships between specimens/taxa in which it is observed (e.g. Bräuer, 2013; Hershkovitz et al., 2017; Li et al., 2017). Currently, most perspectives on the etiology of the suprainiac depression can be summarized under the following three hypotheses.

The first scenario sees the suprainiac fossa as an autapomorphy specific for the Neanderthal lineage and, by extension, most suprainiac depressions on Late Pleistocene Eurasian *H. sapiens* as significant phenotypic markers of recent Neanderthal/*H. sapiens* admixture (Frayer, 1992; Kramer et al., 2001; Trinkaus, 2004, 2007, 2011; Wolpoff et al., 2001). In the second hypothesis, the Neanderthal suprainiac fossae and *H. sapiens* suprainiac depressions are considered homologous traits which are inherited from a common ancestor (Nowaczewska et al., 2019; Trinkaus, 2004). The third hypothesis proposes a biomechanical framework, in which Neanderthal suprainiac fossae and *H. sapiens* suprainiac depressions could be convergent traits due to the biomechanics of the nuchal musculature and a possible correlation with both occipital and cranial shape (Caspari, 2005; Nowaczewska, 2011). In order to resolve this discussion on the etiology of the suprainiac depression, it is necessary that the aforementioned hypotheses are all investigated in holistic studies which include comparable qualitative and quantitative methods.

The Cioclovina calvaria might prove critical to the assessment of the first of these hypotheses in particular, as it plays an important role in the continued discussion on recent admixture between Neanderthal and *H. sapiens* (Bae et al., 2017; Li et al., 2017; Soficaru et al., 2007; Trinkaus, 2007, 2011; Wolpoff & Caspari, 2013; Wu et al., 2019). Dated to 28,510 ± 170 ^{14}C years BP, it has been proposed the Cioclovina specimen represents a possible Neanderthal/*H. sapiens* hybrid due to the presence of several Neanderthal autapomorphies (Soficaru et al., 2007; Trinkaus, 2007). However, recent research has suggested that this individual is well within the range of recent *H. sapiens* variation and that its cranial phenotype does not demonstrate any obvious signs of admixture (Harvati et al., 2007; Kranioti et al., 2011; Uhl et al., 2016). For example, Harvati et al. (2007) have argued that the suprainiac area of the Cioclovina specimen exhibits none of the structures present in the classic Neanderthal suprainiac morphology but rather demonstrates superficial remodeling of the ectocranial surface. As such, this specimen constitutes an excellent case study to investigate the interbreeding hypothesis. In the context of the second and third objectives of this dissertation, **Appendix III** details an analytical framework in which qualitative observations of the external surface of the Cioclovina suprainiac area are

combined with qualitative and morphometric analyses of the internal structures (i.e. external table, diploic layer, and internal table; Balzeau & Rougier, 2010), though the use of (micro) computed tomography (Materials and Methods section).

Appendix IV: Are suprainiac depressions in later *Homo* symplesiomorphic?

There has been an ongoing debate about the homology of suprainiac depressions and the surrounding occipital bone morphology in Pleistocene hominins. Whereas most previous studies have only considered the external morphology and/or frequency of this trait (e.g. Caspari, 2005; Frayer, 1992; Trinkaus, 2004), in **Appendix III** the internal structures of the Cioclovina suprainiac area are discussed in detail, as these components of the cranium have been shown to possess distinctive patterns of relative thickness which differentiate Neanderthal suprainiac fossae from *H. sapiens* suprainiac depressions (Balzeau & Rougier, 2010, 2013; Nowaczewska et al., 2019). Moreover, this study on the Cioclovina specimen tests the quantitative framework on the internal morphology and is designed to inform whether Neanderthal/*H. sapiens* interbreeding could be a possible cause for the apparent homology between the suprainiac depressions in these two taxa.

So far, however, there have been no studies on the internal morphology of suprainiac depressions which include eastern African *H. sapiens* from the late Middle and Late Pleistocene. As this geographic area and these time periods were likely key in the emergence of autapomorphic *H. sapiens* traits, as well as the eventual dispersal of *H. sapiens* out of Africa (e.g. Bräuer, 2008, 2013; Day, 1969; Reyes-Centeno et al., 2015; Sahle et al., 2018, 2019a, 2019b; White et al., 2003), such specimens are critical in resolving the debate on the homology and etiology of suprainiac depressions in *H. sapiens* and Neanderthals. Especially the hypothesis about common ancestry of the suprainiac depression (symplesiomorphy) should be assessed by investigating specimens that date close to the appearance of *H. sapiens* autapomorphic traits. Additionally, while the hypothesis on the influence of biomechanics (convergence) has been discussed to some extent (Caspari, 2005; Nowaczewska, 2011), this scenario has not been extensively evaluated with data on the internal structures of the cranium (however see Nowaczewska et al., 2019). Thus, in order

to investigate these hypotheses and meet the second and third objectives of this dissertation, the suprainiac morphologies of two Middle-Late Pleistocene eastern African individuals, Eyasi I and ADU-VP-1/3, are analyzed in **Appendix IV**. Eyasi I was found in Tanzania and is generally considered an early *H. sapiens*, even though its taxonomic attribution is contentious (e.g. Bräuer, 2013; Trinkaus, 2004). Although unresolved, the geochronology of this specimen is broadly placed between 375-88 ka. ADU-VP-1/3 is more securely dated to between 105-79 ka (Yellen et al., 2005). Moreover, its cranial morphology has generally been described as anatomically modern (Haile-Selassie et al., 2004).

In **Appendix IV**, these specimens are directly compared with one recent anatomically modern human with a distinct suprainiac depression from Tanzania (Masai 12), and two classic Neanderthals from France (La Chapelle-aux-Saints 1 & La Ferrassie 1). By making use of and elaborating on the combined qualitative and quantitative framework utilized in **Appendix III**, both the external and internal morphologies of the suprainiac areas of these individuals are evaluated and compared to a larger reference sample consisting of both Neanderthal and *H. sapiens* specimens (Balzeau and Rougier, 2010). Since comparable methods are used to investigate the three aforementioned hypotheses in **Appendix III** and **Appendix IV**, these independent studies can be directly compared to each other and their results placed more firmly within the larger context of *H. sapiens* evolution. Moreover, if the depressions on Eyasi I and ADU-VP-1/3 are found to be quantitatively and qualitatively similar to the Neanderthal condition, then the status of the suprainiac fossa as a diagnostic Neanderthal-derived trait must be reconsidered, complicating the taxonomic assignment of isolated occipital bones in the fossil record. Alternatively, if the depressions above inion on Eyasi I and ADU-VP-1/3 are found to differ from the Neanderthal condition, then the suprainiac fossa can be tentatively retained as an autapomorphic trait.

2.3. Materials & Methods

To answer the research questions outlined above, this cumulative dissertation combines virtual anthropology, computer based tomographic imaging, and state of the art three-dimensional geometric morphometrics (Figure 1). The following sections introduces some of the used methods and the concepts behind them. More in-depth discussions, specific protocols, and reviews of applied techniques can be found in the appendices and the references therein.

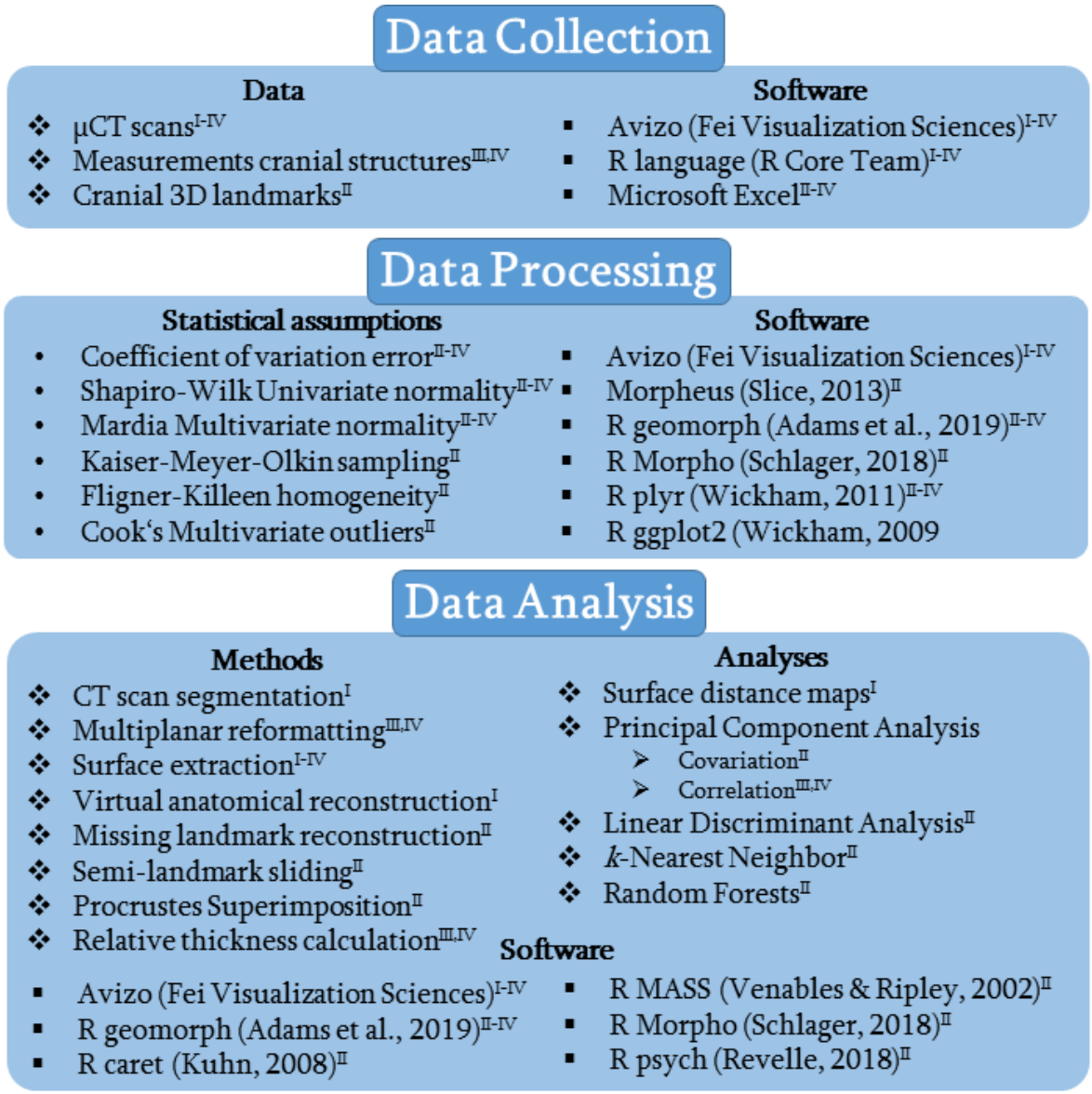

Figure 1. General workflow followed in this dissertation. Superscript numbers indicate appendices.

Appendix I

The Kabua 1 cranium was scanned with a Nikon Metrology HMX ST 225 micro-computed tomography (μCT) machine, located at the Natural History Museum in London. The scanning parameters were optimized for variable sizes, densities, and states of mineralization of the separate fragments (average: kV = 183, mA = 178, number of slices = 1532, voxel size = 0.07). In short, CT scanning creates two-dimensional images, or so-called "slices" of an object, as it is scanned in successive layers from a multitude of angles by a beam of X-rays. Subsequently, absorption values of the scanned materials across all layers are computed and used to construct a cross-sectional image that can be rendered as a 3D model in a virtual environment (Ambrose, 1973; Hounsfield, 1973; Jungers et al., 1979). Effectively, CT scans can be used to explore hidden areas of fossil/skeletal material which are otherwise inaccessible barring destructive sampling (Weber & Bookstein, 2011). Recent improvements in these techniques have led to the development of industrial μCT scanners, which involve scanning resolutions in the range of micrometers. This technology increases the level of detail of scans due to a higher resolution, a wider range of absorption values, as well as better penetration of fossilized remains and matrix (Du Plessis et al., 2017). As such, this was the ideal method to digitize the Kabua 1 cranium, as this fossil contains a large amount of sediment and several dense inclusions.

Subsequent to data acquisition, matrix clinging to Kabua 1 was removed virtually from the CT-scans through the application of manual thresholding, distorted fragments were restored to their original condition, and fragments were pieced back together (e.g. Abel et al., 2012; Di Vincenzo et al., 2017; Weber, 2015; Weber & Bookstein, 2011). During the virtual anatomical reconstruction of the separate fragments, a bottom-up approach was followed in order to maintain a high amount of reproducibility (Zollikofer & Ponce De León, 2005). As such, the reconstruction was primarily based on anatomical information present in the fragments, which meant both following biological constraints when fragments were thought to articulate, as well as identification of taphonomic distortion/deformation through observations of deviations from symmetry (e.g. Gunz et al., 2009b; White, 2003). Most fragments of the parietal and occipital bones could be directly

articulated, following break patterns and cranial sutures. Major taphonomic distortions were assessed and corrected for using affine transformations (Zollikofer & Ponce de León, 2005).

As soon as direct anatomical information could not be relied on to reconstruct portions of the Kabua 1 cranium, alternative hypotheses were followed which are valid not only for a specific taxon but rather for the ancestral state. For Kabua 1, this was limited to bilateral symmetry, as it is an attested symplesiomorphic condition in the animal kingdom (Finnerty et al., 2004). This hypothesis entails that, in the scenario that a specimen presents extensive damage or distortion on one side, this portion can be reconstructed by reflecting the other, better preserved side (Bookstein, 1991; Gunz et al., 2009b; Mardia et al., 2000). This principle was followed to restore the Kabua 1 maxilla and mandible to approximate their original condition. However, due to the presence of expanding matrix distortion (Weber & Bookstein, 2011; White, 2003), these methods were not applied to the parietal and temporal bones, as it would give a more skewed perspective of the cranium which could not be corrected for systematically using only affine transformations (Weber & Bookstein, 2011).

In order to join together the frontal and parietal portions of Kabua 1, which could not be reconstructed through articulation or bilateral symmetry, it was necessary to rely on interpolation of data from an *a priori* defined reference sample (e.g. Gunz et al., 2009b; Weber & Bookstein, 2011; Zollikofer et al., 2005). As the nature of the reference sample is critical in the final outcome, these reference crania are ideally selected in order to cover a wide variety of inter- and intra-species variation (Senck et al., 2015). However, as we do not have a secure date for the Kabua material, as well as limited access to CT scanned paleoanthropological material, we had to rely on data available to us. As such, six reference crania from very distinct temporal and geographic localities (Broken Hill, Ngaloba LH 18, Skhūl V, Mumba X, Masai 03, and Masai 10) were used to limit the degrees of freedom that the disarticulated Kabua fragments could move in virtual space. These crania were used as a general framework to position the Kabua 1 fragments, without overly relying on the degree of similarity between the fragments and the reference crania, in order to prevent a

substantial bias towards the reference (Figure 2). The virtual models of the reference crania used during the reconstruction procedure were based on µCT scans as well as 3D surface scans obtained from the Natural History Museum in London, the Virtual Anthropology Laboratory in Vienna, and the Eberhard Karls University of Tübingen. The creation of multiple independent reconstructions by using several distinct reference crania provides a range of possible morphologies, rather than one single solution (e.g. Gunz et al., 2009b; Harvati et al., 2019; Neubauer et al., 2018; Zollikofer et al., 2005). Moreover, the robusticity of the resulting virtual reconstructions was evaluated through surface distance maps, which display the amount of surface overlap between two objects by calculating the minimal distance between them.

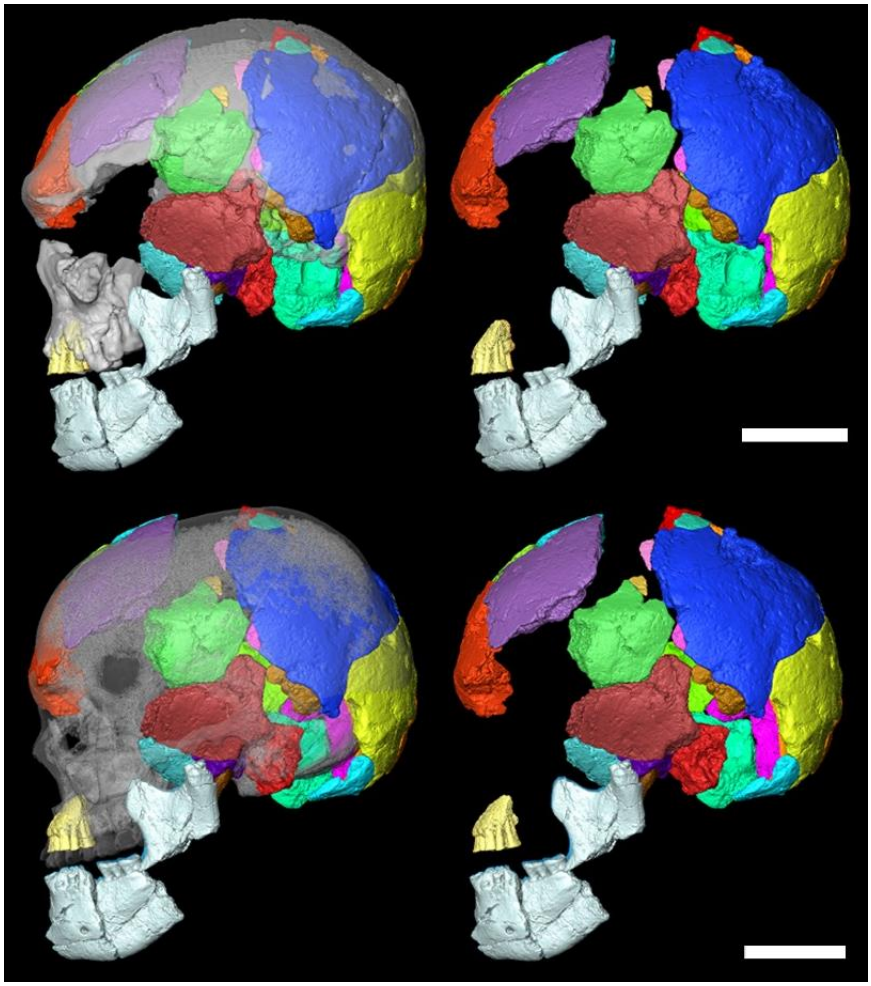

Figure 2. Virtual reconstructions of Kabua 1. Top-left: reconstruction based on LH18, with the reference superimposed (gray, transparant); top-right: reconstruction based on LH18; bottom-left: reconstruction based on Masai 03, with the reference superimposed (gray, transparant); bottom-right: reconstruction based on Masai 03 (scale bars = 10 cm).

Appendix II

The reconstructions described in **Appendix I** were further analyzed with landmark-based geometric morphometrics. Traditionally, morphometrics as a field has been concerned with linear distances and angles between designated metric points. These measurements have been used to study variation in the morphology of hominin remains to great effect (e.g. Howells, 1973; Lahr, 1996). Morphometrics can also be used to measure internal structures of bones and fossils, as demonstrated in **Appendix III** and **Appendix IV**. However, these measurements convey no information on the geometric structure of three-dimensional objects. In geometric morphometrics (GM), components of a specimen can be defined in three-dimensional shape-space where their relative position and distribution are meaningful, thus allowing for the quantitative comparison of anatomy and shape (Rohlf, 1990; Rohlf & Marcus, 1993). The most commonly applied technique in GM is the landmark-based approach. Landmarks are discrete, biologically homologous two/three dimensional Cartesian coordinates, meaning that they represent the same locations on every single individual in a sample. These landmarks can be used to investigate underlying patterns of variation and test hypotheses about function, development, ontogeny, life history, adaptation, and taxonomy (e.g. Athreya, 2009; Dryden & Mardia, 1998; Harvati & Weaver, 2006a; Hublin et al., 2017; Mitteroecker & Gunz, 2009; Mitteroecker et al., 2013).

In **Appendix II,** the landmarks on the Kabua reconstructions were designated with Avizo Lite (FEI Visualization Sciences Group, versions 9.0.1 and 9.2.0), and were distributed to capture neurocranial shape along the midsagittal and lambdoidal sutures, as these areas of the cranium have been used in previous studies to accurately classify Middle-Late Pleistocene hominins (e.g. Harvati et al., 2011, 2019). The landmark dataset consisted of both "fixed" landmarks and semi-landmarks. Fixed landmarks represent homologous points within a specimen and are generally located at the discrete juxtaposition of tissues or extremes of curvature. Semi-landmarks are instead used to represent the areas which are not covered by fixed landmarks, such as curves or surfaces. These structures are matched between specimens by iteratively sliding coordinates under the control of several adjustable parameters (e.g. Weber & Bookstein, 2011).

The sample to which the Kabua reconstructions were compared consisted of Microscribe data (Immersion Corp) collected by Harvati et al (2011) and Reyes-Centeno et al. (2014a). This sample includes hominin and *H. sapiens* crania from Middle Pleistocene, Late Pleistocene, and Holocene Eurasia and Africa. Processing of Microscribe data was performed in DVLR, Resample.exe (http://www.nycep.org/nmg/programs.html), Morpheus (Slice, 2013), Evan Toolbox (http://evan-society.org), and R version 3.5.0 (R Core Team, 2019). The data were subsequently processed with a Generalized Procrustes Analysis, which is a least-squares method which estimates parameters for location and orientation that minimize the sum of squared distances between corresponding landmarks on two or more configurations, and thus makes them directly comparable (Gower, 1975; Rohlf & Slice, 1990). After this transformation, groups were specified and the data were explored using a Principal Component Analysis (PCA) and associated plots (Darroch & Mosimann, 1985). In short, PCA computes new linear combinations of any set of variables and maximizes variance among individuals. Effectively, PCA reduces the number of variables in an analysis, thereby allowing for the application of both parametric and non-parametric statistics. Afterwards, standard tests were used to test mathematical assumptions. These include Shapiro-Wilk tests for univariate normality (Shapiro & Wilk, 1965), Mardia measures of multivariate skewness and kurtosis (Mardia, 1970), Kaiser-Meyer-Olkin test for sampling adequacy (Kaiser, 1970; Kaiser & Rice, 1974), Fligner-Killeen test of homogeneity of variance (Fligner & Kileen, 1976), and Cook's distance for multivariate outliers (Cook & Weisberg, 1982).

Procrustes distances (Adams et al., 2004; Bookstein et al., 2004; Gower, 1975; Rohlf & Slice, 1990), and Linear Discriminant Analysis (Bookstein, 1991; Gunz et al., 2009b; Slice, 2011) were used to statistically test the robusticity of the analyses and to correctly classify the Kabua 1 reconstructions. Procrustes distances represent the square root of the sum of squared differences between the positions of optimally superimposed configurations within a sample and can be used to describe similarity (or dissimilarity) between specimens. Linear Discriminant Analysis takes a vector of observations from an unknown specimen and uses coefficients to produce a score that is compared to other pre-defined groups, in order to

classify the unknown specimen. These methods were complemented by two machine-learning algorithms applied on the neurocranial shape data: *k*-Nearest Neighbors (*k*-NN; Ripley, 1996) and Random Forests (RF; Breiman, 2001). In short, both of these methods are non-parametric and rely on iteratively subsampling a training dataset in order to classify unknown individuals based on the provided data. *k*-NN uses the distances between specimens and bases a classification on a plurality vote of an adjustable number of nearest neighbors (Ripley, 1996). RF models are based on classification trees, which predict group membership of an unknown dependent variable based on a measurement at a predictor variable at each (decision) node, and can be directly applied to (Procrustes) shape data (Feldesman, 2002; Hefner et al., 2014). However, instead of only using a single tree which has access to all predictor variables, RF models use shape data to construct a large number of classification trees that incorporate randomized distribution of the original variables (Breiman, 2001). Both *k*-NN and Random Forests were trained on the fossil reference sample in four sets, with manually adjusted numbers of randomly resampled recent *H. sapiens*, repeated over 10.000 iterations. The recent *H. sapiens* were randomly resampled in order to combat the class imbalance problem, as this group contained a higher number of individuals than any of the fossil groups. All classification analyses were trained with leave-one-out crossvalidation. All statistical tests were peformed in R version 3.5.0 (R Core Team, 2019), using the following packages: caret (Kuhn, 2008), extrafont (Chang, 2014), geomorph (Adams et al., 2019), ggplot2 (Wickham, 2009), ggrepel (Slowikowski, 2017), MASS (Venables & Ripley, 2002), Morpho (Schlager, 2018), MVN (Korkmaz et al., 2014), PCDimensions (Wang et al., 2018), plyr (Wickham, 2011), psych (Revelle, 2018), and shapes (Dryden, 2018).

Appendix III and Appendix IV

The CT scans of Cioclovina were procured using a Siemens Sensation 64 medical CT scanner in Centrul De Sanatate Pro-Life SRL, Bucharest. The direction of scanning was coronal (transverse) with a slice thickness of 0.625 mm, 120 kV tube voltage, and 304 mA tube current (Kranioti et al., 2011). Eyasi I was scanned with a "General Electric Phoenix" µCT scanner (model v|tome|x s) at the Paleoanthropology High Resolution CT Laboratory

(University of Tübingen) with scan parameters set to 180 kV, 100 µA, 3000 images, and a voxel size of 0.1319100 (mm/pixel). ADU-VP-1/3 was scanned in the National Museum of Ethiopia (Addis Ababa) with a High Energy Desktop Micro-CT System Skyscan 117, with parameters set to 130 kV, 40 µA, 1334 images, and a voxel size of 0.14269408 (mm/pixel). These fossil specimens were analyzed in the virtual environment of Avizo Lite (FEI Visualization Sciences Group, versions 9.0.1 and 9.2.0). Masai 12 was scanned with a "General Electric Phoenix" µCT scanner (model v|tome|x s) at the Paleoanthropology High Resolution CT Laboratory (University of Tübingen) with parameters set to 170 kV, 170 µA, 2500 images, and a voxel size of 0.12915161 (mm/pixel). La Chapelle-aux-Saints 1 and La Ferrassie 1 were scanned with General Electric µCT scanner (model "v|tome|x L 240") at the *Muséum National d'Histoire naturelle* in Paris, with voxel sizes of 0.122739 and 0.13155056 (mm/pixel), respectively.

The morphometric aspect of the combined framework mentioned in the second and third research questions consisted of a set of measurements of the thickness of the internal structures of each cranium (external table, diploic layer, internal table). These measurements were taken on a singular vertical slice obtained from the CT dataset, which was computed to cross the midsagittal plane between lambda and the most posterior point of the occipital superstructures. Measurements were obtained in Avizo Lite (FEI Visualization Sciences Group, versions 9.0.1 and 9.2.0), distributed equidistantly in three areas of the occipital bone: (1) the area from lambda to the upper limit of the suprainiac depression, (2) the area from the superior limit of the depression to the most posteriorly prominent point of the occipital, and (3) a single measurement of the center of the depression. These absolute measurements were converted into relative values by first assessing the total thickness of the cranial vault at each measurement location. Subsequently, the relative contributions of the internal structures were calculated as percentages of the total cranial thickness. This standardization procedure makes the measurements from different specimens comparable without the need for scaling or further manipulation of data (Figure 2).

The observations and measurements obtained through the application of this framework were subsequently compared to a sample of Neanderthals and Holocene *H. sapiens* from North Africa and Europe with clearly defined suprainiac depressions. This reference sample was derived from Balzeau and Rougier (2010) and, together with the newly acquired data on the Cioclovina, Eyasi I and ADU-VP-1/3 specimens, subjected to a Principal Component Analysis in order to assess whether the relative densities of the internal structures of suprainiac morphologies could differentiate between Neanderthal and *H. sapiens* suprainiac phenotypes. To check for inter-observer error, La Ferrassie 1 and La Chapelle-aux-Saints 1 were measured and compared to the data on these specimens reported by Balzeau and Rougier (2010). Additionally, the data on Cioclovina, Eyasi I and ADU-VP-1/3 were projected in the PCA. All analyses were performed in R version 3.5.0 (R Core Team, 2019) using the following R packages: extrafont (Chang, 2014), ggplot2 (Wickham, 2009), ggrepel (Slowikowski, 2017), and plyr (Wickham, 2011).

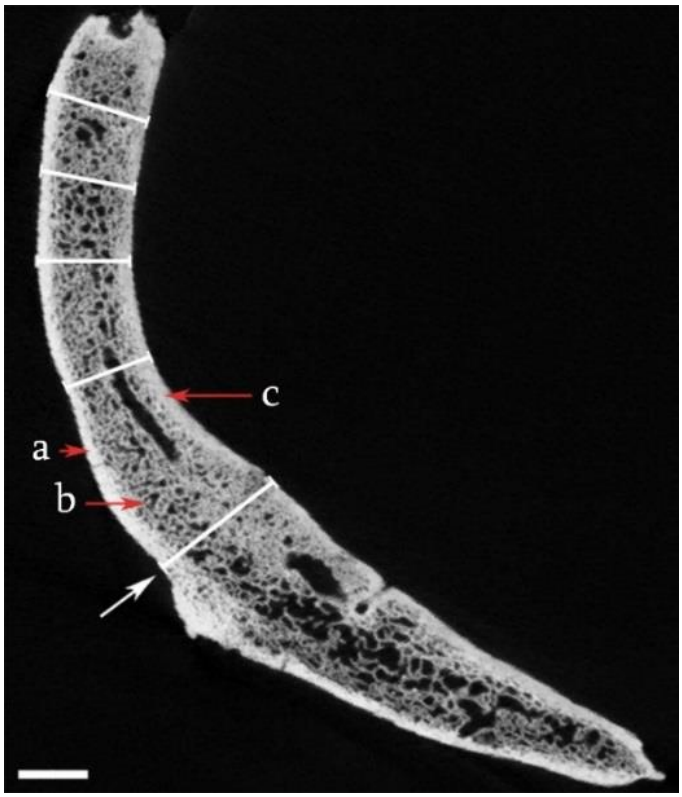

Figure 3. Internal structures of the occipital bone of Masai 12. A white arrow indicates the position of the suprainiac depression. Red arrows and associated letters indicate the internal components of the cranium. White bars represent examples of 5 measurements of the internal components (not equidistant). a: external table; b: diploic layer; c: internal table (scale bar = 1 cm).

3. Key Results and Discussion

3.1. Appendix I: The Kabua 1 cranium: Virtual anatomical reconstructions

This study is the first since 1966 to comprehensively evaluate the Kabua 1 cranium. It tentatively confirms the hypothesis set out for this study, in which it was stated that Kabua 1 can be considered anatomically modern human, consistent with previous suggestions (Bräuer, 1978; Rightmire, 1975; Schepartz, 1987). Kabua 1 exhibits relatively gracile features, such as minimally expressed supraorbital tori, superior nuchal lines that extend laterally along the entire occipital bone, and no indication of a retromolar gap. All virtual reconstructions of the Kabua 1 cranium presented a fairly globular form—a proposed hallmark trait of anatomically modern *H. sapiens* (Gunz et al., 2012; Neubauer et al., 2018; Pearson, 2008). The reconstructions were at their widest in the mid-parietal region, and did not present a posterior extension of the occipital squama—a feature that is present on the Broken Hill cranium. Moreover, the Kabua 1 fragments did not exhibit the same robusticity as the Skhūl V cranium but were rather gracile and more comparable to the Masai 03 and Masai 10 individuals. In addition, some of the cranial traits present in Kabua 1 (nuchal crest, mastoid process, supraorbital margin, and glabella) were found to be minimally expressed. This might signify that Kabua 1 was female, rather than male, as suggested by Schepartz (1987). However, the lack of other skeletal elements that can contribute to the estimation of sex, such as the pelvis, precludes a definitive assessment.

In light of the first research question set out for this dissertation, a fully anatomically modern *H. sapiens* designation would be in line with the current results. This stands in contrast with the plesiomorphic affinities proposed for the Kabua 1 cranium upon its first examination (Whitworth, 1960, 1966). The designation of Kabua 1 as recent *H. sapiens* is supported by the fact that the recent *H. sapiens* reference crania helped establish virtual reconstructions of Kabua 1 that have the most anatomical cohesion, which is confirmed with surface distance maps. In these reconstructions, the fragments of Kabua 1 align well with the frontal bone, the anterior portion of the parietals, and the superior portion of the occipital bone. The posterior protrusion of the occipital bone overlaps the most with its

reference in the reconstruction based on a recent African specimen from Tanzania, Masai 03 (Kohl-Larsen, 1941). However, while a recent *H. sapiens* designation is most parsimonious based on the current material, this is only assessed through a qualitative investigation of the newly created reconstructions. This hypothesis is further tested by evaluating the virtual reconstructions in a combined qualitative and quantitative framework (**Appendix II**), in line with the first and third objectives of this dissertation. This combined framework includes the analysis of overall neurocranial shape in order to test the *H. sapiens* taxonomic attribution put forward here and to assess the robusticity and repeatability of the virtual reconstructions.

Finally, due to the incompleteness of the diagnostically most important areas, as well as the pronounced taphonomic distortion present in some of the fragments, the separate sections of Kabua 1 could be spatially manipulated with several degrees of freedom and still resulted in acceptable anatomical configurations. Thus, this study has confirmed that the reference-based approach is useful in limiting the spatial distribution of the fragments with respect to each other. Although it was not considered how size and allometric effects on cranial shape in the reference crania might influence the Kabua 1 reconstructions (Freidline et al., 2012; Mitteroecker et al., 2004, 2013), the results presented here stress the need to employ a widely diverging range of reference crania and several reconstructions in order to critically evaluate fragmented material. This approach provides a more unbiased view during the reconstruction procedure, and allows for more research possibilities, instead of treating a certain reconstruction as the "true" form. This study also reaffirms the effectiveness of using virtual anthropological methods to securely separate fragments from surrounding sediment and laboratory adhesives, and adjust the positions of fragments which have previously been fixed together during manual reconstruction (Weber, 2015; Zollikofer & Ponce de León, 2005). Moreover, the results exemplify the value in revisiting materials of inadequately studied sites from eastern Africa. These carefully curated specimens should not be forgotten about in favor of more high profile research areas and excavations, since they can still contribute to current discussions in human evolution.

3.2. Appendix II: A geometric morphometric analysis of the Kabua 1 cranium

Having established a new set of virtual reconstructions, the next logical step is to validate these by using quantitative geometric morphometric analyses. To this end, a set of coordinates consisting of both fixed and curve semi-landmarks is used to capture overall neurocranial shape. The comparative data are obtained from earlier studies (Harvati et al., 2011; Reyes-Centeno et al., 2014a) and consist of Neanderthals, "archaic" or early *H. sapiens* from Eurasia and Africa, as well as a large amount of recent *H. sapiens* from eastern and southern Africa.

The GM analyses confirm that there is an overall consistency in the Kabua 1 reconstructions as they show both relatively small Procrustes distances to each other; all reconstructions have another reconstruction as their closest neighbor. Additionally, none of the reconstructions are located particularly close to their respective reference crania in shape space, showing that the virtual reconstructions described in **Appendix I** are not entirely driven by their respective reference crania and lead to comparable results. The Principal Component Analysis (PCA) separates the *a priori* defined groups to a high degree, consistent with previous work (Athreya, 2009; Harvati & Weaver, 2006a; Hubbe et al., 2009). Most plesiomorphic hominins (Middle Pleistocene European and Neanderthals) are represented by a antero-posteriorly elongated neurocranial vault. On the other hand, recent *H. sapiens* are characterized by rounded, antero-posteriorly short vaults, with a higher degree of globularity, which is especially pronounced high on the parietal bones and in the cerebellar area. On the axes that explain the most variance in the sample, Middle Pleistocene African specimens (Broken Hill, Irhoud, and Saldanha) fall between the Neanderthals and Late Pleistocene/recent *H. sapiens* groups, although there is a slight amount of overlap with the latter. The Kabua 1 reconstructions all consistently fall within the convex hull of recent *H. sapiens*, although there is quite some inter-reconstruction variation. The reconstruction based on Ngaloba LH18 is close to the Middle Pleistocene African group, while the reconstruction based on Skhūl V plots close to the extreme end of the *H. sapiens* group.

Contrary to the results from the PCA, the Linear Discriminant Analysis (LDA) classifies all reconstructions as Middle Pleistocene African (average posterior probability *H. sapiens* = 0.136), with the exception of the reconstruction based on Skhūl V, which is classified as *H. sapiens* (posterior probability MPA = 0.002). However, these results need to be treated with caution, as the fossil groups are quite small (three and four individuals for the Middle Pleistocene European and African groups respectively). Moreover, the data used in the LDA are not normally distributed, even though this specific analysis is sensitive to non-normal data and outliers (e.g. Hefner et al., 2014). Additionally, LDA and related discriminant function techniques have been known to maximize variance between groups, even attaining a separation between "groups" in randomly generated data that have no real biological separation, reducing their reliability for geometric morphometric analyses (Mitteroecker & Bookstein, 2011).

The machine learning models (*k*-Nearest Neighbors and Random Forests) predominantly result in the Kabua 1 reconstructions classifying as recent *H. sapiens*. These results are consistent with the PCA ordination analyses and Procrustes distances and are likely more secure than the LDA as they do not rely on the same statistical assumptions. However, in all *k*-NN and Random Forest analyses, the Kabua 1 reconstructions have high posterior probabilities for the group containing Middle Pleistocene hominins from Africa, signifying that the results are not entirely conclusive. Moreover, a limitation common among machine learning methods is the fact that they are influenced by the composition of the training dataset, which can be quite small for fossil groups due to the paucity of the fossil record and availability of CT/3D scan data. While certain techniques exist to artificially oversample small groups in order to better train ML models (e.g. Chawla et al., 2002), these methods do not reflect the morphological variation present in real fossil specimens, and the reliability of these methods for GM data remains to be tested.

Returning to the research question on the taxonomic affiliation of Kabua 1, it is shown that this specimen presents a neurocranial morphology that is reminiscent of recent *H. sapiens* with retention of some ancestral traits, such as the superiorly positioned posterior canal in

norma lateralis in the inner ear, a relatively low frontal bone, and a very narrow occipital bone in posterior view. Nonetheless, both the anatomical reconstructions in **Appendix I** and the subsequent multivariate analyses summarized here suggest affinity with recent Africans and Late Pleistocene modern humans, even though the reconstructions exhibit some characteristics by which their neurocranial shape fall close to the margin of the known range of phenotypic variation present in the Late Pleistocene African fossil record. As such, the Kabua cranium possibly highlights the broad phenotypic diversity, deep population structure, and a complicated transition to anatomical modernity present in Late Pleistocene Africa (e.g. Crevecoeur et al., 2009; Durvasula & Sankararaman, 2019; Excoffier, 2002; Fagundes et al., 2007; Lorente-Galdos et al., 2019; Marth et al., 2003; Schlebusch et al., 2017). However, while a late Pleistocene-Holocene age was put forward as most likely for this material, the lack of a robust archaeological and geochronological context prevents effective discussion on the Kabua 1 cranium in the context of this Late Pleistocene anatomical variation.

3.3. Appendix III: A virtual assessment of the proposed suprainiac fossa on the early modern European calvaria from Cioclovina, Romania

This study is the first to explore the internal structure of the occipital bone of a Late Pleistocene European *H. sapiens* specimen, namely Cioclovina. This specimen was selected as a case study to test whether qualitative and morphometric analyses of the internal morphology of the suprainiac region can assist in assessing the suprainiac depression as a phenotypic marker for interbreeding between Neanderthals and *H. sapiens*. While this case study might be somewhat spatiotemporally removed from the other specimens discussed in this dissertation, the interbreeding hypothesis simply cannot be tested by means of fossil or modern African individuals, as they possess the lowest amounts of Neanderthal introgressed genetic material when compared to Upper Paleolithic and modern Eurasian specimens (e.g. Fu et al., 2016; Sankararaman et al., 2014).

By using a combined qualitative and quantitative framework, it is found that the suprainiac morphology of the Cioclovina calvaria shares no morphological traits with the Neanderthal

condition (as suggested by e.g. Bräuer, 2013; Harvati et al., 2007). Externally, the medial thickening of the Cioclovina nuchal torus does not match the strongly expressed, often bilaterally protruding, Neanderthal occipital torus (Arsuaga et al., 2014; Balzeau & Rougier, 2010; Klein, 2009). Moreover, the Cioclovina suprainiac depression, unlike the Neanderthal suprainiac fossa, is not clearly defined and is only represented by superficial bone turnover, i.e. small dents and pits on the external surface (Harvati et al., 2007). Additionally, the absence of a true external occipital protuberance in Cioclovina, although similar to Neanderthals as argued by Soficaru et al. (2007) and Trinkaus (2007), is not uncommon among *H. sapiens* (Balzeau & Rougier, 2010; Caspari, 2005; Nowaczewska, 2011). Overall, the suprainiac morphology of Cioclovina primarily resembles the third type of suprainiac depression morphology described for *H. sapiens* by Nowaczewska (2011). This type is characterized by the absence of an external occipital protuberance, and a tall nuchal torus that is confined inferiorly by the superior nuchal lines and superiorly by a transversely, shallow, elongated depression with unclear borders (Nowaczewska, 2011), although the depression in Cioclovina is faint.

Internally, the depression on the Cioclovina calvaria is only characterized by the superficial modification of the ectocranial surface in the area above inion. This modification does not penetrate deep into the external layer of the cranium, and the Cioclovina suprainiac area is similar to most other recent modern humans with some form of depression. Moreover, the relative thickness of the diploic layer is not lower when comparing the area of the proposed depression to the rest of the occipital squama, and thus does not resemble the Neanderthal condition.

In the applied analytical framework and subsequent Principal Component Analysis, Neanderthals and *H. sapiens* groups are well separated. Variation in this sample is mostly driven by changes in the diploic layer, representing the influence of the depression on the internal structures in the Neanderthal group. The Cioclovina calvaria aligns with the recent *H. sapiens* in the studied sample. This finding is consistent with previous analyses of cranial shape and inner ear morphology of the same specimen (Harvati et al., 2007; Kranioti et al.,

2011; Uhl et al., 2016). As such, it can be tentatively concluded that both the external and internal aspects of the Cioclovina suprainiac morphology are consistent with relatively low levels of Neanderthal ancestry, as also indicated by genomic evidence (Fu et al., 2016; Posth et al., 2016). Thus, the results of the current study confirm that these quantitative methods can be used to investigate aspects of the phylogenetic importance of discrete anatomical characteristics such as the suprainiac depression. Additionally, this case study provides evidence that the suprainiac depression in this specimen is likely not the result of interbreeding of Neanderthals and *H. sapiens*. Moreover, these results caution against the use of the presence/absence and external morphology of non-metric cranial traits in isolation in order to characterize interbreeding between hominin taxa.

3.4. Appendix IV: A virtual assessment of the suprainiac depressions on the Eyasi I and ADU-VP-1/3 crania

By building on the methodologies investigated in **Appendix III**, the final study in this dissertation was designed with the aim to discuss the phylogenetic implications of the presence of suprainiac depressions in the Middle Pleistocene and Late Pleistocene African fossil record. Specifically, while the interbreeding scenario was tentatively rejected in **Appendix III**, the common ancestry and biomechanics hypotheses remain untested. As such, the objective of this study was to analyze the external and internal structures of the Eyasi I and ADU-VP-1/3 occipital bones. It was premised at the outset of this particular study that if the Eyasi I and ADU-VP-1/3 suprainiac depressions are similar to that of the Neanderthal suprainiac fossa, a re-assessment of this feature as a Neanderthal autapomorphic trait would be necessary. However, while slight similarities to the Neanderthal condition in the external suprainiac morphology of these two specimens have been suggested previously (Balzeau & Rougier, 2010; Haile-Selassie et al., 2004; Trinkaus, 2004), it is demonstrated in **Appendix IV** that the internal morphologies of these specimens are akin to those of Late Pleistocene/Holocene *H. sapiens*. In short, the internal structures of the suprainiac depressions in Eyasi I and ADU-VP-1/3 are characterized by a slight decrease in the relative thickness of the external table when compared to the rest of the occipital squama, while the diploic layer remains unaffected. This stands in contrast with

the Neanderthal condition, in which the suprainiac fossa is characterized by a decrease in the relative thickness of the diploic layer.

These results are strengthened by the fact that systematic measurements of the internal structures and subsequent Principal Component Analyses align the two specimens more closely to *H. sapiens* than to Neanderthals. Moreover, the external dimensions of the Eyasi I and ADU-VP-1/3 suprainiac depressions fall outside of the range for Neanderthal suprainiac fossae reported in the literature (Trinkaus, 2004; Verna et al., 2010). However, studies have shown that there is a strong relationship between cranial dimensions and non-metric traits on the occipital bone (e.g. Lahr, 1996). Thus, measurements of external dimensions of suprainiac depressions might not be useful in separating *H. sapiens* suprainiac depressions from Neanderthal suprainiac fossae if used in isolation. Together, these results reconcile previous interpretations of Neanderthal similarities in the suprainiac depression of Eyasi I and ADU-VP-1/3 (e.g. Trinkaus, 2004) with the more nuanced interpretations that describe a difference when considering the surrounding occipital squama that differentiates them from Neanderthals, including the variably present occipital superstructures such as the occipital torus, the superior nuchal lines, cruciform eminence, and the external occipital protuberance.

Returning to the three hypotheses proposed in the second and third research questions of this dissertation, the first hypothesis postulated *H. sapiens* suprainiac morphologies as possible phenotypic markers of Neanderthal/*H. sapiens* interbreeding. However, as was already shown in **Appendix III**, this scenario is unlikely and needs to be treated with caution, as we have a limited understanding of the influence of Neanderthal genetic material on the *H. sapiens* phenotype (Dediu & Levinson, 2018; Gunz et al., 2019). Moreover, while admixture between Neanderthals and *H. sapiens* is now well-documented for the Late Pleistocene (e.g. Green et al., 2010; Posth et al., 2016), interbreeding with other archaic hominin groups in the Middle Pleistocene (such as Denisovans; e.g. Vernot et al., 2016) could complicate our limited understanding of the influence of Neanderthal DNA

introgression, as the presence of genetic material from other lineages could also have had an effect on the *H. sapiens* phenotype.

The second hypothesis, which states that the suprainiac fossae/depressions in Neanderthals and *H. sapiens* are possibly derived from a common ancestor, remains difficult to adequately test. At this point, there is limited information on the ancestral lineage of Neanderthals and *H. sapiens*, due to the limited fossil evidence for Middle-Late Pleistocene *H. sapiens* currently in hand. Moreover, recent research suggests that that there were likely multiple *H. sapiens* lineages in Africa, which experienced high levels of population structure and morphological variability (**Appendix II**; Harvati et al., 2011; Scerri et al., 2018). The presence of suprainiac depression in some Middle Pleistocene *H. sapiens* might thus reflect morphological variation that was lost later due to this deep population structure and/or the loss of lineages that were originally present but did not contribute substantially to *H. sapiens* evolution.

The third scenario, in which convergence of Neanderthal suprainiac fossae and *H. sapiens* suprainiac depressions under a biomechanical framework is considered a primary factor, could not be investigated directly in this study, but provides a promising opportunity for future research. It should also be considered that these hypotheses are not necessarily mutually exclusive. To conclude, this study demonstrates the importance of using combined quantitative and qualitative approaches to analyze morphological characteristics that have only been studied qualitatively before. Moreover, this study confirms that, when considering the internal structure of the suprainiac depression, the presence of a superficially similar suprainiac morphology in Middle/Late Pleistocene African specimens does not negate the derived status for the Neanderthal suprainiac fossa. Finally, this study forewarns against the use of such traits in other lineages as phylogenetically informative, as their etiology is not well understood at this point in time.

4. Future Directions

Several future research avenues can be identified from these results. While **Appendix I** and **Appendix II** have described most qualitative and quantitative aspects of the Kabua cranium, the remainder of this fossil assemblage, namely Kabua 2 and 3, is as yet poorly understood. Kabua 2 consists primarily of a heavily distorted frontal bone which preserves the upper borders of the supraorbital margins, while Kabua 3 is represented by a small parietal fragment. While not quantified, it was put forward by Buck and Stringer (2015) that the cranial walls of Kabua 2 are much thinner than those of Kabua 1. It would be a valuable approach to use systematic methods such as retrodeformation (e.g. Tallman et al., 2014) and Thin Plate Spline algorithms (Amano et al., 2015; Bookstein, 1991; Weber & Bookstein, 2011) to fit the distorted Kabua 2 and Kabua 3 fragments to Kabua 1 and compare the three specimens in an equal context.

Additionally, it has to be considered that the current results on the Kabua 1 cranium exist somewhat in a vacuum. While recent literature suggests a Late Pleistocene-Holocene age range for the Kabua material (e.g. Sawchuk & Willoughby, 2015), there has yet to be a formal analysis of the archaeological and geochronological context. Direct dating of the material using U-series and ESR methods is currently in progress. A reliable geochronological placement of the Kabua 1 cranium promises better contextualization and taxonomic attribution.

Moreover, the use of machine learning methods on shape data (**Appendix II**) has proven to be quite effective in testing hypotheses and approaching classification problems in paleoanthropological samples. However, while some studies exist in which *k*-Nearest Neighbor analyses and Random Forest models are applied directly to anthropological shape data (Hefner et al., 2014; Navega et al., 2015), these methods are not prevalent in archaeological/paleoanthropological research. The study on the Kabua 1 cranium has demonstrated that these methods provide possible alternative statistical analyses in the GM workflow, especially in scenarios where more standard classification techniques such as LDA should be applied with caution due to violations of statistical assumptions. These

methods and their potential for shape data need to be explored in future paleoanthropological studies.

The fossils from the Lake Eyasi site in Tanzania, Eyasi I-III (**Appendix IV**), like Kabua 1, suffer from the lack of archaeological context and robust date. This is crucial, since there is no definitive consensus that the Eyasi I-III specimens from the West Bay of Lake Eyasi, and the EH06 frontal bone from the Northeast Bay, which has been dated to between 138 and 88 kya (Domínguez-Rodrigo et al., 2008), are penecontemporaneous. If this would be the case, this means that the Eyasi I cranium could be representative of the persistence of plesiomorphic morphological traits in the Late Pleistocene. On the other hand, if the Eyasi material dates to the Middle Pleistocene, it could instead represent an early emergence of *H. sapiens* autapomorphies. However, while the presence of plesiomorphic traits in the Eyasi I specimen, such as a low frontal bone, posteriorly elongated neurocranium, and a nuchal torus have been recognized (e.g. Bräuer, 2008; Stringer, 2016; Trinkaus, 2004), these traits were only assessed qualitatively and the taxonomic affinities of Eyasi I remain unknown (Stringer, 2000). It is thus critical that this specimen is re-evaluated and virtually reconstructed so that quantitative methods, together with a robust geochronological context, can be used to resolve its phylogenetic affiliation.

While the common ancestry scenario was preliminary rejected for the Eyasi I and ADU-VP-1/3 specimens, these two specimens both post-date the Neanderthal/*H. sapiens* divergence. As such, future testing this scenario could include an evaluation of the internal suprainiac morphology in pre-sapiens specimens which precede the Neanderthal/*H. sapiens* divergence. Although most of the currently available specimens have not been reported to possess a clearly defined suprainiac depression, there exist several African specimens (e.g., KNM-ER 3733: Leakey, 1976; OH 9: Leakey, 1971; OH 12: Leakey, 1971) which possess a laterally elongated supratoral sulcus (sensu Mirazón Lahr, 1996). Investigations of the internal morphology of these traits could help identify possible similarities with suprainiac fossae/suprainiac depressions as well as underlying hypotheses on development and phylogenetic implications.

Furthermore, while **Appendix III** and **Appendix IV** include combined analyses of the external and internal structures of the occipital bone, these results should be considered within the context of the hominin cranium as an integrated system (e.g. von Cramon-Taubadel, 2011; Lieberman et al., 2002). Specifically, the third hypothesis in **Appendix IV** might be supported by possible correlations between the presence/morphology of suprainiac depressions, flexion of the occipital plane, globularity and robusticity of the neurocranium, and associated biomechanics of the cranial musculature (Caspari, 2005; Nowaczewska, 2011). However, the location, size, and specific stress generated by the cranial musculature have only been described qualitatively in a theoretical biomechanical framework. As such, there are many unknown factors that could influence the possible correlation between the morphology of suprainiac depression and the rest of the cranium (see Gunz et al., 2019). A promising field of research are methods such as Finite Element Analysis (FEA). FEA opens up possibilities to test how bony structures react to artificially applied forces in a virtual environment. These methods could for example be applied to 3D models of crania which have some form of suprainiac depression, in order to investigate whether these specimens would have had an increased resistance to stress generated by the nuchal musculature and thus whether suprainiac depressions could have contributed to an 'optimal' cranial form.

5. Concluding Remarks

This dissertation aimed to goal of this cumulative dissertation is **to help fill existing gaps in the fossil record through the analysis of neurocranial shape and distinct morphological traits in a series of understudied fossil crania**. This goal was made approachable by dividing it into three interconnected objectives. To summarize, these objectives are concerned with: the reconstruction of curated fragmented fossil material, the investigation of specific morphological traits proposed as autapomorphic for certain lineages of the genus *Homo*, and the validation of combined qualitative and quantitative frameworks to analyze both discrete anatomical characteristics and continuous shape data. Although these objectives are somewhat separate in their individual designs, they are unified by the application of virtual anthropological methods to crania that are not often discussed in the paleoanthropological literature.

Specifically, in **Appendix I** it was shown that, through the assembly and subsequent investigation of multiple virtual anatomical reconstructions, the Kabua 1 cranium is likely representative of the extensive *H. sapiens* morphological variation present in Late Pleistocene Africa. Moreover, quantitative geometric morphometrics and machine learning algorithms were used in **Appendix II** to systematically evaluate these preliminary results with a large reference sample and place them in a broader context. Together, these studies provide a tentative answer to the first research question on the taxonomic attribution of the Kabua 1 cranium. Moreover, by bringing this individual back to discussions surrounding *H. sapiens* evolution, these studies have contributed to the realization of the dissertation's first and third objectives, emphasizing the effectiveness of combining traditional and virtual methods to study the shape of taphonomically distorted and fragmented paleoanthropological materials without subjecting them to further degradation. These methods can be applied to a wide range of specimens from diverse temporal and geographic origins to fill in the current gaps in the fossil record and contextualize recent finds.

This dissertation has also demonstrated that combined qualitative/quantitative virtual frameworks can be applied in the study of specific morphometric traits in order to help resolve long-standing debates on their phylogenetic importance. The study on the internal structures of the Cioclovina calvaria in **Appendix III** has shown that caution should be exercised in using traits such as the suprainiac depression to characterize possible interbreeding between hominin taxa, even though more research on possible 'hybrid' specimens is necessary. Furthermore, this study attests the effectiveness of the applied virtual framework and thus contributes to the second objective of this dissertation. This is also the first study in which CT scans are used in order to investigate the structural elements of the occipital bone of an Upper Paleolithic European specimen. However, before the effect of interbreeding on the morphology of the suprainiac depression and possibly other anatomical traits is completely rejected, other Middle and Late Pleistocene Eurasian specimens, should be investigated in similar fashion, as the phenotypes of these specimens have been argued to be representative of high levels of archaic genetic introgressed material. Moreover, these quantitative methods can not only be used to estimate the admixture between taxa but also other hypotheses proposed for the etiology of the suprainiac depression, including common ancestry and convergence. This was partly demonstrated in the study on the Eyasi I and ADU-VP-1/3 crania in **Appendix IV**, which reconciles previous interpretations of possible Neanderthal characteristics in the suprainiac depressions of Eyasi I and ADU-VP-1/3 with quantitative data that support affinity with the suprainiac region of anatomically modern *H. sapiens*. Even though the associated research question on common ancestry could not be adequately answered due to the lack of penecontemporaneous comparative data, it was shown that the applied quantitative methods hold much promise for future investigations of the suprainiac depression and possibly other discrete anatomical traits, thus contributing to the second and third objectives of this dissertation. This study additionally stresses that this trait should not only be investigated in terms of their presence/absence but rather incorporated in larger syntheses on the hominin cranium as an integrated system with a phenotype that is influenced by both genetic and epigenetic factors.

To conclude, the studies presented here contribute valuable information about *H. sapiens* evolution in the Middle to Late Pleistocene periods. By applying quantitative virtual anthropological methods and systematic qualitative analyses, this dissertation sheds new light on some of the inadequately studied fossils of the late Middle and Late Pleistocene. While neurocranial shape and specific anatomical traits such as the suprainiac depressions have shown to broadly separate fossil material and recent *H. sapiens*, the studies forming this dissertation ultimately exemplify the extent and complexity of phenotypic variability of the late Middle and Late Pleistocene fossil record. These approaches hold much promise for future investigations of both curated and newly discovered materials. Moreover, specimens from previously neglected areas such as parts of eastern Africa can be analyzed extensively with virtual methods and discussed in regional and global contexts. These efforts therefore aid in bridging the gaps between fossil material from marginalized sites and wider discussions on human evolution and subsequent dispersals from Africa. While some of the discussions on the nature of anatomical modernity as well as the timing of the emergence of modern anatomical traits (e.g. punctuated versus mosaic) are yet to be resolved, this dissertation provides encouraging insights that will, once incorporated into the paleoanthropological literature, contribute to a better understanding of these processes. Finally, the digital data described here, as well as in other studies where virtual methods are applied, should be made freely available to allow for more inclusive discussions in paleoanthropology. As such, this dissertation has affirmed that virtual anthropology, in combination with suitable and comprehensive analytical frameworks, has the ability to provide new perspectives and opportunities for the research of our shared past.

6. References

Abel, R. L., Laurini, C. R., & Richter, M. (2012). A palaeobiologist's guide to 'virtual' micro-CT preparation. *Palaeontologia Electronica, 15*(2), 1-16.

Adams, D. C., Rohlf, F. J., & Slice, D. E. (2004). Geometric morphometrics: ten years of progress following the 'revolution'. *Hystrix: The Italian Journal of Zoology, 71*(1), 5-16.

Adams, D. C., Collyer, M. L., & Kaliontzopoulou, A. (2019). *Geomorph: Software for geometric morphometric analyses*. R package version 3.1.0. https://cran.rproject.org/package=geomorph.

Amano, H., Kikuchi, T., Morita, Y., Kondo, O., Suzuki, H., Ponce de León, M. S., . . . Ogihara, N. (2015). Virtual reconstruction of the Neanderthal Amud 1 cranium. *American Journal of Physical Anthropology, 158*(2), 185-197.

Ambrose, J. (1973). Computerized transverse axial scanning (tomography): Part 2. Clinical application. *British Journal of Radiology*, *46,* 1023-1047.

Ambrose, S. H. (1980). *Elmenteitan and other Late Pastoral Neolithic adaptations in the central highlands of East Africa.* Paper presented at the Proceedings of the 8th Panafrican Congress of Prehistory and Quaternary Studies, 1977, Nairobi.

Arsuaga, J. L., Martínez, I., Arnold, L. J., Aranburu, A., Gracia-Téllez, A., Sharp, W. D., . . . Carbonell, E. (2014). Neandertal roots: Cranial and chronological evidence from Sima de los Huesos. *Science, 344*(6190), 1358-1363.

Athreya, S. (2009). A comparative study of frontal bone morphology among Pleistocene hominin fossil groups. *Journal of Human Evolution, 57*(6), 786-804.

Bae, C. J., Douka, K., & Petraglia, M. D. (2017). On the origin of modern humans: Asian perspectives. *Science, 358*(6368), eaai9067.

Balzeau, A., Crevecoeur, I., Rougier, H., Froment, A., Gilissen, E., Grimaud-Hervé, D., . . . Semal, P. (2010). Applications of imaging methodologies to paleoanthropology: Beneficial results relating to the preservation, management and development of collections. *Comptes Rendus Palevol, 9*(6), 265-275.

Balzeau, A., & Rougier, H. (2010). Is the suprainiac fossa a Neandertal autapomorphy? A complementary external and internal investigation. *Journal of Human Evolution, 58*(1), 1-22.

Balzeau, A., & Rougier, H. (2013). New information on the modifications of the Neandertal suprainiac fossa during growth and development and on its etiology. *American Journal of Physical Anthropology, 151*(1), 38-48.

Bons, P. D., Bauer, C. C., Bocherens, H., de Riese, T., Drucker, D. G., Francken, M., . . . Wißing, C. (2019). Out of Africa by spontaneous migration waves. *PloS One, 14*(4), e0201998.

Bookstein, F. L. (1991). *Morphometric tools for landmark data geometry and biology*. Australia: Cambridge University Press.

Bookstein, F., Slice, D., Gunz, P., & Mitteroecker, P. (2004). Anthropology takes control of morphometrics. *Collegium Antropologicum 28*(2), 121-132.

Bouchneb, L., & Crevecoeur, I. (2009). The inner ear of Nazlet Khater 2 (Upper Paleolithic, Egypt). *Journal of Human Evolution, 56*(3), 257-262.

Bräuer, G. (1978). The morphological differentiation of anatomically modern man in Africa, with special regard to recent finds from East Africa. *Zeitschrift für Morphologie und Anthropologie, 69*(3), 266-292.

Bräuer, G. (2008). The origin of modern anatomy: By speciation or intraspecific evolution? *Evolutionary Anthropology: Issues, News, and Reviews, 17*(1), 22-37.

Bräuer, G. (2013). Origin of Modern Humans. In W. Henke & I. Tattersall (Eds.), *Handbook of Paleoanthropology* (pp. 1749-1779). Heidelberg: Springer.

Breiman, L. (2001). Random Forests. *Machine Learning, 45*(1), 5-32.

Buck, L. T., & Stringer, C. B. (2015). A rich locality in South Kensington: the fossil hominin collection of the Natural History Museum, London. *Geological Journal, 50*(3), 321-337.

Campbell, M. C., & Tishkoff, S. A. (2010). The Evolution of Human Genetic and Phenotypic Variation in Africa. *Current Biology, 20*(4), 166-173.

Campbell, M. C., Hirbo, J. B., Townsend, J. P., & Tishkoff, S. A. (2014). The peopling of the African continent and the diaspora into the new world. *Current Opinion in Genetics and Development, 29*, 120-132.

Caspari, R. (2005). The suprainiac fossa: the question of homology. *Anthropologie (Brno), 43*(2-3), 229-39.

Caspari, R., & Wolpoff, M. (2013). The Process of Modern Human Origins: The Evolutionary and Demographic Changes Giving Rise to Modern Humans. In F. H. Smith & J. C. M. Ahern (Eds.), *The origins of modern humans: Biology reconsidered* (pp. 355-391). Hoboken: Wiley.

Chang, W. (2014). extrafont: Tools for using fonts. Retrieved from https://CRAN.R-project.org/package=extrafont.

Chawla, N. V., Bowyer, K. W., Hall, L. O., & Kegelmeyer, W. P. (2002). SMOTE: Synthetic Minority Over-sampling Technique. *Journal of Artificial Intelligence Research, 16,* 321-357.

Collard, M., & Wood, B. A. (2015). Defining the Genus *Homo*. In W. Henke & I. Tattersall (Eds.), *Handbook of Paleoanthropology* (pp. 2107-2144). Heidelberg: Springer.

Cook, R. D., & Weisberg, S. (1982). Residuals and Influence in Regression. New York: Chapman and Hall.

von Cramon-Taubadel, N. (2011). The relative efficacy of functional and developmental cranial modules for reconstructing global human population history. *American Journal of Physical Anthropology, 146*(1), 83-93.

Crevecoeur, I., Rougier, H., Grine, F., & Froment, A. (2009). Modern human cranial diversity in the Late Pleistocene of Africa and Eurasia: Evidence from Nazlet Khater, Peştera cu Oase, and Hofmeyr. *American Journal of Physical Anthropology, 140*(2), 347-358.

Darroch J.N. & Mosimann J.E. (1985). Canonical and principal components of shape. *Biometrika, 72*(2), 241-252.

Day, M. H. (1969). Early *Homo sapiens* Remains from the Omo River Region of South-west Ethiopia: Omo Human Skeletal Remains. *Nature, 222*(5199), 1135-1138.

Day, M. H., & Stringer, C. B. (1982). A reconsideration of the Omo Kibish remains and the *erectus-sapiens* transition. In M. A. de Lumley (Ed.). Homo erectus *et la place de l'Homme de Tautavel parmi les hominidés fossiles. Première congrès international de paléontologie humaine* (pp. 814–846). UNESCO: Colloque International du Centre National de la Récherche Scientifique.

Dediu, D., & Levinson, S. C. (2018). Neanderthal language revisited: not only us. *Current Opinion in Behavioral Sciences, 21*, 49-55.

Di Vincenzo, F., Profico, A., Bernardini, F., Cerroni, V., Dreossi, D., Schlager, S., . . . Manzi, G. (2017). Digital reconstruction of the Ceprano calvarium (Italy), and implications for its interpretation. *Scientific Reports, 7*(13974).

Domínguez-Rodrigo, M., Mabulla, A., Luque, L., Thompson, J. W., Rink, J., Bushozi, P., . . . Alcala, L. (2008). A new archaic *Homo sapiens* fossil from Lake Eyasi, Tanzania. *Journal of Human Evolution, 54*(6), 899-903.

Dryden, I. L. (2018). shapes: Statistical shape analysis. R package version 1.2.4.

Dryden, I. L., & Mardia, K. V. (1998). *Statistical shape analysis*. New York: John Wiley & Sons.

Durvasula, A., & Sankararaman, S. (2019). Recovering signals of ghost archaic introgression in African populations. *bioRxiv*, 285734.

Endicott, P., Ho, S. Y. W., & Stringer, C. B. (2010). Using genetic evidence to evaluate four palaeoanthropological hypotheses for the timing of Neanderthal and modern human origins. *Journal of Human Evolution, 59*(1), 87-95.

Eriksson, A., & Manica, A. (2012). Effect of ancient population structure on the degree of polymorphism shared between modern human populations and ancient hominins. *Proceedings of the National Academy of Sciences, 109*(35), 13956-13960.

Excoffier, L. (2002). Human demographic history: refining the recent African origin model. *Current Opinion in Genetics and Development, 12*(6), 675-682.

Fagundes, N. J., Ray, N., Beaumont, M., Neuenschwander, S., Salzano, F. M., Bonatto, S. L., & Excoffier, L. (2007). Statistical evaluation of alternative models of human evolution. *Proceedings of the National Academy of Sciences, 104*(45), 17614-17619.

Feldesman, M.R., 2002. Classification trees as an alternative to linear discriminant analysis. *American Journal of Physical Anthropology, 119*, 257-275.

Finnerty, J. R., Pang, K., Burton, P., Paulson, D., & Martindale, M. Q. (2004). Origins of Bilateral Symmetry: Hox and Dpp Expression in a Sea Anemone. *Science, 304*(5675), 1335.

Fligner, M. A., & Killeen, T. J. (1976). Distribution-Free Two-Sample Tests for Scale. *Journal of the American Statistical Association, 71*(353), 210-213.

Forster, P. (2004). Ice Ages and the mitochondrial DNA chronology of human dispersals: a review. *Philosophical Transactions of the Royal Society of London. Series B: Biological Sciences, 359*(1442), 255-264.

Frayer, D. W. (1992). The persistence of Neanderthal features in post-Neanderthal Europeans. In G. Bräuer & F. H. Smith (Eds.), *Continuity or Replacement: Controversies in Homo sapiens Evolution* (pp. 179-88). Rotterdam: Balkema.

Fu, Q., Hajdinjak, M., Moldovan, O. T., Constantin, S., Mallick, S., Skoglund, P., … Pääbo, S. (2015). An early modern human from Romania with a recent Neanderthal ancestor. *Nature, 524*, 216-219.

Galway-Witham, J., Cole, J., & Stringer, C. (2019). Aspects of human physical and behavioural evolution during the last 1 million years. *Journal of Quaternary Science, 34*(6), 355-378.

Gower J. (1975). Generalized procrustes analysis. Psychometrika 40(1):33-51.

Green, R. E., Krause, J., Briggs, A. W., Maricic, T., Stenzel, U., Kircher, M., . . . Pääbo, S. (2010). A Draft Sequence of the Neandertal Genome. *Science, 328*(5979), 710-722.

Grine, F. E. (2016). The Late Quaternary Hominins of Africa: The Skeletal Evidence from MIS 6-2. In S. C. Jones & B. A. Stewart (Eds.), *Africa from MIS 6-2: Population Dynamics and Paleoenvironments* (pp. 323-381). Dordrecht: Springer Netherlands.

Grine, F. E., Gunz, P., Betti-Nash, L., Neubauer, S., & Morris, A. G. (2010). Reconstruction of the late Pleistocene human skull from Hofmeyr, South Africa. *Journal of Human Evolution, 59*(1), 1-15.

Gronau, I., Hubisz, M. J., Gulko, B., Danko, C. G., & Siepel, A. (2011). Bayesian inference of ancient human demography from individual genome sequences. *Nature Genetics, 43*, 1031-1034.

Groucutt, H. S., Petraglia, M. D., Bailey, G., Scerri, E. M. L., Parton, A., Clark-Balzan, L., . . . Scally, A. (2015). Rethinking the dispersal of Homo sapiens out of Africa. *Evolutionary Anthropology: Issues, News, and Reviews, 24*(4), 149-164.

Grün, R., Stringer, C. B., McDermott, F., Nathan, R., Porat, N., Robertson, S., . . . McCulloch, M. (2005). U-series and ESR analyses of bones and teeth relating to the human burials from Skhul. *Journal of Human Evolution, 49*(3), 316-334.

Gunz, P., Bookstein, F. L., Mitteroecker, P., Stadlmayr, A., Seidler, H., & Weber, G. W. (2009a). Early modern human diversity suggests subdivided population structure and a complex out-of-Africa scenario. *Proceedings of the National Academy of Sciences, 106*(15), 6094-6098.

Gunz, P., Mitteroecker, P., Neubauer, S., Weber, G. W., & Bookstein, F. L. (2009b). Principles for the virtual reconstruction of hominin crania. *Journal of Human Evolution, 57*(1), 48-62.

Gunz, P., Tilot, A. K., Wittfeld, K., Teumer, A., Shapland, C. Y., van Erp, T. G. M., . . . Fisher, S. E. (2019). Neandertal Introgression Sheds Light on Modern Human Endocranial Globularity. *Current Biology, 29*(1), 120-127.e125.

Haile-Selassie, Y., Asfaw, B., & White, T. D. (2004). Hominid cranial remains from upper pleistocene deposits at Aduma, Middle Awash, Ethiopia. *American Journal of Physical Anthropology, 123*(1), 1-10.

Hammer, M. F., Woerner, A. E., Mendez, F. L., Watkins, J. C., & Wall, J. D. (2011). Genetic evidence for archaic admixture in Africa. *Proceedings of the National Academy of Sciences, 108*(37), 15123-15128.

Harvati, K. (2003). The Neanderthal taxonomic position: models of intra-and inter-specific craniofacial variation. *Journal of Human Evolution, 44*(1), 107-132.

Harvati, K. (2015). Neanderthals and their contemporaries. In W. Henke & I. Tattersall (Eds.), *Handbook of Paleoanthropology* (pp. 2243-2279). Heidelberg: Springer.

Harvati, K., & Weaver, T. D. (2006a). Human cranial anatomy and the differential preservation of population history and climate signatures. *The Anatomical Record Part A: Discoveries in Molecular, Cellular, and Evolutionary Biology, 288*(12), 1225-1233.

Harvati, K., & Roksandic, M. (2016). The Human Fossil Record from Romania: Early Upper Paleolithic European Mandibles and Neanderthal Admixture. In K. Harvati & M. Roksandic (Eds.), *Paleoanthropology of the Balkans and Anatolia: Human Evolution and its Context* (pp. 51-68). Dordrecht: Springer Netherlands.

Harvati, K., Gunz, P., & Grigorescu, D. (2007). Cioclovina (Romania): affinities of an early modern European. *Journal of Human Evolution, 53*(6), 732-46.

Harvati, K., Hublin, J.-J., & Gunz, P. (2010). Evolution of middle-late Pleistocene human cranio-facial form: A 3-D approach. *Journal of Human Evolution, 59*(5), 445-464.

Harvati, K., Stringer, C. B., Grün, R., Aubert, M., Allsworth-Jones, P., & Folorunso, C. A. (2011). The Later Stone Age Calvaria from Iwo Eleru, Nigeria: Morphology and Chronology. *PloS One, 6*(9), e24024.

Harvati, K., Röding, C., Bosman, A. M., Karakostis, F. A., Grün, R., Stringer, C. B., . . . Kouloukoussa, M. (2019). Apidima Cave fossils provide earliest evidence of Homo sapiens in Eurasia. *Nature, 571*, 500-504.

Hefner, J. T., Spradley, M. K., & Anderson, B. (2014). Ancestry Assessment Using Random Forest Modeling. *Journal of Forensic Sciences, 59*(3), 583-589.

Henn, B. M., Steele, T. E., & Weaver, T. D. (2018). Clarifying distinct models of modern human origins in Africa. *Current Opinion in Genetics and Development, 53*, 148-156.

Hershkovitz, I., Marder, O., Ayalon, A., Bar-Matthews, M., Yasur, G., Boaretto, E., . . . Barzilai, O. (2015). Levantine cranium from Manot Cave (Israel) foreshadows the first European modern humans. *Nature, 520*(7546), 216-9.

Hershkovitz, I., Latimer, B., Barzilai, O., & Marder, O. (2017). Manot 1 calvaria and recent modern human evolution: an anthropological perspective. *Bulletins et Mémoires de la Société d'Anthropologie de Paris, 29*(3), 119-130.

Hershkovitz, I., Weber, G. W., Quam, R., Duval, M., Grün, R., Kinsley, L., . . . Weinstein-Evron, M. (2018). The earliest modern humans outside Africa. *Science, 359*(6374), 456-459.

Hounsfield, G. N. 1973. Computerized transverse axial scanning (tomography): Part I. Description of system. British Journal of Radiology, 46: 1016-1022.

Howell, F. C. (1999). Paleo-Demes, Species Clades, and Extinctions in the Pleistocene Hominin Record. *Journal of Anthropological Research, 55*(2), 191-243.

Howells, W.W., 1973. Cranial variation in man: A study by multivariate analysis of patterns of difference among recent human populations., Papers of the Peabody Museum of Archaeology and Ethnology. Harvard University, Cambridge.

Hubbe, M., Hanihara, T., & Harvati, K. (2009). Climate Signatures in the Morphological Differentiation of Worldwide Modern Human Populations. *The Anatomical Record: Advances in Integrative Anatomy and Evolutionary Biology, 292*(11), 1720-1733.

Hubbe, M., Neves, W. A., Harvati, K. (2010). Testing Evolutionary and Dispersion Scenarios for the Settlement of the New World. PLOS One 5 (6), 1 – 9.

Hublin, J.-J. (1978). Quelques caractères apomorphes du crâne néandertalien et leur interprétation phylogénique. *Comptes rendus de l'Académie des sciences. Série III, Sciences de la vie., D287*, 923-926.

Hublin, J.-J., Ben-Ncer, A., Bailey, S. E., Freidline, S. E., Neubauer, S., Skinner, M. M., . . . Gunz, P. (2017). New fossils from Jebel Irhoud, Morocco and the pan-African origin of Homo sapiens. *Nature, 546*(7657), 289-292.

Immersion Corp. (1998). *Microscribe 3D User's Guide*. Immersion Corporation, San Jose, CA.

Jacobs, G. S., Hudjashov, G., Saag, L., Kusuma, P., Darusallam, C. C., Lawson, D. J., . . . Cox, M. P. (2019). Multiple Deeply Divergent Denisovan Ancestries in Papuans. *Cell, 177*(4), 1010-1021.

Jungers, W. L., & Minns, R. J. (1979). Computed tomography and biomechanical analysis of fossil long bones. *American Journal of Physical Anthropology, 50*(2), 285-290.

Kaiser, H. F. (1970). A second generation little jiffy. *Psychometrika, 35*(4), 401-415.

Kaiser, H. F., & Rice, J. (1974). Little Jiffy, Mark IV. *Educational and Psychological Measurement, 34*(1), 111-117.

Klein, R. G. (2009). *The Human Career: Human Biological and Cultural Origins*. Chicago: University of Chicago Press.

Kohl-Larsen, L. (1941). Meine Expedition in Deutsch-Ostafrika (1934–1936 und 1937–1939). *Zeitschrift der Gesellschaft für Erdkunde, 1-4*, 126-144.

Korkmaz, S., Goksuluk, D., & Zararsiz, G. (2014). MVN: An R Package for Assessing Multivariate Normality. *The R Journal, 6*(2), 151-162.

Kramer, A., Crummett, T. L., & Wolpoff, M. H. (2001). Out of Africa and into the Levant: replacement or admixture in Western Asia? *Quaternary International, 75*(1), 51-63.

Kranioti, E. F., Holloway, R., Senck, S., Ciprut, T., Grigorescu, D., & Harvati, K. (2011). Virtual Assessment of the Endocranial Morphology of the Early Modern European Fossil Calvaria From Cioclovina, Romania. *The Anatomical Record: Advances in Integrative Anatomy and Evolutionary Biology, 294*(7), 1083-1092.

Kuhn, M. (2008). Caret package. *Journal of Statistical Software,* 28(5).

Lacruz, R. S., Stringer, C. B., Kimbel, W. H., Wood, B., Harvati, K., O'Higgins, P., . . . Arsuaga, J.-L. (2019). The evolutionary history of the human face. *Nature Ecology & Evolution*, *3*, 726-736.

Lahr, M. M. (1994). The Multiregional Model of modern human origins: a reassessment of its morphological basis. *Journal of Human Evolution, 26*(1), 23-56.

Lahr, M. M. (1996). *The evolution of modern human diversity: a study of cranial variation* (Vol. 18): Cambridge University Press.

Lahr, M. M., & Foley, R. (1994). Multiple dispersals and modern human origins. *Evolutionary Anthropology: Issues, News, and Reviews, 3*(2), 48-60.

Le Cabec, A., & Toussaint, M. (2017). Impacts of curatorial and research practices on the preservation of fossil hominid remains. *Journal of Anthropological Science, 95*, 7-34.

Li, Z.-Y., Wu, X.-J., Zhou, L.-P., Liu, W., Gao, X., Nian, X.-M., & Trinkaus, E. (2017). Late Pleistocene archaic human crania from Xuchang, China. *Science, 355*(6328), 969-972.

Lieberman, D. E., McBratney, B. M., & Krovitz, G. (2002). The evolution and development of cranial form in *Homo sapiens*. *Proceedings of the National Academy of Sciences, 99*(3), 1134-1139.

Lorente-Galdos, B., Lao, O., Serra-Vidal, G., Santpere, G., Kuderna, L. F. K., Arauna, L. R., . . . Comas, D. (2019). Whole-genome sequence analysis of a Pan African set of samples reveals archaic gene flow from an extinct basal population of modern humans into sub-Saharan populations. *Genome Biology, 20*(77), 1-15.

Mahalanobis, P.C. (1930). A statistical study of certain anthropometric measurements from Sweden. *Biometrika, 22*(1/2), 94-108.

Mahalanobis, P.C. (1936). *On the generalized distance in statistics*. Proceedings of the national institute of sciences of India: New Delhi, 49-55.

Mardia, K. V. (1970). Measures of Multivariate Skewness and Kurtosis with Applications. *Biometrika, 57*(3), 519-530.

Mardia, K. V., Bookstein, F. L., & Moreton, I. J. (2000). Statistical Assessment of Bilateral Symmetry of Shapes. *Biometrika, 87*(2), 285-300.

Marth, G., Schuler, G., Yeh, R., Davenport, R., Agarwala, R., Church, D., . . . Kholodov, M. (2003). Sequence variations in the public human genome data reflect a bottlenecked population history. *Proceedings of the National Academy of Sciences, 100*(1), 376-381.

Mirazón Lahr, M. (2016). The shaping of human diversity: filters, boundaries and transitions. *Philosophical Transactions of the Royal Society of London. Series B: Biological Sciences, 371*(1698).

Mirazón Lahr, M., & Foley, R. A. (2016). Human Evolution in Late Quaternary Eastern Africa. In S. C. Jones & B. A. Stewart (Eds.), *Africa from MIS 6-2: Population Dynamics and Paleoenvironments* (pp. 215-231). Dordrecht: Springer Netherlands.

Mitteroecker, P., & Gunz, P. (2009). Advances in Geometric Morphometrics. *Evolutionary Biology, 36*(2), 235-247.

Mitteroecker, P., Gunz, P., Windhager, S., & Schaefer, K. (2013). A brief review of shape, form, and allometry in geometric morphometrics, with applications to human facial morphology. *Hystrix: The Italian Journal of Mammalogy, 24*(1), 8.

Mounier, A., & Mirazón Lahr, M. (2016). Virtual ancestor reconstruction: Revealing the ancestor of modern humans and Neandertals. *Journal of Human Evolution, 91*, 57-72.

Mounier, A., & Mirazón Lahr, M. (2019). Deciphering African late middle Pleistocene hominin diversity and the origin of our species. *Nature Communications, 10*(1), 3406.

Navega, D., Coelho, C., Vicente, R., Ferreira, M. T., Wasterlain, S., & Cunha, E. (2015). AncesTrees: ancestry estimation with randomized decision trees. *International Journal of Legal Medicine, 129*(5), 1145-1153.

Neubauer, S., Gunz, P., Leakey, L., Leakey, M., Hublin, J.-J., & Spoor, F. (2018). Reconstruction, endocranial form and taxonomic affinity of the early *Homo* calvaria KNM-ER 42700. *Journal of Human Evolution, 121*, 25-39.

Nielsen, R., Akey, J. M., Jakobsson, M., Pritchard, J. K., Tishkoff, S., & Willerslev, E. (2017). Tracing the peopling of the world through genomics. *Nature, 541*, 302.-310.

Nowaczewska, W. (2011). Are *Homo sapiens* nonsupranuchal fossa and Neanderthal suprainiac fossa convergent traits? *American Journal of Physical Anthropology, 144*(4), 552-563.

Nowaczewska, W., Binkowski, M., Kubicka, A. M., Piontek, J., & Balzeau, A. (2019). Neandertal-like traits visible in the internal structure of non-supranuchal fossae of some recent *Homo sapiens*: The problem of their identification in hominins and phylogenetic implications. *PloS One, 14*(3), e0213687.

Pagani, L., Lawson, D. J., Jagoda, E., Mörseburg, A., Eriksson, A., Mitt, M., . . . Metspalu, M. (2016). Genomic analyses inform on migration events during the peopling of Eurasia. *Nature, 538*, 238.

Pearson, O. M. (2008). Statistical and biological definitions of "anatomically modern" humans: suggestions for a unified approach to modern morphology. *Evolutionary Anthropology: Issues, News, and Reviews, 17*(1), 38-48.

Ponce de León, M. S., Koesbardiati, T., Weissmann, J. D., Milella, M., Reyna-Blanco, C. S., Suwa, G., . . . Zollikofer, C. P. E. (2018). Human bony labyrinth is an indicator of population history and dispersal from Africa. *Proceedings of the National Academy of Sciences, 115*(16), 4128-4133.

Porraz, G., Val, A., Dayet, L., de la Pena, P., Douze, K., Miller, C., . . . Sievers, C. (2015). Bushman Rock Shelter (Limpopo, South Africa): a perspective from the edge of the highveld. *South African Archaeological Bulletin, 70*(202), 166-179.

Posth, C., Renaud, G., Mittnik, A., Drucker, Dorothée G., Rougier, H., Cupillard, C., . . . Krause, J. (2016). Pleistocene Mitochondrial Genomes Suggest a Single Major Dispersal of Non-Africans and a Late Glacial Population Turnover in Europe. *Current Biology, 26*(6), 827-833.

Posth, C., Wißing, C., Kitagawa, K., Pagani, L., van Holstein, L., Racimo, F., . . . Krause, J. (2017). Deeply divergent archaic mitochondrial genome provides lower time boundary for African gene flow into Neanderthals. *Nature Communications 8,* 1-9.

Quam, R., Lorenzo, C., Martínez, I., Gracia-Téllez, A., & Arsuaga, J. L. (2016). The bony labyrinth of the middle Pleistocene Sima de los Huesos hominins (Sierra de Atapuerca, Spain). *Journal of Human Evolution, 90*, 1-15.

R Core Team (2019). R: A language and environment for statistical computing. R Foundation for Statistical Computing, Vienna, Austria, https://www.R-project.org/. R version 3.5.0.

Revelle, W. (2018) psych: Procedures for Personality and Psychological Research, Northwestern University, Evanston, Illinois, USA, https://CRAN.R-project.org/package=psych.

Reyes-Centeno, H., Ghirotto, S., Détroit, F., Grimaud-Hervé, D., Barbujani, G., & Harvati, K. (2014a). Genomic and cranial phenotype data support multiple modern human dispersals from Africa and a southern route into Asia. *Proceedings of the National Academy of Sciences, 111*(20), 7248-7253.

Reyes-Centeno, H., Buck, L. T., Stringer, C. B., & Harvati, K. (2014b). *The inner ear of the Eyasi I (Tanzania) and Kabua I (Kenya) hominin fossils*. Paper presented at the African Human Fossil Record, Toulouse.

Reyes-Centeno, H., Hubbe, M., Hanihara, T., Stringer, C. B., & Harvati, K. (2015). Testing modern human out-of-Africa dispersal models and implications for modern human origins. *Journal of Human Evolution, 87*, 95-106.

Rightmire, G. P. (1975). Problems in the Study of Later Pleistocene Man in Africa. *American Anthropologist, 77*(1), 28-52.

Rightmire, G. P. (2008). *Homo* in the Middle Pleistocene: Hypodigms, variation, and species recognition. *Evolutionary Anthropology: Issues, News, and Reviews, 17*(1), 8-21.

Rightmire, G. P. (2009). Middle and later Pleistocene hominins in Africa and Southwest Asia. *Proceedings of the National Academy of Sciences, 106*(38), 16046-16050.

Rightmire, G. P. (2012). The evolution of cranial form in mid-Pleistocene Homo. *South African Journal of Science, 108*, 68-77.

Ripley, B. D. (1996). *Pattern recognition and neural networks*. Cambridge: Cambridge University Press.

Rohlf, F. J. (1990). Morphometrics. *Annual Review of Ecology and Systematics, 21*(1), 299-316.

Rohlf F. J., & Slice D. (1990). Extensions of the Procrustes method for the optimal superimposition of landmarks. *Systematic Biology, 39*(1), 40-59.

Rohlf, F. J., & Marcus, L. F. (1993). A revolution in morphometrics. *Trends in Ecology & Evolution, 8*(4), 129-132.

Sahle, Y., Reyes-Centeno, H., & Bentz, C. (2018). Modern human origins and dispersal: current state of knowledge and future directions. *Evolutionary Anthropology: Issues, News, and Reviews, 27*, 64-67.

Sahle, Y., Beyene, Y., Defleur, A., Asfaw, B., WoldeGabriel, G., Hart, W. K., . . . White, T. D. (2019a). Human emergence: Perspectives from Herto, Afar Rift, Ethiopia. In Y. Sahle, H. Reyes-Centeno, & C. Bentz (Eds.), *Modern Human Origins and Dispersal* (pp. 105-136). Tübingen: Kerns Verlag.

Sahle, Y., Reyes-Centeno, H., & Bentz, C. (2019b). *Modern Human Origins and Dispersal*. Tübingen: Kerns Verlag.

Sankararaman, S., Mallick, S., Dannemann, M., Prüfer, K., Kelso, J., Pääbo, S., . . . Reich, D. (2014). The genomic landscape of Neanderthal ancestry in present-day humans. *Nature, 507*, 354-357.

Santa Luca, A. P. (1978). A re-examination of presumed Neandertal-like fossils. *Journal of Human Evolution, 7*(7), 619-636.

Sawchuk, E. A., & Willoughby, P. R. (2015). Terminal Pleistocene Later Stone Age Human Remains from the Mlambalasi Rock Shelter, Iringa Region, Southern Tanzania. *International Journal of Osteoarchaeology, 25*(5), 593-607.

Scerri, E. M., Thomas, M. G., Manica, A., Gunz, P., Stock, J. T., Stringer, C. B., . . . Rightmire, G. P. (2018). Did our species evolve in subdivided populations across Africa, and why does it matter? *Trends in Ecology & Evolution, 33*(8), 582-594.

Scozzari, R., Massaia, A., Trombetta, B., Bellusci, G., Myres, N. M., Novelletto, A., & Cruciani, F. (2014). An unbiased resource of novel SNP markers provides a new chronology for the human Y chromosome and reveals a deep phylogenetic structure in Africa. *Genome Research, 24*(3), 535-544.

Shapiro, S. S., & Wilk, M. B. (1965). An Analysis of Variance Test for Normality (Complete Samples). *Biometrika, 52*(3/4), 591-611.

Schepartz, L. A. (1987). *From hunters to herders: subsistence pattern and morphological change in eastern Africa.* (Ph.D.), University of Michigan, Ann Arbor.

Schlager, S. (2018). Morpho: calculations and visualizations related to geometric morphometrics (R package version 2.6).

Schlebusch, C. M., Malmström, H., Günther, T., Sjödin, P., Coutinho, A., Edlund, H., . . . Jakobsson, M. (2017). Southern African ancient genomes estimate modern human divergence to 350,000 to 260,000 years ago. *Science, 358*(6363), 652-655.

Schwartz, J. H. (2016). What constitutes Homo sapiens? Morphology versus received wisdom. *Journal of Anthropological Sciences, 94*, 65-80.

Schwartz, J. H., & Tattersall, I. (2010). Fossil evidence for the origin of Homo sapiens. *American Journal of Physical Anthropology, 143*(S51), 94-121.

Senck, S., Bookstein, F. L., Benazzi, S., Kastner, J., & Weber, G. W. (2015). Virtual Reconstruction of Modern and Fossil Hominoid Crania: Consequences of Reference Sample Choice. *The Anatomical Record*, *298*(5), 827-841.

Slice, D. E. (2007). Geometric Morphometrics. *Annual Review of Anthropology, 36*(1), 261-281.

Slice, D. E. (2011). *Modern morphometrics in physical anthropology*. New York: Kluwer.

Slice, D. E. (2013). Morpheus et al., Java Edition. Department of Scientific Computing, The Florida State University, Tallahassee, Florida. Retrieved from http:/morphlab.sc.fsu.edu/.

Slowikowski, K. (2017). ggrepel: Repulsive Text and Label Geoms for 'ggplot2'. Retrieved from https://CRAN.R-project.org/package=ggrepel.

Stringer, C. B. (2000). Eyasi. In E. Delson, I. Tattersall, J. Van Couvering, & A. S. Brooks (Eds.), *Encyclopedia of Human Evolution and Prehistory* (pp. 263). New York: Garland Publishing.

Stringer, C. B. (2016). The origin and evolution of Homo sapiens. *Philosophical Transactions of the Royal Society B: Biological Sciences, 371*(20150237).

Stringer, C. B., Hublin, J.-J., & Vandermeersch, B. (1984). The origin of anatomically modern humans in Western Europe. In H. Smith & F. Spencer (Eds.), *The Origins of Modern Humans: a World Survey of the Fossil Evidences* (pp. 51-135). New York: Alan R. Liss.

Stringer, C. B., & Buck, L. T. (2014). Diagnosing Homo sapiens in the fossil record. *Annals of Human Biology, 41*(4), 312-322.

Smith, F., Janković, I., & Karavanić, I. (2005). The assimilation model, modern human origins in Europe, and the extinction of Neandertals. *Quaternary International, 137*(1), 7-19.

Soficaru, A., Doboş, A., & Trinkaus, E. (2006). Early modern humans from the Peştera Muierii, Baia de Fier, Romania. *Proceedings of the National Academy of Sciences, 103*(46), 17196-17201.

Soficaru, A., Petrea, C., Doboş, A., & Trinkaus, E. (2007). The human cranium from the Peştera Cioclovina Uscată, Romania: context, age, taphonomy, morphology, and paleopathology. *Current Anthropology, 48*(4), 611-9.

Tattersall, I. (2009). Human origins: Out of Africa. *Proceedings of the National Academy of Sciences, 106*(38), 16018-16021.

Tattersall, I., & Schwartz, J. H. (2008). The morphological distinctiveness of Homo sapiens and its recognition in the fossil record: Clarifying the problem. *Evolutionary Anthropology: Issues, News, and Reviews, 17*(1), 49-54.

Tallman, M., Amenta, N., Delson, E., Frost, S. R., Ghosh, D., Klukkert, Z. S., . . . Sawyer, G. J. (2014). Evaluation of a New Method of Fossil Retrodeformation by Algorithmic Symmetrization: Crania of Papionins (Primates, Cercopithecidae) as a Test Case. *PloS One, 9*(7), e100833.

Trinkaus, E. (2004). Eyasi 1 and the suprainiac fossa. *American Journal of Physical Anthropology, 124*(1), 28-32.

Trinkaus, E. (2007). European early modern humans and the fate of the Neandertals. *Proceedings of the National Academy of Sciences, 104*(18), 7367-72.

Trinkaus, E. (2011). Late Neandertals and Early Modern Humans in Europe, Population Dynamics and Paleobiology. In S. Condemi & G.-C. Weniger (Eds.), *Continuity and Discontinuity in the Peopling of Europe: One Hundred Fifty Years of Neanderthal Study* (pp. 315-329). Dordrecht: Springer.

Tryon, C. A., Crevecoeur, I., Faith, J. T., Ekshtain, R., Nivens, J., Patterson, D., . . . Spoor, F. (2015). Late Pleistocene age and archaeological context for the hominin calvaria from GvJm-22 (Lukenya Hill, Kenya). *Proceedings of the National Academy of Sciences, 112*(9), 2682-2687.

Tryon, C. A., Lewis, J. E., & Ranhorn, K. (2019). Excavating the archives: The 1956 excavation of the late Pleistocene-Holocene sequence at Kisese II (Tanzania). In Y. Sahle, H. Reyes-Centeno, & C. Bentz (Eds.), *Modern Human Origins and Dispersal*. Tübingen: Kerns Verlag.

Uhl, A., Reyes-Centeno, H., Grigorescu, D., Kranioti, E. F., & Harvati, K. (2016). Inner ear morphology of the cioclovina early modern European calvaria from Romania. *American Journal of Physical Anthropology, 160*(1), 62-70.

Venables, W. N. & Ripley, B. D. (2002) Modern Applied Statistics with S. Fourth Edition. Springer, New York.

Verna, C., Hublin, J.-J., Debenath, A., Jelinek, A., & Vandermeersch, B. (2010). Two new hominin cranial fragments from the Mousterian levels at La Quina (Charente, France). *Journal of Human Evolution, 58*(3), 273-278.

Wang, M., Kornblau, S. M., & Coombes, K. R. (2018). Decomposing the Apoptosis Pathway into Biologically Interpretable Principal Components. *Cancer Informatics, 17*, 1-13.

Weaver, T. D. (2012). Did a discrete event 200,000–100,000 years ago produce modern humans? *Journal of Human Evolution, 63*(1), 121-126.

Weber, G. W., Recheis, W., Scholze, T., & Seidler, H. (1998). Virtual anthropology (VA): methodological aspects of linear and volume measurements--first results. *Collegium Antropologicum, 22*(2), 575-584.

Weber, G. W., & Bookstein, F. L. (2011). *Virtual Anthropology: A Guide to a New Interdisciplinary Field*. Vienna/New York: Springer.

Weber, G. W. (2015). Virtual Anthropology. *American Journal of Physical Anthropology, 156*, 22-42.

Webster, M., & Sheets, H. D. (2010). A practical introduction to landmark-based geometric morphometrics. *Quantitative Methods in Paleobiology, 16*, 168-188.

White, T. D., (2003). Early Hominids--Diversity or Distortion? *Science, 299*(5615), 1994.

White, T. D., Asfaw, B., DeGusta, D., Gilbert, H., Richards, G. D., Suwa, G., & Clark Howell, F. (2003). Pleistocene Homo sapiens from Middle Awash, Ethiopia. *Nature, 423*(6941), 742-747.

Whitworth, T. *Unpublished documents*. Archive of Natural History Museum. London.

Whitworth, T. (1960). Fossilized Human Remains from Northern Kenya. *Nature, 185*(4717), 947-948.

Whitworth, T. (1965a). Artifacts from Turkana, Northern Kenya. *The South African Archaeological Bulletin, 20*(78), 75-78.

Whitworth, T. (1965b). The Pleistocene lake beds of Kabua, northern Kenya. *Durham University Journal, 57*, 88-100.

Whitworth, T. (1966). A Fossil Hominid from Rudolf. *The South African Archaeological Bulletin, 21*(83), 138-150.

Wickham, H. (2009). *ggplot2: Elegant Graphics for Data Analysis*. New York: Springer-Verlag.

Wickham, H. (2011). The Split-Apply-Combine Strategy for Data Analysis. *Journal of Statistical Software, 40*(1), 1-29.

Wilshaw, A. (2016). The Current Status of the Kenya Capsian. *The African Archaeological Review, 33*, 13-27.

Wolpoff, M. H., Hawks, J., Frayer, D. W., & Hunley, K. (2001). Modern Human Ancestry at the Peripheries: A Test of the Replacement Theory. *Science, 291*(5502), 293-297.

Wolpoff, M. H., & Caspari, R. (2013). The origin of modern east Asians. *Acta Anthropologica Sinica, 32*, 377-410.

Yellen, J., Brooks, A., Helgren, D., Tappen, M., Ambrose, S., Bonnefille, R., . . . Renne, P. (2005). The archaeology of Aduma Middle Stone Age sites in the Awash Valley, Ethiopia. *Paleoanthropology, 10*(2).

Zollikofer, C. P. E., Ponce de León, M. S., Lieberman, D. E., Guy, F., Pilbeam, D., Likius, A., . . . Brunet, M. (2005). Virtual cranial reconstruction of *Sahelanthropus tchadensis*. *Nature, 434*(7034), 755-759.

Zollikofer, C. P., & Ponce de León, M. S. (2005). *Virtual reconstruction: a primer in computer-assisted paleontology and biomedicine*: Wiley-Interscience.

7. Acknowledgements

The last words of this dissertation are for the people who were critical in this entire process. First of all, I would like to express my deepest gratitude to my two supervisors: Dr. Yonatan Sahle and Prof. Dr. Katerina Harvati, who gave me the opportunity to have a Ph.D. position at the Eberhard Karls University in Tübingen and the DFG Center for Advanced Studies: Words, Bones, Genes, and Tools: Tracking Linguistic, Cultural, and Biological Trajectories of the Human Past. Thank you both so much for your instrumental support during all stages of this dissertation and of course your valued comments and assistance which helped perfect the manuscripts included here. I would also like to thank Prof. Dr. Gerhard Jäger, co-PI of the Words, Bones, Genes, and Tools Advanced Center. Although we did not interact on a frequent basis, I am grateful for your trust in my scientific capabilities. Additionally, I am honored to have Prof. Dr. Joachim Wahl and Prof. Dr. Nicholas Conard in my doctoral committee. I thank the German Research Foundation (DFG FOR 2237: Project "Words, Bones, Genes, Tools: Tracking Linguistic, Cultural, and Biological Trajectories of the Human Past") and the Eberhard Karls University of Tübingen for their funding of my Ph.D.

Further thanks go to the various collaborators who I have worked with over the last few years. First of all, I thank Dr. Andrea Waters-Rist, Dr. Dan Dediu, and Dr. Scott Moisik for their guidance throughout my Master thesis and ultimately my journey in the fields of geometric morphometrics and interdisciplinary research. Thanks also go to my co-authors Prof. Dr. Chris Stringer, Prof. Dr. Mirazón Lahr, Dr. Hugo Reyes-Centeno, and Dr. Laura Buck. Moreover, I thank the following persons for giving me the opportunity to work with the material/data discussed in this dissertation: Prof. Dr. Chris Stringer from the Natural History Museum, London, United Kingdom; Prof. Dr. Marta Mirazón Lahr from the University of Cambridge; The Middle Awash Project team, in particular Dr. Berhane Asfaw, Dr. Yonas Beyene, and Prof. Dr. Tim White, as well as the Authority for Research and Conservation of Cultural Heritage of Ethiopia; Dr. Antoine Balzeau and Dr. Dominique Grimaud-Hervé from the National Museum of Natural History, Paris, France; Prof. Dan Grigorescu from the Department of Paleontology, University of Bucharest, Romania;

Dr. Tudor Ciprut from the Radiology Department, Centrul De Sanatate Pro-Life SRL, Bucharest, Romania; Wieland Binczik, Prof. Dr. Nicholas Conard, Dr. Michael Francken; Prof. Dr. Katerina Harvati Dr. Hugo Reyes-Centeno and Dr. Yonatan Sahle from the Eberhard Karls University of Tübingen.

My time at the WoBoGeTo center was enriched by the many people that walked those halls. Special thanks go to both Yonatan and Hugo. Your work ethic and scientific rigor have greatly inspired me. I would also like to thank Dr. Monika Doll, for all her help in navigating German bureaucracy. Additionally, I had the pleasure to meet many fellows and students that were affiliated with the center, many of whom I also consider good friends. The same goes for all the wonderful people part of the Institute for Archaeological Sciences (INA), who made the Institute and Tübingen in general a great place to work. Specifically, I would like to thank Carolin Röding for helping out with the German "Zusammenfassung". Moreover, special thanks go to the members of the Dragon Slayers (f.k.a. the Goblin Slayers) for the awesome D&D nights.

Finally, on a personal note, I thank my friends and family for their support. In particular, I thank María, for the Spanish lessons and good conversations about this crazy world we live in. Also thanks to Kevin for continuing to be my best friend since High School and providing the necessary distractions from the doctoral life. I also want to thank my parents Gieljan and Marionne, and my brother Kobus for their patience, love, and encouragement, without which this dissertation would have never seen the light of day. Last but certainly not least, words cannot express my gratitude and love for my partner, Evelien. Your continued support has certainly kept me sane during this, often stressful period. Even though we had to find ways to physically bridge the distance between us, you were always with me, and for that I am deeply grateful. This dissertation is dedicated to you.

8. Abbreviated Curriculum Vitae

Abel Marinus Bosman
Date of birth: February 15, 1992
Place of birth: Nijmegen, The Netherlands
Nationality: Dutch

Education

2016 – pres.	**Ph.D. Palaeoanthropology**, Eberhard Karls University of Tübingen, Department of Natural Sciences, Baden-Württemberg, Germany.
2014 – 2015	**Master of Science Archaeology *cum laude*,** Faculty of Archaeology, Leiden University, The Netherlands.
2010 – 2014	**Bachelor of Arts Archaeology**, Faculty of Archaeology, Leiden University, The Netherlands.

Field experience

2015	Rhenen, The Netherlands, Late Medieval Cemetery. Echt-Bocage, The Netherlands, Iron Age Merovingian Cemetery.
2014	Enkhuizen-Rikkert, The Netherlands Bronze Age site. Oss Horzak West Excavation, The Netherlands, Iron Age site. Kampen, The Netherlands, Late Medieval Cemetery.
2013	Alta Valle del Tappino, Molise, Italy, Field Survey Barnham, United Kingdom, Middle Pleistocene site.
2012	NWO-research program 'Odyssee'. Nijmegen, The Netherlands, Digitizing Project. Agrigento, Sicily Italy, Roman period Museum project.

Publications

2019	Harvati, K., Röding, C., **Bosman, A. M.**, Karakostis, F. A., Grün, R., Stringer, C., . . . Kouloukoussa, M. (2019). Apidima Cave fossils provide earliest evidence of Homo sapiens in Eurasia. *Nature, 571*, 500-504.

Bosman, A. M., & Harvati, K. A virtual assessment of the proposed suprainiac fossa on the early modern European calvaria from Cioclovina, Romania. *American Journal of Physical Anthropology, 169*(3), 567-574.

Bosman, A. M., Buck, L. T., Reyes-Centeno, H., Mirazón Lahr, M., Stringer, C., & Harvati, K. The Kabua 1 cranium: Virtual anatomical reconstructions. In Y. Sahle, H. Reyes-Centeno, & C. Bentz (Eds.), Modern Human Origins and Dispersal (pp. 137-170). Tübingen: Kerns Verlag.

2017 **Bosman, A.M.**, Moisik, S.R., Dediu, D., & Waters-Rist, A. Talking heads: Morphological variation in the human mandible over the last 500 years in the Netherlands. *HOMO, 68*(5), 329-342.

Conference abstracts

2019 **Bosman, A.M.** and Harvati, K. A virtual assessment of the proposed suprainiac fossa on the early modern European calvaria from Cioclovina, Romania. 88th Annual Meeting of the American Association of Physical Anthropologists, Cleveland, Ohio, United States of America.

2017 **Bosman, A.M.** and Harvati, K. A virtual approach to the investigation of the suprainiac depressions on the Eyasi 1 and Aduma (ADU-VP-1/3) crania. Annual Meeting of Students in Evolution and Ecology, Tübingen, Germany.

Bosman, A.M. and Harvati, K. A virtual investigation of the suprainiac depressions on the Eyasi 1 and Aduma VP-1/3 crania. Third Annual Symposium of the DFG Center for Advanced Studies: "Words, Bones, Genes, Tools", Tübingen, Germany.

Bosman, A.M., Moisik, S.R., Dediu, D., & Waters-Rist, A. Talking heads: Morphological variation in the human mandible over the last 500 years in the Netherlands. Annual Meeting of the European Society of Human Evolution (ESHE), Leiden, The Netherlands.

Bosman, A. M., Buck, L. T., Reyes-Centeno, H., Mirazón Lahr, M., Stringer, C., & Harvati, K. Filling in the gaps: virtual reconstruction of the Kabua 1 cranium. East African Association for Paleoanthropology and Paleontology (EAAPP) Sixth Biennial Conference, Addis Ababa, Ethiopia.

Reviewer for scientific journals

2019 – pres. American Journal of Physical Anthropology

Appendix I

"Our inability to imagine a world without Homo sapiens has a profound impact on our view of ourselves; it becomes seductively easy to imagine that our evolution was inevitable. And inevitability gives meaning to life, because there is a deep security in believing that the way things are is the way they were meant to be."

Richard E Leakey (1995) – *The sixth extinction: patterns of life and the future of humankind*. New York: Anchor Books.

The Kabua 1 cranium: Virtual anatomical reconstructions

Abstract

Our current knowledge of the emergence of anatomically modern humans, and the human lineage in general, is limited, in large part because of the lack of a well preserved and well dated fossil record from Pleistocene Africa. Thus, the primary aim of our research is to partly relieve this problem by virtually reconstructing and analyzing the hominin cranial remains of Kabua 1, found in Kenya in the 1950s. Most scholars have argued that Kabua 1 represents an anatomically modern *Homo sapiens*, although the fragmentary nature of the remains and lack of a chronometric date hinder robust phylogenetic and taxonomic assessments. This manuscript presents the first steps taken to resolve this issue, namely a set of reconstructions of the specimen that would allow comparison with the fossil record. First, we virtually removed sediment and laboratory adhesives from µCT scans of the fragments. Subsequently, all fragments were separated by segmentation of the µCT data and described. Finally, virtual surface projections were used in the creation of several anatomical reconstructions, based on separate reference crania. These first steps provide a framework that will be used for quantitative shape analyses that aim to more firmly place these remains in the context of human evolution.

Publication

Bosman, A. M., Buck, L. T., Reyes-Centeno, H., Mirazón Lahr, M., Stringer, C., & Harvati, K. (2019). The Kabua 1 cranium: Virtual anatomical reconstructions. In Y. Sahle, H. Reyes-Centeno, & C. Bentz (Eds.), *Modern Human Origins and Dispersal* (pp. 137-170). Tübingen: Kerns Verlag.

1. Introduction

During the last few years, interest in the evolution of *H. sapiens* has increased greatly, as reflected by several scientific and popular publications (e.g. Hublin et al., 2017; Stringer, 2016). However, we still have limited knowledge of the specifics of the evolution of *H. sapiens* and the emergence of a "modern" anatomy characterized by a suite of traits present, or found at high frequency, in populations living today. This is partially due to the fact that a well preserved and well dated fossil record from of sub-Saharan Africa is lacking, excluding several fossils from the Middle Pleistocene (Fleagle et al., 2008; Hublin et al., 2017; White et al., 2003) and the Late Pleistocene (Crevecoeur et al., 2009, 2016; Grine et al., 2007; Harvati et al., 2011; Tryon et al., 2015). Specifically, hypotheses about the emergence of diagnostic *H. sapiens* traits cannot be rigorously tested because of the limited paleoanthropological record. This gap in our current knowledge can be partially filled by reconstructing and re-analyzing known fragmentary remains. The Kabua hominin remains are critical in this regard. This material was excavated in 1959, west of Lake Turkana in Kenya, near the Kabua Gorge and consists of at least three individuals (Whitworth, 1966). The material is curated by the Natural History Museum in London as part of the Palaeoanthropology collection (Buck & Stringer, 2015). Kabua 1 (K1) is the most complete individual and is represented by a fragmented calvaria, a right hemimandible, and a small right maxillary fragment. This individual is commonly considered adult (Schepartz, 1987; Whitworth, 1966) and possibly male (Schepartz, 1987). Kabua 2 (K2) consists of several frontal fragments, while Kabua 3 (K3) is represented by a small parietal fragment. There are also two isolated molars which were found in close association with K1 (Buck & Stringer, 2015; Whitworth, 1966).

Even though the material from the Kabua locality is not often discussed in the palaeoanthropological literature, there has been some discourse on the K1 cranium. According to Whitworth (1966), this specimen exhibits a set of distinct features, such as thick vault bones, a receding forehead, pronounced brow ridges, an inflated glabella, and an extremely robust mandible that possesses a chin. He particularly emphasized some of

these traits as "Neanderthaloid" (Whitworth, 1966), a statement linked to the common idea at this time that human evolution in the Old World went through a Neanderthal phase (Hrdlička, 1927; Hublin, 2009). However, most other scholars have disagreed with these findings. Schepartz (1987) and Rightmire (1975) have argued that the robusticity, inflated glabella, large mandible, and presence of a chin are comparable to other Holocene *H. sapiens* specimens from eastern Africa. Additionally, Phenice (1972), Rightmire (1975), and Bräuer (1978) have reasoned that the interpretation of a receding frontal bone and low vault is the result of the reconstruction line drawings provided by Whitworth (1966), rather than accurately reflecting the morphology of the fossil. Finally, a recent investigation of the bony labyrinth of K1 and a multivariate analysis based on ten metric variables suggested a closer affinity to anatomically modern humans than to Neanderthals (Reyes-Centeno et al., 2014). However, despite these multiple lines of evidence, there is currently no definite consensus on the taxonomic affiliation of the Kabua remains.

This manuscript will pave the way to addressing some of these issues by presenting an exhaustive description of the K1 material, which has not been undertaken since the initial publications by Whitworth (1960, 1966), together with several new virtual anatomical reconstructions. To this end, we use a suite of methods from the field of virtual anthropology or computer-assisted paleoanthropology (Gunz et al., 2009; Weber, 2001, 2015; Weber & Bookstein, 2011; Zollikofer et al., 1998; Zollikofer & Ponce de León, 2005). These methods include (1) the separation of bony material from surrounding matrix and laboratory adhesives by virtual segmentation of (μ)CT-scans, (2) generation of three-dimensional (3D) rendered models, (3) reconstructing 3D models of fragments in a virtual environment, and (4) adapting these reconstructions according to several anatomical guidelines and evolutionary hypotheses (Zollikofer & Ponce de León, 2005). The benefit of using a virtual environment is that it minimizes fossil handling and thus contributes to a specimen's preservation. It also provides access to a large corpus of sophisticated exploratory and analytical tools that are otherwise unavailable. Additionally, digital data allows

multiple researchers to try multiple variations on reconstructions, while also making visualizations more accessible and allowing for easy data sharing.

The aims of this manuscript are twofold. First, our evaluation of the available anatomical information will help re-contextualize the K1 material, as general knowledge of Middle/Late Pleistocene hominins has increased greatly since the 1960s. Second, through the use of several virtual techniques, we intend to gain new information on the Kabua 1 cranium. These preliminary results, together with a detailed description on how we approached the reconstruction of this cranium, will aid us in our future quantitative analyses of the taxonomic affiliation of this specimen when a chronometric date can be determined.

1.1. Historical and archaeological context

On 8 September 1959, a team of geologists led by Thomas Whitworth from the University of Durham discovered two localities containing skeletal material on the western shore of Lake Turkana in Kenya (Whitworth, 1960). The remains were excavated from lake sediments on the eastern flank of the Lothidok Hill range, immediately south of the Kalokol River and near the Kabua Gorge, approximate position 35° 47′E., 3° 26′ N. (Whitworth, 1960). The material was located near a watering hole referred to as 'Kabua' by the research team and as 'Kadokorinyang' by the local people (Shea & Hildebrand, 2010). K1 was found about 1 km SSE from the Kabua watering hole, while K2 and K3 were found at an unreported distance from K1, but a measurement on a published map (Whitworth, 1965a) yields an approximate distance of 1200 meters.

There is much uncertainty about the actual antiquity of the Kabua remains. According to Whitworth (1965a), the matrix encasing the hominin remains was of Late Pleistocene antiquity, as determined by Arambourg et al. (in Whitworth, 1965a) and Fuchs (1934) on the basis of mollusks and faunal remains (Buck & Stringer, 2015; Whitworth, 1960, 1965a, 1965b, 1966). However, Owen et al. (1982) argue that these lake sediments are part of a

larger complex of deposits, known as the Galana Boi Formation, and regard them as early- to mid-Holocene in age. Moreover, oral tradition and archaeological evidence suggest that the faunal remains belonged to animals that survived in this area until recently (Robbins, 1972). Attempts at establishing a chronometric context for the Kabua remains have had limited success. Uranium and fluorine relative dating carried out by Kenneth Oakley at the Natural History Museum, London were inconclusive (Buck & Stringer, 2015). Shells from a layer ~15m above the base of the Kabua lake beds were radiocarbon dated to between 5500 and 7500 years BP (Buck & Stringer, 2015). While no directly associated artifacts were found *in situ* with the hominin remains, a stone tool assemblage was recovered from the surface near the Kabua lake beds. This assemblage included artifacts that Whitworth (1965a) referred to as consisting of Kenya Stillbay lithics, Upper Kenya Capsian microliths, and some Sangoan handaxes. Whitworth (1965a) reported that the Sangoan handaxes, which were possibly derived from a horizon that overlay the Kabua skeletal material, were ascribed to the Early, Middle, and Late Sangoan industries by independent specialists, although names of these specialists were not given. Additionally, none of these handaxes have been figured or described in detail. Moreover, the so-called Kenya Stillbay and Upper Kenya Capsian industries, the latter of which has been later partly redefined as Eburran (Ambrose, 1980; Wilshaw, 2016), are generally considered to be Middle and Later Stone Age, respectively. Since the handaxes come from distinct archaeological periods and there is a hiatus of several thousand years in between the Stillbay and Eburran industries, it is possible that there has been substantial stratigraphic mixing at the entire Kabua locality. Furthermore, assigning exact dates to broad periods such as the MSA is problematic, as MSA industries occur at different points in time throughout the continent, with the added factor that new sites are being uncovered every year. For example, the oldest MSA-bearing site in eastern Africa as currently considered is in the Olorgesailie Basin, Kenya, dated to around 300 ka (Deino et al., 2018). Several years ago, the oldest MSA-bearing site was part of the Gademotta complex, which was reported to be older than 280 ka (Morgan & Renne, 2008; Sahle et al., 2013), showing how our understanding of the chronology of this tradition is changing rapidly. Moreover, several scholars (e.g. Blegen et al., 2017; Tribolo et al., 2017)

present evidence of MSA technology at sites in eastern Africa that are younger than 36 ka. This variability precludes the use of lithic technologies in securely dating archaeological contexts. In an attempt to resolve the dating issues associated with the Kabua material, direct dating of the hominin remains is currently underway with ESR and U-series methods (Buck & Stringer, 2015).

2. Materials and Methods

The fragments of the K1 cranium were scanned in six segments with a Nikon Metrology HMX ST 225 μCT machine, located at the Natural History Museum in London (Figure 1; Supplementary Table 1), with parameters optimized for the variable sizes, densities, and states of mineralization (Table 1).

Table 1. Parameters used for the scanning of the six segments. All filters were copper.

Segment	Museum Index	Voltage (kV)	Power (mA)	Filter thickness (mm)	Number of slices	Pixel size (μm)
Posterior calvaria	EM2468	215	200	2	1890	0.096
Frontal	EM2469	180	150	0.5	1520	0.083
Left temporal	EM2470	200	165	1	1256	0.083
Right temporal	EM2471	135	200	0.5	1102	0.0427
Mandible	EM2480	210	175	2	1772	0.0863
Maxilla	EM2481	190	175	1	1654	0.0236

Subsequently adhesive, plaster, and sediment were virtually removed in Avizo Lite 9.0.1 (FEI Visualization Sciences Group), using manual and semi-automatic segmentation based on thresholding and region growing. Some fragments, especially the fragments of the right temporal bone, are so heavily mineralized and affected by expanding matrix distortion that it was impossible to securely distinguish bone from sediment, which made subsequent estimation of anatomical features unreliable. Therefore, these fragments (EM2471) were not included in the anatomical reconstructions. Surface models were extracted after segmentation and together with high quality photographs of the K1 material, were used to describe each fragment and any recognizable anatomical features. In order to standardize

our observations of several non-metric traits (Supplementary Table 2), we used the scoring systems compiled and published by Buikstra and Ubelaker (1994).

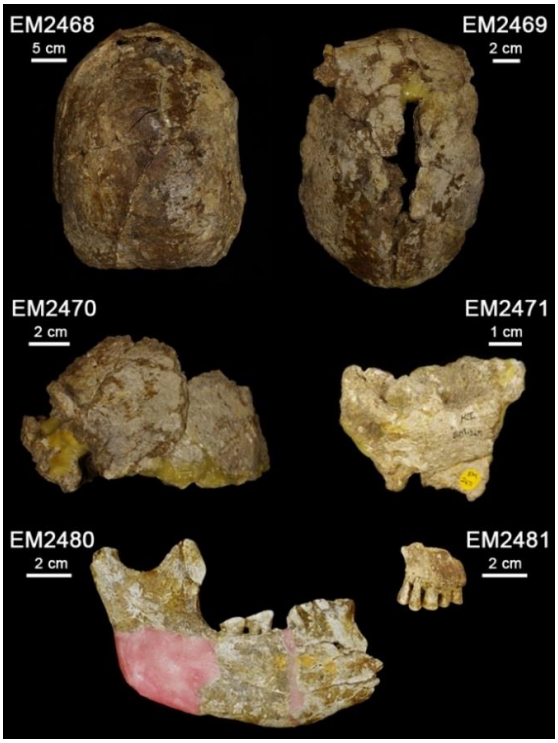

Figure 1. Selection of Kabua 1 cranial fragments. Top-left: occipital and parietals in norma occipitalis; top-right: frontal bone in *norma verticalis*, anterior faces up; middle-left: left temporal with petrous portion and parietal fragment in lateral view, with anterior facing up; middle-right: right temporal bone in inferolateral view with anterior facing left; bottom: preserved right hemimandible and maxillary fragment in buccal view, anterior facing right. Photographs courtesy of the Natural History Museum, London.

To reassemble the cranium, we used evidence of direct articulation, anatomical features, and geometric similarities of fracture surfaces wherever possible. This follows general best practice, which dictates that one should rely on the morphological information obtained from the fossil(s) in question (Zollikofer & Ponce de León, 2005). Articulation between fragments was independently assessed by three of the authors (AB, HRC, and LTB) and fragments were only fixed in place when a consensus was reached. To reassemble the non-articulated fragments, extrinsic information was employed to locate and register 'floating' fragments in an anatomically sensible location. This process relies on inference based on symplesiomorphic crania (Weber & Bookstein, 2011). However, since the K1 cranium

purportedly displays a mix of plesiomorphic and autapomorphic features, and the possible range of antiquity is quite large, it was deemed necessary to use a variety of possible crania in order to explore different scenarios, a practice that is common in virtual anthropology (Weber & Bookstein, 2011). The crania used in this manuscript were selected for their state of preservation, diverging morphologies, geographical location, possible peri-contemporaneity with Kabua, and availability of CT scan data. These reference crania include Broken Hill (Kabwe), Ngaloba LH18, Skhūl V, Mumba X, Masai 03 and Masai 10 (Table 2). We used these crania as a general framework to position the fragments of K1, without relying overly on the degree of similarity between the K1 fragments and the reference crania. That is to say, we prioritized the articulation between the Kabua fragments over direct superimposition of the fragments on the reference crania, in order to prevent a substantial bias towards the reference. By using the reference sample presented in Table 2, we aimed to capture a significant amount of possible variation with the data available to us. To determine whether our reconstructions are robust, in a future study we will use a set of geometric morphometric analyses that includes a larger comparative sample. Additionally, this comparative sample will be expanded to include less complete crania by, for example, limiting the quantitative analyses to specific areas of the cranium.

The following protocol was used for the superimposition of the K1 fragments on the reference. First, we manually aligned the posterior calvaria of K1 (EM2468) to the reference cranium by using the occipital superstructures (external occipital protuberance, asterion, cruciform eminence, superior nuchal lines, and parietal notch). Then, we manually aligned the frontal of K1 (EM2469) with the reference by using the frontal crest, glabella, and the supraorbital margins. The posterior of the frontal was rotated until it attained a smooth curvature with the posterior calvaria. The fragments of the left temporal (EM2470) were aligned to the posterior calvaria and the frontal by estimating the position of the coronal sutures and using the smooth outline in *norma frontalis* and *norma lateralis*. The K1 maxilla (EM2481) was aligned manually to the reference, while using the frontal of K1 as a guideline. The mandible (EM2480) was aligned to the maxilla by using dental occlusion and

the estimated position of the mandibular fossa on the left temporal bone. This procedure was repeated for all reference crania.

Thus, we created several distinct anatomical reconstructions, each based on a different phylogenetic and chronological scenario. However, each reconstruction was not entirely biased by the choice of reference, as smooth continuation of fragments and symmetry of the K1 cranium were favored over direct articulation with the reference crania. At the same time, using a reference-based approach ensures reproducibility by limiting the degree to which individual fragments can be spatially manipulated. In order to test the anatomical cohesion between the reconstructions and the references, we created several surface deviation models (Figure 6; Supplementary Figures 11-15) in Avizo, using the surface distance module, that display the amount of surface overlap between two objects by calculating the minimal distance between them. It has to be noted here that the Ngaloba LH18 reference cranium consists of two separately scanned fragments, the calvaria and the splanchnocranium, which had to be manually reconstructed. As described in the original publication of this specimen (Day et al., 1980), there is no direct anatomical articulation between these fragments and the reconstruction must therefore remain speculative. We nevertheless approximated the original reconstruction by Day et al. (1980) and note that the degree of facial prognathism can otherwise vary depending on the positioning of the splanchnocranium relative to the calvaria. In addition, the LH18 cranium is somewhat distorted in the frontal/facial area. These limitations of the reference might result in some uncertainty associated with the reconstruction of K1.

To investigate the form of the dental arcade of K1, we applied a specific mirroring protocol. In this procedure, we used a set of semilandmarks to compute a plane of symmetry at the area medial to the first incisor. Subsequently, we duplicated the original fragment and reflected it along the artificially created plane of symmetry; a procedure that has been described by several authors (Gunz et al., 2009; Weber & Bookstein, 2011). This mirrored copy of the maxilla was registered to the original fragment by using landmark surface

registration with rigid transformation (Supplementary Figure 1). However, points to define the mid-sagittal plane are only located in the most anterior portion of the maxilla, which makes the reconstruction of the dental arcade uncertain. The same procedure was applied to mirror the mandible.

Table 2. Summary of comparative specimens used in the anatomical reconstructions and their proposed antiquity.

Specimen	Broken Hill	LH 18	Skhūl V	Mumba X	Masai 03 & Masai 10
Locality	Kabwe, Zambia	Laetoli, Tanzania	Skhūl Cave, Israel	Mumba rockshelter, Tanzania	Lake Eyasi region, Tanzania
Taxon	*H. heidelbergensis* s.l.	early *H. sapiens*	early *H. sapiens*	recent *H. sapiens*	recent *H. sapiens*
Antiquity	300 - 250 ka	490 – 121 ka	130 – 100 ka	>5 ka	Holocene; ~200 ya
Dating method	ESR, U-series	Thorium and protactinium dating on giraffe vertebra	ESR, U-series	Minimum radiocarbon based on stratigraphically superior burial	Uncalibrated radiocarbon on charcoal found in grave of Masai 1
References	Buck & Stringer (2015); Balzeau et al. (2017)	Hay (1987); Millard (2008)	Grün et al. (2005)	Mehlman (1979)	Bräuer (1983)
Location	NHML	NMT/VAV	NHML/PMH	EKUT	EKUT

Abbreviations: NHML = National History Museum, London, NMT = National Museum Tanzania, VAV = Virtual Anthropology Vienna, PMH = Peabody Museum, Harvard University, Cambridge, EKUT = Eberhard Karls University of Tübingen.

2.1. Inventory and description of the fragments

The K1 material (Figures 1-2, Supplementary Table 1) has been described to some extent by Whitworth (1960, 1965b). In this manuscript, we summarize these descriptions and add information where needed or where we differ from Whitworth's findings.

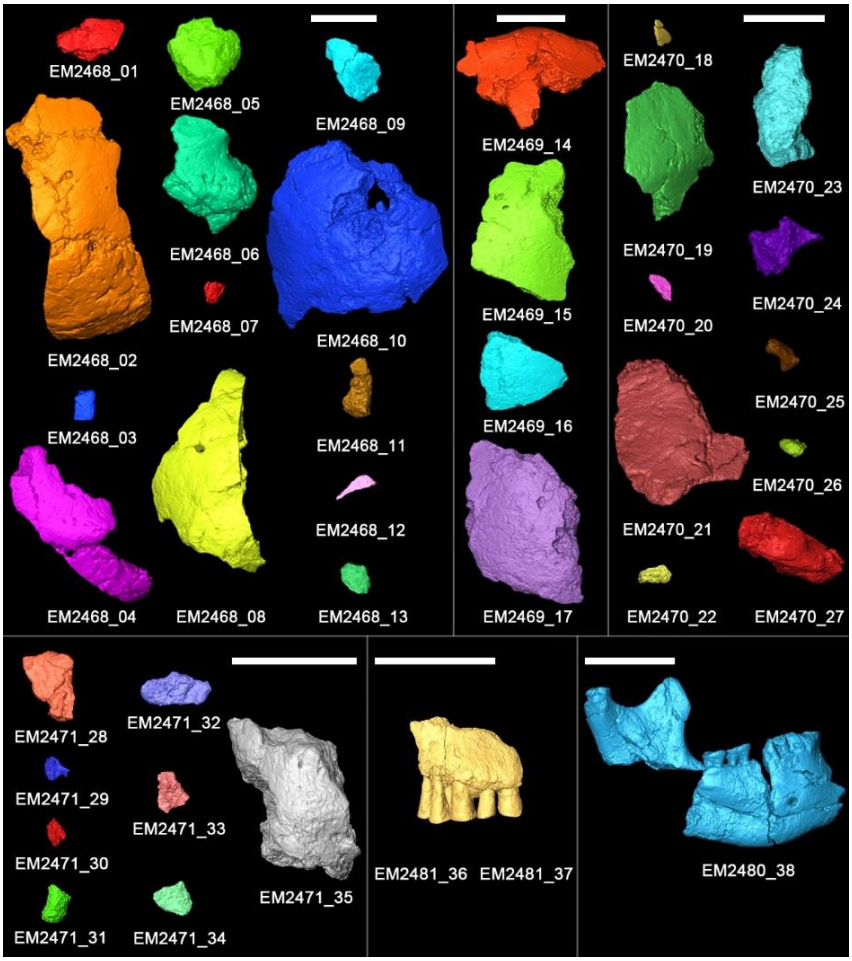

Figure 2. Inventory of the Kabua 1 remains as surface reconstructions. For EM2468, EM2469, EM2470, and EM2471, the ectocranial surfaces are facing the viewer and the anterior sides are facing up. For EM2480, the buccal side is facing the viewer, with anterior facing right. For EM2481, the anterior side is facing the viewer and superior sides face up. Labels as in Supplementary Table 1 (scale bars = 5 cm).

Occipital bone (EM2468)

The occipital squama is preserved up to a point behind opisthion, while the basilar occipital is absent (Whitworth, 1966). The lambdoid suture is visible on the right side, where it is distorted by taphonomy, and the external table is degraded. This distorts the articulation with the posterior temporal bone, EM2468_06. In the area of lambda, the lambdoid suture can only be faintly traced on the left half of the occipital plane. The occipital does not project posteriorly below lambda. The superior nuchal lines are robust and extend laterally towards asterion. There is a medial thickening present on the superior nuchal lines, but the external occipital protuberance is not pronounced; its inferior border is rounded and does

not extend inferiorly of the superior nuchal lines (score 1; Buikstra & Ubelaker, 1994). The cruciform eminence and transverse sulci are also not pronounced. The cerebellar fossae are of similar size as the cerebral fossae, although most of the basilar portion is not preserved. The neurocranium is high and medio-laterally compressed, partially due to taphonomic processes.

Approximately nine millimeters above the superior nuchal lines, there is a shallow oval depression, with uneven borders, that has a maximum extension in the transverse direction. It does not correspond to the suprainiac fossa commonly described for Neanderthal specimens, which are discrete, elliptical depressions with an uneven floor that extend laterally between the bilateral aches of an occipital torus (Balzeau & Rougier, 2010; Hublin, 1978; Santa Luca, 1978). Moreover, its external surface is not characterized by localized rugosity and pitting, but is instead marked by macroscopic dents and abrasion of the external table of the cranial vault, suggesting that the depression may be the result of extensive taphonomic processes. Moreover, when analyzing a µCT slice that crosses the maximum vertical extent of the depression on K1, it is clear that only the external table is influenced (Supplementary Figure 2). The diploë is not affected by the presence of the depression. This pattern corresponds to suprainiac depressions found in *H. sapiens* and contrasts with that observed in the Neanderthal suprainiac fossa (Balzeau & Rougier, 2010).

Frontal bone (EM2469)

The frontal bone is fairly complete and consists primarily of the medial segments of the superciliary arches, the area surrounding glabella, and most of the posterior frontal bone. It is damaged around the area of the frontal suture by a long fissure that originates behind the position of glabella and separates the frontal nearly in two distinct halves. According to Whitworth (1966), this suggests imperfect metopic suture closure at the time of death. While some traces of the metopic suture persist superior of nasion in most known cases of metopism (Ajmani et al., 1983), metopic sutures of the partial type can either extend upward from nasion or downward from bregma (Zdilla et al., 2018). Moreover, the prevalence of

metopism varies among different populations and sexes (Ajmani et al., 1983; Zdilla et al., 2018). In K1, the taphonomic damage extends from the area of bregma but does not reach the area around glabella or the post-toral sulcus. However, it is also possible that the frontal bone fissure is exclusively caused by postmortem taphonomic processes. As there is no conclusive evidence for metopism, we consider the latter a more conservative interpretation. Endocranially, the frontal crest is broken off just as it bifurcates into the sagittal sulcus.

Both supraorbital margins are present to some extent, with the left being better preserved than the right (Whitworth, 1966). Neither margin shows supraorbital notches, but the areas where these should be present are not fully preserved. The supraorbital margins seem fairly sharp and minimally expressed (score 2; Buikstra & Ubelaker, 1994). Similarly, glabella and the supraorbital ridge are also minimally expressed (score 1; Buikstra & Ubelaker, 1994). There are no clear signs of a post-toral sulcus or postorbital constriction. The lateral parts of the supraorbital region are differentiated from the medial segment—a condition that is often described as anatomically modern and differs from the continuous supraorbital morphology seen in Neanderthal specimens (Harvati et al., 2007; Smith & Ranyard, 1980).

According to Whitworth (1966), the frontal bone of K1 displays pronounced median frontal keeling. However, this median frontal keeling seems to be mainly caused by a slight mismatch between the anterior (EM2469_14) and posterior (EM2469_15, EM2469_16, and EM2469_17) fragments in the original manual reconstruction. After positioning the fragments so that there is direct articulation between EM2469_14 and the posterior frontal fragments (right: EM2469_15, left: EM2469_17), the pronounced sagittal keel is reduced significantly (Supplementary Figure 3).

Parietals (EM468 and EM2470)

The left parietal is better preserved than the right, although most of the anterior portion is missing, especially around bregma and posterior to the left orbit. There is a hint of a weak

parietal eminence on the left parietal. The right parietal is missing a large anterior portion and is damaged by perforations near the midsagittal plane (Whitworth, 1966). On the right side, the area where the parietal eminence would be located is not fully preserved and distorted by post-depositional processes. There does seem to be a trace of the posterior portion of the inferior temporal line on the right parietal (EM2468_05). The coronal suture is not preserved on either parietal bone.

Temporal bones (EM2470)

Most of the squamous portion of the left temporal is intact, including the petrous portion. While the petrous portion is displaced inwards, it is generally well preserved, which allowed for the reconstruction of the bony labyrinth (Figure 3; Reyes-Centeno et al., 2014). The proximal portion of the postglenoid process is intact. Also present is the posterior base of the zygomatic process. The glenoid fossa, entoglenoid process, zygomatic process, parietal notch, and most of the tympanic plate are not preserved. Concerning the mastoid process, the ectocranial surface is damaged. On the right side, only the posterior aspect of the temporal bone is present, which includes the mastoid process and a fairly pronounced supramastoid crest. While they are quite broad, the mastoid processes do not extend inferiorly (score 2; Buikstra & Ubelaker, 1994). Concerning the right temporal bone, Whitworth (1966) only describes the posterior aspect. However, the K1 material includes a very heavily mineralized fragment catalogued as a squamous portion of a right temporal bone (EM2471). This fragment includes the articular eminence and the mandibular fossa but the presence of these features cannot be established with much certainty, as the entire temporal is afflicted by expanding matrix distortion (Figure 1), which makes an accurate assessment of its anatomical features extremely difficult. However, as far as can be determined, the tympanic part, petrous portion, and other diagnostic features such as the styloid process or the auditory meatus are not preserved.

While most of basilar calvaria is not preserved (Whitworth, 1966), the distal portion of the left greater wing of the sphenoid articulates with the left temporal bone (EM2470_21 and

EM2470_23; Figure 2). On the right side, there is a singular fragment that resembles the inferodistal part of the right greater wing (EM2471_32), but this assessment cannot be determined with certainty due to the extensive expanding matrix distortion, as earlier described for the right temporal.

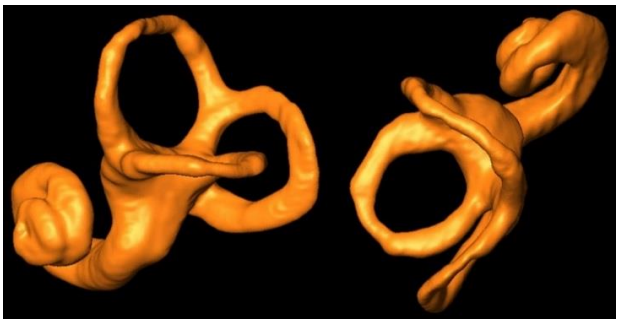

Figure 3. Reconstruction of the Kabua 1 left bony labyrinth in lateral (left) and superior (right) view.

Mandible (EM2480)

The right hemi-mandible is well preserved, as most of the right sigmoid sulcus, inferior portion of the articular condyle, coronoid process, mandibular ramus, and mandibular corpus are present. Just behind the second premolar, the mandible is almost completely separated into two pieces, but the inferior border and adhesives from Whitworth's reconstruction hold the two fragments together. The gonial area is reconstructed as well. There is some post-depositional deformation in the form of a large oval depression on the buccal side of the mandibular corpus, inferior to the first and second molars (Figures 1-2). Overall, the corpus of the mandible is robust, primarily in the lingual area, which is dominated by a mylohyoid ridge that develops into a pronounced mandibular torus. The mandibular corpus has been described as deep by Wood (2011). Moreover, Whitworth (1966) and several other authors (e.g. Schepartz, 1987; Wood, 2011) have argued that there is an unequivocal presence of a chin. While there is a posteriorly oriented slope between the alveolar process around the first incisor and the area where the mental protuberance would be located, there is not sufficient bone preserved to ascertain the exact morphology of this area. Behind the third molar, there is a narrow space that Wood (2011) describes as a retromolar gap. The retromolar gap is commonly referred to as a Neanderthal

autapomorphy (e.g. Franciscus & Trinkaus, 1995; Stringer et al., 1984; but see Harvati, 2015) and has been related to processes such as mid-facial prognathism (Rak, 1986; Rosas, 2001) and a decrease in size of the buccal teeth (Brace, 1979). However, Rosas and Bastir (2004) and Nicholson and Harvati (2006) found that the retromolar gap was related to increasing mandibular size and is not autapomorphic for *H. neanderthalensis*. Thus, there is some uncertainty regarding the Neanderthal derived status of the retromolar gap, and the narrow space behind the third molar in the K1 mandible might simply be related to the relative large size and robusticity of the mandibular corpus and its comparably small dentition.

The K1 lower dentition (I_2 to P_4, M_2, and M_3) is heavily worn and the enamel is mostly abraded. While most of the traits present are common in *H. sapiens* (i.e., smaller bucco-lingual diameter of the first molar when compared to the second molar, vertical lingual wall versus an inflated buccal wall), Whitworth (1966) notes that the roots of the second lower molar seem to consist of two external roots and one, "pillar-like" median internal root. Similarly, he argues that the third molar only presents a singular fused root (Whitworth, 1966). He equates these structures to the enlarged pulp chambers in molars, taurodontism, found in the Neanderthal dentition from Krapina (Whitworth, 1966). While taurodontism is more common in Neanderthals, it is also found in varying frequencies in Late Pleistocene *H. sapiens* (Kupczik & Hublin, 2010). However, while the external morphology of the roots is unclear due to the presence of sediment, a series of ortho slices show that both M_2, and M_3 possess two major external roots with an early invagination (Supplementary Figure 4), a condition typical for *H. sapiens* (Kupczik & Hublin, 2010).

Maxilla (EM2481)

The maxilla is represented by a small fragment of the right medial alveolar process and is heavily damaged around the midline. In general, the labial surface of the alveolar process is quite flat and not pronounced. There is no evidence of a pronounced naso-alveolar clivus. Likewise, what is preserved of the palate is not robust. There is no evidence of a greater palatine groove, although most of the area where this structure would be located is not

preserved. In contrast to what has been stated by Whitworth (1966), not enough of the maxilla is preserved to securely estimate the position of the anterior root of the zygomatic arch, nor of the presence of a canine fossa.

After reflection of the maxilla along the sagittal plane, the dental arcade has a parabolic, semi-circular appearance (Supplementary Figure 1). The incisors, canine, and premolars (I^1 to P^4 along the dental row) are preserved, although heavily affected by abrasion. The anterior teeth are particularly small (Schepartz, 1987). As with the mandibular dentition, most of the enamel has degraded due to abrasion, especially on the lingual side of the incisors, where the cervical margin has completely worn away. On the labial side, the proximal portion of the cervical margin is still present, primarily on P^3 and P^4.

3. Results and Discussion

While we used several morphologically distinct reference crania in the virtual reconstruction of K1, there is an overall consistency between the reconstructions in regards to general cranial shape. (Figures 4-6, Supplementary Figures 5-15). All anatomical reconstructions present fairly globular crania—a hallmark trait of anatomical modernity (Gunz et al., 2012; Neubauer et al., 2018; Pearson, 2008), which could be established with some confidence, as the preserved cranial vault is located fairly close to the frontal bone. Moreover, the anatomically correct curvature between the frontal and temporal sections on the left side is preserved to some extent, even though direct articulation could not be established. The reconstructions are at their widest in the mid-parietal region, and do not present a posterior extension of the occipital squama—a feature that is present on the Broken Hill cranium. Moreover, the K1 fragments are not as robust as the Skhūl V cranium but seem to be quite gracile and more comparable to the Masai 03 and Masai 10 individuals. In addition, some of the cranial traits present on K1 (nuchal crest, mastoid process, supraorbital margin, and glabella) were found to be minimally expressed. This might signify that the K1 cranium was female, rather than male, as suggested by Schepartz (1987).

However, the lack of other skeletal elements, such as the pelvis, that can contribute to the estimation of sex precludes a definitive assessment.

Overall, the recent *H. sapiens* reference crania (Figure 6; Supplementary Figures 8-10, 14-15) result in reconstructions that have the most anatomical cohesion, together with the reconstruction based on Skhūl V. In these reconstructions, the fragments of K1 align well to the frontal, the anterior portion of the parietals, and the superior area of the occipital bone. The posterior protrusion of the occipital bone overlaps the most with its reference in the reconstruction based on Masai 03 (Figure 6) It should be noted that in all reconstructions, the surface deviation models highlight that the lower scale of the occipital and inferior portions of the temporal bones of K1 extend further than the references used here. When comparing all reconstructions, the specimens with fewer anatomically modern traits (specifically Broken Hill and Ngaloba) do not display as great a degree of anatomical cohesion as the reconstructions based on Skhūl V, Mumba X, Masai 03, and Masai 10.

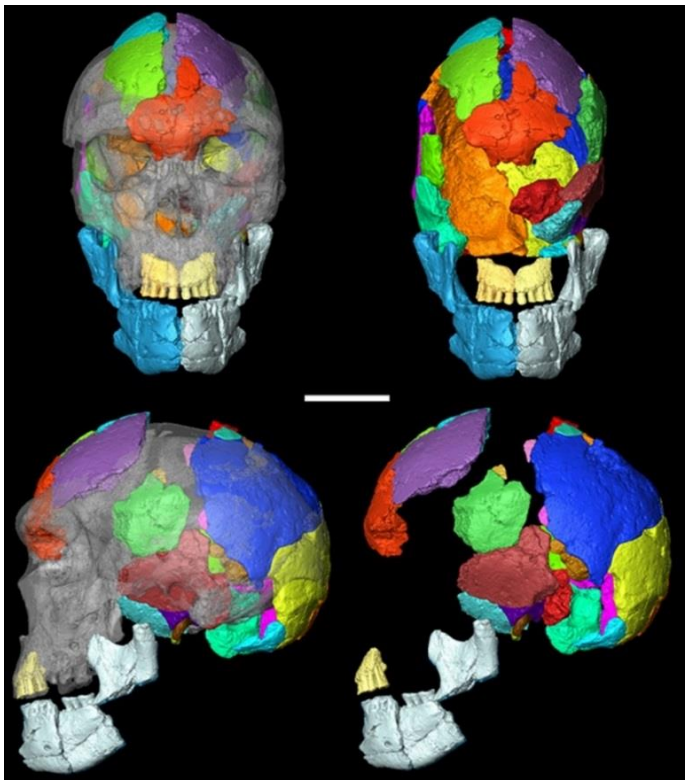

Figure 4. Reconstruction of Kabua 1, with Broken Hill as the reference. Top-left: *norma frontalis* with Broken Hill superimposed; top-right: *norma frontalis*; bottom-left: *norma lateralis sinister* with Broken Hill superimposed; bottom-right: *norma lateralis sinister* (scale bar = 10 cm). For more orientations, see Supplementary Figure 5.

In particular, the reconstruction based on Ngaloba LH18 is problematic. In this reconstruction, the orientation of the K1 frontal does not align well with the frontal of LH18. Furthermore, the left temporal/parietal portion does not form a smooth continuation of the coronal outline between the posterior calvaria and frontal bone. This can be partially explained by the fact that the LH18 specimen shows some degree of taphonomic deformation (see above), which likely contributes to the final reconstruction. Likewise, the reconstruction deviates from Broken Hill in very specific areas, such as the medial part of the frontal and around the position of lambda. However, since a qualitative assessment of the robustness of the reconstructions and anatomical cohesion displayed by the surface deviation models is limited in usefulness, we will use geometric morphometrics in a future study in order to better evaluate the results presented here.

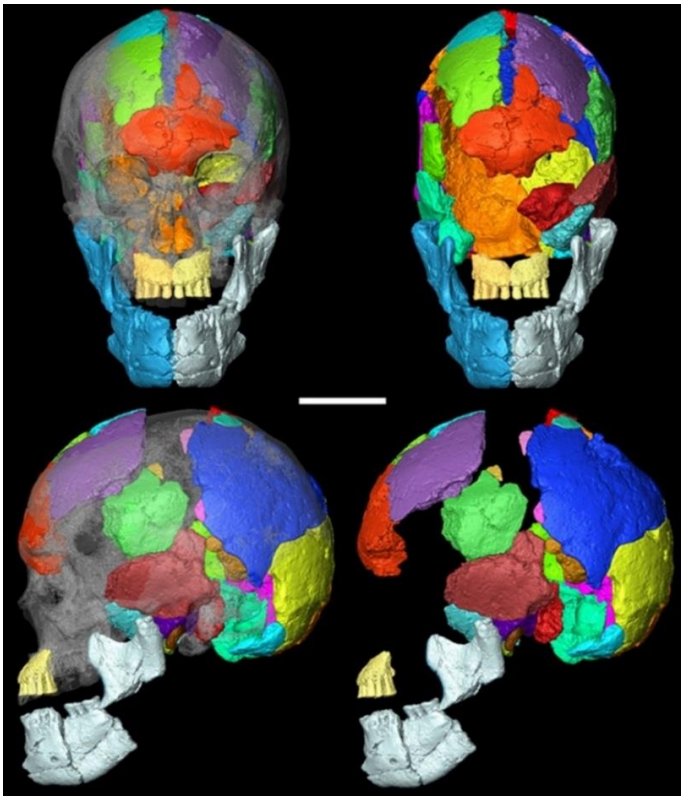

Figure 5. Reconstruction of Kabua 1, with Masai 10 as the reference. Top-left: *norma frontalis* with Masai 10 superimposed; top-right: *norma frontalis*; bottom-left: *norma lateralis sinister* with Masai 10 superimposed; bottom-right: *norma lateralis sinister* (scale bar = 10 cm). For more orientations, see Supplementary Figure 10.

As stated in the materials and methods, the reference crania were used as frameworks to correctly register fragments of K1, after inherent anatomical guidelines and articulation were exhausted. Therefore, in some of the reconstructions, there are slight mismatches between the reference cranium and the K1 fragments. This is especially evident in the reconstructions based on Broken Hill, Ngaloba LH18 and Skhūl V. Particularly troublesome was the placement of the left temporal/parietal section and the reconstruction of its relationship with the frontal. This was even more true for the maxilla and mandible. As the glenoid area in K1 is not preserved, we had to rely on the occlusion between the upper and lower dentition to position the mandible. Due to the significant amount of dental abrasion, this placement is uncertain, which results in a large amount of variation in this area between reconstructions. Additionally, in all reconstructions K1 seems to be more inferiorly extended in the occipital and temporal regions (Figures 4-6). This is exemplified by the especially inferiorly located temporal bone and the long nuchal crest. Moreover, all reconstructions of K1 are quite narrow at the temporo-parietal area. This is primarily caused by post-mortem distortion of the right parietal/temporal region, which caused the fragments EM2468_05 and EM2468_06 to be moved medially, as well as endocranially distorting a small area superior of where the temporal line should be. In our reconstructions, we have attempted to remedy this distortion by moving EM2468_05 and EM2468_06 laterally, relative to the superior right parietal fragments. However, most of the distortion could not be solved by manually positioning fragments according to a framework; another solution should be sought for this problem.

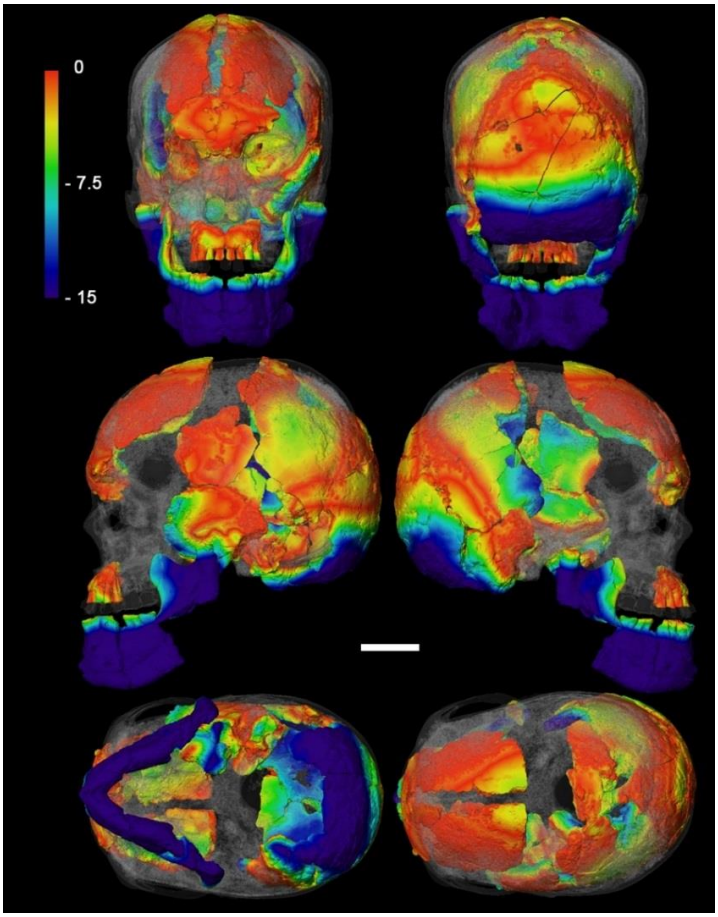

Figure 6. Surface displacement model of Kabua 1 reconstruction and Masai 03 as the reference (transparent). Scale of colormap: 0 – 15 mm deviation. Top-left: *norma frontalis*; top-right: *norma occipitalis*; center-left: *norma lateralis sinister*; center-right: *norma lateralis dexter*; bottom-left: *norma basilaris*; bottom-right: *norma verticalis* (scale bar = 5 cm).

Finally, our reconstructions present a severe limitation of the methodology that was applied. Since there is no direct articulation between the cranial vault, temporal, frontal bone, and the maxilla and mandible, these sections could be placed with several degrees of freedom and still result in anatomically viable reconstructions. Since data interpolation methods, such as thin plate spline warping, rely on the correct initial placement of the available fragments, we are unable to apply them to K1 in order to create reconstructions that would resemble what the specimen would have looked like just after deposition. This is a limitation we cannot easily overcome. In addition, we have not considered how size and allometric effects on cranial shape in our reference crania might influence our reconstructions (Freidline et al., 2012; Mitteroecker et al., 2004, 2013). Such limitations

highlight the need to employ a widely diverging range of reference crania, as well as the creation of several reconstructions, instead of treating a certain reconstruction as the "true" form of the K1 cranium.

In conclusion, the K1 material has presented us with a challenge, due to the incompleteness of the most diagnostically important areas, as well as the pronounced taphonomic distortion in the parieto-temporal region. Our reconstructions show that, even though direct articulation between several fragments is retained, the separate sections can be spatially manipulated with several degrees of freedom and still result in acceptable anatomical configurations. As such, the reference-based approach was useful in limiting the spatial distribution of the fragments with respect to each other and to the reference specimen.

To return to the results presented in this manuscript, we found that, in general, the K1 cranium exhibits a globular neurocranium and relatively gracile features, without substantial evidence for plesiomorphic traits, such as a sharp occipital angle, a low and sloping frontal bone, and pronounced supraorbital and occipital tori. Thus, in this regard, we tentatively agree with Rightmire (1975), Bräuer (1978), and Schepartz (1987) that the morphology of the K1 cranium is within the range of anatomically modern *H. sapiens* variation. This hypothesis is strengthened by the fact that it was quite difficult to fit these fragments with reference to pre-modern specimens without violating basic anatomical principles. The findings presented in this manuscript stand in contrast with the proposed 'Neanderthaloid' affinities put forth by Whitworth (1966) for the Kabua material. However, his hypothesis should be viewed within the context of the knowledge of human evolution at the time of its initial description. We have the benefit of working with a more abundant fossil record, a wealth of knowledge generated in the last decades, and sophisticated technology that allowed us to investigate this fossil in minute detail. In addition, we were able to explore multiple scenarios without the potential dangers involved in handling these delicate materials.

Outstanding questions on this material include the phylogenetic affinities of the Kabua 1 specimen, as well as the antiquity of both assemblages. This manuscript has presented the first steps towards evaluating its taxonomic affiliation by investigating the preserved qualitative traits. Moreover, the anatomical reconstructions described here will be used for geometric morphometric analyses of the Kabua material in order to determine the taxonomic affiliation of this specimen and its place in the African fossil record. Finally, the Kabua skeletal assemblages contain a wealth of other information that should now be more widely incorporated in the context of human evolution for years to come.

4. Acknowledgements

Support for this research was provided by the German Research Foundation (DFG FOR 2237: Project "Words, Bones, Genes, Tools: Tracking Linguistic, Cultural, and Biological Trajectories of the Human Past" and DFG INST 37/706-1 FUGG: Paleoanthropology High Resolution CT Laboratory). LTB was additionally supported by the Human Origins Research Fund of the Natural History Museum London. CS's research is supported by the Calleva Foundation and the Human Origins Research Fund. We thank Julia Galway-Witham for the photographs of the Kabua material. We thank the editors and two anonymous reviewers for their comments, which greatly improved this manuscript.

5. References

Ajmani, M. L., Mittal, R. K., & Jain, S. P. (1983). Incidence of the metopic suture in adult Nigerian skulls. *Journal of Anatomy, 137*, 177-183.

Ambrose, S. H. (1980). *Elmenteitan and other Late Pastoral Neolithic adaptations in the central highlands of East Africa.* Paper presented at the Proceedings of the 8th Panafrican Congress of Prehistory and Quaternary Studies, 1977, Nairobi.

Balzeau, A., & Rougier, H. (2010). Is the suprainiac fossa a Neandertal autapomorphy? A complementary external and internal investigation. *Journal of Human Evolution, 58*(1), 1-22.

Balzeau, A., Buck, L. T., Albessard, L., Becam, G., Grimaud-Hervé, D., Rae, T. C., & Stringer, C. B. (2017). The Internal Cranial Anatomy of the Middle Pleistocene Broken Hill 1 Cranium. *Paleoanthropology*, 107-138.

Blegen N., Faith J. T., Mant-Melville A., Peppe D. J. & Tryon C. A. (2017). The Middle Stone Age after 50,000 years ago: New evidence from the Late Pleistocene sediments of the Eastern Lake Victoria Basin, Western Kenya. *PaleoAnthropology*, 139–169.

Brace, C. L. (1979). Krapina, "Classic" Neanderthals, and the evolution of the European face. *Journal of Human Evolution, 8*(5), 527-550.

Bräuer, G. (1978). The morphological differentiation of anatomically modern man in Africa, with special regard to recent finds from East Africa. *Zeitschrift für Morphologie und Anthropologie, 69*(3), 266-292.

Bräuer, G. (1983). Die menschlichen Skelettfunde des" Later Stone Age" aus der Mumba-Höhle und anderen Lokalitäten nahe des Eyasi-Sees (Tanzania) und ihre Bedeutung für die Populationsdifferenzierung in Ostafrika. In H. Müller-Beck (Ed.), *Die archäologischen und anthropologischen Ergebnisse der Kohl-Larsen-Expeditionen in Nord-Tanzania, 1933–1939* (Vol. 4). Tübingen: Verlag Archaeologica Venatoria.

Buck, L. T., & Stringer, C. B. (2015). A rich locality in South Kensington: the fossil hominin collection of the Natural History Museum, London. *Geological Journal, 50*(3), 321-337.

Buikstra, J. E., & Ubelaker, D. H. (1994). *Standards for Data Collection from Human Skeletal Remains.* Fayetteville, Arkansas: Arkansas Archaeological Survey Report Number 44.

Crevecoeur, I., Rougier, H., Grine, F., & Froment, A. (2009). Modern human cranial diversity in the Late Pleistocene of Africa and Eurasia: Evidence from Nazlet Khater, Peştera cu Oase, and Hofmeyr. *American Journal of Physical Anthropology, 140*(2), 347-358.

Crevecoeur, I., Brooks, A., Ribot, I., Cornelissen, E., & Semal, P. (2016). Late Stone Age human remains from Ishango (Democratic Republic of Congo): New insights on Late Pleistocene modern human diversity in Africa. *Journal of Human Evolution, 96*, 35-57.

Day, M. H., Leakey, M. D., & Magori, C. (1980). A new hominid fossil skull (L.H. 18) from the Ngaloba Beds, Laetoli, northern Tanzania. *Nature, 284*(5751), 55-56.

Deino, A. L., Behrensmeyer, A. K., Brooks, A. S., Yellen, J. E., Sharp, W. D., & Potts, R. (2018). Chronology of the Acheulean to Middle Stone Age transition in eastern Africa. *Science*, *360*(6384), 95-98.

Fleagle, J. G., Assefa, Z., Brown, F. H., & Shea, J. J. (2008). Paleoanthropology of the Kibish Formation, southern Ethiopia: Introduction. *Journal of Human Evolution, 55*(3), 360-365.

Franciscus, R. G., & Trinkaus, E. (1995). Determinants of retromolar space presence in Pleistocene Homo mandibles. *Journal of Human Evolution, 28*(6), 577-595.

Freidline, S. E., Gunz, P., Harvati, K., & Hublin, J.-J. (2012). Middle Pleistocene human facial morphology in an evolutionary and developmental context. *Journal of Human Evolution, 63*(5), 723-740.

Fuchs, V. E. (1934). The Geological Work of the Cambridge Expedition to the East African Lakes, 1930–31. *Geological Magazine, 71*(3), 97-112.

Grine, F. E., Bailey, R. M., Harvati, K., Nathan, R. P., Morris, A. G., Henderson, G. M., . . . Pike, A. W. (2007). Late Pleistocene human skull from Hofmeyr, South Africa, and modern human origins. *Science, 315*(5809), 226-229.

Grün, R., Stringer, C., McDermott, F., Nathan, R., Porat, N., Robertson, S., . . . McCulloch, M. (2005). U-series and ESR analyses of bones and teeth relating to the human burials from Skhul. *Journal of Human Evolution, 49*(3), 316-334.

Gunz, P., Mitteroecker, P., Neubauer, S., Weber, G. W., & Bookstein, F. L. (2009). Principles for the virtual reconstruction of hominin crania. *Journal of Human Evolution, 57*(1), 48-62.

Gunz, P., Neubauer, S., Golovanova, L., Doronichev, V., Maureille, B., & Hublin, J.-J. (2012). A uniquely modern human pattern of endocranial development. Insights from a new cranial reconstruction of the Neandertal newborn from Mezmaiskaya. *Journal of Human Evolution, 62*(2), 300-313.

Harvati, K. (2015). Neanderthals and their contemporaries. In W. Henke & I. Tattersall (Eds.), *Handbook of Paleoanthropology* (pp. 2243-2279). New York: Springer.

Harvati, K., Gunz, P., & Grigorescu, D. (2007). Cioclovina (Romania): affinities of an early modern European. *Journal of Human Evolution*, *53*(6), 732-746.

Harvati, K., Stringer, C., Grün, R., Aubert, M., Allsworth-Jones, P., & Folorunso, C. A. (2011). The Later Stone Age Calvaria from Iwo Eleru, Nigeria: Morphology and Chronology. *PloS One, 6*(9), e24024.

Hay, R. L. (1987). Geology of the Laetoli area. In M. D. Leakey & J. M. Harris (Eds.), *Laetoli: A Pliocene site in northern Tanzania* (pp. 23-47). Oxford: Oxford University Press.

Hublin, J.-J. (1978). Quelques caractères apomorphes du crâne néandertalien et leur interprétation phylogénique. *Comptes rendus de l'Académie des sciences. Série III, Sciences de la vie., D287*, 923-926.

Hublin, J. J. (2009). The origin of Neandertals. *Proceedings of the National Academy of Sciences, 106*(38), 16022-16027.

Hublin, J.-J., Ben-Ncer, A., Bailey, S. E., Freidline, S. E., Neubauer, S., Skinner, M. M., . . . Gunz, P. (2017). New fossils from Jebel Irhoud, Morocco and the pan-African origin of Homo sapiens. *Nature, 546*(7657), 289-292.

Hrdlička, A. (1927). The Neanderthal Phase of Man. *The Journal of the Royal Anthropological Institute of Great Britain and Ireland, 57*, 249-274.

Kupczik, K., & Hublin, J.-J. (2010). Mandibular molar root morphology in Neanderthals and Late Pleistocene and recent Homo sapiens. *Journal of Human Evolution, 59*(5), 525-541.

Mehlman, M. J. (1979). Mumba-Hohle Revisited: The Relevance of a Forgotten Excavation to Some Current Issues in East African Prehistory. *World Archaeology, 11*(1), 80-94.

Millard, A. R. (2008). A critique of the chronometric evidence for hominid fossils: I. Africa and the Near East 500–50ka. *Journal of Human Evolution, 54*(6), 848-874.

Mitteroecker, P., Gunz, P., Bernhard, M., Schaefer, K., & Bookstein, F. L. (2004). Comparison of cranial ontogenetic trajectories among great apes and humans. *Journal of Human Evolution, 46*(6), 679-698.

Mitteroecker, P., Gunz, P., Windhager, S., & Schaefer, K. (2013). A brief review of shape, form, and allometry in geometric morphometrics, with applications to human facial morphology. *Hystrix, the Italian Journal of Mammalogy, 24*(1), 8.

Morgan, L. E., & Renne, P. R. (2008). Diachronous dawn of Africa's Middle Stone Age: New 40Ar/39Ar ages from the Ethiopian Rift. *Geology, 36*(12), 967-970.

Neubauer, S., Hublin, J.-J., & Gunz, P. (2018). The evolution of modern human brain shape. *Science Advances, 4*(1).

Nicholson, E., & Harvati, K. (2006). Quantitative analysis of human mandibular shape using three-dimensional geometric morphometrics. *American Journal of Physical Anthropology, 131*(3), 368-383.

Owen, R. B., Barthelme, J. W., Renaut, R. W., & Vincens, A. (1982). Palaeolimnology and archaeology of Holocene deposits north-east of Lake Turkana, Kenya. *Nature, 298*(5874), 523-529.

Pearson, O. M. (2008). Statistical and biological definitions of "anatomically modern" humans: suggestions for a unified approach to modern morphology. *Evolutionary Anthropology: Issues, News, and Reviews, 17*(1), 38-48.

Phenice, T. W. (1972). *Hominid fossils: an illustrated key*. Iowa: W. C. Brown Co.

Rak, Y. (1986). The Neanderthal: A new look at an old face. *Journal of Human Evolution, 15*(3), 151-164.

Reyes-Centeno, H., Buck, L. T., Stringer, C., & Harvati, K. (2014). *The inner ear of the Eyasi I (Tanzania) and Kabua I (Kenya) hominin fossils*. Paper presented at the African Human Fossil Record, Toulouse.

Rightmire, G. P. (1975). Problems in the Study of Later Pleistocene Man in Africa. *American Anthropologist, 77*(1), 28-52.

Robbins, L. (1972). Archeology in the Turkana District, Kenya. *Science, 176*(4033), 359-366.

Rosas, A. (2001). Occurrence of Neanderthal features in mandibles from the Atapuerca-SH site. *American Journal of Physical Anthropology, 114*(1), 74-91.

Rosas, A., & Bastir, M. (2004). Geometric morphometric analysis of allometric variation in the mandibular morphology of the hominids of Atapuerca, Sima de los Huesos site. *The Anatomical Record Part A: Discoveries in Molecular, Cellular, and Evolutionary Biology, 278A*(2), 551-560.

Sahle, Y., Hutchings, W. K., Braun, D. R., Sealy, J. C., Morgan, L. E., Negash, A., & Atnafu, B. (2013). Earliest Stone-Tipped Projectiles from the Ethiopian Rift Date to >279,000 Years Ago. *PloS One, 8*(11), e78092.

Santa Luca, A. P. (1978). A re-examination of presumed Neandertal-like fossils. *Journal of Human Evolution, 7*(7), 619-636.

Schepartz, L. A. (1987). *From hunters to herders: subsistence pattern and morphological change in eastern Africa.* (Ph.D.), University of Michigan, Ann Arbor.

Shea, J. J., & Hildebrand, E. A. (2010). The Middle Stone Age of West Turkana, Kenya. *Journal of Field Archaeology, 35*(4), 355-364.

Smith, F. H., & Ranyard, G. C. (1980). Evolution of the supraorbital region in Upper Pleistocene fossil hominids from South-Central Europe. *American Journal of Physical Anthropology, 53*(4), 589-610.

Stringer, C. (2016). The origin and evolution of Homo sapiens. *Philosophical Transactions of the Royal Society B: Biological Sciences, 371*(1698).

Stringer, C. B., Hublin, J.-J., & Vandermeersch, B. (1984). The origin of anatomically modern humans in Western Europe. In H. Smith & F. Spencer (Eds.), *The Origins of Modern Humans: a World Survey of the Fossil Evidences* (pp. 51-135). New York: Alan R. Liss.

Tribolo, C., Asrat, A., Bahain, J.-J., Chapon, C., Douville, E., Fragnol, C., Hernandez, M., Hovers, E., Leplongeon, A., & Martin, L. 2017. Across the gap: geochronological and sedimentological analyses from the Late Pleistocene-Holocene sequence of Goda Buticha, southeastern Ethiopia. *PloS One*, *12*, e0169418.

Tryon, C. A., Crevecoeur, I., Faith, J. T., Ekshtain, R., Nivens, J., Patterson, D., . . . Spoor, F. (2015). Late Pleistocene age and archaeological context for the hominin calvaria from GvJm-22 (Lukenya Hill, Kenya). *Proceedings of the National Academy of Sciences, 112*(9), 2682-2687.

Weber, G. W. (2001). Virtual anthropology (VA): A call for Glasnost in paleoanthropology. *The Anatomical Record, 265*(4), 193-201.

Weber, G. W. (2015). Virtual Anthropology. *American Journal of Physical Anthropology, 156*, 22-42.

Weber, G. W., & Bookstein, F. L. (2011). *Virtual Anthropology: A Guide to a New Interdisciplinary Field*. Vienna/New York: Springer.

White, T. D., Asfaw, B., DeGusta, D., Gilbert, H., Richards, G. D., Suwa, G., & Clark Howell, F. (2003). Pleistocene Homo sapiens from Middle Awash, Ethiopia. *Nature, 423*(6941), 742-747.

Whitworth, T. (1960). Fossilized Human Remains from Northern Kenya. *Nature, 185*(4717), 947-948.

Whitworth, T. (1965a). Artifacts from Turkana, Northern Kenya. *The South African Archaeological Bulletin, 20*(78), 75-78.

Whitworth, T. (1965b). The Pleistocene lake beds of Kabua, northern Kenya. *Durham University Journal, 57*, 88-100.

Whitworth, T. (1966). A Fossil Hominid from Rudolf. *The South African Archaeological Bulletin, 21*(83), 138-150.

Wilshaw, A. (2016). The Current Status of the Kenya Capsian. *The African Archaeological Review, 33*, 13-27.

Wood, B. A. (2011). *Wiley-Blackwell encyclopedia of human evolution*. Oxford, UK: Blackwell.

Zollikofer, C. P. E., Ponce De León, M. S., & Martin, R. D. (1998). Computer-assisted paleoanthropology. *Evolutionary Anthropology: Issues, News, and Reviews, 6*(2), 41-54.

Zollikofer, C. P., & Ponce de León, M. S. (2005). *Virtual reconstruction: a primer in computer-assisted paleontology and biomedicine*: Wiley-Interscience.

6. Supplementary Material

Supplementary Table 1. Kabua 1 fragments and their corresponding indices. Four fragments, here designated as Un-900 to Un-903, were too small to be identified securely and were thus not incorporated in the reconstructions. Fragments grouped under EM2471 have been described here but were not included in the reconstructions (see text).

Number	Description
EM2468_01	This fragment is composed of both parietals, as it lies on the sagittal plane, located some distance posterior of bregma. There is slight taphonomic damage on the anterior and posterior portions. Articulates with EM2468_02 and EM2468_13.
EM2468_02	Fragment composed of the posterior right parietal and superolateral right of the occipital bone. Its occipital part consists of both the *planum occipitale*, and the *planum nuchale*. The parietal and occipital parts are separated by the lambdoidal suture, which is expanded due to taphonomic influence and resembles a large fissure. The fragment shows extensive degradation of the external table and multiple circular or semicircular cavities. A true perforation is present in the middle of the lambdoidal suture. Anatomical characteristics include internal occipital protuberance, part of the cruciform eminence, part of the nuchal torus, and superior nuchal lines. Articulates with EM2468_01 to EM2468_08, and EM2468_10.
EM2468_03	Rectangular parietal fragment, positioned anteromedially. This fragment is glued on the ectocranial surface of EM2468_04.
EM2468_04	Lateral right fragment of the *planum occipitale* and *planum nuchale*. The fragment extends towards asterion. Anatomical characteristics: lambdoidal suture and superior nuchal lines. Articulates with EM2468_02, EM2468_03, EM2468_05, EM2468_06, and EM2468_07.
EM2468_05	Lateral right parietal fragment, located inferiorly and of endocranially EM2468_04 due to taphonomic distortion. Articulates with EM2468_04 and EM2468_05 but this articulation is distorted.
EM2468_06	Posterior portion of the right temporal bone. Anatomical characteristics: posteroinferior portion of supramastoid crest and mastoid process. Articulates with EM2468_03, EM2468_05, and EM2468_07.
EM2468_07	Small, triangular shaped, posterior fragment of the right portion of the *planum nuchale*. Articulates with EM2468_04.
EM2468_08	Large fragment that represents the left posterior portion of the left parietal, posterosuperior portion of the right parietal, and the occipital bone. It presents several small cavities and one large perforation, which is roughly 6 mm superior to inferior and 5 mm lateral to medial. Anatomical characteristics include the superior nuchal lines, lambdoidal suture, lambda, and the cruciform eminence. Articulates with EM2468_02, EM2468_09, and EM2468_10.
EM2468_09	Left inferolateral fragment of the *planum nuchale* of the occipital bone. Articulates with EM2468_08.
EM2468_10	This large fragment represents the superior part of the right parietal, left parietal and a small part of the occipital, although this is uncertain due to the absence of a clear lambdoidal suture on this side. Superomedially, there is a large, roughly triangular cavity (13 mm posteroanteriorly) where the outer layers of cranial bone gradually degrade. Anatomical characteristic: temporal line. Articulates with EM2468_01, EM2468_02, EM2468_08, EM2468_11, EM2468_12, EM2468_13, EM2470_18, and EM2470_20.
EM2468_11	Inferolateral fragment of left parietal. Located near the parietomastoid suture. Slight erosion of external table. Articulates with EM2468_10 and EM2471_21

EM2468_12	Small fragment that belongs to the superolateral portion of the left parietal. Articulates with EM2468_10.
EM2468_13	Rounded parietal fragment, posterolateral left of bregma. Articulates with EM2468_10 and EM2468_01.
EM2469_14	Anteriorly positioned frontal fragment. Anatomical characteristics: supraorbital margin, superciliary arch, glabella, lacrimal fossa, and frontal crest. There is a large, likely taphonomic, break on the posterior medial portion, which starts as erosion of the external table and extends as a large fissure that separates EM2469_15 and EM2469_16 Articulates with EM2469_15, and EM2469_17.
EM2469_15	Right lateral, anterior frontal fragment. Forms the right portion of the frontal bone. Large presence of taphonomic fissure in the medial region.
EM2469_16	Right lateral posterior frontal fragment. There seems to be a very weak presence of the coronal suture. Articulates with EM2469_15 and EM2469_17.
EM2469_17	Left lateral frontal fragment. Forms the left portion of the frontal bone. Articulates with EM2469_14 and EM2469_16.
EM2470_18	Small triangular fragment, posterior portion of the left parietal. Articulates with EM2470_19.
EM2470_19	Lateral right parietal fragment. It is broken off around the coronal suture but there are no clear traces of this suture on this fragment. Anatomical characteristic: temporal line. Articulates with EM2470_18, and EM2471_21.
EM2470_20	Small posterosuperior parietal fragment. Articulates with EM2468_10.
EM2470_21	Portion of the left temporal bone and inferior portion of the left parietal. Anatomical characteristics include the temporal squama and parietomastoid suture. Shows extensive erosion of the endocranial surface Articulates with EM2470_22, EM2470_23, EM2470_24, and EM2470_27.
EM2470_22	Small, rectangular, endocranial fragment of the left parietal bone. Articulates with EM2470_20.
EM2470_23	Inferior portion of left temporal squama. Expanded due to matrix in diploic layer. Articulates with EM2470_21, EM2470_24, and EM2470_27.
EM2470_24	Anteroinferior fragment, base of the postglenoid process, located in between the superior and inferior fragments of the left squama. Articulates with EM2470_21, EM2470_23, EM2470_25, and EM2470_27.
EM2470_25	Posterosuperior part of the postglenoid process. Articulates with EM2470_24 and EM247026.
EM2470_26	Anteroinferior part of the postglenoid process and lateral part of the articular eminence. Articulates with EM2470_25.
EM2470_27	Petrous portion of the left temporal. Anatomical characteristics: internal auditory meatus, part of the mastoid process. Articulates with EM2470_21 and EM2470_23.
EM2471_28	Anterosuperior fragment of the right temporal squama, separated into two pieces but joined by sediment. Articulates with EM2471_35.
EM2471_29	Fragment of right temporal squama, protruding anteriorly from EM2471_35. Covered in sediment and separated into two pieces. Superior fragment.
EM2471_30	Fragment of right temporal squama, protruding anteriorly from EM2471_35. Covered in sediment and separated into two pieces. Inferior fragment. Does not articulate directly with EM2471_35.
EM2471_31	Lateral portion of right articular eminence. Articulates with EM2471_35.
EM2471_32	Separate endocranial fragment, medial of the right temporal squama. Articulates with EM2471_35.
EM2471_33	Part of the right sphenoid greater wing (?). Articulates with EM2471_34 and EM2471_35.
EM2471_34	Triangular fragment, anteroinferior endocranial. Articulates with EM2471_33 and EM2471_35.

EM2471_35	Body of the right temporal. Articulates with EM2471_28, EM2471_30, EM2471_31, EM2471_32, EM2471_33, and EM2471_34.
EM2481_36	Anterior fragment of the right maxilla. Retains the first upper incisor, the second upper incisor and the upper canine. Articulates with EM2481_37. Since the articulation seems to be perfect and presence of sediment minimal, this fragment was not segmented.
EM2481_37	Posterior fragment of the right maxilla. Retains P^3 and P^4. Articulates with EM2481_36. Was not segmented.
EM2480_38	Right hemimandible. Retains the second lower incisor, the first lower premolar, the second lower premolar, the second lower molar and the third lower molar. Anatomical characteristics include the upper ascending ramus, coronoid process, sigmoid notch, base of the mandibular condyles, and mandibular corpus. The pieces are not entirely separated, as there is still bone preserved between the middle portion and mandibular corpus and the mandibular ramus, as well as between the middle portion and the anterior part of the mandible. However, as can be seen in Figure 1, most of the gonial angle and the area around the absent first molar have been glued and reconstructed.
Un-900	Small fragment of bone superior of EM2468_06.
Un-901	Small fragment inferior of the left parietal.
Un-902	Small fragment inferior of the left parietal.
Un-903	Very small fragment, located anteroinferior of the maxilla.

Supplementary Table 2. Morphological features described in the manuscript, and associated scores when applicable. For the estimation of sex, numbers range from 1 (feminine) to 5 (masculine).

	Trait	Sex estimation score
Posterior calvaria	Laterally expressed superior nuchal lines	-
	Weakly expressed external occipital protuberance	1
	Weakly expressed cruciform eminence	-
	Shallow suprainiac depression	-
	No projection below lambda	-
	Parietal eminence	-
	Temporal line	-
Frontal	Sharp supraorbital margins	2
	Gracile glabella	1
	Discontinuous supraorbital tori	-
	Metopic suture	-
	Absence of post-toral sulcus	-
	Absence of postorbital constriction	-
	Minimal frontal keeling	-
Temporal	Small mastoid process	2
	Pronounced supramastoid crest	-
Mandible & Maxilla	Robust mylohyoid ridge	-
	Mandibular torus	-
	Deep mandibular corpus	-
	Mandibular symphysis (area not fully preserved)	-
	Possible retromolar gap	-
	Second and third lower molars with distinct roots	-
	Canine fossa (area not preserved)	-

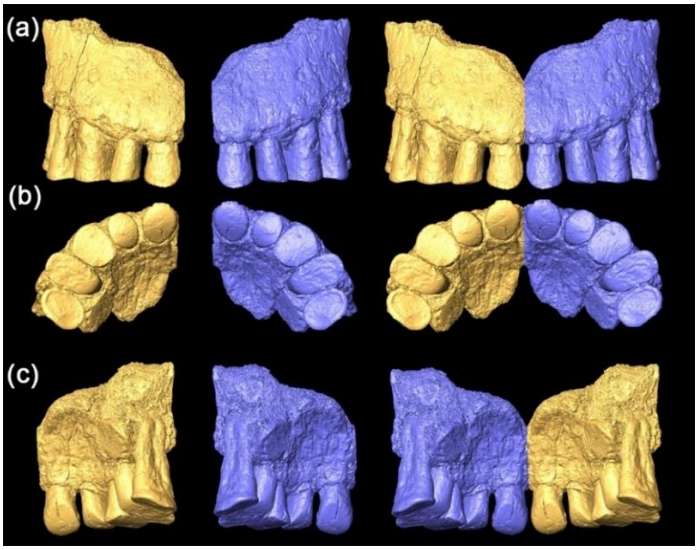

Supplementary Figure 1. Reconstruction of the dental arcade. Yellow: Original fragment, blue: reflection. Each row shows the original fragment, followed by the mirrored fragment and the reconstruction after aligning and merging the original with the mirrored counterpart. (a) Labial view; (b) Ventral view; (c) Lingual view.

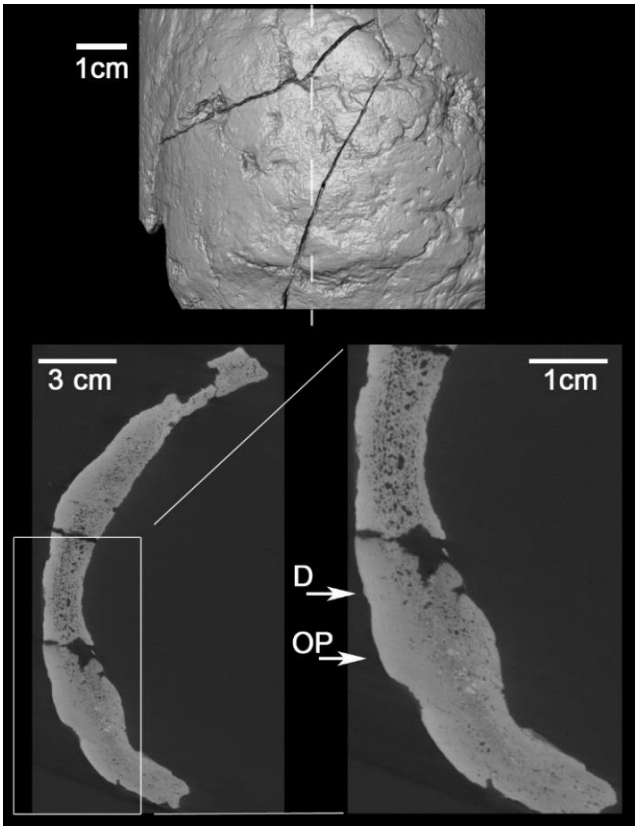

Supplementary Figure 2. Overview image of depression above inion on Kabua 1. Top: Zoom of Kabua 1 in *norma occipitalis*. Dashed line has been added to depict the location of the vertical slice; bottom-left: Vertical slice through the Kabu 1 occipital bone; bottom-right: Zoom on the vertical slice, showing the depression (D) and external occipital protuberance (OP) in detail.

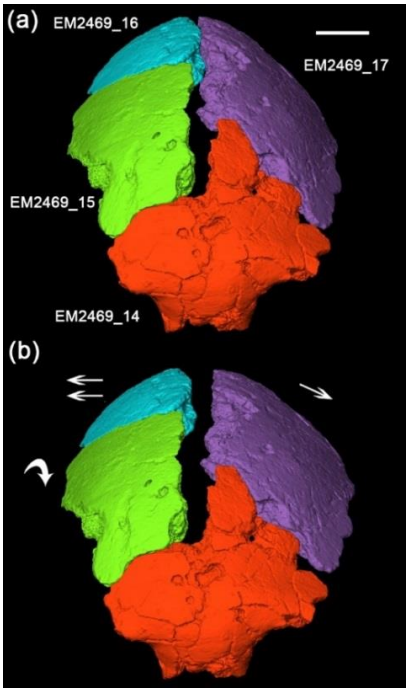

Supplementary Figure 3. Reconstruction of the anatomical articulation between the fragments of the frontal bone. (a) Original position of fragments, segmented from the µCT scanned volume; (b) Fragments EM2469_15 and EM2469_16 are rotated medially and subsequently moved laterally in order to achieve a better articulation between EM2469_14 and EM2469_15 (scale bar = 3 cm).

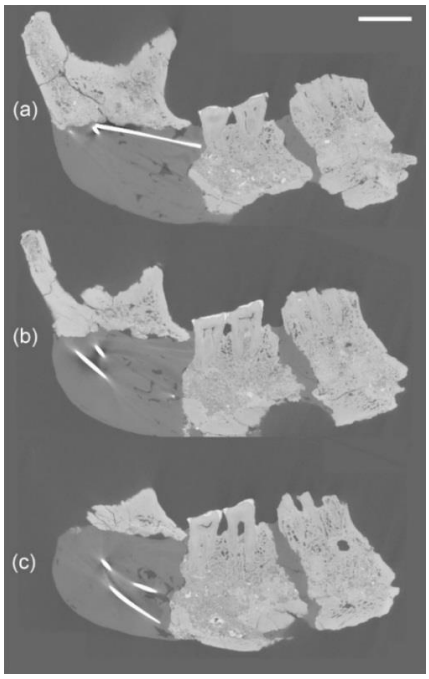

Supplementary Figure 4. Sequence of transverse CT slices through the mandible, buccal to lingual, showing the root morphology of M_2 and M_3. (a) Lingual aspect of M_2 and M_3; (b) Middle of M_2 and M_3; (c) Buccal aspect of M_2 and M_3 (scale bar = 2 cm).

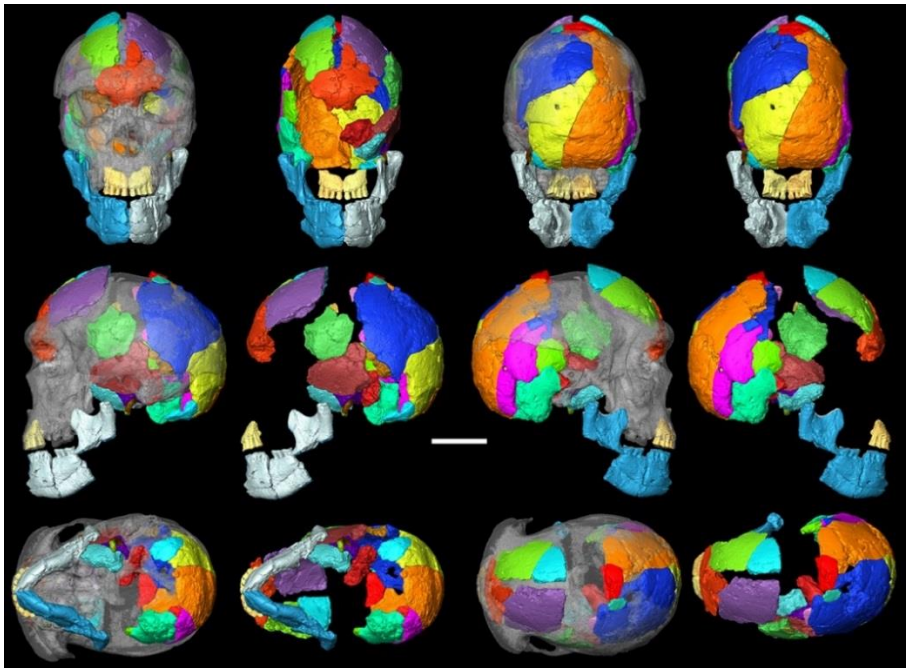

Supplementary Figure 5. Reconstruction of Kabua 1, with Broken Hill as the reference. Each pair of orientations shows the Kabua 1 material, either with or without Broken Hill transparent and superimposed. Top-left: *norma frontalis*; top-right: *norma occipitalis*; center-left: *norma lateralis sinister*; center-right: *norma lateralis dexter*; bottom-left: *norma basilaris*; bottom-right: *norma verticalis* (scale bar = 10 cm).

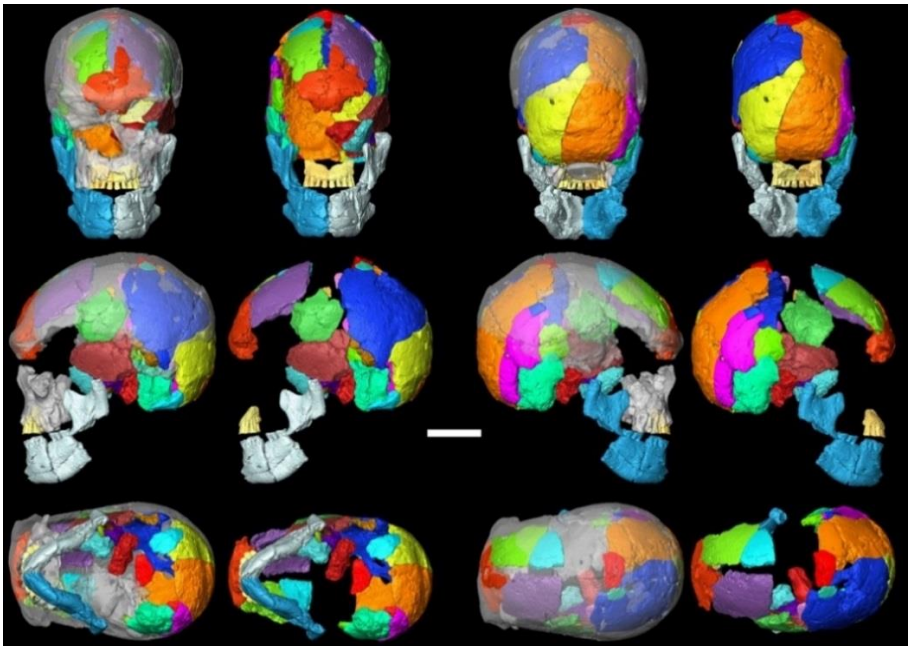

Supplementary Figure 6. Reconstruction of Kabua 1, with Ngaloba LH18 as the reference. Each pair of orientations shows the Kabua 1 material, both with and without Ngaloba LH18 transparent and superimposed. Top-left: *norma frontalis*; top-right: *norma occipitalis*; center-left: *norma lateralis sinister;* center-right: *norma lateralis dexter*; bottom-left: *norma basilaris*; bottom-right: *norma verticalis* (scale bar = 10 cm).

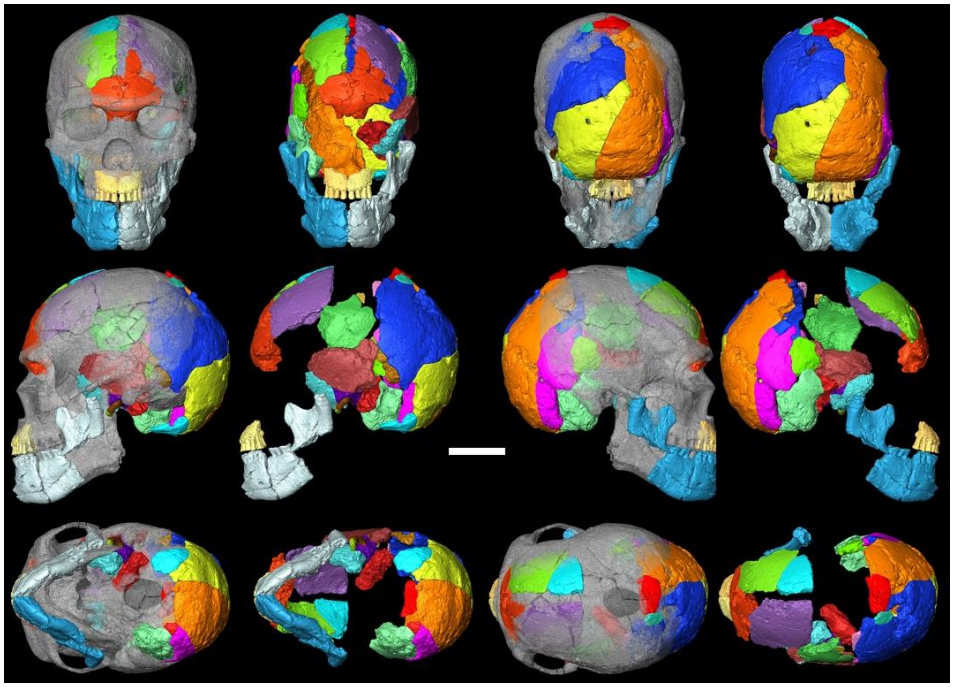

Supplementary Figure 7. Reconstruction of Kabua 1, with Skhūl V as the reference. Each pair of orientations shows the Kabua 1 material, both with and without Skhūl V transparent and superimposed. Top-left: *norma frontalis*; top-right: *norma occipitalis*; center-left: *norma lateralis sinister*; center-right: *norma lateralis dexter*; bottom-left: *norma basilaris*; bottom-right: *norma verticalis* (scale bar = 10 cm).

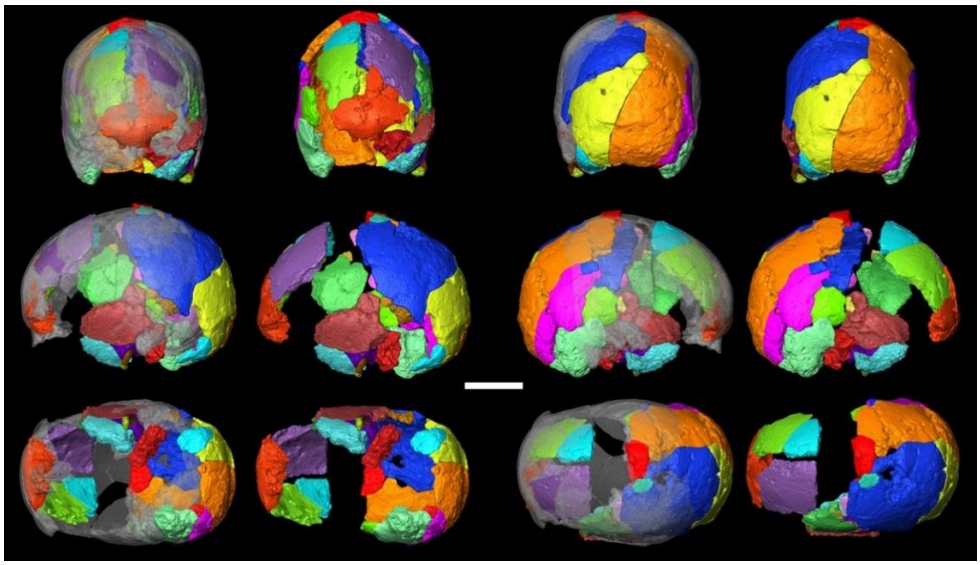

Supplementary Figure 8. Reconstruction of Kabua 1, with Mumba X as the reference. Each pair of orientations shows the Kabua 1 material, both with and without Mumba X transparent and superimposed. Top-left: *norma frontalis*; top-right: *norma occipitalis*; center-left: *norma lateralis sinister*; center-right: *norma lateralis dexter*; bottom-left: *norma basilaris*; bottom-right: *norma verticalis* (scale bar = 10 cm).

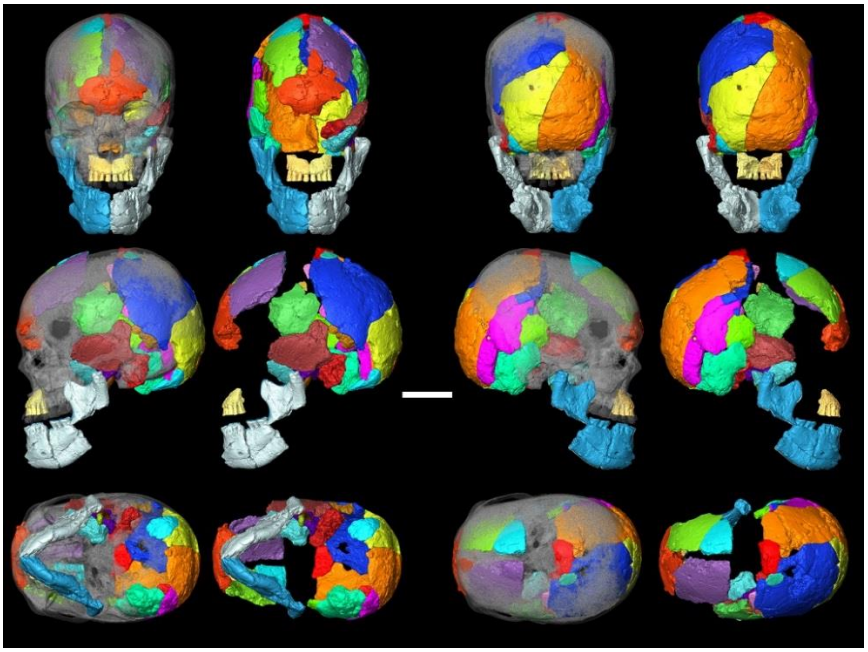

Supplementary Figure 9. Reconstruction of Kabua 1, with Masai 03 as the reference. Each pair of orientations shows the Kabua 1 material, both with and without Masai 03 transparent and superimposed. Top-left: *norma frontalis*; top-right: *norma occipitalis*; center-left: *norma lateralis sinister*; center-right: *norma lateralis dexter*; bottom-left: *norma basilaris*; bottom-right: *norma verticalis* (scale bar = 10 cm).

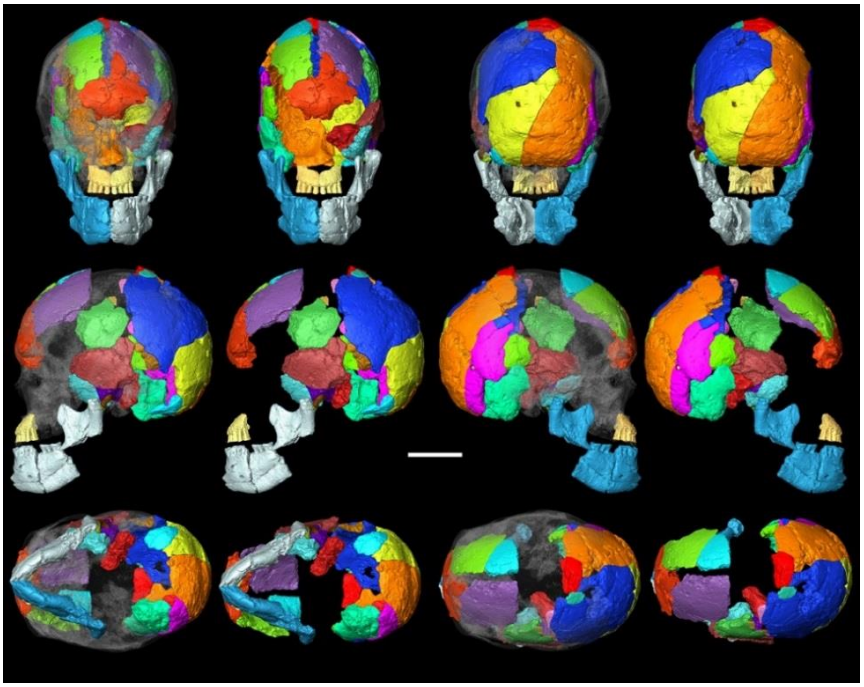

Supplementary Figure 10. Reconstruction of Kabua 1, with Masai 10 as the reference. Each pair of orientations shows the Kabua 1 material, both with and without Masai 10 transparent and superimposed. Top-left: *norma frontalis*; top-right: *norma occipitalis*; center-left: *norma lateralis sinister*; center-right: *norma lateralis dexter*; bottom-left: *norma basilaris*; bottom-right: *norma verticalis* (scale bar = 10 cm).

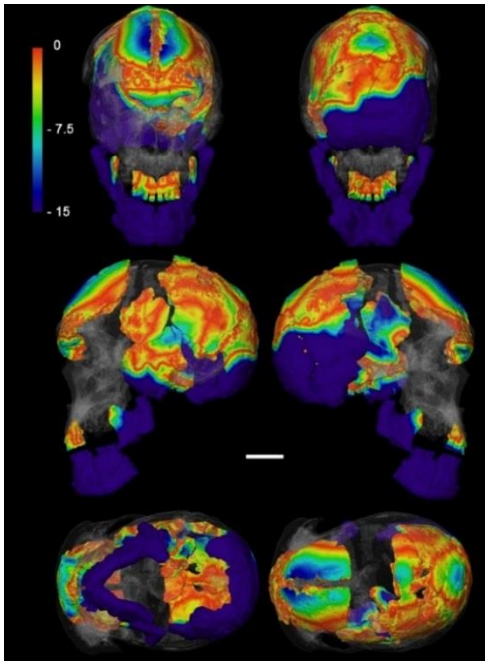

Supplementary Figure 11. Surface displacement model of the Kabua 1 reconstruction and Broken Hill as the reference (transparent). Scale of colormap: 0 – 15 mm deviation. Top-left: *norma frontalis*; top-right: *norma occipitalis*; center-left: *norma lateralis sinister*; center-right: *norma lateralis dexter*; bottom-left: *norma basilaris*; bottom-right: *norma verticalis* (scale bar = 5 cm).

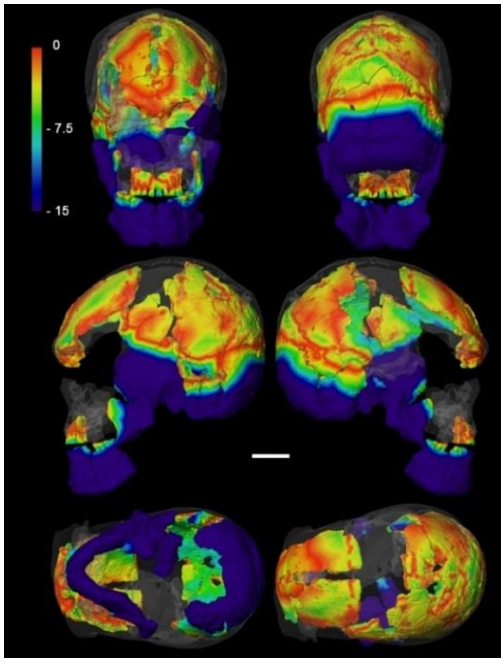

Supplementary Figure 12. Surface displacement model of the Kabua 1 reconstruction and Ngaloba LH18 as the reference (transparent). Scale of colormap: 0 – 15 mm deviation. Top-left: *norma frontalis*; top-right: *norma occipitalis*; center-left: *norma lateralis sinister*; center-right: *norma lateralis dexter*; bottom-left: *norma basilaris*; bottom-right: *norma verticalis* (scale bar = 5 cm).

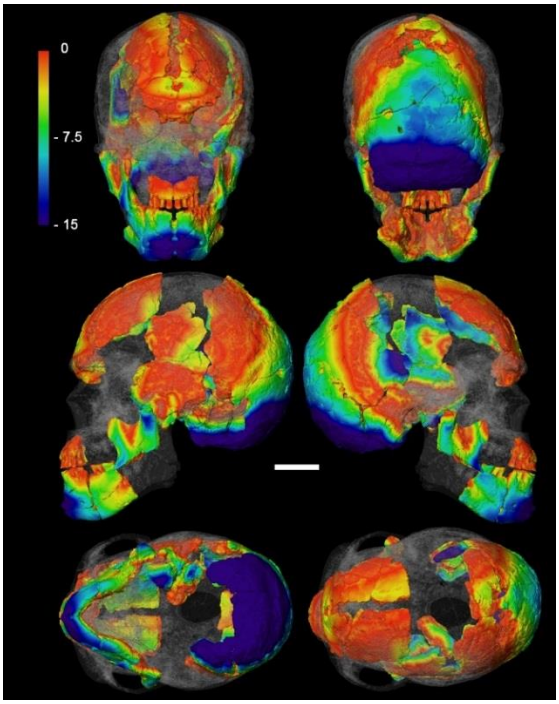

Supplementary Figure 13. Surface displacement model of the Kabua 1 reconstruction and Skhūl V as the reference (transparent). Scale of colormap: 0 – 15 mm deviation. Top-left: *norma frontalis*; top-right: *norma occipitalis*; center-left: *norma lateralis sinister*; center-right: *norma lateralis dexter*; bottom-left: *norma basilaris*; bottom-right: *norma verticalis* (scale bar = 5 cm).

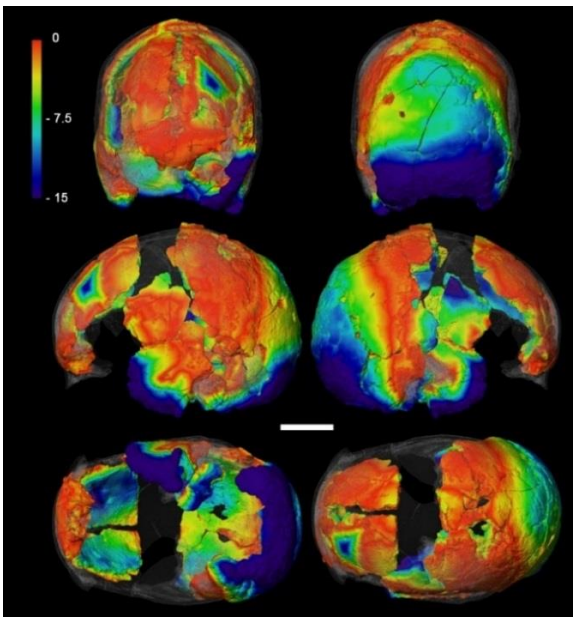

Supplementary Figure 14. Surface displacement model of the Kabua 1 reconstruction and Mumba X as the reference (transparent). Scale of colormap: 0 – 15 mm deviation. Top-left: *norma frontalis*; top-right: *norma occipitalis*; center-left: *norma lateralis sinister*; center-right: *norma lateralis dexter*; bottom-left: *norma basilaris*; bottom-right: *norma verticalis* (scale bar = 5 cm).

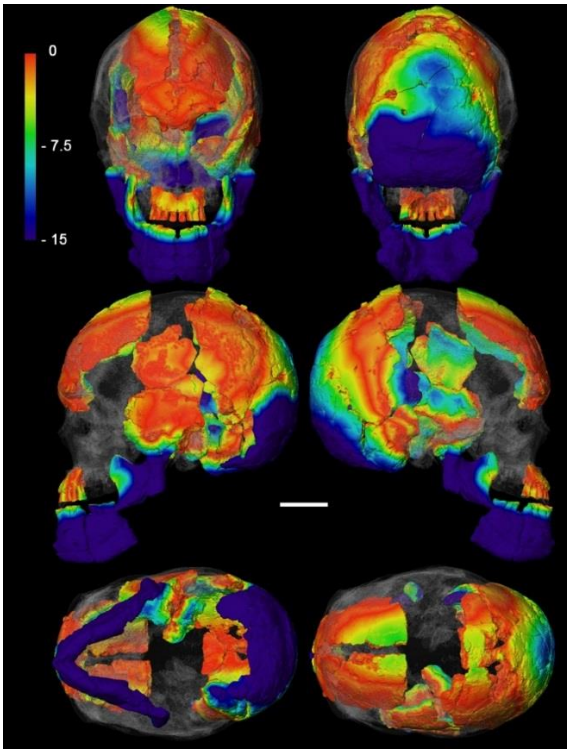

Supplementary Figure 15. Surface displacement model of the Kabua 1 reconstruction and Masai 10 as the reference (transparent). Scale of colormap: 0 – 15 mm deviation. Top-left: *norma frontalis*; top-right: *norma occipitalis*; center-left: *norma lateralis sinister*; center-right: *norma lateralis dexter*; bottom-left: *norma basilaris*; bottom-right: *norma verticalis* (scale bar = 5 cm).

Appendix II

"*[The stones] began to lose their rigidity and hardness, and after a while softened, and once softened acquired new form. Then after growing, and ripening in nature, a certain likeness to a human shape could be vaguely seen, like marble statues at first inexact and roughly carved. The earthy part, however, wet with moisture, turned to flesh; what was solid and inflexible mutated to bone…*"

Ovid – *Metamorphoses Book I*, 381-415. Translated by A.S. Kline.

A geometric morphometric analysis of the Kabua 1 cranium

Abstract

The taxonomic affiliation of the adult fossilized Kabua 1 cranium from Turkana (Kenya) remains unknown. While initial descriptions stress the presence of multiple plesiomorphic characteristics, researchers have suggested that this specimen instead falls within recent anatomically modern human variation. This is supported by a recently constructed set of virtual anatomical reconstructions. However, the reproducibility of these reconstructions as well as all assessments of taxonomic affiliation were primarily qualitative in nature. Here we apply 3D geometric morphometric analyses to the previously created set of virtual reconstructions of the Kabua 1 cranium. We also apply advanced machine learning algorithms (*k*-Nearest Neighbors and Random Forests) directly to the acquired shape data. The comparative sample includes Neanderthals, Middle Pleistocene European and African specimens, as well as a wide variety of Late Pleistocene and recent anatomically modern *H. sapiens*. A Principal Component analysis, Procrustes distances and the majority of *k*-Nearest Neighbor and Random Forest models result in the Kabua 1 reconstructions plotting within the range of variation of our recent *H. sapiens* sample. In contrast, a Linear Discriminant analysis classifies the reconstructions primarily as Middle Pleistocene African. Overall, our results strengthen the hypothesis that Kabua 1 is representative of recent modern variation, while retaining several plesiomorphic characteristics by which it falls on the border of known Late Pleistocene/recent *H. sapiens* variation. As a result, Kabua 1 might be an example of deep population structure in the African Late Pleistocene, similar to specimens such as Nazlet Khater, Iwo Eleru, and Hofmeyr. As such, it potentially affords an insight into the morphological variation present in eastern Africa and the African continent in general.

In preparation for the American Journal of Physical Anthropology

Bosman, A. M., Buck, L. T., Reyes-Centeno, H., Mirazón Lahr, M., Stringer, C., & Harvati, K. (in prep). A geometric morphometric analysis of the Kabua 1 cranium.

1. Introduction

New techniques and advances in virtual anthropological methods have enabled us to study the evolution of *H. sapiens* in great detail (e.g. Gunz et al., 2019). However, partially due to the fragmented nature of the fossil record, large gaps in our knowledge about the emergence of anatomically modern traits in the late Middle and Late Pleistocene remain (e.g. Bräuer, 2008; Pearson, 2013; Schwartz & Tattersall, 2010; Stringer, 2016). Moreover, the fossil record of the African continent is generally underrepresented when compared to the European record, even though certain regions within Africa have been proposed as critical in the emergence of early *H. sapiens* (e.g. Grine et al., 2007; Hublin et al., 2019; Rightmire, 2001, 2009; White et al., 2003), as well as eventual dispersals of anatomically modern *H. sapiens* into Eurasia (Gunz et al., 2009a; Mirazón Lahr, 2016; Reyes-Centeno et al., 2014a). Additionally, lesser known sites from Africa are disregarded in favor of finds from new excavations and surveys in more well-known localities, even though these carefully curated materials hold the potential to frame more recent materials and can shed light on current issues in paleoanthropology (e.g. Buck & Stringer, 2015; Tryon et al., 2015, 2019). As such, the hominin remains from Kabua, currently located in the Natural History Museum in London as part of the Palaeoanthropology collection (Buck & Stringer, 2015), might constitute a critical contribution. These skeletal assemblages were excavated in 1959 in Kenya and consist of at least three individuals (Kabua 1-3; Whitworth, 1966). Kabua 1 (K1) is the most complete individual and is represented by a fragmented calvaria, a right hemimandible, and a right maxillary fragment. Possibly representing an adult male (Schepartz 1987), this individual has been proposed to date to the Late Pleistocene (Whitworth, 1960, 1965a, 1965b), although the lack of a robust geochronological and archaeological context prohibits a robust assessment (Bosman et al., 2019; Buck & Stringer, 2015). While direct ESR and U-series dating is currently underway, a Late Pleistocene-Holocene geochronological age range seems to be the most conservative estimate, based on circumstantial evidence gathered from the sediment from which the Kabua fossils were presumably recovered (e.g. Buck & Stringer, 2015; Owen et al., 1982; Robbins, 1992).

As for the taxonomic affiliation of the K1 cranium, Whitworth (1960, 1966) proposed that this specimen retained several plesiomorphic traits such as thick cranial walls, a low and sloping frontal bone, thick supraorbital tori, and a retromolar gap, which resulted in Whitworth suggesting certain "Neanderthaloid" affinities for the fossil material. In contrast, other scholars have argued that K1 possesses a more modern morphology (Phenice, 1972; Rightmire, 1975; Schepartz, 1987). Through an extensive analysis of the K1 cranium, Bosman et al. (2019) demonstrated that this specimen mostly exhibits anatomically modern features, suggesting a *H. sapiens* taxonomic attribution. This was supported by a set of virtual anatomical reconstructions, in which six reference crania were used to limit the degrees of freedom that non-articulating fragments could move in virtual space (Figure 1). However, the results presented in this study were primarily qualitative in nature and the robusticity and repeatability of the applied reconstruction procedures as well as the taxonomic affiliation of the K1 cranium could not be rigorously determined.

We address these issues in the current study by performing a quantitative analysis the aforementioned virtual reconstructions. We focus on neurocranial shape, as this skeletal element has been proposed to have evolved primarily under neutral conditions (Athreya, 2009; Harvati & Weaver, 2006; Hubbe et al., 2009), and is the taxonomically most diagnostic area of the K1 cranium. Based on previous works (e.g. Bosman et al., 2019, Rightmire, 1975), we hypothesize that the K1 cranium can be designated as *H. sapiens.* As such, we predict that the overall neurocranial shape of the K1 reconstructions will align with other *H. sapiens* and thus will fall within the range of variation of this group. This hypothesis is rejected if K1 reconstructions align with more pleisomorphic fossil specimens, such as those from Middle Pleistocene Africa or Eurasia.

To this end, we use a suite of methods that are often used concertedly and have been collected under the denomination of geometric morphometrics (Adams et al., 2004; Mitteroecker & Gunz, 2009; Mitteroecker et al., 2013). These methods include the placement of three-dimensional Cartesian coordinates, otherwise known as landmarks, to

capture neurocranial shape and asses the morphological variation present in the K1 reconstructions. These data are then compared to shape data derived from a larger comparative sample which consists of late Middle and Late Pleistocene specimens of the genus *Homo,* as well as a number of recent *H. sapiens* crania from Africa, through the application of Generalized Procrustes Analysis (GPA) and Principal Component Analysis (PCA). Furthermore, the shape data generated by these analyses are used in a set of classification procedures, including Linear Discriminant Analysis (LDA), and two machine learning (ML) algorithms: *k*-Nearest Neighbors (*k*-NN), and Random Forests (RF). These results are combined with previous qualitative observations on the K1 fragments and reconstructions, in order better discuss this fossil within the context of hominin cranial shape variation and evolution of *H. sapiens* in eastern Africa from the Middle-Late Pleistocene onwards.

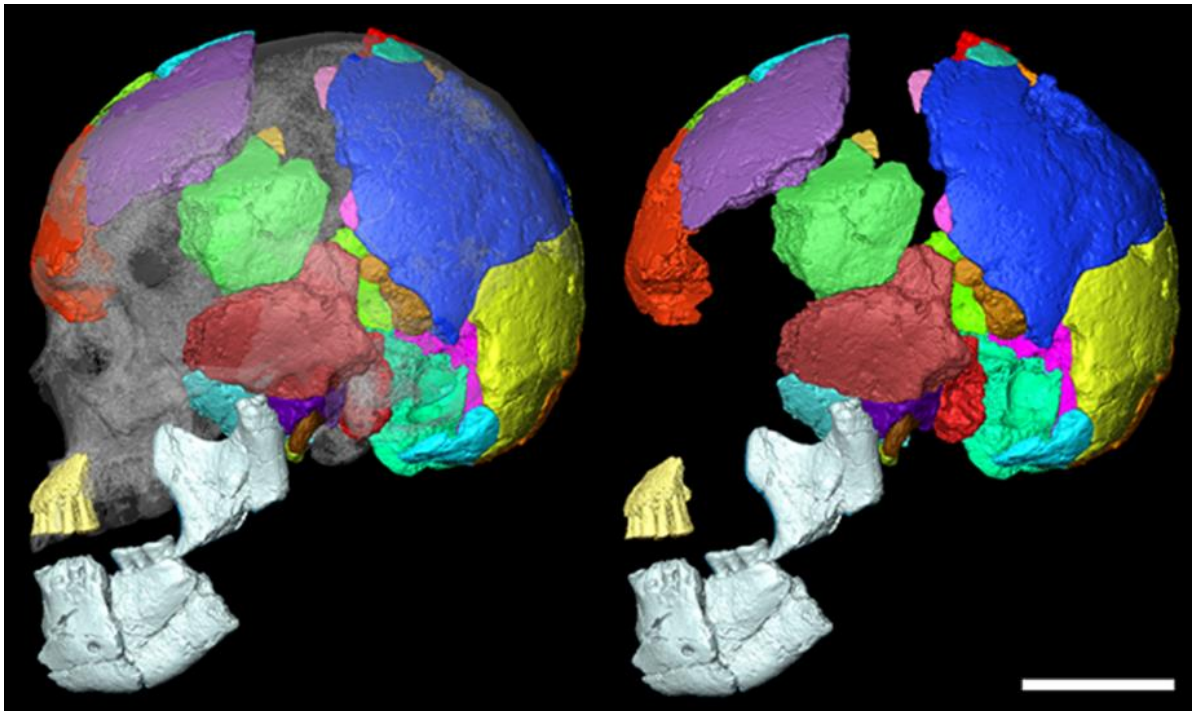

Figure 1. Virtual anatomical reconstruction of the Kabua 1 cranium (colored fragments) in *norma lateralis sinister*. On the left, the fragments are superimposed on the anatomically modern *H. sapiens* reference cranium Masai 10, Tanzania (gray, transparent). All virtual reconstructions referred to in the text are described and visualized in Bosman et al., 2019 (scale bar = 10 cm).

2. Materials and Methods

The K1 fragments were scanned with a Nikon Metrology HMX ST 225 µCT scanner, located at the Natural History Museum in London. Detailed descriptions of the specimen can be found in Whitworth (1960, 1966) and Bosman et al. (2019). Both the geometric similarities of the fracture surfaces and anatomical features were used to reassemble the fragments. In order to reassemble fragments that do not directly articulate and limit their degrees of freedom, the relevant anatomical information was interpolated from a variety of symplesiomorphic crania. Six crania were selected for their morphology, state of preservation, geographical location, availability, and assumed peri-contemporaneity with Kabua. These crania were additionally selected to represent different geochronological periods and morphologies present in the genus *Homo*, in order to test several competing evolutionary scenarios, given the hypothesis outlined in the introduction and the unknown geological context of the K1 specimen. These crania include; Broken Hill (Woodward, 1921), Ngaloba LH18 (Day, 1980), Skhūl V (McCown, 1939), Mumba X (Bräuer, 1983; Reck & Kohl-Larsen, 1936) Masai 3 (Kohl-Larsen, 1941), and Masai 10 (Kohl-Larsen, 1941; Figure 1). This procedure resulted in six virtual reconstructions of the K1 cranium, each based on a different reference cranium (Bosman et al., 2019).

The comparative sample used in the geometric morphometric analyses comprises several Middle-Late Pleistocene hominin fossils from Africa and Eurasia. This dataset was primarily collected by one of the authors (KH) using a Microscribe G2X portable digitizer (Immersion Corp, 1998). The remainder of the dataset consists of 109 recent anatomically modern *H. sapiens* crania from eastern Africa and South Africa, collected by HRC and KH respectively, also using a Microscribe digitizer. The crania were previously selected on the basis of adult ontogeny and the absence of any pathologies or severe taphonomic distortions (Table 1).

Table 1. Comparative sample used in the geometric morphometric analyses.

Group	n	Specimens
Middle Pleistocene Europeans (MPE)	3	Dali (Dali)*, Sima 5 (SH05), Petralona (Petr)
Middle Pleistocene Africans (MPA)	4	Broken Hill (BrH)†, Saldanha (Sald), Ihroud 1 (Ir01), Ihroud 2 (Ir02)
H. neanderthalensis (NEA)	8	Amud 1 (Am01), Feldhofer 1 (Fel1)* , Guattari 1 (Gua1)†, La Chapelle 1(LaC1), La Ferrassie 1 (LaF1), Quina 5 (LQn5), Spy I (Sp01), Spy II (Sp02)
Recent H. sapiens (RHS)	130	
Late Pleistocene	21	Afalou 12 (AF12)†, Brno 2 (BRN2), Cro-Magnon 1 (CRM1), Cro-Magnon 2 (CRM2), Cro-Magnon 3 (CRM3), Dolní Věstonice 3 (DV03), Dolní Věstonice 13 (DV13), Dolní Věstonice 15 (DV15), Dolní Věstonice 16 (DV16), Mumba 10 (Mumb)†, Nazlet Khater 2 (NZKH), Ngaloba LH18 (LH18)†, Pavlov 1 (PAV1), Predmosti 3 (PRD3)*, Predmosti 4 (PRD4)*, Qafzeh 9 (Qa09), Skhūl 5 (Skl5), Taforalt 11 C1U (IT11)†, Taforalt 15 C4U (IT54)†, Taforalt 15 C5U (IT55)†, Taforalt 18 C1U (IT18)†
Holocene	109	Amhara (n =2; AM), Danakil (n =2; DA), Ethiopian (n = 10; ET), Igai (n = 1; IGAI), Kenya (n = 3; Ke), Kokoro (n = 1; Koko), Masai (n = 2; MA)†, Pouma (n = 1; Poum), San from Museum of Cape Town (n = 54; SA), San from University of Cape Town (n = 7; UC), Somalia (n = 1; Soma), Turkana (n = 2; TU), Zulu (n = 23; ZU)
Kabua reconstructions	6	Kabua-Broken Hill (K-BrH), Kabua-Ngaloba LH18 (K-LH18), Kabua- Skhūl V (K-Skl5), Kabua-Mumba X (K-Mumb), Kabua-Masai 3 (K-Ma03), Kabua-Masai 10 (K-Ma10).

* Specimens for which high-quality casts or stereolithographs were measured.
† Specimens for which we had access to CT-data.

Six fixed landmarks (Type I and Type II; Weber & Bookstein, 2011) were placed on the multiple anatomical reconstructions of the K1 cranium (Bosman et al., 2019; Table 2) using the Avizo Lite (FEI Visualization Sciences Group, versions 9.0.1 and 9.2.0). Additionally, two curves of Type IV semi-landmarks were designated in the same virtual environment (Table 2). These coordinates were chosen to adequately represent neurocranial morphology. As for the comparative sample, the dorsal-ventral-left-right fitting program (DLVR; http://pages.nycep.org/nmg/programs.html) was used to process the Microscribe-derived data. Subsequently, Resample (http://pages.nycep.org/nmg/programs.html) was used to make the Type IV curve semi-landmarks equidistant via weighted linear interpolation. Missing landmarks and curve semi-landmarks were reconstructed by reflected relabeling of

the bilateral homologue (Mardia et al., 2000; Supplementary Table 1) in the program Morpheus (Slice, 2013) or by applying a function based on the publication by Claude (2008) in R, version 3.5.0 (R Core Team, 2019). All subsequent data preparation steps and analyses were also performed in R, version 3.5.0.

Table 2. Landmarks used in this study. (B) indicates which landmarks are bilateral. Additionally, for the curve semi-landmarks (Type IV) the number of landmarks are noted.

Landmark	Description	Type
Asterion (B)	Meeting point of the temporal, parietal, and occipital bones	I
Glabella	Most anterior midline point on the frontal bone	II
Inion	Point at which the superior nuchal lines merge in the midline	I
Parietal Notch (B)	Point on the posterosuperior border of the temporal bone	I
Midsagittal Profile	Curve from glabella to inion, through bregma and lambda	IV (n=26)
Lambdoid Suture (B)	From asterion (right) to lambda to asterion (left)	IV (n=14)

To assess intra-observer error, one of the crania from the comparative sample (Skhūl V) was landmarked five times. These repetitions were used in the determination of the coefficient of variation (CV; Corner et al., 1992), which is calculated according to the formula:

$$CV = \frac{\sigma}{\mu} * 100$$

where μ is the mean and σ is the standard deviation of each fixed landmark across the five repetitions. Subsequently, the landmarks and semi-landmarks were superimposed with a Generalized Procrustes Analysis (GPA; geomorph: Adams et al., 2019). This is a least-squares method which estimates the parameters for the location and orientation that minimize the sum of squared distances between corresponding points on the individuals in the sample (Slice, 2011). Because all differences in location, isometric scale, and orientation are removed during this procedure, any differences between corresponding landmarks will be the result of differences in shape or allometric size (Webster & Sheets, 2010). During this procedure, the semi-landmarks were slid along their curves to make them homologous between specimens, using the minimized bending energy criterion (Gunz et al., 2009b; Perez et al., 2006). Mardia's test (MVN: Korkmaz, Goksuluk, & Zararsiz, 2014) was used to assess multivariate normality. The Procrustes superimposed coordinates were subsequently

analyzed using Principal Component Analysis (PCA) and Procrustes distances, which represent the square root of the summed squared distances between homologous landmarks. The PCA was performed by first computing the eigenvalues and PC scores using the entire sample, excluding the K1 reconstructions. The latter were projected in PC shape space by using the computed PC scores. Differences between the maximal PC scores were visualized using thin plate spline (TPS) relative warps (Bookstein, 1989). The Auer-Gervini method (Auer & Gervini, 2008, PCDimensions: Wang et al., 2018) was used to retrieve the number of significant Principal Components. Additionally, we computed a neurocranial shape index, following Gunz et al. (2019) and Harvati et al. (2019), using the mean PC scores of the Neanderthal and the Holocene *H. sapiens* groups and projecting all other specimens on this axis.

Statistical assumptions concerning the Procrustes superimposed coordinates and significant PC scores were tested using Shapiro-Wilk tests for univariate normality (Shapiro & Wilk, 1965), Mardia measures of multivariate skewness and kurtosis (Mardia, 1970), Kaiser-Meyer-Olkin test for sampling adequacy (Kaiser, 1970; Kaiser & Rice, 1974; psych: Revelle, 2018), Fligner-Killeen test of homogeneity of variance (Fligner & Kileen, 1976), and Cook's distance for multivariate outliers (Cook & Weisberg, 1982). Subsequent to this assumption testing, a Linear Discriminant Analysis (LDA) was performed on the significant PC's, with equal prior probabilities for all groups, and jackknife cross-validation. LDA is a supervised classification procedure that separates or classifies specimens through linear combination of features and maximization of variance between groups. However, LDA is sensitive to multicollinearity, non-normal distributions, outliers, and highly dimensional data. As such, classifications of the K1 reconstructions were verified with two non-parametric ML algorithms, *k*-Nearest Neighbors (*k*-NN) and Random Forests (RF). *k*-NN is a supervised technique, which uses Euclidean (in this case Procrustes) distances between individuals in order to classify unknowns based on a plurality vote by its *k*-nearest neighbors (Ripley, 1996). The number of nearest neighbors considered for the *k*-NN analysis was arbitrarily set at three, as the smallest group in our sample (MPE) contains only three individuals.

RF similarly fall under the non-parametric machine learning methods (Breiman, 2001) and predict a categorical dependent variable based on measurements and/or observations on multiple continuous or nominal variables through a set of nodes. In this, RF are similar to normal classification trees, which can take any type or multiple types (nominal, ordinal, continuous) of input variables and classify new individuals according to a training data set which selects the most relevant variables (Hefner et al., 2014). As such, changes in the training dataset will result in different trees and results. However, RF differ from standard classification trees as they bootstrap the original training set, leading to a randomized subset of the training data used for each tree (Breiman, 2001). Additionally, while in standard classification trees all variables are used at each node to make a decision, RF incorporate random bagging of variables, which are split or separated at each node. Essentially, bagging is a method of generating new sets of randomly selected variables from the complete set of variables (Breiman, 2001). This procedure averages many low-bias and high-variance predictors, thereby reducing the variance without increasing bias and thus reduces the effect of multicollinearity (Navega et al., 2015). In our study, we let the model search for the best performing number of variables to split at each node, ranging from one to the maximal number of variables in the sample.

One downside of ML models such as *k*-NN and RF is that they are affected by the so called class imbalance problem (Japkowicz, 2000). This problem arises if one class or group is only represented by a few specimens, while another contains a large number of specimens. Consequently, the classification of unknown individuals will be skewed towards the larger group. In our study, the RHS group is represented by 130 individuals, while the other groups contain fewer specimens (Table 1). As such, the *k*-NN and RF analyses were applied on an adjusted dataset in which the RHS group was reduced in size by random resampling over 1000 iterations. To check for multiple scenarios arising from differences in sample sizes, we ran the *k*-NN four times, each of the 1000 iterations possessing a set number of randomly resampled RHS. These randomly resampled RHS groups were set at the number of

individuals in each of the other represented groups (n =3, n = 4, n = 8) and one arbitrary number (n = 10). All classification analyses were run with the caret package (Kuhn, 2008), with dependencies on the ranger (Wright & Ziegler, 2017) and MASS (Venables & Ripley, 2002) packages in R, version 3.5.0. Additionally, the agreement between prior and posterior group assignments was determined on a validation set randomly extracted from the training data with a confusion-matrix derived estimation of correct classification as well as the Cohen's Kappa statistic. This statistic returns a result between zero and one, where zero represents an agreement equivalent to chance and one represents perfect agreement (Cohen, 1960).

3. Results

Descriptions of Kabua 1 and comparisons of the six virtual reconstructions are detailed in Bosman et al. (2019) and thus not discussed here. The intra-observer measurement error for the fixed landmarks, as calculated with the coefficient of variation (CV), is quite low with an average CV of 0.436% across all landmarks, while the highest CV is 1.23 % at inion (Table 3).

Table 3. Summary statistics for the error test, based on a single specimen (Skhūl V). The means and standard deviations per landmark are calculated on the square root of the sum of squared coordinates.

Landmark	Mean	Standard deviation	Coefficient of variation (cv) in %
Asterion Left	20.793	0.073	0.353
Asterion Right	25.91	0.034	0.132
Glabella	25.002	0.075	0.302
Inion	18.292	0.225	1.230
Parietal Notch Left	23.235	0.075	0.322
Parietal Notch Right	22.294	0.062	0.279
Average of landmarks	21.923	0.091	0.436

The results from the PCA with the groups outlined in Table 1 show that the first principal component (PC1) accounts for 26.9% of the total variance and separates Neanderthals and Middle Pleistocene European specimens from recent *H. sapiens* (Figure 2). This component reflects differences in the overall antero-posterior shape of the neurocranium, which varies

from an elongated and low vault, to a rounded and antero-posteriorly short vault (Figure 2; Supplementary Figure 1). Additionally, the negative end of PC1 is represented by medio-laterally wide lambdoidal sutures. On the positive end of PC1, the upper parts of the lambdoidal sutures are closer to the midline, representing an ovoid occipital bone. The Neanderthal and Middle Pleistocene hominins are located on the extreme negative of this axis, which represents their generally elongated neurocranial shape in lateral view. On the other hand, recent *H. sapiens* are situated predominantly on the positive end of PC1. The Middle Pleistocene African specimens are positioned on the negative end of PC1 but without overlapping with the Neanderthal and Middle Pleistocene European groups. All of the K1 reconstructions are located within the hull of the recent *H. sapiens*. The K-LH18 reconstruction is closest to the MPA group but still within the recent *H. sapiens* convex hull. The K-Skl5 reconstruction is somewhat of an outlier of the K1 reconstructions, as this specimen is near the extreme positive of the first principal component, corresponding to the globular shape of its neurocranium in lateral view. The other four reconstructions (K-BrH, K-Ma03, K-Ma10, K-Mumb) all plot within the RHS convex hull, close to each other and RHS individuals.

The second principal component (PC2) accounts for 16.5 % of total variance (Figure 2). This principal component does not reflect a strong separation between groups, but rather represents intragroup variation. Crania with positive scores on PC2 display a more vertically oriented frontal bone and a somewhat greater occipital curvature in lateral view. Medio-laterally, these crania have wide shapes, with the lambdoid suture located relatively high, resulting in an "egg"-like appearance of the *planum occipitale*. Crania with negative scores exhibit sloping, more horizontally oriented frontals, low lambdoidal sutures, and a lower occipital curvature. The occipital bones of these specimens are more squat and square-like in shape (Figure 2, Supplementary Figure 2). The specimens that belong to the Neanderthal and recent *H. sapiens* groups are spread around the entirety of PC2, with Feldhofer, Amud, and Mumba 10 nearing the extremes. The MPA specimens are positioned mostly on the negative end of this axis, reflecting their low lambdoid sutures and short nuchal planes.

Similarly, the K1 reconstructions are located on the negative end of this axis, reflecting their short nuchal planes, more sloping frontal bone, flat glabellar region, and overall narrow neurocranium.

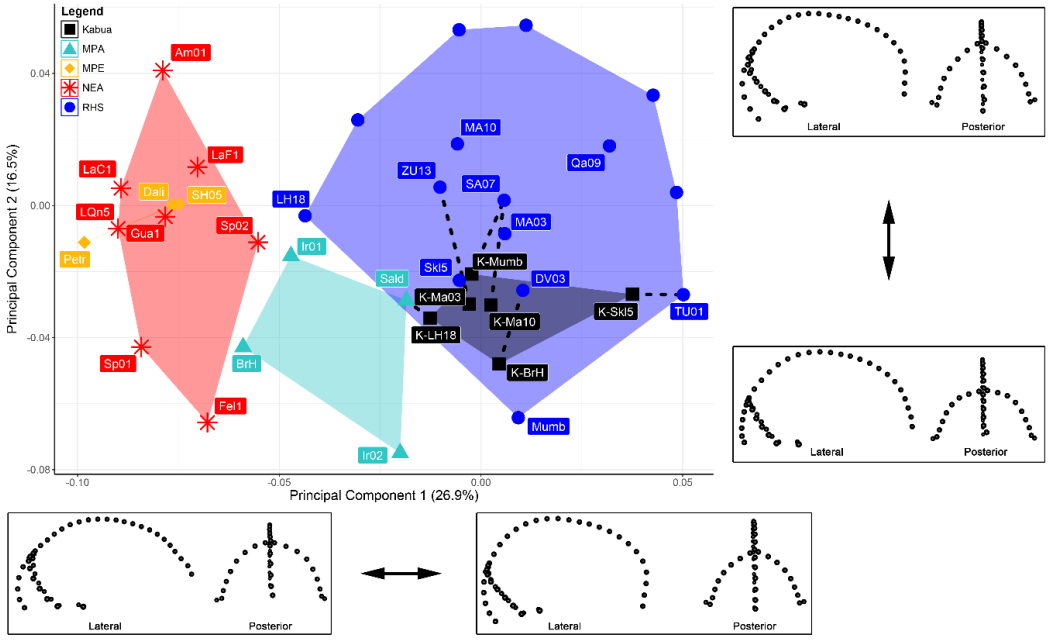

Figure 2. PCA of comparative sample (PC1 vs PC2). Of the RHS group, only nearest neighbors to reconstructions and the reference crania used in the virtual reconstructions are depicted. PC1 shape changes below the plot reflect the modern human-like rounded neurocranium (positive) vs low and elongated neurocranium. PC2 shape changes to the right of the plot reflect intraspecific variation in flatness of the anterior frontal bone and curvature of the lambdoid suture. Abbreviations specified in Table 1.

The K1 reconstructions have relatively large Procrustes distances to the comparative sample in Procrustes shape space (Figure 3). Additionally, all of the reconstructions have another reconstruction as their closest neighbor. None of the reconstructions are particularly close to their respective reference crania, except the reconstruction based on Masai 3 (Table 4; K-Ma03). Moreover, the reconstruction based on Masai 3 is the basal node of all reconstructions, in turn displaying the shortest inter-individual Procrustes distance to a recent modern Zulu from South Africa (0.067). After linking to the other reconstructions, the reconstruction based on Broken Hill is closest to Dolní Věstonice 03, an Upper Paleolithic modern human from Europe (0.065). The other reconstructions plot close to a recent modern individual from South Africa (K-Ma10; 0.062 and K-Mumb; 0.066), Saldanha

1 (or Elandsfontein) (K-LH18; 0.067), and a recent modern individual from Turkana (K-Skl5; 0.062) (Figure 2 & Figure 3).

Table 4. Distances between reconstructions and their respective reference crania. Count indicates the position of the reference crania when Procrustes distances are ordered from lowest to highest. Closest neighbors indicated in this table ignore other reconstructions.

Reconstruction	Distance to Reference	Count of Reference	Closest Neighbor
K-BrH	0.086	52/151	DV03
K-Ma03	0.070	11/151	ZU13
K-Ma10	0.083	39/151	SA07
K-Mumb	0.096	69/151	SA07
K-LH18	0.088	46/151	Sal1
K-Skl5	0.082	35/155	Tur1

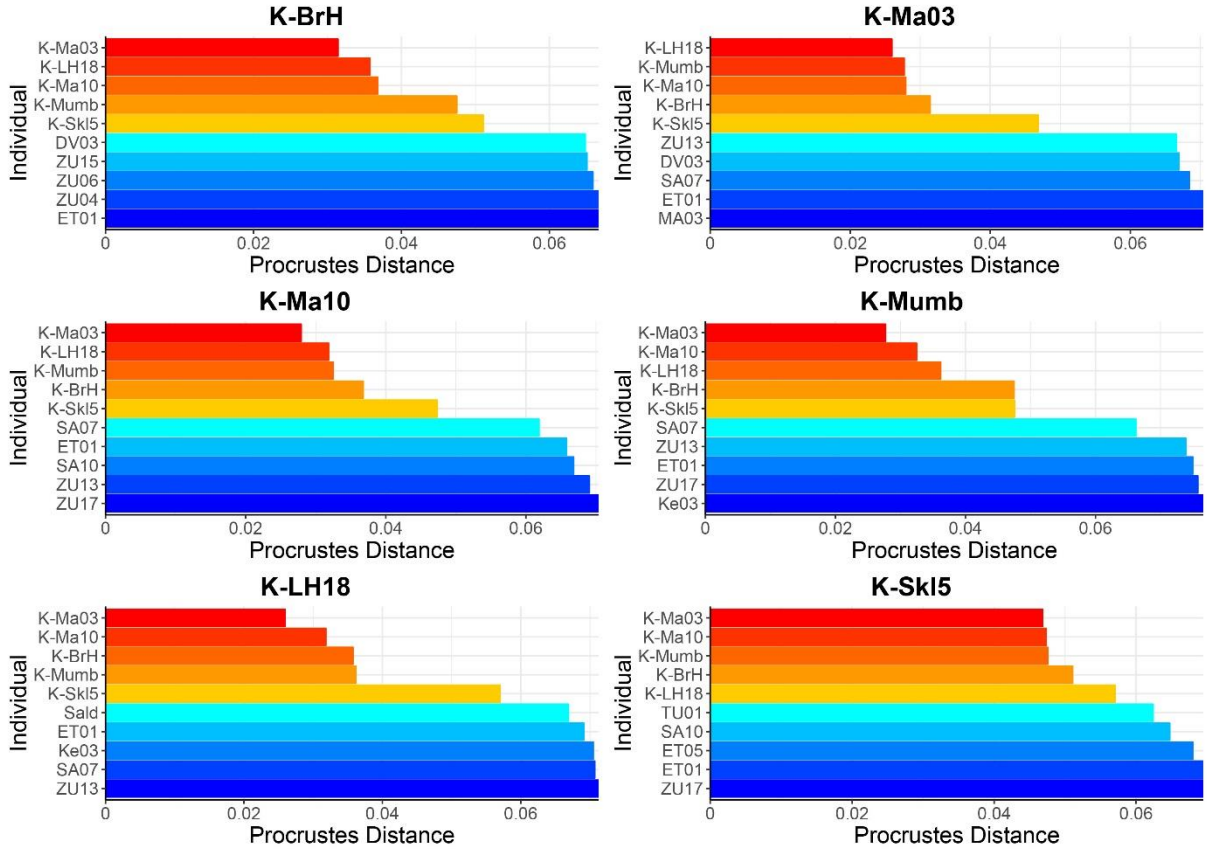

Figure 3. Procrustes distances of the Kabua reconstructions and the comparative sample. Only the first ten specimens are shown per plot. Abbreviations of individuals specified in Table 1.

The neurocranial shape index (Figure 4) demonstrates a similar separation between *H. sapiens* and Middle Pleistocene European specimens as observable in the PCA plot (Figure 2). Both the Neanderthal and Middle Pleistocene European groups are situated on the negative end of this axis, while the RHS group is spread between the origin and the positive extreme of the axis. The MPA group is located between the former two groups, with substantial overlap between MPA specimens and recent *H. sapiens*. The LH18 cranium plots close to Irhoud 1, Broken Hill, and Spy 2. Additionally, Irhoud 2 and Saldanha overlap with several recent *H. sapiens*, and are located close to Masai 10 and Skhūl V. All reconstructions of K1 are located close to the origin, within the range of *H. sapiens*. The reconstruction based on LH18 is closest to the MPA group, while the reconstruction based on Skhūl V is located near the extreme positive end of the axis.

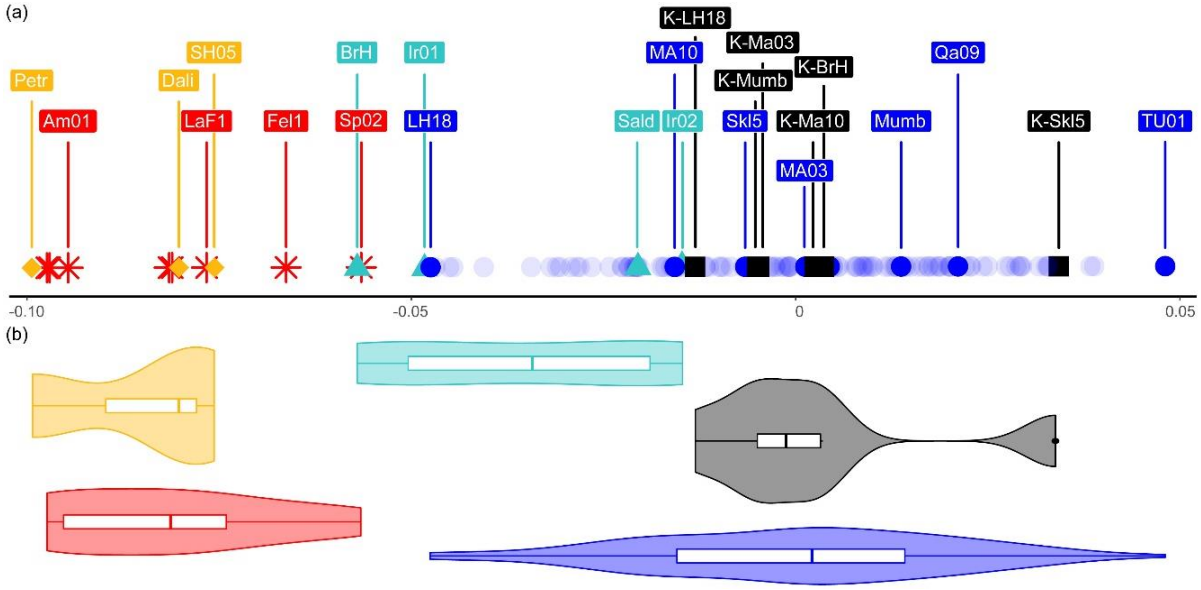

Figure 4. (a) Neurocranial shape index. Symbols and colors specified in Figures 2 & 3, abbreviations specified in Table 1. Recent *H. sapiens* have their opacity reduced in order to increase readability of the plot. (b) Violin plots reflect the variation in (a). Whiskers of boxplots show minimum and maximum values of the calculated shape indices per group, while boxes show 25-75% quartiles, lines in boxplots show median values. In this analysis, the Kabua 1 reconstructions are treated as a group, in which the Kabua reconstruction based on Skhūl V can be considered an outlier (filled circle).

Mardia's test for multivariate normality on the Procrustes superimposed coordinates show the comparative sample has a high measure of skewness (-9081.82) and kurtosis (692.83), due to the non-parametric distribution of this dataset (Supplementary Figure 3). As such, a systematic stopping rule (Auer-Gervini) was used to estimate the number of statistically significant components from the PCA, which shows that the first 12 PC's are significant. Together, these components explain 85.2% of cumulative variance. Note that our PC selection method somewhat conforms to the common practice of excluding PC's that explain less than 1% of variance. However, principal components 13 and 14 both explained about 1.1% of variance and could be included if a manual approach is preferred over a statistical one. Tests for univariate normality (Supplementary Table 2) and multivariate normality (Mardia skewness = 668.53, p-value = <0.01; Mardia kurtosis 5.57, p-value = <0.01) on the significant PC's show that these scores do not approximate a normal distribution (Supplementary Figure 4). As such, the sample contains several outliers, namely: Feldhofer, Amud, Spy 1, Irhoud 1, Irhoud 2, and Petralona (Supplementary Figure 5). The KMO test returns a mediocre overall Measure of Sampling Adequacy of 0.68, while the Fligner-Killeen test shows overall homogeneity of variance among groups (Chi^2 = 15.557, df = 9, p-value= 0.077).

Table 5. Posterior probabilities for the LDA. As the posterior probabilities for the MPE and NEA groups were close to 0, these were excluded.

Method	Group	K-BrH	K-Ma03	K-Ma10	K-Mumb	K-LH18	K-Skl5
LDA	MPA	0.958	0.694	0.910	0.997	0.994	0.002
	RHS	0.031	0.443	0.127	0.077	0.004	0.998
Result		MPA	MPA	MPA	MPA	MPA	RHS

The linear discriminant analysis (jackknife correct classification = 93.8%, Cohen's Kappa = 0.687) classifies all reconstructions as Middle Pleistocene African (with the exception of K-Skl5, which is classified as recent *H. sapiens*; Table 5). The four *k*-Nearest Neighbor algorithms on the Procrustes superimposed coordinates show slight diverging results. When the RHS group is randomly subsampled to three and four *H. sapiens*, all reconstructions are classified as MPA, except K-Skl5, which is classified as RHS (RHS n = 3, correct classification

of 62.4%, Cohen's Kappa = 0.378; RHS n = 4, correct classification of 62.8%, Cohen's Kappa = 0.403). Randomly subsampling the RHS group to eight individuals causes the K-BrH and K-LH18 reconstructions to be classified as MPA, while the other reconstructions are classified as RHS (correct classification of 68.6%, Cohen's Kappa = 0.550). When subsampling the RHS to the arbitrarily chosen number of 10 individuals, all reconstructions are classified as recent *H. sapiens*, with the exception of the K-LH18 which is classified as MPA (correct classification of 73.1% Cohen's Kappa = 0.599; Table 6).

Table 6. Posterior probabilities for the *k*-NN analyses. Each *k*-NN analysis is based on a different class size of RHS (see Methods). Additionally, the posterior probabilities for the *k*-NN indicated here are mean probabilities and their standard deviations over 1000 iterations. As there were no posterior probabilities for MPE and NEA groups, these were excluded.

Method	Group	K-BrH	K-Ma03	K-Ma10	K-Mumb	K-LH18	K-Skl5
	MPA	0.741 ±	0.706 ±	0.687 ±	0.677 ±	0.85 ±	0.347 ±
k-NN 1		0.197	0.242	0.214	0.237	0.186	0.102
RHS = 3	RHS	0.259 ±	0.294 ±	0.313 ±	0.323 ±	0.150 ±	0.653 ±
		0.197	0.242	0.214	0.237	0.186	0.102
Result		MPA	MPA	MPA	MPA	MPA	RHS
	MPA	0.689 ±	0.628 ±	0.621 ±	0.598 ±	0.811 ±	0.315±
k-NN 2		0.204	0.253	0.220	0.241	0.201	0.090
RHS = 4	RHS	0.311 ±	0.372 ±	0.379 ±	0.402 ±	0.189 ±	0.685 ±
		0.204	0.253	0.220	0.241	0.201	0.09
Result		MPA	MPA	MPA	MPA	MPA	RHS
	MPA	0.509 ±	0.410 ±	0.415 ±	0.400 ±	0.648 ±	0.186 ±
k-NN 3		0.221	0.192	0.184	0.158	0.220	0.166
RHS = 8	RHS	0.491 ±	0.590 ±	0.585 ±	0.600 ±	0.352 ±	0.814 ±
		0.221	0.192	0.184	0.158	0.220	0.166
Result		MPA	RHS	RHS	RHS	MPA	RHS
	MPA	0.448 ±	0.359 ±	0.363 ±	0.355 ±	0.598 ±	0.136 ±
k-NN 4		0.219	0.168	0.162	0.128	0.214	0.164
RHS = 10	RHS	0.552 ±	0.641 ±	0.637 ±	0.645 ±	0.402 ±	0.864 ±
		0.219	0.168	0.162	0.128	0.214	0.164
Result		RHS	RHS	RHS	RHS	MPA	RHS

Finally, the four RF models on the Procrustes superimposed coordinates also yield somewhat diverging results. A random subsample of three RHS results in the reconstructions being classified as MPA (correct classification of 67.8%, Cohen's Kappa = 0.379). When this random subsample is increased to four RHS individuals, the results are similar, with the exception that the K-Skl5 is now classified as RHS (correct classification

of 69.4%, Cohen's Kappa = 0.466). Subsampling to eight and 10 RHS leads to all reconstructions except K-LH18 to be classified as RHS (RHS n = 8, correct classification of 68.5%, Cohen's Kappa = 0.524; RHS n =10, correct classification of 72.9%, Cohen's Kappa = 0.581; Table 7).

Table 7. Posterior probabilities for the Random Forest Models. Each Random Forest is based on a different class size of RHS (see Methods). Additionally, the posterior probabilities indicated here are mean probabilities and their standard deviations over 1000 iterations.

Method	Group	K-BrH	K-Ma03	K-Ma10	K-Mumb	K-LH18	K-Skl5
	MPA	0.546 ± 0.061	0.529 ± 0.061	0.502 ± 0.061	0.495 ± 0.058	0.544 ± 0.056	0.461 ± 0.074
	MPE	0.066 ± 0.024	0.092 ± 0.029	0.088 ± 0.029	0.100 ± 0.030	0.089 ± 0.028	0.050 ± 0.022
RF 1							
RHS = 3	NEA	0.129 ± 0.035	0.119 ± 0.035	0.123 ± 0.036	0.152± 0.039	0.189 ± 0.042	0.081 ± 0.030
	RHS	0.259 ± 0.063	0.260 ± 0.067	0.286 ± 0.066	0.253 ± 0.062	0.178 ± 0.056	0.408 ± 0.080
Result		MPA	MPA	MPA	MPA	MPA	MPA
	MPA	0.549 ± 0.070	0.528 ± 0.072	0.505 ± 0.071	0.497 ± 0.070	0.562 ± 0.064	0.436 ± 0.085
	MPE	0.064 ± 0.026	0.090 ± 0.029	0.084 ± 0.029	0.100 ± 0.031	0.084 ± 0.028	0.045 ± 0.022
RF 2							
RHS = 4	NEA	0.102 ± 0.036	0.079 ± 0.031	0.081 ± 0.032	0.108 ± 0.038	0.153 ± 0.042	0.05 ± 0.025
	RHS	0.285 ± 0.072	0.304 ± 0.078	0.330 ± 0.076	0.295 ± 0.073	0.201 ± 0.064	0.469 ± 0.089
Result		MPA	MPA	MPA	MPA	MPA	RHS
	MPA	0.455 ± 0.070	0.403 ± 0.076	0.377 ± 0.073	0.386 ± 0.072	0.488 ± 0.064	0.229 ± 0.075
	MPE	0.053 ± 0.023	0.067 ± 0.028	0.060 ± 0.026	0.070 ± 0.027	0.070 ± 0.027	0.021 ± 0.016
RF 3							
RHS = 8	NEA	0.087 ± 0.032	0.066 ± 0.028	0.065 ± 0.029	0.086 ± 0.033	0.136 ± 0.039	0.026 ± 0.019
	RHS	0.405 ± 0.083	0.464 ± 0.093	0.498 ± 0.090	0.458 ± 0.091	0.306 ± 0.076	0.724 ± 0.087
Result		MPA	RHS	RHS	RHS	MPA	RHS
	MPA	0.430 ± 0.073	0.368 ± 0.080	0.344 ± 0.077	0.357 ± 0.074	0.464 ± 0.067	0.179 ± 0.070
	MPE	0.051 ± 0.023	0.062 ± 0.027	0.057 ± 0.026	0.065 ± 0.027	0.067 ± 0.027	0.017 ± 0.015
RF 4							
RHS = 10	NEA	0.087 ± 0.033	0.062 ± 0.027	0.061 ± 0.026	0.081 ± 0.031	0.131 ± 0.036	0.022 ± 0.017
	RHS	0.433 ± 0.091	0.508 ± 0.100	0.538 ± 0.094	0.497 ± 0.095	0.338 ± 0.084	0.781 ± 0.083
Result		RHS	RHS	RHS	RHS	MPA	RHS

4. Discussion

The geometric morphometric analyses presented in this paper demonstrate that the virtual anatomical reconstructions of K1 (Bosman et al., 2019) are robust. Most of the reconstructions resulted in more or less similar outcomes, as there was sufficient anatomical information present to place non-articulating fragments in similar positions. However, during the reconstruction process, it was sometimes difficult to determine the correct location of fragments based on anatomical information and break-patterns. This resulted in some variation in location in shape space between the several reconstructions, as observed in the PCA. Thus, the choice of reference cranium in a virtual reconstruction can influence the resulting model, just as the entire comparative sample will influence any analysis. However, by primarily relying on the inherent anatomical information that is present in the K1 cranium, our reconstructions are sufficiently comparable.

Additionally, the applied neurocranial dataset is shown to be adequate in separating Middle Pleistocene hominins from Europe/Africa from more recent *H. sapiens* (Late Pleistocene and Holocene) and can thus be used in assessments of taxonomic attribution, which is consistent with past work (e.g. Athreya, 2009; Gunz et al., 2009a; Harvati et al., 2011, 2019). The location of the K1 reconstructions within this PCA plot support the hypothesis that the neurocranial shape of the K1 cranium is reflective of its affiliation with recent modern *H. sapiens*. This is further supported by the neurocranial shape index, although this plot does indicate that there is substantial overlap between the MPA and RHS groups. This could have been caused by the fact that we used a broad *a priori* grouping factor to classify our comparative sample, which has precedence in the relevant literature (e.g. Brewster et al., 2014; Harvati et al., 2011; Harvati et al., 2019; Hublin et al., 2017). Consequently, when using these groups, the overall classification rate is quite high and leads to a higher Cohen's Kappa statistic. One could argue that a separation between Late Pleistocene specimens and recent anatomically modern humans would be prudent. However, as the analyses are based on a limited number of shape variables which are primarily located on the neurocranium and the occipital bone, it might not be the most useful to separate recent modern humans

on account of more recent population history (Reyes-Centeno et al., 2017). Moreover, the inclusion of additional groups with low sample sizes reduces the reliability of any classification due to multiple violations of minimal group size as well as the presence of significant overlap between the Late Pleistocene fossils and recent modern *H. sapiens* (Supplementary Figure 6).

The Procrustes distance analysis generally support the results of the PCA, as all reconstructions link together and are close to late Pleistocene *H. sapiens* (DV03) and recent modern humans (South African 07, Turkana 01, and Zulu 13). However, the Kabua reconstruction based on Ngaloba LH18 is close to the Saldanha specimen (broadly dated to the Middle Pleistocene; Potts and Deino, 1995; Singer, 1954) in Procrustes Distance. In the process of reconstructing K1 using Ngaloba LH18 as a reference cranium, we encountered some difficulties as this specific reference had to be manually reconstructed, since its fragments were scanned separately. As described in the original publication (Day et al., 1980), there is no direct anatomical articulation between the splanchocranium and the posterior part of the neurocranium. Moreover, there is some distortion present in the frontal bone, which demonstrates substantial lateral deviation from the midline in the anterior part of the frontal bone. During the process of reconstruction, we approximated the original reconstruction by Day et al. (1980) and note that the degree of facial prognathism will change depending on the positioning of the splanchnocranium relative to the calvaria (Bosman et al., 2019). Thus, the issues associated with this specific reconstruction could potentially explain its proximity to specimens belonging to the MPA group in both the PCA and neurocranial shape index plots.

As for the classification of the K1 virtual reconstructions, our three classification techniques (LDA, *k*-NN and RF) show somewhat disparate results. The LDA is inconsistent with the PCA and Procrustes distances. This analysis classifies five of the K1 reconstructions as Middle Pleistocene Africans, except for the reconstruction based on Skhūl V. However, this analysis is based on the distance between a reconstruction (in other words, a group with

only a singular specimen) and the other group means, cross-validated with a leave-one-out procedure. LDA only accounts for unequal sample sizes by assigning an equal prior probability for all classes. Additionally, the assumption tests returned that our data violates normality, and LDA is sensitive to non-normal data and outliers (e.g. Hefner et al., 2014). Furthermore, specifically for this sample, half of the MPA group (n = 4) can be considered outliers in tangent space (Irhoud 1 and Irhoud 2), which reduces the reliability of this analysis considerably. Moreover, LDA and related techniques maximize variance between groups, even attaining a separation between "groups" in randomly generated data that have no real biological separation (Mitteroecker & Bookstein, 2011).

On the contrary, non-parametric analyses such as *k*-NN are robust against departures of normality and the presence of outliers. Moreover, *k*-NN relies on Procrustes distances, which are computed from the Procrustes superimposed coordinates, resulting in a more complete picture when compared to only the significant principal components used in the LDA. We attempted to account for the imbalance between classes by applying randomized subsampling. In general, the results from the *k*-NN analyses are consistent with the results from the PCA and Procrustes Distances. While most reconstructions classify as recent *H. sapiens*, they have high posterior probabilities for the Middle Pleistocene African group. The posterior probabilities for the other groups are zero, as the maximal count of *k*-nearest neighbors is only three, nullifying the likelihood that a Neanderthal or Middle Pleistocene European specimen participates in the classification vote. K-LH18 classifies consistently as a Middle Pleistocene African specimen, reaffirming its low Procrustes Distance the Saldanha specimen. K-BrH tends to classify either as MPA or as RHS, depending on the number of RHS included in the analyses. The other reconstructions classify primarily as RHS, which is also reflected in the PCA and Procrustes distances. In all, the *k*-NN had a decent Cohen's Kappa score, which is inversely affected by the amount of morphological overlap between groups and the large amount of intra-group variation.

The Random Forest models are also resistant to departures of normality and outliers. Moreover, the random bagging of variables reduces the problem of multicollinearity, without the need to apply ordination techniques. Even if these ordination techniques are applied on the Procrustes shape data before applying the RF models, the results are similar to the outcomes presented here, although with lower Cohen's Kappa scores (Supplementary Table 3). The RF models demonstrated correct classification percentages and Cohen's Kappa scores similar to the *k*-NN models, albeit slightly lower. The K-LH18 and K-BrH classify primarily as MPA, while K-Skl5 classifies exclusively as a RHS, with the other three reconstructions falling somewhere between these two extremes. As the number of randomly subsampled RHS is increased, the reconstructions are more likely to classify as such, demonstrating the effect of the class imbalance problem in our sample.

While *k*-NN and RF are not often applied in the context of geometric morphometrics (Hefner et al., 2014), these two ML applications seem to be quite effective in classifying unknown individuals on the basis of neurocranial shape data, even in a dataset that exhibits large amounts of intra-group variation. As these methods might provide robust alternatives to the problems associated with LDA (Hefner et al., 2014; Navega et al., 2015), their potential for geometric morphometrics and paleoanthropology should be explored further. However, one downside of both *k*-NN and RF is the fact that they are influenced by the composition of the training dataset, which can quite small for the fossil groups due to the paucity of the Middle Pleistocene fossil record and availability of CT/3D scan data. These violations of minimum group size as well as the class imbalance problem negatively affect the generation of any ML model, which reduces overall classification confidence. While certain techniques exist to artificially oversample small groups in order to better train ML models (Chawla et al., 2002; Japkowicz, 2000), these methods do not reflect the morphological variation present in real fossil specimens, and their reliability for GM data remains to be tested. As such, we should not blindly trust the classifications provided by either the LDA or the ML models presented here but rather compare the resulting

classifications to the data obtained from arguably more straightforward analyses such as Principal Component Analysis and Procrustes distances.

To conclude, both our anatomical reconstructions and our subsequent multivariate analyses suggest affinity with recent Africans and Late Pleistocene modern *H. sapiens*, thereby confirming the hypothesis set out in the beginning of this study. As such, our results agree with what has been put forward by Rightmire (1975, page 37), who argues that: "if it is accepted as early… Kabua 1 is something of an anomaly. But if it is late and not of Pleistocene origin, then there is probably little difficulty in including it within the ranks of modern *Homo sapiens."* However, some features of the K1 cranium cause it to be close to the borders of the currently known range of variation of the Late Pleistocene and anatomically modern individuals. This includes a relatively low frontal bone, narrow neurocranium, possible plesiomorphic affinities in the bony labyrinth (Bosman et al., 2019; Reyes-Centeno et al., 2014b), as well as the proximity of the Kabua 1 reconstructions to Middle Pleistocene African specimens. The presence of these traits does not preclude an anatomically modern *H. sapiens* designation. Instead, it alludes to the broad phenotypic diversity present in Late Pleistocene Africa and the possible persistence of phenotypes representing deep population structure in specific regions across the African continent (e.g. Crevecoeur et al., 2009; Excoffier, 2002; Fagundes et al., 2007; Marth et al., 2003). Whether this phenotypic diversity was caused by interbreeding between other hominin taxa and anatomically modern *H. sapiens* or by other, non-mutually exclusive, processes such as a larger effective size for African populations and an older onset of population demographic expansion within Africa (e.g. Forster, 2004), or population size fluctuations and positive selection through adaptation to new environments outside Africa (e.g. Excoffier, 2002), cannot be investigated with the results presented this manuscript.

Nonetheless, the Kabua material presents a similar scenario as has been argued for Nazlet Khater (Crevecoeur et al., 2009), Hofmeyr (Grine et al., 2007), and Iwo Eleru (Harvati et al., 2011), respectively dated to 38 ka, 36 ka, and 14 ka. These specimens all

display a mix of archaic and derived features and each of these individuals has been interpreted as phenotypic evidence for the presence of deep population structure in Africa (Crevecoeur et al., 2009; Harvati et al., 2011). K1 might be a part of this Late-Pleistocene group of anatomically modern humans which show a retention of specific "archaic" traits, and thus represent a complicated transition to anatomical modernity. This aligns with what has been suggested by Gunz et al. (2009a), on the basis of a large neurocranial dataset. They propose that this Late Pleistocene *H. sapiens* phenotypic diversity is caused by intra-African population expansions, which possibly led to temporally subdivided and isolated groups (e.g. Garrigan & Hammer, 2006). Kabua might be representative of such an isolated group. However, while a late Pleistocene date was put forward as most likely for this material, the lack of a robust archaeological and geochronological context, as well as the patchiness of the African fossil record, prevent us from effectively discussing the Kabua 1 cranium in the context of this Late Pleistocene anatomical variation. As such, the Kabua 1 cranium currently cannot contribute to discussions on the aforementioned processes (e.g. deep population or transitions to anatomical modernity) at this point in time. What our research does show, however, is the importance of revisiting older fossils and applying new methods in order to broaden our knowledge about the emergence and development of *H. sapiens*, expand the currently available fossil record for study and comparison, and diversify the discussion on hominin evolution. Fossils like Kabua 1 are untapped wells of potential knowledge, and should be treated with much care and consideration, for they are essential for our understanding of our shared past.

5. Acknowledgements

Support for this research was provided by the German Research Foundation (DFG FOR 2237: Project "Words, Bones, Genes, Tools: Tracking Linguistic, Cultural, and Biological Trajectories of the Human Past" and DFG INST 37/706-1 FUGG: Paleoanthropology High Resolution CT Laboratory). LTB was additionally supported by the Human Origins Research Fund of the Natural History Museum London. CS's research is supported by the Calleva Foundation and the Human Origins Research Fund. KH is supported by the European Research Council (ERC CoG no. 724703). We thank Yonatan Sahle for his extensive comments on earlier versions of this manuscript

6. References

Adams, D. C., Rohlf, F. J., & Slice, D. E. (2004). Geometric morphometrics: ten years of progress following the 'revolution'. *Hystrix: Italian Journal of Zoology, 71*(1), 5-16.

Adams, D. C., Collyer, M. L., & Kaliontzopoulou, A. (2019). *Geomorph: Software for geometric morphometric analyses*. R package version 3.1.0. https://cran.rproject.org/package=geomorph.

Athreya, S. (2009). A comparative study of frontal bone morphology among Pleistocene hominin fossil groups. *Journal of Human Evolution, 57*(6), 786-804.

Auer, P., & Gervini, D. (2008). Choosing Principal Components: A New Graphical Method Based on Bayesian Model Selection. *Communications in Statistics - Simulation and Computation, 37*(5), 962-977.

Bookstein, F. L. (1989). Principal warps: thin-plate splines and the decomposition of deformations. *IEEE Transactions on Pattern Analysis and Machine Intelligence, 11*(6), 567-585.

Bosman, A. M., Buck, L. T., Reyes-Centeno, H., Mirazón Lahr, M., Stringer, C., & Harvati, K. (2019). The Kabua 1 cranium: Virtual anatomical reconstructions. In Y. Sahle, H. Reyes-Centeno, & C. Bentz (Eds.), *Modern Human Origins and Dispersal* (pp. 137-170). Tübingen: Kerns Verlag.

Bräuer, G. (1983). Die menschlichen Skelettfunde des" Later Stone Age" aus der Mumba-Höhle und anderen Lokalitäten nahe des Eyasi-Sees (Tanzania) und ihre Bedeutung für die Populationsdifferenzierung in Ostafrika. In H. Müller-Beck (Ed.), *Die archäologischen und anthropologischen Ergebnisse der Kohl-Larsen-Expeditionen in Nord-Tanzania, 1933–1939 (Vol. 4)*. Tübingen: Verlag Archaeologica Venatoria.

Bräuer, G. (2008). The origin of modern anatomy: By speciation or intraspecific evolution? *Evolutionary Anthropology: Issues, News, and Reviews, 17*(1), 22-37.

Breiman, L. (2001). Random Forests. *Machine Learning, 45*(1), 5-32.

Brewster, C., Meiklejohn, C., von Cramon-Taubadel, N., & Pinhasi, R. (2014). Craniometric analysis of European Upper Palaeolithic and Mesolithic samples supports discontinuity at the Last Glacial Maximum. *Nature Communications, 5*(4094).

Buck, L. T., & Stringer, C. B. (2015). A rich locality in South Kensington: the fossil hominin collection of the Natural History Museum, London. *Geological Journal, 50*(3), 321-337.

Chawla, N. V., Bowyer, K. W., Hall, L. O., & Kegelmeyer, W. P. (2002). SMOTE: Synthetic Minority Over-sampling Technique. *Journal of Artificial Intelligence Research, 16,* 321-357.

Claude, J. (2008). *Morphometrics with R*. New York: Springer.

Cohen, J. (1960). A Coefficient of Agreement for Nominal Scales. *Educational and Psychological Measurement, 20*(1), 37-46.

Cook, R. D., & Weisberg, S. (1982). Residuals and Influence in Regression. New York: Chapman and Hall.

Corner BD, Lele S, & Richtsmeier JT. (1992). Measuring precision of three-dimensional landmark data. *Journal of Quantitative Anthropology, 3*, 347-359.

Crevecoeur, I., Rougier, H., Grine, F., & Froment, A. (2009). Modern human cranial diversity in the Late Pleistocene of Africa and Eurasia: Evidence from Nazlet Khater, Peştera cu Oase, and Hofmeyr. *American Journal of Physical Anthropology, 140*(2), 347-358.

Day, M. H., Leakey, M. D., & Magori, C. (1980). A new hominid fossil skull (L.H. 18) from the Ngaloba Beds, Laetoli, northern Tanzania. *Nature, 284*(5751), 55-56.

Excoffier, L. (2002). Human demographic history: refining the recent African origin model. *Current Opinion in Genetics and Development, 12*(6), 675-682.

Fagundes, N. J., Ray, N., Beaumont, M., Neuenschwander, S., Salzano, F. M., Bonatto, S. L., & Excoffier, L. (2007). Statistical evaluation of alternative models of human evolution. *Proceedings of the National Academy of Sciences, 104*(45), 17614-17619.

Fligner, M. A., & Killeen, T. J. (1976). Distribution-Free Two-Sample Tests for Scale. *Journal of the American Statistical Association, 71*(353), 210-213.

Forster, P. (2004). Ice Ages and the mitochondrial DNA chronology of human dispersals: a review. *Philosophical Transactions of the Royal Society of London. Series B: Biological Sciences, 359*(1442), 255-264.

Garrigan, D., & Hammer, M. F. (2006). Reconstructing human origins in the genomic era. *Nature Reviews Genetics, 7*(9), 669-680.

Grine, F. E., Bailey, R. M., Harvati, K., Nathan, R. P., Morris, A. G., Henderson, G. M., . . . Pike, A. W. (2007). Late Pleistocene human skull from Hofmeyr, South Africa, and modern human origins. *Science, 315*(5809), 226-229.

Gunz, P., Bookstein, F. L., Mitteroecker, P., Stadlmayr, A., Seidler, H., & Weber, G. W. (2009a). Early modern human diversity suggests subdivided population structure and a complex out-of-Africa scenario. *Proceedings of the National Academy of Sciences, 106*(15), 6094-6098.

Gunz, P., Mitteroecker, P., Neubauer, S., Weber, G. W., & Bookstein, F. L. (2009b). Principles for the virtual reconstruction of hominin crania. *Journal of Human Evolution, 57*(1), 48-62.

Gunz, P., Tilot, A. K., Wittfeld, K., Teumer, A., Shapland, C. Y., van Erp, T. G. M., . . . Fisher, S. E. (2019). Neandertal Introgression Sheds Light on Modern Human Endocranial Globularity. *Current Biology, 29*(1), 120-127.

Harvati, K., & Weaver, T. D. (2006). Reliability of cranial morphology in reconstructing Neanderthal phylogeny. In K. Harvati, & T. Harrison (Eds.), *Neanderthals Revisited: New Approaches and Perspectives* (pp. 239-254). Dordrecht: Springer Netherlands.

Harvati, K., Stringer, C., Grün, R., Aubert, M., Allsworth-Jones, P., & Folorunso, C. A. (2011). The Later Stone Age Calvaria from Iwo Eleru, Nigeria: Morphology and Chronology. *PloS One, 6*(9), e24024.

Harvati, K., Röding, C., Bosman, A.M., Karakostis, F.A., Grün, R., Stringer, C., Karkanas, P., Thompson, N.C., Koutoulidis, V., Moulopoulos, L.A., Gorgoulis, V.G., Kouloukoussa, M., 2019. Apidima Cave fossils provide earliest evidence of Homo sapiens in Eurasia. Nature 571, 500-504.

Hefner, J. T., Spradley, M. K., & Anderson, B. (2014). Ancestry Assessment Using Random Forest Modeling. *Journal of Forensic Sciences, 59*(3), 583-589.

Hubbe, M., Hanihara, T., & Harvati, K. (2009). Climate Signatures in the Morphological Differentiation of Worldwide Modern Human Populations. *The Anatomical Record: Advances in Integrative Anatomy and Evolutionary Biology, 292*(11), 1720-1733.

Hublin, J.-J., Ben-Ncer, A., Bailey, S. E., Freidline, S. E., Neubauer, S., Skinner, M. M., . . . Gunz, P. (2017). New fossils from Jebel Irhoud, Morocco and the pan-African origin of Homo sapiens. *Nature, 546*(7657), 289-292.

Immersion Corp. (1998). *Microscribe 3D User's Guide*. Immersion Corporation, San Jose, CA.

Japkowicz, N. (2000). *The Class Imbalance Problem: Significance and Strategies*. Proceedings of the 2000 International Conference on Artificial Intelligence (IC-AI'2000): Special Track on Inductive Learning, Las Vegas, Nevada.

Kaiser, H. F. (1970). A second generation little jiffy. *Psychometrika, 35*(4), 401-415.

Kaiser, H. F., & Rice, J. (1974). Little Jiffy, Mark IV. *Educational and Psychological Measurement, 34*(1), 111-117.

Korkmaz, S., Goksuluk, D., & Zararsiz, G. (2014). MVN: An R Package for Assessing Multivariate Normality. *The R Journal, 6*(2), 151-162.

Kuhn, M. (2008). Caret package. *Journal of Statistical Software, 28*(5).

Mardia, K. V. (1970). Measures of Multivariate Skewness and Kurtosis with Applications. *Biometrika, 57*(3), 519-530.

Mardia, K. V., Bookstein, F. L., & Moreton, I. J. (2000). Statistical Assessment of Bilateral Symmetry of Shapes. *Biometrika, 87*(2), 285-300.

Marth, G., Schuler, G., Yeh, R., Davenport, R., Agarwala, R., Church, D., . . . Kholodov, M. (2003). Sequence variations in the public human genome data reflect a bottlenecked population history. *Proceedings of the National Academy of Sciences, 100*(1), 376-381.

McCown, T. D., & Keith, A. (1939). *The Stone Age of Mount Carmel II: The Fossil Human Remains from the Levalloiso-Mousterian*. Oxford: Clarendon Press.

Mirazón Lahr, M. (2016). The shaping of human diversity: filters, boundaries and transitions. *Philosophical Transactions of the Royal Society of London. Series B: Biological Sciences, 371*(1698).

Mitteroecker, P., & Gunz, P. (2009). Advances in Geometric Morphometrics. *Evolutionary Biology, 36*(2), 235-247.

Mitteroecker, P., & Bookstein, F. (2011). Linear Discrimination, Ordination, and the Visualization of Selection Gradients in Modern Morphometrics. *Evolutionary Biology, 38*(1), 100-114.

Mitteroecker, P., Gunz, P., Windhager, S., & Schaefer, K. (2013). A brief review of shape, form, and allometry in geometric morphometrics, with applications to human facial morphology. *Hystrix, the Italian Journal of Mammalogy, 24*(1), 8.

Navega, D., Coelho, C., Vicente, R., Ferreira, M. T., Wasterlain, S., & Cunha, E. (2015). AncesTrees: ancestry estimation with randomized decision trees. *International Journal of Legal Medicine, 129*(5),1145-53

Neeser, R., Ackermann, R. R., & Gain, J. (2009). Comparing the accuracy and precision of three techniques used for estimating missing landmarks when reconstructing fossil hominin crania. *American Journal of Physical Anthropology, 140*(1), 1-18.

Owen, R. B., Barthelme, J. W., Renaut, R. W., & Vincens, A. (1982). Palaeolimnology and archaeology of Holocene deposits north-east of Lake Turkana, Kenya. *Nature, 298*(5874), 523-529.

Perez, S.I., Bernal, V., Gonzalez, P.N. (2006). Differences between sliding semi-landmark methods in geometric morphometrics, with an application to human craniofacial and dental variation. *Journal of Anatomy, 208*, 769-784.

Phenice, T. W. (1972). *Hominid fossils: an illustrated key*. Iowa: W. C. Brown Co.

Potts, R., Deino, A., 1995. Mid-Pleistocene Change in Large Mammal Faunas of East Africa. *Quaternary Research, 43*, 106-113.

R Core Team (2019). *R: A language and environment for statistical computing*. R Foundation for Statistical Computing, Vienna, Austria, https://www.R-project.org/. R version 3.5.0.

Revelle, W. (2018) *psych: Procedures for Personality and Psychological Research*, Northwestern University, Evanston, Illinois, USA, https://CRAN.R-project.org/package=psych.

Reck, H., & Kohl-Larsen, L. (1936). Erster Überblick über die jungdiluvialen Tier- und Menschenfunde Dr. Kohl-Larsens im nordöstlichen Teil des Njarasa-Grabens (Ostafrika). *Geologische Rundschau: Zeitschrift für Allgemeine Geologie, 27*(5), 401-441.

Reyes-Centeno, H., Ghirotto, S., Détroit, F., Grimaud-Hervé, D., Barbujani, G., & Harvati, K. (2014a). Genomic and cranial phenotype data support multiple modern human dispersals from Africa and a southern route into Asia. *Proceedings of the National Academy of Sciences, 111*(20), 7248-7253.

Reyes-Centeno, H., Buck, L. T., Stringer, C., & Harvati, K. (2014b). *The inner ear of the Eyasi I (Tanzania) and Kabua I (Kenya) hominin fossils*. The African Human Fossil Record, Toulouse.

Reyes-Centeno, H., Ghirotto, S., & Harvati, K. (2017). Genomic validation of the differential preservation of population history in modern human cranial anatomy. *American Journal of Physical Anthropology, 162*(1), 170-179.

Rightmire, G. P. (1975). Problems in the Study of Later Pleistocene Man in Africa. *American Anthropologist, 77*(1), 28-52.

Rightmire, G. P. (2001). Morphological Diversity in Middle Pleistocene Homo. In P. V. Tobias, M. A. Raath, J. Moggi-Cecchi, & G. A. Doyle (Eds.), *Humanity from African Naissance to Coming Millennia*. Firenze University Press.

Rightmire, G. P. (2009). Middle and later Pleistocene hominins in Africa and Southwest Asia. *Proceedings of the National Academy of Sciences, 106*(38), 16046-16050.

Ripley, B. D. (1996). *Pattern recognition and neural networks*. Cambridge: Cambridge University Press.

Robbins, L. (1972). Archeology in the Turkana District, Kenya. *Science, 176*(4033), 359-366.

Sahle, Y., Reyes-Centeno, H., & Bentz, C. (2019). *Modern Human Origins and Dispersal*. Tübingen: Kerns Verlag.

Schepartz, L. A. (1987). *From hunters to herders: subsistence pattern and morphological change in eastern Africa*. (Ph.D.), University of Michigan, Ann Arbor.

Schwartz, J. H., & Tattersall, I. (2010). Fossil evidence for the origin of Homo sapiens. American *Journal of Physical Anthropology, 143*(51), 94-121.

Shapiro, S. S., & Wilk, M. B. (1965). An Analysis of Variance Test for Normality (Complete Samples). *Biometrika, 52*(3/4), 591-611.

Singer, R., 1954. The Saldanha skull from Hopefield, South Africa. *American Journal of Physical Anthropology, 12*, 345-362.

Slice, D. E. (2011). *Modern Morphometrics in Physical Anthropology*. New York: Kluwer.

Slice, D. E. (2013). *Morpheus et al., Java Edition*. Department of Scientific Computing, The Florida State University, Tallahassee, Florida.

Stringer, C. B. (1984). The definition of Homo erectus and the existence of the species in Africa and Europe. *Courier Forschungsinstitut Senckenberg, 69*, 131-143.

Tryon, C. A., Crevecoeur, I., Faith, J. T., Ekshtain, R., Nivens, J., Patterson, D., . . . Spoor, F. (2015). Late Pleistocene age and archaeological context for the hominin calvaria from GvJm-22 (Lukenya Hill, Kenya). *Proceedings of the National Academy of Sciences, 112*(9), 2682-2687.

Tryon, C. A., Lewis, J. E., & Ranhorn, K. (2019). Excavating the archives: The 1956 excavation of the late Pleistocene-Holocene sequence at Kisese II (Tanzania). In Y. Sahle, H. Reyes-Centeno, & C. Bentz (Eds.), *Modern Human Origins and Dispersal*. Tübingen: Kerns Verlag.

Venables, W. N. & Ripley, B. D. (2002) *Modern Applied Statistics with S*. Fourth Edition. Springer, New York.

Wang, M., Kornblau, S. M., & Coombes, K. R. (2018). Decomposing the Apoptosis Pathway into Biologically Interpretable Principal Components. *Cancer Informatics, 17*, 1-13.

Weber, G. W., & Bookstein, F. L. (2011). *Virtual Anthropology: A Guide to a New Interdisciplinary Field*. Vienna/New York: Springer.

Webster, M., & Sheets, H. D. (2010). A practical introduction to landmark-based geometric morphometrics. *Quantitative Methods in Paleobiology, 16*, 168-188.

White, T. D., Asfaw, B., DeGusta, D., Gilbert, H., Richards, G. D., Suwa, G., & Clark Howell, F. (2003). Pleistocene Homo sapiens from Middle Awash, Ethiopia. *Nature, 423*(6941), 742-747.

Whitworth, T. (1960). Fossilized Human Remains from Northern Kenya. *Nature, 185*(4717), 947-948.

Whitworth, T. (1965a). Artifacts from Turkana, Northern Kenya. *The South African Archaeological Bulletin, 20(*78), 75-78.

Whitworth, T. (1965b). The Pleistocene lake beds of Kabua, northern Kenya. *Durham University Journal, 57*, 88-100.

Whitworth, T. (1966). A Fossil Hominid from Rudolf. *The South African Archaeological Bulletin, 21*(83), 138-150.

Wright, M. N., & Ziegler, A. (2017). ranger: A Fast Implementation of Random Forests for High Dimensional Data in C++ and R. *Journal of Statistical Software, 77*(1), 17.

Woodward, A. S. (1921). A New Cave Man from Rhodesia, South Africa. Nature, 108(2716), 371-372.

7. Supplementary Material

Supplementary Table 1. Specimens in the comparative sample with bilateral landmarks reconstructed through reflection. Abbreviations: AST = Asterion; L = Left; LAMB = Lambdoid Suture; PAR = Parietal Notch; R = Right.

Specimen	Reconstructed landmarks
Amud	PAR-R
Cro Magnon 2	AST-R; PAR-R; LAMB-R
Dali	LAMB-R
Feldhofer	AST-L
La Ferrassie 1	AST-L; LAMB-R
Irhoud 2	AST-R; PAR-R; LAMB-R
Broken Hill	AST-L; PAR-L; LAMB-L
Ngaloba LH18	PAR-L
Pavlov 1	PAR-R
Predmosti 4	PAR-L
Saldanha	PAR-L
Spy I	PAR-L
South African (Museum) 38	LAMB-R
South African (University) 8	AST-L; LAMB-L
Igiai 17930	AST-R; LAMB-R
Somalia 23575	AST-L

Supplementary Table 2. Shapiro-Wilk tests for Univariate Normality on significant PC scores.

Variable	Statistic	p-value
PC 1	0.892	<0.001*
PC 2	0.987	0.182
PC 3	0.985	0.101
PC 4	0.969	0.002*
PC 5	0.985	0.100
PC 6	0.987	0.181
PC 7	0.961	3e-04*
PC 8	0.995	0.902
PC 9	0.991	0.426
PC 10	0.992	0.548
PC 11	0.992	0.539
PC 12	0.995	0.869

*Indicates significant deviation from univariate normality

Supplementary Table 3. Posterior probabilities for the RF on the 12 significant PC scores. Each RF model is based on a different class size of RHS (see Methods), as indicated in the "Groups" column. Additionally, the posterior probabilities indicated here represent mean probabilities and their standard deviations over 1000 iterations. CA = Classification accuracy; Kap = Cohen's Kappa statistic.

Method	Groups	K-BrH	K-Ma03	K-Ma10	K-Mumb	K-LH18	K-Skl5
RF 1	MPA	0.311 ±	0.465 ±	0.293 ±	0.646 ±	0.350 ±	0.646 ±
RHS = 3		0.066	0.069	0.068	0.078	0.072	0.078
CA =	MPE	0.080 ±	0.076 ±	0.112 ±	0.044 ±	0.115 ±	0.034 ±
52.5%		0.030	0.029	0.036	0.022	0.036	0.019
Kap =	NEA	0.235 ±	0.144 ±	0.205 ±	0.060 ±	0.212 ±	0.057 ±
0.204		0.054	0.043	0.051	0.025	0.052	0.025
	RHS	0.374 ±	0.314 ±	0.390 ±	0.251 ±	0.323 ±	0.264 ±
		0.093	0.082	0.100	0.081	0.106	0.081
Result		RHS	MPA	RHS	MPA	MPA	MPA
RF 2	MPA	0.234 ±	0.382 ±	0.224 ±	0.551 ±	0.301 ±	0.545 ±
RHS = 4		0.086	0.090	0.086	0.106	0.097	0.107
CA =	MPE	0.054 ±	0.053 ±	0.077 ±	0.022 ±	0.098 ±	0.016 ±
64.7%		0.025	0.025	0.031	0.016	0.041	0.014
Kap =	NEA	0.137 ±	0.082 ±	0.110 ±	0.021 ±	0.149 ±	0.020 ±
0.356		0.050	0.036	0.043	0.015	0.058	0.015
	RHS	0.575 ±	0.484 ±	0.589 ±	0.406 ±	0.453 ±	0.419 ±
		0.109	0.104	0.112	0.109	0.150	0.110
Result		RHS	RHS	RHS	MPA	RHS	MPA
RF 3	MPA	0.208 ±	0.303 ±	0.19 ±	0.388 ±	0.260 ±	0.406 ±
RHS = 8		0.077	0.088	0.075	0.100	0.084	0.103
CA =	MPE	0.037 ±	0.037 ±	0.055 ±	0.035 ±	0.064 ±	0.026 ±
65.3%		0.022	0.020	0.026	0.020	0.033	0.017
Kap =	NEA	0.128 ±	0.096 ±	0.136 ±	0.061 ±	0.146 ±	0.062 ±
0.458		0.046	0.038	0.045	0.027	0.056	0.028
	RHS	0.627 ±	0.565 ±	0.619 ±	0.515 ±	0.530 ±	0.506 ±
		0.099	0.099	0.101	0.105	0.128	0.108
Result		RHS	RHS	RHS	RHS	RHS	RHS
RF 4	MPA	0.156 ±	0.230 ±	0.144 ±	0.290 ±	0.214 ±	0.310 ±
RHS = 10		0.086	0.103	0.084	0.112	0.099	0.121
CA =	MPE	0.019 ±	0.019 ±	0.030 ±	0.021 ±	0.044 ±	0.015 ±
65.5%		0.016	0.015	0.020	0.016	0.032	0.013
Kap =	NEA	0.076 ±	0.057 ±	0.082 ±	0.037 ±	0.105 ±	0.039 ±
0.490		0.037	0.029	0.035	0.021	0.055	0.022
	RHS	0.748 ±	0.693 ±	0.743 ±	0.652 ±	0.636 ±	0.636±
		0.103	0.111	0.105	0.116	0.147	0.125
Result		RHS	RHS	RHS	RHS	RHS	RHS

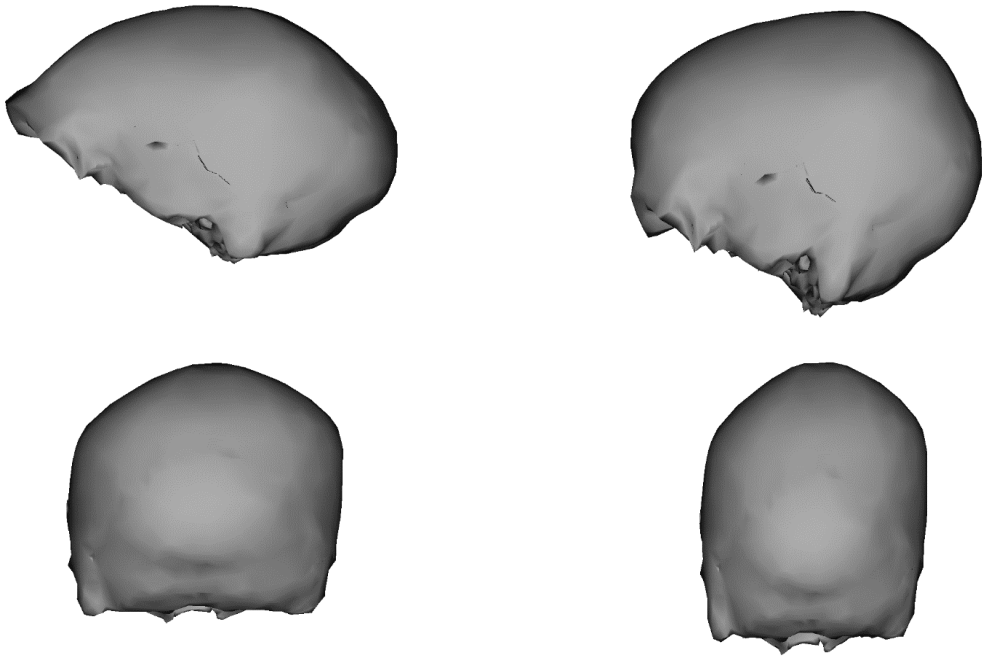

Supplementary Figure 1. Surface warps for the first principal component with the Masai 03 cranium as the reference. Left is PC1 negative, right is PC1 positive. Top is *norma lateralis sinister*, bottom is *norma occipitalis*. The largest difference between PC1 negative and PC1 positive is the distance between glabella and lambda, followed by the difference in the point of highest superior extension on the neurocranium and the surrounding flexion.

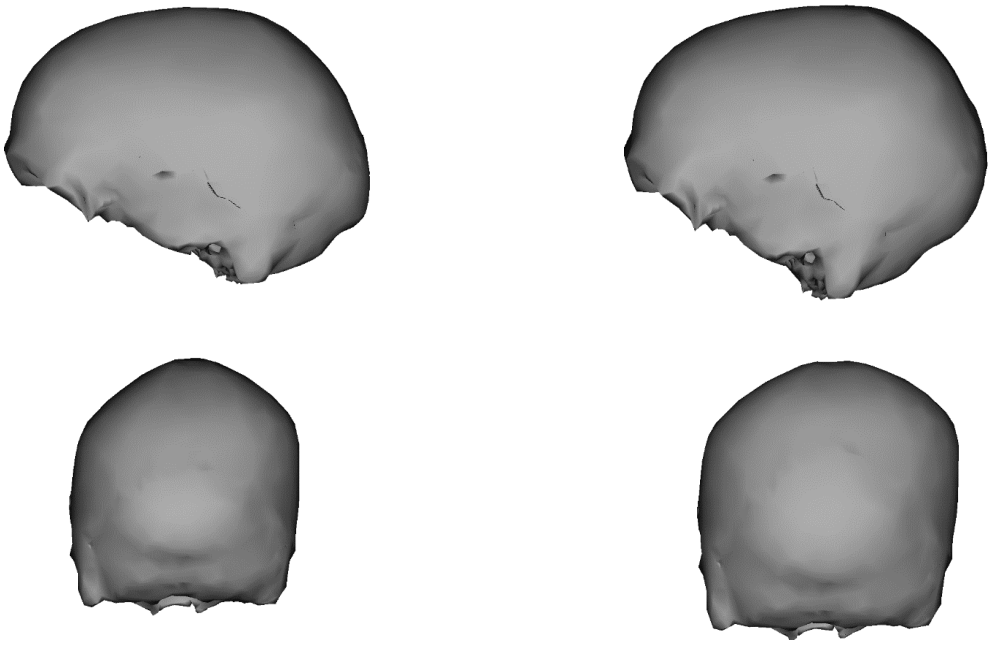

Supplementary Figure 2. Surface warps for the second principal component with Masai 03 as the reference cranium. Left is PC2 negative, right is PC2 positive. Top is *norma lateralis sinister*, bottom is *norma occipitalis*. Largest difference between PC2 negative and PC2 positive is the distance between the points of largest coronal breadth, followed by the distance between lambda and inion.

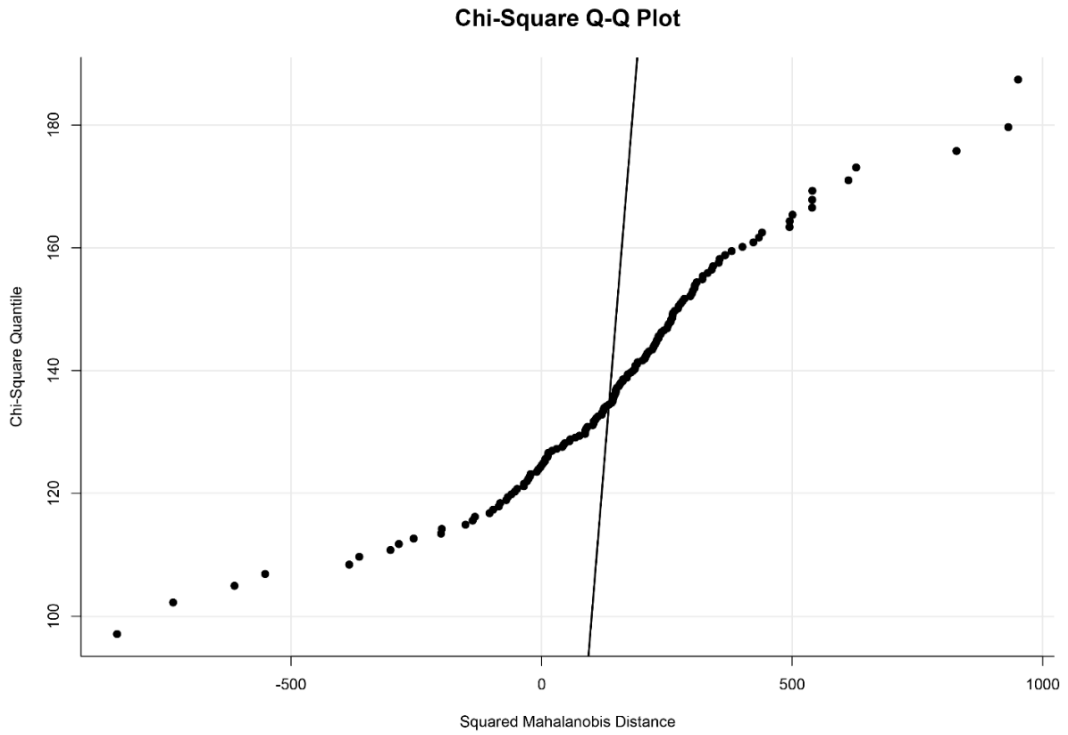

Supplementary Figure 3. Chi-Square quantile-quantile plot on the Procrustes superimposed coordinates (n = 151, p = 138). The diagonal trend line shows the non-normal distribution of the data.

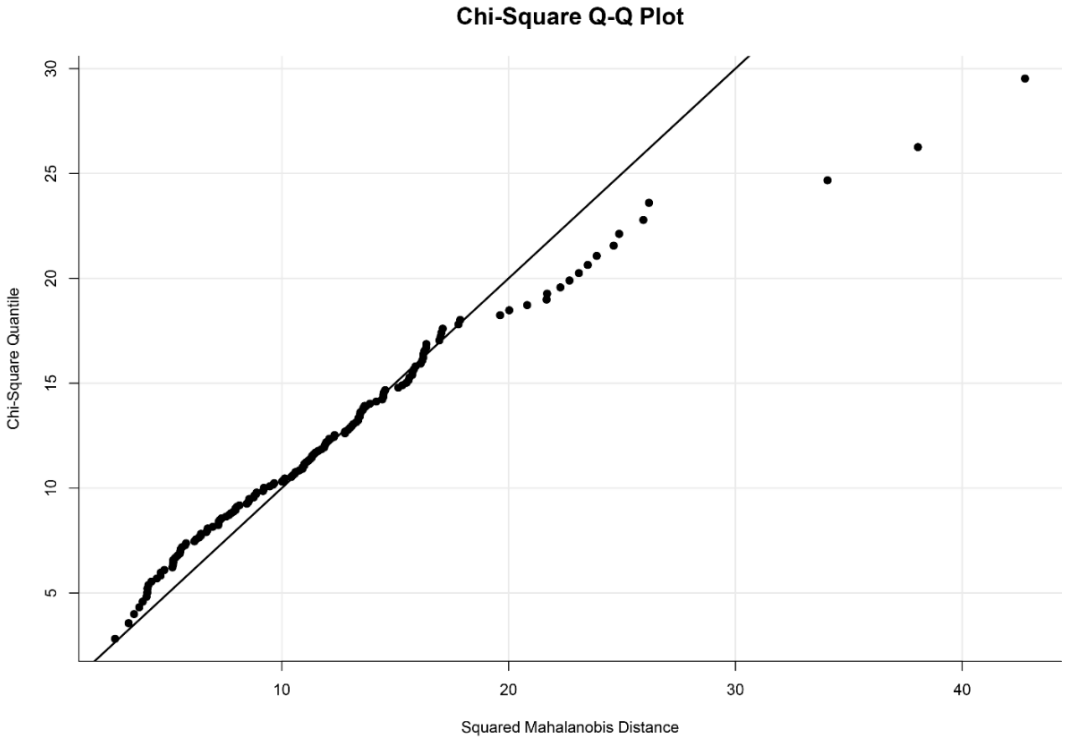

Supplementary Figure 4. Chi-Square quantile-quantile plot on the significant PC scores (n = 151, p = 12). The diagonal trend line represents the non-normal distribution of the data.

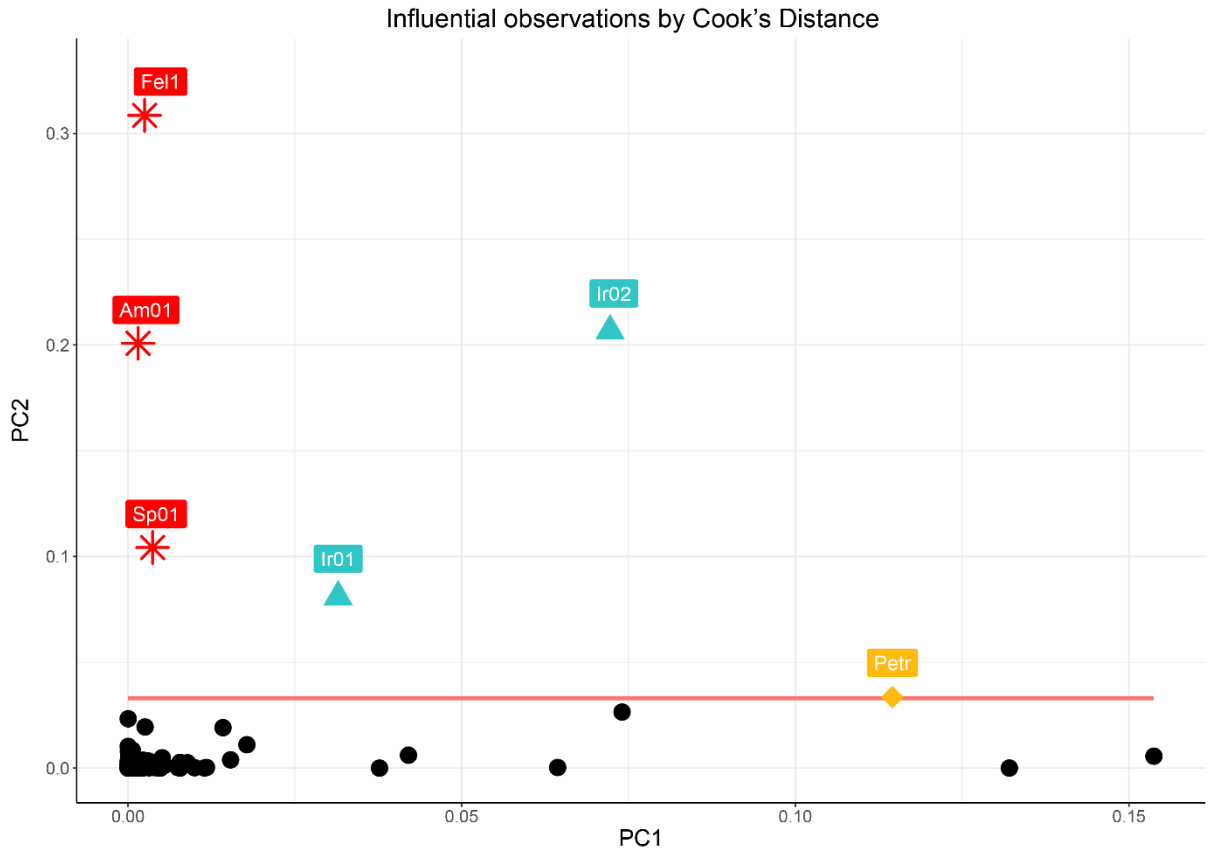

Supplementary Figure 5. Cooks distances on the significant PC scores, here showing PC1 against PC2. The red line represents the mean of all PC scores, multiplied by four. As such, labeled individuals above or on the red line can be considered outliers of the comparative data. Abbreviations specified in Table 1 (main text).

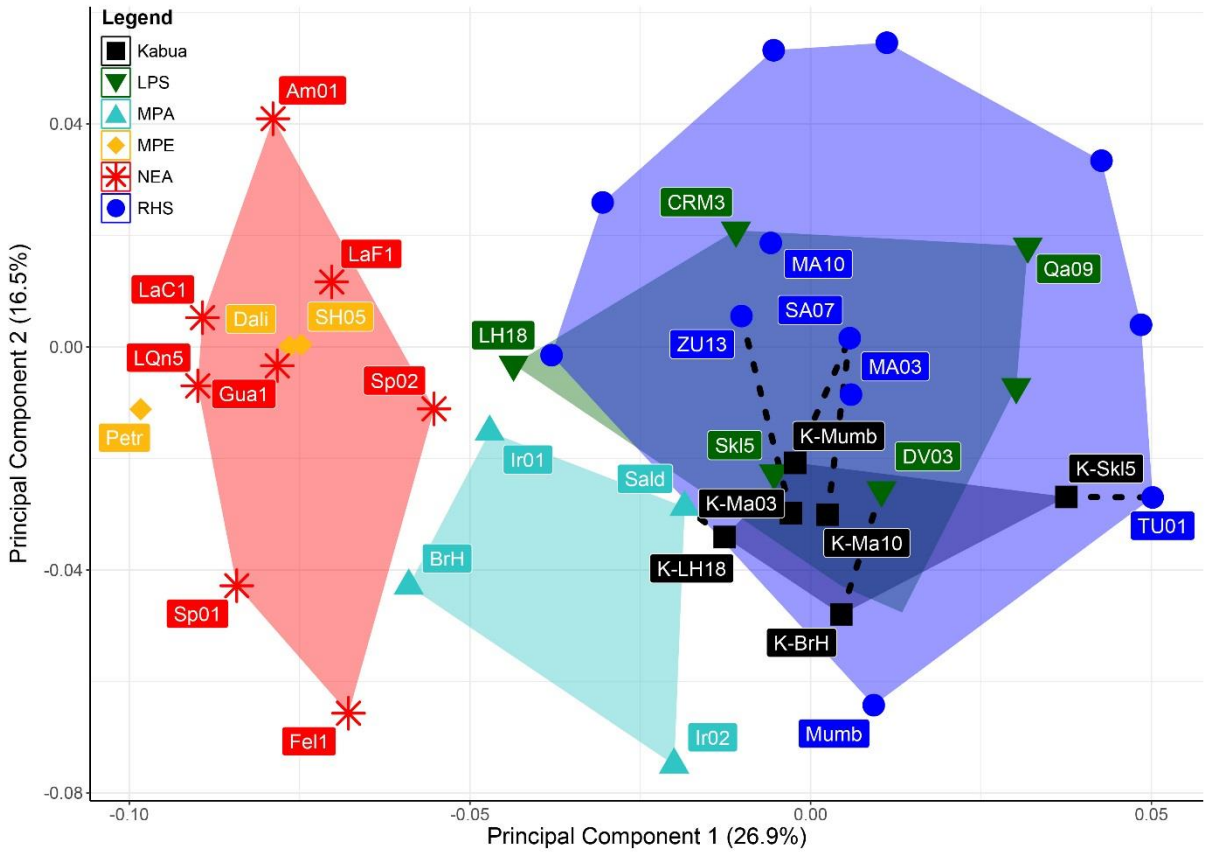

Supplementary Figure 6. PCA of comparative sample (PC1 vs PC2), with the Late Pleistocene (LPS) fossil specimens separated from the RHS group. In both the LPS and RHS groups, only nearest neighbors to reconstructions and reference crania are depicted. Abbreviations specified in Table 1 (main text).

Appendix III

"Somewhere in our DNA must lie the key mutation (or, more probably, mutations) that set us apart - the mutations that make us the sort of creature that could wipe out its nearest relative, then dig up its bones and reassemble its genome."

Elizabeth Kolbert (2014) – *The sixth extinction: an unnatural history*. New York: Henry Holt and Company.

A virtual assessment of the proposed suprainiac fossa on the early modern European calvaria from Cioclovina, Romania.[1]

Abstract

The calvaria from Cioclovina (Romania) has been argued to possess some traits commonly ascribed to individuals belonging to the Neanderthal lineage, including a suprainiac fossa. However, its supranuchal morphology has only been evaluated with a qualitative analysis of the ectocranial surface. We evaluate whether the morphology of the supranuchal area of this specimen is homologous to the Neanderthal condition. We described in detail the external morphology, and, using computed tomography, investigated the internal morphology of the Cioclovina supranuchal area. We took measurements of the internal structures and calculated their relative contributions to total cranial vault thickness, which were compared to published data and evaluated with a principal component analysis (PCA). The Cioclovina supranuchal region is characterized by superficial resorption present on the outer layer of the external table. Neither the diploic layer nor the external table decrease in relative thickness in the area above inion. In the PCA, Cioclovina falls within the convex hulls of recent modern *H. sapiens*. Our results show that the morphology of the Cioclovina supranuchal region does not correspond to the external and internal morphology of the typical Neanderthal suprainiac fossa. It cannot be characterized as a depression, but rather as an area presenting superficial bone turnover. Together with earlier results, there is little phenotypic evidence that Cioclovina has high levels of Neanderthal ancestry. Our study demonstrates the usefulness of this quantitative method in assessing proposed Neanderthal-like suprainiac depressions in Upper Paleolithic and other fossil specimens.

Publication

Bosman, A. M., & Harvati, K. A virtual assessment of the proposed suprainiac fossa on the early modern European calvaria from Cioclovina, Romania. *American Journal of Physical Anthropology, 169(3), 567-574.*

[1] The contents of this article were reprinted with permission by Wiley due to retained author rights that allow authors to include their articles in a thesis or dissertation for non-commercial purposes. A copy of the permissions can be requested from the author.

1. Introduction

The Cioclovina specimen is one of the earliest reliably dated and relatively complete adult anatomically modern human crania from Europe. Found in 1941 during phosphate mining in the Peştera Cioclovina cave, South Transylvania, Romania (Harvati, Gunz, & Grigorescu, 2007; Soficaru, Petrea, Doboş, & Trinkaus, 2007), it was initially described by Rainer and Simionescu (1942) and has been dated with direct Accelerator Mass Spectrometry ^{14}C to 29,000 ± 700 ^{14}C years BP (Olariu et al., 2005) and 28,510 ± 170 ^{14}C years BP (ultrafiltration pretreatment; Soficaru et al., 2007).

Here we evaluate the morphology of the Cioclovina supranuchal region, which has been described as "a shallow but distinct, irregularly rugose, transversely oval depression", located above a nuchal torus together with a conspicuous lack of an external occipital protuberance (Soficaru et al., 2007). This morphology has been argued to reflect the Neanderthal autapomorphic feature known as the suprainiac fossa (Balzeau & Rougier, 2010; Harvati, 2015; Hublin, 1978; Nowaczewska, 2011; Santa Luca, 1978; Stringer, Hublin, & Vandermeersch, 1984), which has been described as a discrete elliptical depression with an uneven floor, confined to the area directly above inion, between the bilateral arches of an occipital torus, with an apex on the midline, and surrounded by a triangular uplifted area of bone (Caspari, 2005; Hublin, 1978; Santa Luca, 1978). However, this autapomorphic status has been disputed, as morphologically similar, though not necessarily homologous, features have been found in Upper Paleolithic specimens (Frayer, 1992; Kramer, Crummett, & Wolpoff, 2001; Trinkaus, 2007), early *H. sapiens* (Haile-Selassie, Asfaw, & White, 2004; Hershkovitz et al., 2015; Li et al., 2017; Trinkaus, 2004) and recent anatomically modern humans (Caspari, 2005; Klein, 2009; Nowaczewska, 2011). Consequently, several scholars (Ahern, Janković, Voisin, & Smith, 2013; Soficaru et al., 2007; Trinkaus, 2007) proposed that the combination of traits found in Cioclovina, and other Upper Paleolithic European *H. sapiens* specimens (Ahern et al., 2013; Trinkaus, 2007), represented a possible phenotypic expression of substantial levels of introgression of Neanderthal genetic material in modern human populations during the dispersal of the latter across Europe (Fu et al., 2016; Smith,

Janković, & Karavanić, 2005; Wolpoff, Hawks, Frayer, & Hunley, 2001). This interpretation was disputed by Harvati et al. (2007), and by Gunz and Harvati (2007), who argued that the overall cranial morphology of Cioclovina, midsagittal convexity of the posterior neurocranium, and the specific anatomy of its supranuchal region lie well within the range of modern human variation. However, while previous works relied on qualitative observations of the external morphology to evaluate whether classic Neanderthal suprainiac fossae and *H. sapiens* supranuchal depressions can be considered homologous structures, recent work by Balzeau and Rougier (2010) on internal bone configurations supports the status of the Neanderthal morphology as derived for this lineage. Through measurements, they demonstrated that the Neanderthal suprainiac fossa primarily affects the thickness of the diploic layer, leaving the thickness of the external table of the upper scale of the occipital bone mostly unaffected (Balzeau & Rougier, 2010). This condition contrasts with that shown by depressions present on *H. sapiens* specimens, which are formed through extensive modification of the external table and leave the diploic layer unaffected (Balzeau & Rougier, 2010).

Furthermore, several genetic studies after 2007 have revealed that Neanderthals and recent *H. sapiens* in Europe did interbreed in various geographic and temporal settings (Fu et al., 2015; Green et al., 2010; Kuhlwilm et al., 2016; Posth et al., 2017; Sankararaman et al., 2014; Vernot & Akey, 2014, 2015). Therefore, the current discussion has shifted from the question whether Neanderthals and modern *H. sapiens* interbred at all, to other issues, such as the extent of admixture or the level of Neanderthal ancestry present in specific fossil *H. sapiens* (Fu et al., 2016). As for Cioclovina, aDNA analysis of this specimen found a Neanderthal genomic component of 4.1% (Fu et al., 2016), similar to levels observed in living non-Africans, although the exact range of Neanderthal ancestry in living non-Africans is debated (e.g. Green et al., 2010; Prüfer et al., 2017; Vernot & Akey, 2014). Because of this relatively low Neanderthal genomic component, especially when compared with other Upper Paleolithic European specimens such as Oase 1 (Fu et al., 2015), an investigation of proposed Neanderthal-like morphologies such as the supranuchal area is of particular

interest. Moreover, to what extent the percentage of genetic ancestry, or the presence of particular Neanderthal alleles, affect the skeletal phenotype remains poorly understood (Dediu & Levinson, 2018; Harvati & Roksandic, 2016; however see Gregory et al., 2017 and Gunz et al., 2019 for recent advances). Studying the fossil material and gaining a better understanding of the underlying biology is thus still relevant. In this manuscript we evaluate both the external and internal morphology of the Cioclovina occipital bone, using the methods published by Balzeau and Rougier (2010). A detailed assessment of the suprainiac morphology of the early Upper Paleolithic calvaria from Cioclovina will help evaluate this morphology as possible phenotypic evidence of partial Neanderthal ancestry for this specimen and ultimately other Upper Paleolithic individuals.

2. Materials and Methods

This study was conducted on a computed tomography (CT) scan of the Cioclovina calvaria, procured using a Siemens Sensation 64 medical CT scanner in the facilities of the Centrul De Sanatate Pro-Life SRL, Bucharest. The direction of scanning was coronal (transverse) with a slice thickness of 0.625 mm, 120 kV tube voltage, and 304 mA tube current (Kranioti et al., 2011). The reconstruction diameter and pixel resolution were 223 and 0.44 mm, respectively, and all slices were formatted to the same size of 512 x 512 pixels (Kranioti et al., 2011). Additionally, we used μCT scans of the La Chapelle-aux-Saints 1 and La Ferrassie 1 Neanderthal specimens obtained from the Musée de l'Homme in Paris, which were included in our analysis to test the comparability of our measurements with the data reported by Balzeau and Rougier (2010). All scans were loaded in Avizo Lite 9.2.0 (FEI Visualization Sciences Group) and were subjected to standard imaging techniques, such as volume rendering and isosurface extraction (Figure 1a-c). Following the methodological framework detailed by Balzeau and Rougier (2010), we used multiplanar reformatting to compute two slices (Figure 1d-e). The first slice was computed over the midsagittal plane, crossing the maximum vertical extension of the depression. The second slice was placed orthogonally on the vertical slice and crosses the maximum horizontal (transverse) direction of the depression. These slices were used to illustrate and quantify the relative

contribution of the internal structures (external table, diploic layer and internal table) to the total thickness of the upper scale of the occipital bone. The quantitative analysis was performed by taking 16 measurements on the vertical slice, at equidistant locations between lambda and the most posterior projecting point of the occipital structures (Balzeau & Rougier, 2010). Subsequently, the area of interest was divided into two zones: the section from lambda to the supranuchal region (Table 1; Area above SD), and the supranuchal area itself, which is inferiorly delimited by the most posteriorly prominent point of the occipital structures (Table 1; Area of SD). As the Cioclovina supranuchal area is not clearly defined superiorly, we used the most posteriorly projecting point of the "hemi-bun" as the superior limit for the supranuchal zone in this specimen. We report the mean relative thickness for the internal structures in the two zones, instead of localized absolute values, as these variables would not be comparable between specimens (Balzeau & Rougier, 2010). These relative values were calculated by first assessing the total thickness of the cranial vault at each equidistant location. Then, the absolute thickness of all internal components was measured. Subsequently, the relative contributions of the internal structures were calculated as percentages of the total thickness of the cranial vault. Additionally, we report both relative and absolute values for the most concave point of the supranuchal area (Table 1; Center of SD).

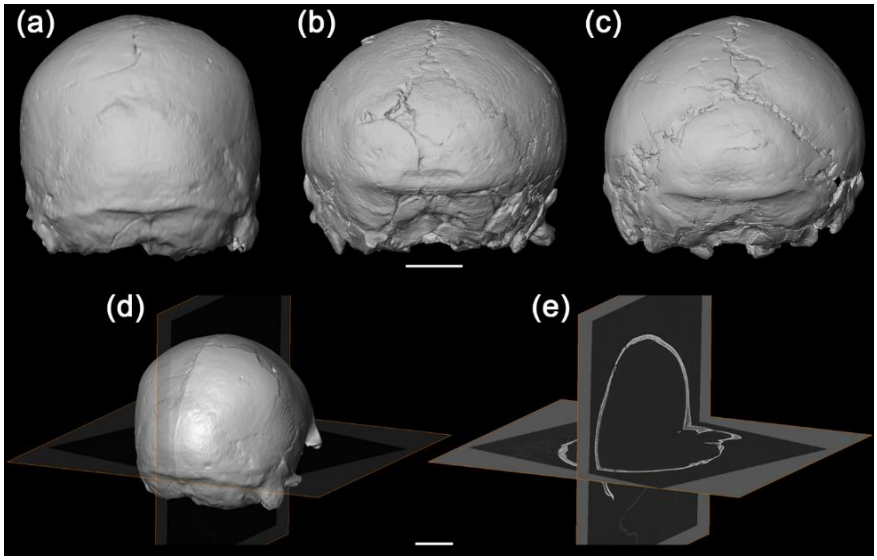

Figure 1. Occipital views of (a) the Cioclovina calvaria, (b) La Chapelle-aux-Saints 1, and (c) La Ferrassie 1 (scale bar = 2 cm); (d) Multiplanar reformatting was used to align two slices to the maximum vertical and transverse extensions of the depression/resorptive area above inion; (e) Slices from Figure 1d, showing the internal structures of the Cioclovina cranial vault (scale bar = 2 cm).

We performed an error test on the Cioclovina specimen by measuring it five times across five days. Subsequently, we computed the coefficient of variation (CoV) to investigate the intra-observer error. To assess whether the combined sample followed a multivariate normal distribution, we used Mardia's test for kurtosis and skewness in the MVN package (Korkmaz, Goksuluk, & Zararsiz, 2014) in R, version 3.5.0 (R Core Team, 2019). Subsequently, we performed a Principal Component Analysis (PCA) on the measurements of the relative contribution of the internal structures throughout the occipital squama. As the internal structures differ greatly in their relative contribution (e.g. a thick diploic layer versus a thin internal table), we used the correlation matrix in the calculation of the PCA. In order to test for inter-observer error between our measurements and the data obtained from the literature, we computed the PCA with the data from Balzeau and Rougier (2010) and projected our measurements on Cioclovina, La Chapelle-aux-Saints 1, and La Ferrassie 1. The PCA plots (Figure 3; Supplementary Figure 1) were generated with the following packages available for R: extrafont (Chang, 2014), ggplot2 (Wickham, 2009), ggrepel (Slowikowski, 2017), and plyr (Wickham, 2011).

3. Results

The vertical slice (Figure 2a) demonstrates that for Cioclovina, the thickness of the external table is more or less constant across most of its occipital scale. Inferior to the supranuchal region, the external table is increased in relative thickness, due to the development of the nuchal torus. In the supranuchal region itself, the external table does not decrease in thickness, which attests to the shallowness of this area. Moreover, the outer and inner layers of the external table have a parallel course throughout the occipital scale, and any possible depression is only represented by superficial changes of the outer layer of the external table.

The diploic layer has the largest contribution to the total occipital scale thickness. Similar to the external table, it is constant in thickness through the occipital scale, with a slight decrease from lambda to the most posterior projection of the occipital squama. There are no signs that the interfaces between the diploic layer and the external table, or between the diploic layer and the internal table, change in course in the supranuchal region. Below the nuchal torus, the diploic layer increases in relative thickness due to the formation of internal occipital crest. Likewise, the internal table of Cioclovina shows almost no variation in relative thickness throughout the occipital scale. This table primarily follows the shape of the occipital lobes and is not affected by changes in the development of the ectocranial structures. There is a slight decrease in internal component thickness at the center of the supranuchal region, due to a medially positioned, vertically oriented groove on the superior sagittal sulcus, just before it enters the internal occipital protuberance (Supplementary Figure 2). The transverse slice (Figure 2f) demonstrates that there are no observable changes in relative thickness of the external table across the horizontal plane. A superficial modification of the outer layer of the external table can be detected, which is possibly related to the small resorptive area visible on the ectocranial surface. The diploic layer increases in thickness due to the development of the internal occipital protuberance, while the thickness of the internal table stays relatively constant and follows the shape of the occipital lobes.

Through the use of the methodological framework described above, we quantified the relative contribution of each internal structure. These data (Table 1) show that the Cioclovina supranuchal region is characterized by almost no variation in relative thickness of the tables. The only observed change in relative thickness of the external table is due to the development of the nuchal torus. Likewise, the diploic layer is constant in its contribution to total cranial vault thickness. It decreases somewhat at the level of nuchal torus development, likely because the external table has a much larger contribution to the total thickness in this area.

Table 1. Linear measurements of Cioclovina and comparative sample[a]

	Area above SD: mean (%)			Area of SD: mean (%)			Center of SD (mm)			Center of SD (%)		
	ET	DL	IT	ET	DL	IT	ET	DL	IT	ET	DL	IT
Cioclovina[b]	31	50	19	39	44	17	1.9	3.0	1.0	33	50	17
La Chapelle-aux-Saints 1	24	57	19	26	55	19	2.7	6.2	1.7	25	58	16
Chapelle 1[b]	27	55	18	28	54	18	2.5	6.4	1.7	24	60	16
La Ferrassie 1	21	64	15	24	63	13	2.2	6.1	1.5	24	62	14
Ferrassie 1[b]	22	64	14	24	62	14	2.3	6.0	1.2	24	63	13
La Quina H5	24	56	20	-	-	-	-	-	-	-	-	-
Spy 1	19	65	16	27	56	17	2.5	6.9	2.0	22	61	18
Spy 10	18	60	22	23	53	24	2.3	4.8	2.6	24	49	27
Salzgitter-Lebenstedt 1	18	64	18	24	57	19	2.1	5.1	1.7	24	57	19
Krapina 5	24	54	22	37	43	20	2.9	4.8	2.5	28	47	25
Le Moustier 1	28	48	24	-	-	-	-	-	-	29	45	26
Swanscombe	32	41	27	33	39	28	2.7	3.3	2.4	32	39	29
Rochereil	35	43	22	36	50	14	3.5	6.5	1.5	30	57	13
Téviec 8	33	48	19	37	49	14	4.1	7.5	1.6	31	57	12
Téviec 9	34	40	26	36	49	15	4.8	7.4	1.8	34	53	13
Téviec 16	35	41	24	35	46	19	4.8	7.1	2.8	33	48	19
Afalou 2	24	59	17	40	46	14	3.5	4.9	1.4	36	50	14
Taforalt XII c1	27	57	16	45	45	10	7.8	8.7	1.8	43	48	10
Taforalt XV c2	29	50	21	57	23	20	3.3	2.5	2.3	41	31	28
Taforalt XV c4	26	55	19	32	49	19	5.2	8.1	2.7	33	51	17
Taforalt XVII	23	61	16	31	51	18	3.1	5.0	1.8	31	51	18

Abbreviations: DL = Diploic layer; ET = External table; IT = Internal table; SD = Suprainiac depression.

[a]Data on Neanderthal specimens and *H. sapiens* from Balzeau and Rougier (2010).

[b]Data collected in this study.

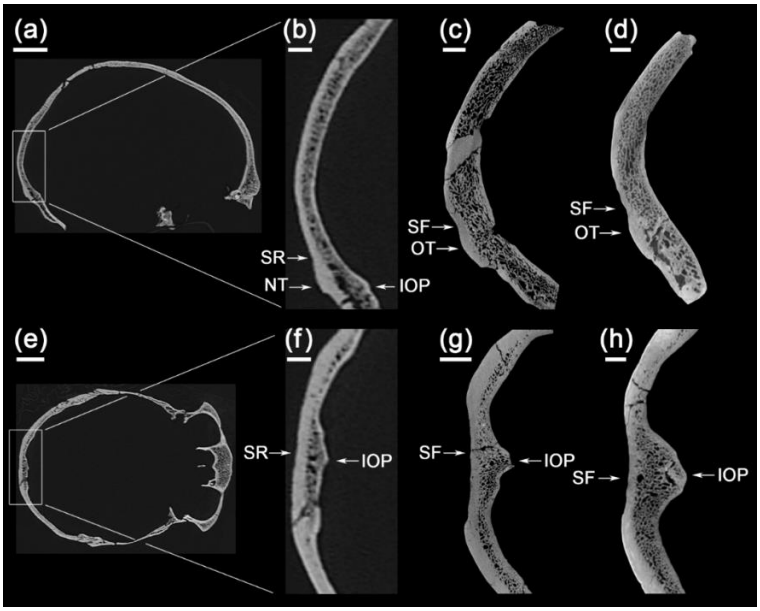

Figure 2. Slices extracted from the volume rendering of Cioclovina, La Chapelle-aux-Saints 1, and La Ferrassie 1, depicting the maximum vertical and transverse extension of the resorptive area above inion. Locations of slices are shown in Figure 1. Boxes and segments show the location of both the vertical and the transverse close-ups. Arrows indicate several relevant occipital structures. (a) Vertical slice of Cioclovina, showing the sagittal plane (scale bar = 2 cm); (b) Zoom of the Cioclovina vertical slice (scale bar = 0.5 cm); (c) La Chapelle-aux-Saints 1 vertical slice (scale bar = 0.5 cm); (d) La Ferrassie 1 vertical slice (scale bar = 0.5 cm); (e) Transverse slice of Cioclovina, showing the coronal plane (scale bar = 2 cm); (f) Zoom of the Cioclovina transverse slice (scale bar = 0.5 cm); (g) La Chapelle-aux-Saints 1 transverse slice (scale bar = 0.5 cm); (h) La Ferrassie 1 transverse slice (scale bar = 0.5 cm). Abbreviations: IOP = Internal occipital protuberance; NT = Nuchal torus; OT = Occipital torus; SF = Suprainiac fossa; SR = Supranuchal region.

3.1. Metric Analysis

The CoV calculated for our measurements of the thickness of the Cioclovina internal structures is around 5 percent. The structure with the highest CoV is the internal table (5.03%), probably due to the very low thickness values for this table. Mardia's test for multivariate normality shows that, in the combined sample, all values are approximately normally distributed (skewness small sample corrected = 14.91, p = 0,135; kurtosis = 0.268, p = 0.789). When projecting our measurements on La Chapelle-aux-Saints 1 and La Ferrassie 1, they plot close to the same specimens by Balzeau and Rougier (2010), which gives us confidence that our methodology and results are comparable to their data (Figure 3).

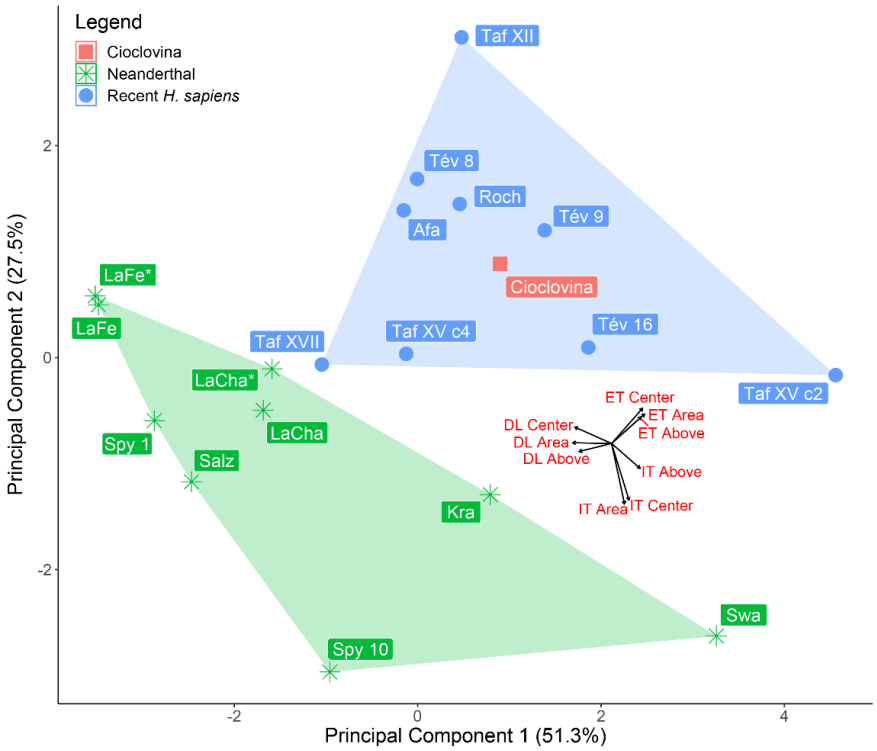

Figure 3. Principal Component Analysis on the correlation matrix, showing PC1 and PC2 (which explain 78.8% of cumulative variance). Data collected in this study (Cioclovina, La Chapelle-aux-Saints 1, and La Ferrassie 1) were projected. Cioclovina: red filled square; Neanderthals: green stars; Recent *H. sapiens*: blue circles. Black arrows represent the loadings of each variable (red). Loadings were plotted some distance from the origin in order to increase readability of the figure. Abbreviations: Afa = Afalou; Kra = Krapina 5; LaCha = La Chapelle-aux-Saints 1; LaCha* = Data on La Chapelle-aux-Saints 1 collected in this manuscript; LaFe = La Ferrassie 1; LaFe* = Data on La Ferrassie 1 collected in this manuscript; Roch = Rochereil; Salz = Salzgitter-Lebenstedt 1; Swa = Swanscombe; Taf = Taforalt; Tév = Téviec.

The PCA, based on the correlation matrix of the relative contribution of all internal structures of the occipital squama, reveals that Neanderthals and recent modern humans are not well separated on the first axis, which explains 51.3 % of total variation. However, the two groups are well separated on the second axis, which explains 27.5% of variation (Figure 3). The external table has positive loadings along this axis, indicating that Neanderthals are characterized by relatively low values and little variation in the relative thickness of the external table. In contrast, recent modern humans are characterized by a large amount of variation in the external table across the occipital squama. The diploic layer is associated with negative loadings along the first and the second axes, indicating that most

Neanderthals show relatively high values and a large amount of variation in the relative thickness of the diploë. Cioclovina falls well within the range of the recent modern *H. sapiens,* also when analyzing each zone separately (Supplementary Figure 1).

4. Discussion

Externally, the occipital bone of Cioclovina shares very few similarities with the Neanderthal occipital morphology, even though the latter show some morphological variability in these features. For example, a geographic trend has been proposed in the morphology of several traits, such as the occipital torus and rounding of the occipital bun (Condemi, 1992; Voisin, 2006). As for the suprainiac fossa, there does not seem to be a temporal/geographic trend in its morphology, as it is already present and fully formed on preneanderthals/early Neanderthals from Europe, such as Swanscombe (Marston, 1937), Biache-Saint-Vaast 1 (Vandermeersch, 1978), Krapina 5 (Caspari, 2006; Radovčić, Smith, Trinkaus & Wolpoff, 1988), and several crania from Sima de los Huesos (Arsuaga, Martínez, Gracia, & Lorenzo, 1997). The feature has also been documented on Western Asian individuals such as Shanidar (Trinkaus, 1983), Amud 1 (Suzuki, 1970; but see Hershkovitz, Latimer, Barzilai, & Marder, 2017 and Tillier, 2005 for a different interpretation), and Tabun C1 (Trinkaus, 1983; but see Tillier, 2005 for a different interpretation).

The medial thickening of the Cioclovina nuchal torus does not match the strongly expressed, often bilaterally projecting, Neanderthal occipital torus (Arsuaga et al., 2014; Balzeau & Rougier, 2010; Klein, 2009). Furthermore, the superior nuchal lines of Cioclovina are robust across the entire occipital bone. Moreover, the Cioclovina supranuchal region, unlike those of Neanderthals, does not evidence a clearly defined depression (Harvati et al., 2007). Additionally, the absence of a true external occipital protuberance on Cioclovina, although similar to Neanderthals as argued by Soficaru et al. (2007) and Trinkaus (2007), is not uncommon among modern humans (Balzeau & Rougier, 2010; Caspari, 2005; Nowaczewska, 2011). Overall, the suprainiac morphology of Cioclovina most resembles the third type of nuchal morphology described for *H. sapiens* by Nowaczewska (2011). This

type is characterized by the absence of an external occipital protuberance, and a tall nuchal torus that is confined inferiorly by the superior nuchal lines and superiorly by a transversely, shallow, elongated depression with unclear borders (Nowaczewska, 2011). Morphologies that can be classified as this type have been observed on recent modern crania from multiple contexts, including, but not limited to, Africa (Lahr, 1994), East Asia (Lahr, 1994), and Oceania (Nowaczewska, 2011). Additionally, several subfossil crania from Europe, including Rochereil and Téviec 8 (Balzeau & Rougier, 2010) resemble this type, but an exhaustive study on nuchal morphologies of recent crania is out of the scope of this paper.

Furthermore, the pattern of internal morphology in Cioclovina is unlike the Neanderthal condition, as exemplified by La Chapelle-aux-Saints 1 and La Ferrassie 1 in this study (Figures 1-2), and described for other Neanderthal specimens by Balzeau and Rougier (2010). It is also not similar to other recent modern humans with some form of depression, as neither our qualitative observations nor our metric analysis could detect any changes in the relative contribution of the diploic layer or the external table to the total bone thickness of the occipital in the supranuchal area. In other words, Cioclovina is only characterized by superficial modification of the ectocranial surface of the area above inion, possibly associated with some form of resorption, as was suggested by Harvati et al. (2007).

The question remains what are the biological mechanisms and processes underlying differences in supranuchal morphology between the classic Neanderthal configuration and that of *H. sapiens*. It has been proposed that the Neanderthal suprainiac fossae and *H. sapiens* supranuchal depressions might have a shared functional morphological etiology (e.g. strain induced by the nuchal musculature) but diverging developmental pathways which are expressed as differences in the development of other occipital structures, different positions of ossification centers above and below the occipital torus, and even differences in overall ecto/endocranial shape (Bräuer, Collard, & Stringer, 2004; Caspari, 2005; Lieberman, 1995; Nowaczewska, 2011; Srivastava, 1992). This last factor is potentially

interesting, as it has been recently suggested that the presence of Neanderthal alleles on specific chromosomes in modern humans is associated with a reduced endocranial globularity (Gunz et al., 2019). Thus, it is possible that the development of supranuchal depressions in *H. sapiens* is correlated with ectocranial morphology (Caspari, 2005), which is in turn integrated with endocranial shape variation (Zollikofer, Bienvenu, & Ponce de León, 2017); all regulated by genes that are potentially affected by the presence of Neanderthal genetic material (Gunz et al., 2019). Therefore, the modern human-like midsagittal convexity of the Cioclovina cranium (Gunz & Harvati, 2007) and its supranuchal morphology described here could potentially be the result not only of its relatively low amount of Neanderthal-derived DNA, but also possibly indicates the lack of specific Neanderthal alleles affecting cranial shape (Gunz et al., 2019). However, other factors such as differences in growth, developmental pathways, and bone thickness between Neanderthals, Cioclovina, and other *H. sapiens* could obscure a possible initial genetic component that resulted from interbreeding.

Returning to the results presented in this manuscript, we conclude that the Cioclovina nuchal morphology falls within the range of anatomically modern human supranuchal variation, in accordance with earlier studies on its inner ear morphology (Uhl, Reyes-Centeno, Grigorescu, Kranioti, & Harvati, 2016), as well as its overall ectocranial (Harvati et al., 2007) and endocranial shape (Kranioti et al., 2011). Taken together, the cranial phenotype of this specimen is consistent with relatively low levels of Neanderthal ancestry, as also indicated by genomic evidence (Fu et al., 2016; Posth et al., 2016). Our study demonstrates that a quantitative approach is useful in assessing the phenotypes of individual Upper Paleolithic specimens as well as how such morphologies compare to the Neanderthal condition. Future analyses of CT scans of additional individuals, including early *H. sapiens* and recent modern humans from other geographic and temporal settings, together with studies on the relationship between endo/ectocranial shape, supranuchal and suprainiac morphology, as well as the functional anatomy of hominin crania will further shed light on this question.

5. Acknowledgements

This research was funded by the German Research Foundation (DFG FOR 2237: Project "Words, Bones, Genes, Tools: Tracking Linguistic, Cultural, and Biological Trajectories of the Human Past"). We thank Prof. Dan Grigorescu from the Department of Paleontology, University of Bucharest, Romania for access to the Cioclovina CT-data, as well as Dr. Tudor Ciprut from the Radiology Department, Centrul De Sanatate Pro-Life SRL, Bucharest, Romania for scanning the specimen. We thank Dr. Antoine Balzeau and Dr. Dominique Grimaud-Hervé from the Musée de l'Homme in Paris for providing us with the µCT scans of the La Ferrassie 1 and La Chapelle-aux-Saints 1 specimens. We also thank the Editor, Associate Editor, and the two reviewers for their comments and suggestions which have greatly improved this manuscript.

6. References

Ahern, J. C., Janković, I., Voisin, J.-L., & Smith, F. H. (2013). Modern human origins in Central Europe. In F. H. Smith & J. C. M. Ahern (Eds.), *The origins of modern humans: Biology reconsidered* (pp. 151-221). Hoboken, New Jersey: John Wiley & Sons.

Arsuaga, J. L., Martínez, I., Gracia, A., & Lorenzo, C. (1997). The Sima de los Huesos crania (Sierra de Atapuerca, Spain). A comparative study. *Journal of Human Evolution, 33*(2), 219-281.

Arsuaga, J. L., Martínez, I., Arnold, L. J., Aranburu, A., Gracia-Téllez, A., Sharp, W. D.,… Carbonell, E. (2014). Neandertal roots: Cranial and chronological evidence from Sima de los Huesos. *Science, 344*(6190), 1358-1363.

Balzeau, A., & Rougier, H. (2010). Is the suprainiac fossa a Neandertal autapomorphy? A complementary external and internal investigation. *Journal of Human Evolution, 58*(1), 1-22.

Bräuer, G., Collard, M., & Stringer, C. (2004). On the reliability of recent tests of the Out of Africa hypothesis for modern human origins. *Anatomical Record, 279A*(2), 701-707.

Caspari, R. (2005). The suprainiac fossa: the question of homology. *Anthropologie (Brno), 43*(2-3), 229-239.

Caspari, R. (2006). The Krapina occipital bones. *Periodicum biologorum, 108*(3), 299-307.

Chang, W. (2014). extrafont: Tools for using fonts. Retrieved from https://CRAN.R-project.org/package=extrafont.

Condemi, S. (1992). *Les Hommes Fossiles de Saccopastore et leur Relation Phylogénétiques* Paris: CNRS.

Dediu, D., & Levinson, S. C. (2018). Neanderthal language revisited: not only us. *Current Opinion in Behavioral Sciences, 21*, 49-55.

Frayer, D. W. (1992). The persistence of Neanderthal features in post-Neanderthal Europeans. In G. Bräuer & F. H. Smith (Eds.), *Continuity or Replacement: Controversies in Homo sapiens Evolution* (pp. 179-188). Rotterdam: Balkema.

Fu, Q., Hajdinjak, M., Moldovan, O. T., Constantin, S., Mallick, S., Skoglund, P., … Pääbo, S. (2015). An early modern human from Romania with a recent Neanderthal ancestor. *Nature, 524*, 216.

Fu, Q., Posth, C., Hajdinjak, M., Petr, M., Mallick, S., Fernandes, D., . . . Reich, D. (2016). The genetic history of Ice Age Europe. *Nature, 534*, 200.

Green, R. E., Krause, J., Briggs, A. W., Maricic, T., Stenzel, U., Kircher, M., ... Pääbo, S. (2010). A Draft Sequence of the Neandertal Genome. *Science, 328*(5979), 710-722.

Gregory, M. D., Kippenhan, J. S., Eisenberg, D. P., Kohn, P. D., Dickinson, D., Mattay, V. S., ... Berman, K. F. (2017). Neanderthal-Derived Genetic Variation Shapes Modern Human Cranium and Brain. *Scientific Reports, 7*(1), 6308.

Gunz, P., & Harvati, K. (2007). The Neanderthal "chignon": variation, integration, and homology. *Journal of Human Evolution, 52*(3), 262-274.

Gunz, P., Tilot, A. K., Wittfeld, K., Teumer, A., Shapland, C. Y., van Erp, T. G. M., … Fisher, S. E. (2019). Neandertal Introgression Sheds Light on Modern Human Endocranial Globularity. *Current Biology, 29*(1), 120-127.

Haile-Selassie, Y., Asfaw, B., & White, T. D. (2004). Hominid cranial remains from upper pleistocene deposits at Aduma, Middle Awash, Ethiopia. *American Journal of Physical Anthropology, 123*(1), 1-10.

Harvati, K. (2015). Neanderthals and their contemporaries. In W. Henke & I. Tattersall (Eds.), *Handbook of Paleoanthropology* (pp. 2243-2279). New York: Springer.

Harvati, K., & Roksandic, M. (2016). The Human Fossil Record from Romania: Early Upper Paleolithic European Mandibles and Neanderthal Admixture. In K. Harvati & M. Roksandic (Eds.), *Paleoanthropology of the Balkans and Anatolia: Human Evolution and its Context* (pp. 51-68). Dordrecht: Springer Netherlands.

Harvati, K., Gunz, P., & Grigorescu, D. (2007). Cioclovina (Romania): affinities of an early modern European. *Journal of Human Evolution, 53*(6), 732-746.

Hershkovitz, I., Marder, O., Ayalon, A., Bar-Matthews, M., Yasur, G., Boaretto, E., . . . Barzilai, O. (2015). Levantine cranium from Manot Cave (Israel) foreshadows the first European modern humans. *Nature, 520*(7546), 216-219.

Hershkovitz, I., Latimer, B., Barzilai, O., & Marder, O. (2017). Manot 1 calvaria and recent modern human evolution: an anthropological perspective. *Bulletins et Mémoires de la Société d'Anthropologie de Paris, 29*(3), 119-130.

Hublin, J.-J. (1978). Quelques caractères apomorphes du crâne néandertalien et leur interprétation phylogénique. *Comptes rendus de l'Académie des sciences. Série III, Sciences de la vie, D287*, 923-926.

Klein, R. G. (2009). *The Human Career: Human Biological and Cultural Origins*. Chicago: University of Chicago Press.

Korkmaz, S., Goksuluk, D., & Zararsiz, G. (2014). MVN: An R Package for Assessing Multivariate Normality. *The R Journal, 6*(2), 151-162.

Kramer, A., Crummett, T. L., & Wolpoff, M. H. (2001). Out of Africa and into the Levant: replacement or admixture in Western Asia? *Quaternary International, 75*(1), 51-63.

Kranioti, E. F., Holloway, R., Senck, S., Ciprut, T., Grigorescu, D., & Harvati, K. (2011). Virtual Assessment of the Endocranial Morphology of the Early Modern European Fossil Calvaria From Cioclovina, Romania. *The Anatomical Record: Advances in Integrative Anatomy and Evolutionary Biology, 294*(7), 1083-1092.

Kuhlwilm, M., Gronau, I., Hubisz, M. J., de Filippo, C., Prado-Martinez, J., Kircher, M., . . . Castellano, S. (2016). Ancient gene flow from early modern humans into Eastern Neanderthals. *Nature, 530*, 429.

Lahr, M. M. (1994). The Multiregional Model of modern human origins: a reassessment of its morphological basis. *Journal of Human Evolution, 26*(1), 23-56.

Li, Z.-Y., Wu, X.-J., Zhou, L.-P., Liu, W., Gao, X., Nian, X.-M., & Trinkaus, E. (2017). Late Pleistocene archaic human crania from Xuchang, China. *Science, 355*(6328), 969-972.

Lieberman, D. E. (1995). Testing hypotheses about recent human evolution from skulls: integrating morphology, function, development, and phylogeny. *Current Anthropology, 36*(2), 159-197.

Marston, A. T. (1937). The Swanscombe Skull. *The Journal of the Royal Anthropological Institute of Great Britain and Ireland, 67*, 339-406.

Nowaczewska, W. (2011). Are *Homo sapiens* nonsupranuchal fossa and neanderthal suprainiac fossa convergent traits? *American Journal of Physical Anthropology, 144*(4), 552-563.

Olariu, A., Skog, G., Hellborg, R., Stenström, K., Faarinen, M., Persson, P., & Alexandrescu, E. (2005). Dating of two Paleolithic human fossil bones from Romania by accelerator mass spectrometry. In A. Olariu, K. Stenström, & R. Hellborg (Eds.), *Applications of High-Precision Atomic and Nuclear Methods* (pp. 222-226). Bucharest: Editura Academiei Romaine.

Posth, C., Renaud, G., Mittnik, A., Drucker, Dorothée G., Rougier, H., Cupillard, C., . . . Krause, J. (2016). Pleistocene Mitochondrial Genomes Suggest a Single Major Dispersal of Non-Africans and a Late Glacial Population Turnover in Europe. *Current Biology, 26*(6), 8278-33.

Posth, C., Wißing, C., Kitagawa, K., Pagani, L., van Holstein, L., Racimo, F., . . . Krause, J. (2017). Deeply divergent archaic mitochondrial genome provides lower time boundary for African gene flow into Neanderthals. *Nature Communications*, *8*, 16046.

Prüfer, K., de Filippo, C., Grote, S., Mafessoni, F., Korlević, P., Hajdinjak, M., . . . Pääbo, S. (2017). A high-coverage Neandertal genome from Vindija Cave in Croatia. *Science, 358*(6363), 655-658.

R Core Team (2019). R: A language and environment for statistical computing. R Foundation for Statistical Computing, Vienna, Austria, https://www.R-project.org/.

Radovčić, J., Smith, F. H., Trinkaus, E., & Wolpoff, M. H. (1988). *The Krapina hominids: an illustrated catalog of skeletal collection*. Zagreb: Croatian Natural History Museum.

Rainer, F., & Simionescu, I. (1942). Sur le premier crâne d'homme Paléolithique trouvé en Roumanie. *Analele Academiei Romane, Memoriile Sectiunii Sçtiintifice Seria III, 17*, 489-503.

Sankararaman, S., Mallick, S., Dannemann, M., Prüfer, K., Kelso, J., Pääbo, S., . . . Reich, D. (2014). The genomic landscape of Neanderthal ancestry in present-day humans. *Nature, 507*, 354-357.

Santa Luca, A. P. (1978). A re-examination of presumed Neandertal-like fossils. *Journal of Human Evolution, 7*(7), 619-636.

Slowikowski, K. (2017). ggrepel: Repulsive Text and Label Geoms for 'ggplot2'. Retrieved from https://CRAN.R-project.org/package=ggrepel.

Smith, F., Janković, I., & Karavanić, I. (2005). The assimilation model, modern human origins in Europe, and the extinction of Neandertals. *Quaternary International, 137*(1), 7-19.

Soficaru, A., Petrea, C., Doboş, A., & Trinkaus, E. (2007). The human cranium from the Peştera Cioclovina Uscată, Romania: context, age, taphonomy, morphology, and paleopathology. *Current Anthropology, 48*(4), 611-619.

Srivastava, H. C. (1992). Ossification of the membranous portion of the squamous part of the occipital bone in man. *Journal of Anatomy, 180*(2), 219-224.

Stringer, C. B., Hublin, J.-J., & Vandermeersch, B. (1984). The origin of anatomically modern humans in Western Europe. In H. Smith & F. Spencer (Eds.), *The Origins of Modern Humans: a World Survey of the Fossil Evidences* (pp. 51-135). New York: Alan R. Liss.

Suzuki, H. (1970). The skull of the Amud man. In H. Suzuki & F. Takai (Eds.), *The Amud man and his cave site*. Tokyo: University of Tokyo Press.

Tillier, A.M. (2005). The Tabun C1 Skeleton: A Levantine Neanderthal? *Mitekufat Haeven: Journal of the Israel Prehistoric Society, 35*, 439-450.

Trinkaus, E. (1983). *The Shanidar Neandertals*. New York: Academic Press.

Trinkaus, E. (2004). Eyasi 1 and the suprainiac fossa. *American Journal of Physical Anthropology, 124*(1), 28-32.

Trinkaus, E. (2007). European early modern humans and the fate of the Neandertals. *Proceedings of the National Academy of Sciences, 104*(18), 7367-7372.

Uhl, A., Reyes-Centeno, H., Grigorescu, D., Kranioti, E. F., & Harvati, K. (2016). Inner ear morphology of the cioclovina early modern European calvaria from Romania. *American Journal of Physical Anthropology, 160*(1), 62-70.

Vandermeersch, B. (1978). Étude préliminaire du crâne humain du gisement paléolithique de Biache-Saint-Vaast (Pas-de-Calais). *Bulletin de l'Association Française pour l'Étude du Quaternaire*, 15, 65-67.

Vernot, B., & Akey, J. M. (2014). Resurrecting Surviving Neandertal Lineages from Modern Human Genomes. *Science, 343*(6174), 1017-1021.

Vernot, B., & Akey, Joshua M. (2015). Complex History of Admixture between Modern Humans and Neandertals. *American Journal of Human Genetics, 96*(3), 448-453.

Voisin, J. L. (2006). Speciation by distance and temporal overlap: a new approach to understanding Neanderthal evolution. In K. Harvati, & T. Harrison (Eds.), *Neanderthals Revisited: New Approaches and Perspectives* (pp. 299-314). Dordrecht: Springer Netherlands.

Wickham, H. (2009). *ggplot2: Elegant Graphics for Data Analysis*. New York: Springer-Verlag.

Wickham, H. (2011). The Split-Apply-Combine Strategy for Data Analysis. *Journal of Statistical Software, 40*(1), 1-29.

Wolpoff, M. H., Hawks, J., Frayer, D. W., & Hunley, K. (2001). Modern Human Ancestry at the Peripheries: A Test of the Replacement Theory. *Science, 291*(5502), 293-297.

Zollikofer, C. P. E., Bienvenu, T., & Ponce de León, M. S. (2017). Effects of cranial integration on hominid endocranial shape. *Journal of Anatomy, 230*(1), 85-105.

7. Supplementary Material

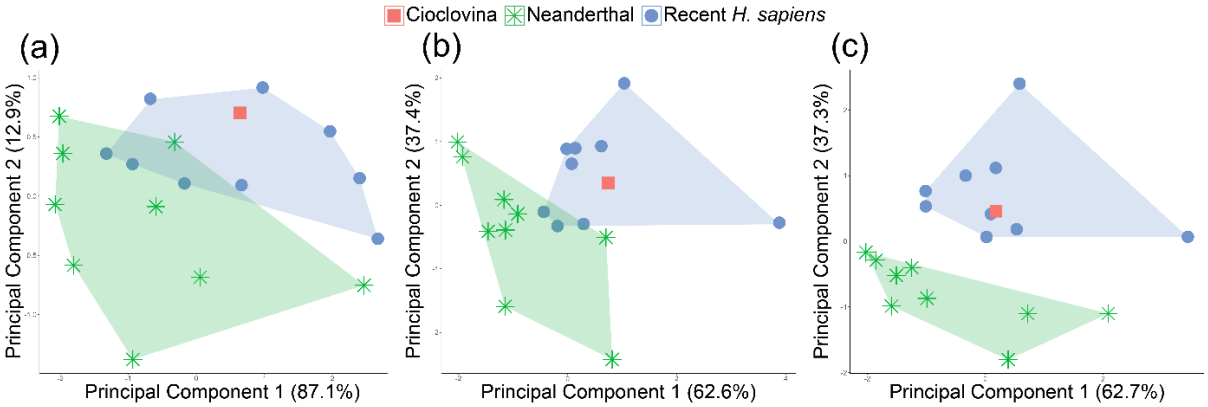

Supplementary Figure 1. Principal Component Analyses on the correlation matrix, showing PC1 and PC2 for each zone indicated in Table 1. (a) Area above the suprainiac depression; (b) Area of the depression; (c) Center of the depression. Data collected in this study (Cioclovina, La Chapelle-aux-Saints 1, and La Ferrassie 1) were projected.

Supplementary Figure 2. Endocranial view of the Cioclovina occipital, showing the endocranial occipital structures. The arrow indicates the groove on the superior sagittal sulcus mentioned in the text (scale bar = 1 cm).

Appendix IV

"*For a species that is both narcissistic and inquisitive, Homo sapiens has so far done a remarkably poor job of defining itself as a morphological entity. The upshot is that scientists have, on the whole, been content to follow in the spirit of Linnaeus, who … contented himself in the case of Homo with "Nosce te ipsum" ("know thyself;" p. 20).*"

Ian Tattersal & Jeffrey Schwartz (2008) – The morphological distinctiveness of Homo sapiens and its recognition in the fossil record: Clarifying the problem. *Evolutionary Anthropology: Issues, News, and Reviews, 17*(1), 49-54.

A virtual assessment of the suprainiac depressions on the Eyasi I and ADU-VP-1/3 crania

Abstract

Despite a steady increase in our understanding of the phenotypic variation of Middle Pleistocene-Late Pleistocene *Homo*, debate continues over phylogenetically informative features. One such trait is the suprainiac fossa, a depression on the occipital bone that is commonly considered an autapomorphy of the Neanderthal lineage. Challenging this convention, depressions in the suprainiac region have also been described for two Middle-Late Pleistocene hominin crania from sub-Saharan Africa: Eyasi I and ADU-VP-1/3. Here we employ a combined quantitative and qualitative approach, using micro-CT imaging to investigate the occipital depressions above inion on these specimens. Results show that both the external and internal morphologies of these depressions do not bear any resemblance to the Neanderthal condition. This is confirmed by linear measurements and Principal Component Analyses, which demonstrate that the relative thickness values for the internal structures in Eyasi I and ADU-VP-1/3 are within the range of *H. sapiens*. Thus, our results support the autapomorphic status of the Neanderthal suprainiac fossa and highlight the need to employ nuanced approaches and multiple lines of evidence when discussing the expression of phenotypic traits, character states, and the relationships between the taxa for which these traits are being described.

Submitted to the Journal of Human Evolution

Bosman, A. M., Reyes-Centeno, H., & Harvati, K. (in prep). A virtual approach to the investigation of the suprainiac depressions on the Eyasi I and ADU-VP-1/3 crania.

1. Introduction

The suprainiac fossa has been widely considered a Neanderthal derived feature, described as a discrete elliptical depression with an uneven floor, confined to the area directly above the inion, between the bilateral arches of the occipital torus (a prominent shelf-like structure between the supreme and superior nuchal lines; Hublin, 1978a, 1978b, 1983), with an apex on the midline (Balzeau & Rougier, 2010; Franciscus & Holliday, 2013; Harvati, 2015; Harvati et al., 2007, 2019; Hublin, 1978a; Hublin, 1984; Nowaczewska, 2011; Nowaczewska et al., 2019; Santa Luca, 1978; Schwartz & Tattersall, 2005a; Stringer et al., 1984). Initially described by Virchow (1872) as a pathological cranial feature on the Neanderthal type specimen, Feldhofer 1, it was later recognized by Klaatsch (1902), Gorjanović-Kramberger (1902), and Boule (1911-1913) as a non-pathological trait present on the Krapina (Croatia), Spy (Belgium), and La Chappelle-aux-Saints (France) Neanderthal crania. According to the accretion hypothesis (Dean et al., 1998; Hublin, 1998), the suprainiac fossa likely became fixed in the Neanderthal lineage, to the extent that some consider it to be present in all Late Pleistocene European Neanderthals (e.g. Smith et al., 2005) and in a less pronounced form in earlier Middle Pleistocene European hominins (Arsuaga et al., 2014).

Depressions above inion proposed as possibly homologous, or at least related, to the Neanderthal suprainiac fossa have been reported on several adult fossil human crania from late Middle and Late Pleistocene Africa (e.g. Balzeau & Rougier, 2010; Haile-Selassie et al., 2004; Trinkaus, 2004), Upper Paleolithic Europe (e.g. Caspari, 2005; Frayer, 1992; Kramer et al., 2001; Soficaru et al., 2006; Soficaru et al., 2007; Trinkaus, 2007), Late Pleistocene Levant (e.g. Skhūl V, Qafzeh VI, and Manot 1; Hershkovitz et al., 2015, 2017; Kramer et al., 2001; Smith et al., 2005), Middle Pleistocene China (Xuchang 2; Li et al., 2017), and Late Pleistocene Australia (e.g. Kow Swamp and Willandra Lakes; Curnoe, 2011; Thorne & Macumber, 1972; Wolpoff et al., 2001). Moreover, similar structures have been described for Holocene specimens from Europe, Africa, and Australia (Balzeau & Rougier, 2010; Lahr, 1994; Nowaczewska, 2011; Nowaczewska et al., 2019). While variable in their morphology,

generally two categories of suprainiac depressions have been reported for fossil and recent *H. sapiens*: supranuchal or non-supranuchal (Caspari, 2005; Nowaczewska, 2011; Nowaczewska et al., 2019). Supranuchal depressions (Sládek 2000, as cited in Caspari, 2005) were used to differentiate depressions on Neanderthal crania from those observed on Early Upper Paleolithic central European modern human crania. The latter are lightly delineated, generally V-shaped in appearance, and associated with the development of a strong superior nuchal line and/or an external occipital protuberance, a trait that is absent in Neanderthals (Caspari, 2005). Most authors agree that these supranuchal depressions are not homologous to the Neanderthal suprainiac fossa (Sládek, 2000 as cited in Caspari, 2005; Trinkaus, 2004; Caspari, 2005; Trinkaus, 2007; Nowaczewska et al., 2019). Non-supranuchal depressions, on the other hand, were defined on Late Pleistocene *H. sapiens* fossils possessing depressions more similar to the Neanderthal condition and not solely defined by the development of an external occipital protuberance (Caspari, 2005). Instead, they are associated with a marked relief for the superior and supreme nuchal lines (Balzeau & Rougier, 2010), or an occipital torus (Nowaczewska, 2011). Especially depressions associated with a bilaterally arched occipital torus have been proposed to reflect the Neanderthal condition (e.g. Caspari, 2005; Nowaczewska, 2011; Nowaczewska et al., 2019).

The presence of suprainiac depressions on specimens from Late Pleistocene Eurasia has been argued to reflect substantial genetic admixture and/or regional continuity between *H. sapiens* and Neanderthals (e.g. Kramer et al., 2001; Li et al., 2017; Smith, 1991; Smith et al., 2005; Trinkaus, 2007, 2011; Wolpoff et al., 2001). On the other hand, the presence of similar features on African Middle and Late Pleistocene hominins (e.g. Bräuer & Leakey, 1987; Haile-Selassie et al., 2004; Saban, 1975; Trinkaus, 2004) puts into question the status of the suprainiac fossa as a Neanderthal autapomorphy, since the trait could possibly be inherited from the common ancestor of modern humans and Neanderthals. Moreover, the presence of occipital depressions above inion across geographically and temporally disparate samples has suggested to some that this feature could be a result of convergent evolution or functional adaptation (e.g. Caspari, 2005; Lieberman, 1995; Nowaczewska, 2011). As a

result, there are currently three competing hypotheses that could explain the external morphological similarity between Neanderthal suprainiac fossae and suprainiac depressions in *H. sapiens* (admixture, common ancestry, and convergence) and the phylogenetic significance of depressions above inion is not well-understood.

In order to systematically evaluate these hypotheses, recent research has focused on the internal morphology of the suprainiac region (i.e. external table, diploic layer, and internal table: Balzeau and Rougier 2010, 2013; Nowaczewska et al., 2019). For example, Balzeau and Rougier (2010, 2013) considered that internal morphologies of depressions and their surrounding occipital bone regions in Middle-Late Pleistocene European Neanderthals differ from those of Late Pleistocene and Holocene *H. sapiens*. By analyzing the internal structures, Balzeau and Rougier (2010) found that the *H. sapiens* suprainiac form is characterized by significant bone remodeling and thinning restricted to the external table. In contrast, the Neanderthal suprainiac form is characterized by remodeling of the diploic layer, while the external table exhibits no remodeling on the occipital squama (Balzeau & Rougier, 2010). These results suggest that the suprainiac fossa found in Neanderthals can be considered an autapomorphic (derived) trait. This was confirmed by Bosman and Harvati (2019) through an investigation of the internal morphology of the proposed suprainiac depression on the Upper Paleolithic European specimen from Cioclovina (Soficaru et al., 2007). By using a combined qualitative and quantitative framework, it was found that the suprainiac morphology of the Cioclovina calvaria shares no morphological traits with the Neanderthal condition. As such, that study concluded that the suprainiac morphology of Cioclovina is consistent with relatively low levels of Neanderthal ancestry, as indicated by genomic evidence (Fu et al., 2016; Posth et al., 2016). This implies that the suprainiac depression in this specimen is likely not the result of recent admixture with Neanderthal populations (Bosman & Harvati, 2019).

However, these studies on the internal morphology of the suprainiac depression have mostly compared the Neanderthal condition to either Upper Paleolithic or recent modern

H. sapiens and are thus primarily relevant to the recent admixture hypothesis. As such, both the common ancestry and convergence hypotheses have yet to be tested using a systematic review of both the external and internal morphology of suitable fossil material. To this end, we investigate here the proposed suprainiac depressions on the Eyasi I (Tanzania) and ADU-VP-1/3 (Ethiopia) specimens. These specimens are especially relevant for the common ancestry scenario, as they date close to currently proposed times of dispersal of anatomically modern humans out of Africa (ADU-VP-1/3) and to the time of appearance of modern human anatomical traits in eastern Africa (Eyasi I) (Reyes-Centeno et al., 2015; Sahle et al. 2018, 2019), respectively. If the depressions on Eyasi I and ADU-VP-1/3 are found to be quantitatively and qualitatively similar to the Neanderthal condition, then the status of the suprainiac fossa as a diagnostic Neanderthal-derived trait must be reconsidered, complicating the taxonomic assignment of isolated occipital bones in the fossil record. Alternatively, if the depressions above inion on Eyasi I and ADU-VP-1/3 are found to differ from the Neanderthal condition, then the suprainiac fossa can be tentatively retained as an autapomorphic trait. Here, we explore these competing hypotheses by performing a qualitative assessment of the external morphology of the putative suprainiac depressions and related occipital superstructures in Eyasi I and ADU-VP-1/3, as well as by making both qualitative and quantitative evaluations of their internal structure using micro-computed tomography (μCT). In addition, we review the current understanding of the suprainiac depression in Neanderthals and modern humans. Finally, we discuss the possible influence of admixture, common ancestry, and convergence in the etiology of this trait in the context of our findings.

1.1. Background: Previous studies on the external morphology of suprainiac depressions in Neanderthals and *H. sapiens*

It has been argued that most known Neanderthal fossils, including juvenile specimens, exhibit the set of morphological characteristics associated with the suprainiac fossa (Ahern, 2006; Smith et al., 2005). In the framework of the accretion hypothesis (Dean et al., 1998; Hublin, 1998), which documents the origin and succession of specific Neanderthal

craniofacial traits across four "stages" of Neanderthal evolution (early-pre-Neanderthals, pre-Neanderthals, early Neanderthals, and classic Neanderthals), some morphological variability in the suprainiac fossa can be observed. For example, Steinheim and Biache-Saint-Vaast 1, respectively defined as a "pre-Neanderthal" (stage 2) and "early Neanderthal" (stage 3), show a relief area in the middle of the suprainiac fossa. This condition has been argued to represent an intermediate position between the early-pre-Neanderthals, which exhibit a so-called "incipient" suprainiac fossa (e.g. the Sima de los Huesos specimens (Arsuaga et al., 1997, 2014) and Swanscombe (Marston, 1937)), and the classic Neanderthal morphology of later specimens such as La Chapelle-aux-Saints 1 and La Ferrassie (Balzeau & Rougier, 2010). However, there is also morphological variability in the suprainiac fossa within these stages (Caspari, 2005; Hublin, 1978a; Santa Luca, 1978; Schwartz & Tattersall, 2005b; Tattersall & Schwartz, 2006). Moreover, while there is no clear geographic variation of this character state, it has been proposed that several Western Asian individuals such as Shanidar, Amud 1, and Tabun C1 do not exhibit a clearly defined suprainiac fossa (e.g. Tillier, 2005; Hershkovitz et al., 2017; but see Trinkaus, 1983; Suzuki, 1970).

The external morphology of the *H. sapiens* suprainiac depression has also been shown to be greatly variable. Using a classification scheme that is more detailed than the previously mentioned supranuchal and non-supranuchal categories (Caspari, 2005), Nowaczewska (2011) distinguished four different forms of depressions above inion in *H. sapiens*, based on Holocene adult crania from Europe (Poland; $n = 44$), Africa (Uganda; $n = 33$) and Australia (Klaatsch collection; $n = 36$). The first form corresponds to the supranuchal fossae defined by Sládek (2000, as cited in Caspari, 2005). Depressions categorized under this type are triangular in shape with an inferiorly pointing apex, constrained by an external occipital protuberance, and have a superior border that is not discrete and flows over into the upper occipital scale (Nowaczewska, 2011). The second and third types are similar to the non-supranuchal depressions described by Caspari (2005). Both types are characterized by a transversely elliptical or round fossa in an area of bone above inion, which is thicker than the rest of the occipital squama, as well as a conspicuous lack of an external occipital

protuberance (Nowaczewska, 2011). In contrast to the second type, depressions of the third type are characterized by the occurrence of an occipital torus. In early and anatomically modern *H. sapiens*, the occipital torus is used to define the projecting area of bone between the superior and supreme nuchal lines (*sensu* Lahr, 1996; Hublin, 1978b). This structure differs from the Neanderthal condition in that it is generally supero-inferiorly taller and not bilaterally arched (Caspari, 2005; Nowaczewska, 2011). Suprainiac depressions grouped under the fourth type bear the greatest resemblance to the Neanderthal condition (Nowaczewska, 2011). These depressions are located above the medial portion of an occipital torus and are elongated in the transverse direction. The occipital tori on these crania are bilaterally arched, poorly expressed laterally, weakly developed, and have an obscure upper margin (Nowaczewska, 2011). Nowaczewska (2011) found all types of these depressions in the Holocene modern human samples, at a relatively moderate frequency (n = 31/113).

1.2. Eyasi I (Tanzania)

The Eyasi hominin fossil assemblage was first discovered in 1935 by Ludwig and Margit Kohl-Larsen in the *Westbuch* (or West Bay) locality along the northeastern shore of Lake Eyasi, Tanzania (Kohl-Larsen, 1941, 1943; Reck & Kohl-Larsen, 1936). It comprises at least three individuals (Eyasi I-III) represented by fragmentary fossils recovered from the surface of the Lake Eyasi shore (Protsch, 1981; Reck & Kohl-Larsen, 1936). The elements assigned to Eyasi I comprise a posterior cranial vault, including a well preserved occipital squama, frontal bone, most of the parietal bones, and several teeth. Both Eyasi II and III include portions of the upper occipital bone but do not preserve the iniac region. In 1993, another fragment of an occipital bone, Eyasi IV, was recovered in the West Bay locality but also lacks the iniac region (Bräuer & Mabulla, 1996).

The Eyasi hominin assemblage is thought to date to the Middle or Late Pleistocene. On geological and biochronological grounds, Reck and Kohl-Larsen (1936) considered the Eyasi I hominin to be of Late Pleistocene antiquity—a view that was shared in later assessments

by Leakey (1936, 1946) and Reeve (1946). Attempts at directly dating the fossil material from the West Bay locality, including fragments from Eyasi I, have thus far been unsuccessful (Mehlman, 1987, 1989; Protsch, 1981). At present, two geochronological interpretations are possible. The first is an approximation based on the stratigraphic association of the Eyasi deposits and other well-dated contexts from the region. Mehlman (1987, 1989) considered the ~130 ka Uranium series dates at the base of the nearby Mumba rock shelter as a minimum date for the top of the Eyasi beds. He speculated that the base of the Eyasi beds could date to ~375 ka, based on approximations of sedimentation rates of the Mumba beds (Mehlman, 1987). Another interpretation for the antiquity of Eyasi I is that it is pene-contemporaneous to a frontal bone fragment, EH06, discovered in 2005 in the locality described by Kohl-Larsen as *Nordostbuch* (or Northeast Bay) (Domínguez-Rodrigo et al., 2008). ESR and U-series age estimates on a wildebeest tooth found in association with EH06 date to between 138 and 88 ka (Domínguez-Rodrigo et al., 2008). Thus, while still unresolved, the geochronology of the Eyasi I specimen is broadly placed between 375-88 ka. While Eyasi I is the holotype for the species *Palaeoanthropus njarasensis* (Reck & Koh-Larsen, 1936), its taxonomic affinities remain unresolved and it is instead often considered an early member of the *Homo sapiens* lineage (e.g. Bräuer, 2012).

1.3. ADU-VP-1/3 (Aduma, Ethiopia)

The Aduma remains were discovered in the Middle Awash, Ethiopia, in the 1990s (Haile-Selassie et al., 2004). Cranial remains representing four adult hominins were recovered from Late Pleistocene sediments at Aduma. The most complete of these, ADU-VP-1/3, was recovered *in situ*, eroding in more than 100 separate fragments from an area of 100 m^2. Although incomplete, the occipital squama of this specimen is preserved and exhibits important diagnostic structures, such as an external occipital protuberance, superior nuchal lines, and a median nuchal crest. While the cranium has not been dated directly, several dating techniques have been applied to materials from the Ardu sequence from which the hominin remains were recovered (Yellen et al., 2005). These include Argon/Argon (on feldspar extracted from pumice); AMS radiocarbon (on *Unio* bivalve shells); amino-acid

racemization (on shells from the silt layers in the Ardu B sequence); Uranium series (on fossilized mammal and crocodile teeth, fossilized mammal bone, and fossilized catfish bone); and optically stimulated luminescence and thermoluminescence (on coarse-grained quartz). Results provided an estimated range of antiquity between 105 and 79 ka for the human remains (Yellen et al., 2005). Because of its proposed chronology and cranial morphology, ADU-VP-1/3 has been commonly described as anatomically modern *H. sapiens* (Haile-Selassie et al., 2004; Klein, 2009; Lieberman, 2011).

2. Materials and Methods

In this study, we analyzed the original Eyasi I and ADU-VP-1/3 fossils. For comparative and illustrative purposes, we also included two Neanderthal crania from Middle Paleolithic France, La Chapelle-aux-Saints 1 and La Ferrassie 1, as well as a recent modern human cranium with a depression above inion. La Chapelle-aux-Saints 1 was found in the Bouffia Bonneval Cave, France (Boule, 1911-1913; Bouyssonie et al., 1908) and has been dated by ESR to between 56 ± 4 and 47 ± 3 ka (Grün & Stringer, 1991). La Ferrassie 1 is part of a skeletal assemblage, consisting of two adult and five sub-adult individuals (Capitan & Peyrony, 1909, 1911, 1912; Schwartz & Tattersall, 2002) and has been dated with OSL between 45-43 ka (Guérin et al., 2015). The recent modern human cranium Masai 12 is part of a skeletal assemblage of 15 well-preserved individuals excavated near the northeastern shores of Lake Eyasi by the Kohl-Larsens in 1938 (Bräuer, 1983; Kohl-Larsen, 1943). The name "Masai" was assigned by the research team, but Kohl-Larsen (1941) acknowledged that it was possibly erroneous. As the ethno-cultural affiliation of these burials remains unresolved, we follow the catalogue system of the curated material and continue to refer to these specimens as Masai in this study. Charcoal found in proximity to another skeleton from the same context, Masai 1, has been radiocarbon dated to 1810±50 CE (Bräuer, 1983).

Eyasi I, ADU-VP-1/3, Masai 12, La Chapelle-aux-Saints 1, and La Ferrassie 1 (Table 1) were scanned with microcomputed tomography (μCT). Acquisition parameters for the μCT data

in this study varied according to the different states of mineralization, general size of the fossils, and thickness of the cranial bones. Eyasi I was scanned with a "General Electric Phoenix" µCT scanner (model v|tome|x s) at the Paleoanthropology High Resolution CT Laboratory (University of Tübingen) with the parameters set to 180 kV, 100 µA, 3000 images, and a voxel size of 0.1319100 (mm/pixel). Masai 12 was scanned with the same scanner, with scan parameters set to 170 kV, 170 µA, 2500 images, and a voxel size of 0.12915161 (mm/pixel). ADU-VP-1/3 was scanned in the National Museum of Ethiopia (Addis Ababa) with a High Energy Desktop Micro-CT System Skyscan 1173, with parameters set to 130 kV, 40 µA, 1334 images, and a voxel size of 0.14269408 (mm/pixel). La Chapelle-aux-Saints 1 and La Ferrassie 1 were scanned with General Electric µCT scanner (model "v|tome|x L 240") at the Muséum National d'Histoire naturelle in Paris, with voxel sizes of 0.122739 and 0.13155056 (mm/pixel), respectively (Balzeau & Rougier, 2013). None of the µCT scans show overflow artifacts nor was beam hardening present to any degree. However, in the case of ADU-VP-1/3, localized sedimentation in the occipital area has caused partial volume averaging artifacts, which obscure the boundaries between the different types of bone, reducing the contrast between tables and the diploë. Scans were loaded into Avizo Lite (FEI Visualization Sciences Group, versions 9.0.1 and 9.2.0) and were subjected to standard imaging techniques, such as volume rendering and isosurface extraction, in order to locate the suprainiac depressions. In all cases, the suprainiac depressions and the surrounding occipital superstructures were analyzed on three-dimensional models created from the µCT slices. In the case of Eyasi I, ADU-VP-1/3, and Masai 12, the original specimens were also directly assessed. We evaluated the external morphology of the suprainiac depressions on all specimens according to the criteria established by Nowaczewska (2011) and followed the qualitative descriptions by Balzeau and Rougier (2010).

Table 1. Inventory of studied data and comparative sample.

Specimen	Repository	Marine Isotope stage	References
Eyasi I	EKUT	MIS 5-11(?)	Reck and Kohl-Larsen (1936)
ADU-VP-1/3	NME	MIS 5	Haile-Selassie et al. (2004)
Masai 12	EKUT	MIS 1	Kohl-Larsen (1941)
La Chapelle-aux-Saints 1	MNH	MIS 3	Bouyssonie et al. (1908)
La Ferrassie 1	MNH	MIS 3	Capitan and Peyrony (1909)

Abbreviations: EKUT = Eberhard Karls University of Tübingen; NME = National Museum of Ethiopia, Addis Ababa; MNHN = Muséum National d'Histoire naturelle, Paris.

Following Balzeau and Rougier (2010), multiplanar reformatting was used to compute two orthogonal slices. The vertical slice was computed over the midsagittal plane, crossing the maximum vertical extension of the depression (Figure 1). The second slice, or the transverse slice, covers the maximum horizontal extension of the depression, perpendicular to the ectocranial surface. We used these slices to systematically quantify the external morphology of the suprainiac depressions. In this protocol, maximum left and right side distances were identified by laterally translating the vertical slice from the center until the depression was indistinguishable from the surrounding occipital bone on either side (Supplementary Figure 1). The same protocol was employed on the transverse slice, which was translated to the superior and inferior borders of the depression. This protocol is useful for delimiting the borders of the depression in what might otherwise be a more subjective assessment when measuring the external surface directly on a specimen. In addition, it provides a systematic method to measure potential asymmetry of the depression, which is useful for specimens like ADU-VP-1/3, where only part of the depression is preserved.

The internal morphology of the sample was assessed and described, utilizing the terminology used by Balzeau and Rougier (2010), and variation in internal bone composition in the upper squama of each occipital bone was quantified following the approach that they developed. It comprises 16 equidistant measurements between lambda and the most posterior point of the occipital superstructures. The measurements were taken in Avizo Lite (FEI Visualization Sciences Group, versions 9.0.1 and 9.2.0) and divided in three categories: (1) the area from lambda to the upper limit of the suprainiac depression, (2) the area from the superior limit of the depression to the most posteriorly prominent

point of the occipital, and (3) a single measurement of the center of the depression. These absolute measurements were converted into relative values by first assessing the total thickness of the cranial vault at each measurement location. Subsequently, the relative contributions of the internal structures were calculated as percentages of the total thickness of the cranial vault. These data were compared to published measurements on Neanderthal (n = 9) and *H. sapiens* (n = 10) specimens (Balzeau & Rougier, 2010; Bosman & Harvati, 2019). An intra-observer error test was performed on the ADU-VP-1/3 and the La Chapelle-aux-Saints 1 specimens by measuring them five times across five days and calculating the coefficient of variation (CoV) for both specimens. Subsequently, a Principal Component Analysis (PCA) was computed on the correlation matrix of the averaged relative contributions of the internal structures in each of the zones, per individual in the comparative sample. The correlation matrix was preferred over the covariation matrix, as the internal structures differ greatly in their relative contribution (e.g. a thick diploic layer versus a thin internal table). In order to explore inter-observer error, the data collected for La Chapelle-aux-Saints 1 and La Ferrassie 1 were projected onto the PCA, thereby comparing their distribution with the previously published measurements (Balzeau & Rougier, 2010; Bosman & Harvati, 2019). Since our goal was to assess the quantitative similarity of Eyasi I, ADU-VP-1/3, and Masai 12 in comparison to the occipital structure of the comparative sample, these specimens were also projected onto the PCA computed with the comparative sample. All analyses were performed in R, version 3.5.0 (R Core Team 2019). The PCA plots were generated with the following R packages: ggplot2 (Wickham, 2009), ggrepel (Slowikowski, 2017), extrafont (Chang, 2014), and plyr (Wickham, 2011).

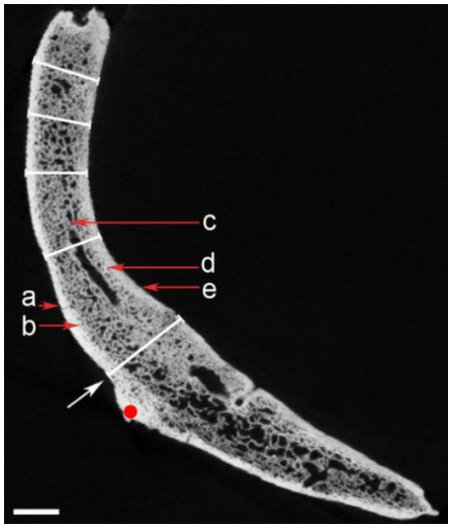

Figure 1. Internal structure of the occipital bone of Masai 12. A white arrow indicates the suprainiac depression. A red landmark shows the position of inion. Red arrows indicate the internal components of the occipital bone. Five white bars represent examples of measurements of the internal components. a: Outer layer of the external table; b: Inner layer of the external table; c: diploic layer; d: inner layer of the internal table; e: outer layer of the internal table (scale bar = 1 cm).

3. Results

Descriptions of the external morphology and internal characteristics of the suprainiac depressions for Eyasi I, ADU-VP-1/3, and Masai 12 (Figure 2a-c), in comparison to the condition exhibited by La Chapelle-aux-Saints 1 and La Ferrassie 1 (Figure 2d-e) are provided in the subsections below and summarized in Table 2. The descriptions of the internal composition are based on the investigation of the entire CT dataset, while orthogonal slices depict the depressions for every specimen (Figure 3). Our observations on La Chapelle-aux-Saints 1 and La Ferrassie match the descriptions by Balzeau and Rougier (2010, 2013) and are thus not reported in detail here.

The CoV calculated for the intra-observer measurements of the thickness of the La Chapelle-aux-Saints internal structures is approximately 1.6 percent. The structure with the highest CoV is the external table (mean CoV: 2.5%, min CoV: 0.8%; max CoV: 4%), showing good repeatability for high quality scans. The CoV calculated for our measurements of the relative internal structure thickness of ADU-VP-1/3 averages to about 3.5%. The structure

with the highest CoV in this specimen is the internal table (mean CoV: 4.5%; min CoV: 1.2%; max CoV: 8.11%), showing a higher intra-observer error when applying this measurement protocol to scans that are affected by partial volume averaging effects.

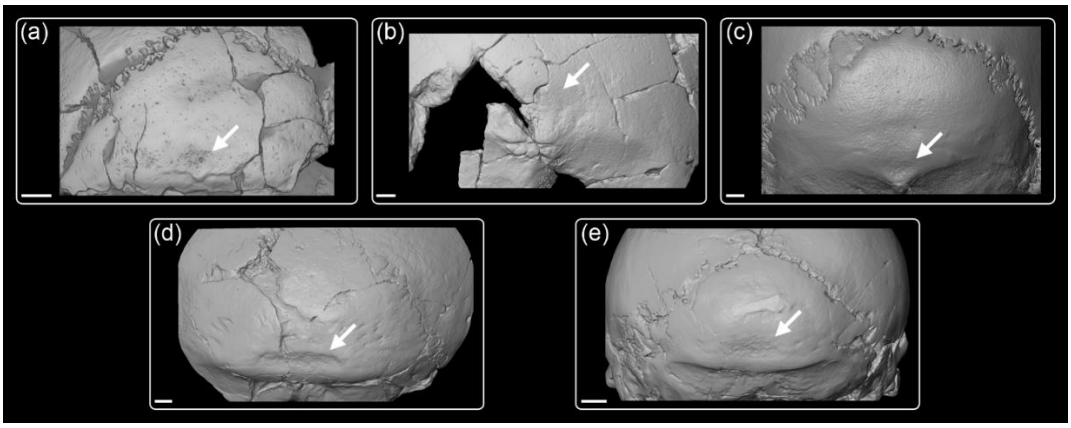

Figure 2. Extracted surfaces of the studied sample in *norma occipitalis*. White arrows indicate the suprainiac depressions/fossae (a) Eyasi I; (b) ADU-VP-1/3; (c) Masai 1; (d) La Chapelle-aux-Saints 1; (e) La Ferrassie 1 (scale bars = 1 cm).

Table 2. Summary of the internal and external morphological characteristics of the suprainiac depressions and surrounding occipital bone features in Eyasi I, ADU-VP-1/3, Masai 12, La Chapelle-aux-Saints 1, and La Ferrassie 1. Observations for La Chapelle-aux-Saints 1 and La Ferrassie 1 are in agreement with Balzeau and Rougier (2010). Abbreviations: DL = Diploic layer; ET = External table.

Characteristics	Eyasi I	ADU-VP-1/3	Masai 12	La Chapelle-aux-Saints 1	La Ferrassie 1
Elliptical in shape	No	Yes	No	No	Yes
Maximum extension on transverse axis	No	Yes	No	Yes	Yes
Deep depression	No	Yes	Yes	Yes	No
Discrete/defined appearance	No	Yes	Yes	Yes	Yes
Straight inferior limit	No	Yes	No	Yes	Yes
Uneven/rugose topography	Yes	Yes	Yes	Yes	Yes
Surrounding triangular shelf†	Yes	Yes	No	No	Yes
Directly above inion	Yes	Yes	Yes	Yes	Yes
Relief dividing depression	No	No	No	Yes	No
Bilaterally arched torus	No*	No	No	No	Yes
Depression defined by protuberance	Yes	No	Yes	N/A	N/A
Type‡	Third	Second	First	N/A	N/A
Outer layer of ET affected	Yes	Yes	Yes	Yes	Yes
Inner layer of ET affected	No	No	No	Yes	Yes
DL affected	No	No	No	Yes	Yes

† Not discussed in Balzeau and Rougier (2010)

‡ As defined by Nowaczewska (2011)

* A torus is present but is not bilaterally arched

3.1. Description of the Eyasi I nuchal morphology

External morphology (Figure 2a)

Eyasi I has a well-preserved occipital plane. The lateral right side of the occipital bone is incomplete, so the extent of the nuchal lines cannot be traced with certainty. The cranium possesses a straight and weakly developed occipital torus. The torus is expressed primarily medially; laterally, it is reduced in prominence. It does not reflect a thickened shelf of bone, which is present in most Neanderthal crania. An external occipital protuberance is present but very weakly developed. This structure is joined medially with the inferior margin of the torus, which has two points of maximal superior projection, although the projection on the lateral right is relatively weak when compared to the lateral left.

There is a vaguely delineated and shallow depression above inion. The depression is located on a posteriorly projecting eminence, or raised shelf of bone. The external surface of the depression is rugose and irregular, related to bone remodeling. The overall morphology of the depression is best described as ovoid, with a maximum in the transverse direction. It extends along the superior margin of the medial portion of the occipital torus, and protrudes slightly into the external occipital protuberance. The depression has been reported to have an approximate breadth of 30.5 mm, a height of 12.5 mm, and an area of 299.5 mm^2, calculated with an ellipse formula (Trinkaus, 2004). However, our slice-based digital protocol yielded a breadth of 25.7 mm and a height of 9 mm, resulting in an area of 181,7 mm^2 (Supplementary Table 1).

Internal morphology (Figure 3a,e)

On the vertical slice, the thickness of the external table is more or less constant across most of the occipital plane, with the exception in the areas immediately superior and inferior to the depression, where it is relatively thicker. Inferiorly, this increased thickness is due to the development of the external occipital protuberance and occipital torus. The relative thickness of the diploic layer is also fairly constant throughout the occipital squama. Only inferior to the external occipital protuberance is the diploic layer relatively thicker

compared to the rest of the occipital squama. The depression is formed by the outer layer of the external table, while the inner layer of the external table follows the shape of the occipital bone and does not change in morphology at the level of the depression. Thus, the outer and inner layers of the external table do not have a parallel course, as the depression is only represented by changes in the outer layer of the external table.

On the transverse slice, the borders between the external table, diploic layer, and internal table are more difficult to discern. In general, the depression is not obvious, as it is quite shallow. Throughout the transverse slice, the external table has a constant relative thickness. Only at the level of the depression is the external table thinner than in the remainder of the occipital bone. At the lateral edges of the depression, the external table has a larger contribution to the total thickness than the diploic layer due to the development of the weak occipital torus.

3.2. Description of the ADU-VP-1/3 nuchal morphology

External morphology (Figure 2b)

The occipital bone of ADU-VP-1/3 is the best-preserved element of the cranium. There is no occipital torus, but the superior nuchal line is robust and tightly arched. The external occipital protuberance is marked and well developed. Its elevated surface is divided by a wide transverse groove that has inferiorly and superiorly directed arms, which separate the external occipital protuberance in four distinct parts (Haile-Selassie et al., 2004). The median nuchal crest is marked and pronounced along the entirety of its extension from inion to opisthion (Haile-Selassie et al., 2004).

There is a relatively deep and bilaterally elongated depression above the external occipital protuberance. The depression is clearly defined in both *norma occipitalis* and *norma lateralis*. Surrounding the depression, there is a slightly uplifted and thickened shelf of bone that forms a discrete border between the depression and the surrounding occipital plane. Only the lateral right side of this depression is still present, but it can be assumed that it

would have extended laterally to the left as well. The external surface of the depression shows some bony spicules and pits. Most of this rugosity is located supero-laterally to the right of the superior margin of the external occipital protuberance. According to Haile-Selassie et al. (2004), measurements of the preserved right half of the depression yield a breadth of approximately 36 mm and a height of 10 mm, which corresponds to an approximate area of 282.7 mm^2. Measurements using our protocol similarly yield a total breadth of 35.2 mm (doubled from 17.6), and a height of 9 mm.

Internal morphology (Figure 3b,f)

In vertical view, the internal morphology of ADU-VP-1/3 is less clear than that of Eyasi I. The diploë is obscure and the borders between the tables are unclear. This is especially obvious around the broken area located left of the depression. While the external table shows constant thickness across the entire occipital bone, it is slightly thicker at the level of the external occipital protuberance. The presence of this structure affects the outer layer of the external table, while the inner layer of the external table is unaffected. At the level of the depression, the relative thickness of the external table is lower than in the surrounding areas. This reduction in thickness affects the outer layer of the external table, as there is a visible concavity, while the inner layer of the external table is not affected and follows the curvature of the occipital bone. Additionally, the interface between the inner layer of the external table and the diploic layer does not change, as the diploic layer has a uniform thickness in most of the occipital bone. At the level of the external occipital protuberance, the diploic layer is thicker in the ectocranial direction, but at the depression, the borders between the diploic layer and the external and internal tables are parallel. Moreover, the transverse slice shows a similar pattern as the vertical slice. While there is a lack of contrast between the layers, only the outer layer of the external table is affected by the presence of the depression. The inner layer of the external table and the diploic layer follow the shape of the occipital bone.

3.3. Description of the Masai 12 nuchal morphology

External morphology (Figure 2c)

The occipital bone of Masai 12 is completely preserved. It exhibits several Wormian bones, which are especially numerous in the left lambdoidal suture. The supreme nuchal lines are robust and slightly arched. The superior nuchal lines are equally pronounced and converge medially and inferiorly to the suprainiac depression into an external occipital protuberance. Inferior to the occipital protuberance is a marked nuchal crest. Superior to the external occipital protuberance is a discrete depression with an irregular external surface and an apex which is delimited by the external occipital protuberance. Its breadth is 21.8 mm, height is 8.7 mm and covers a total area of 149 mm^2. There is no eminence surrounding the depression.

Internal morphology (Figure 3c,g)

The thickness of the external table varies along the occipital squama. At lambda, the external table is relatively thin. The outer layer of the external table is affected by the presence of the depression, whereas the inner layer of the external table and the diploic layer are not. Thus, the outer and inner layers of the external table do not have a parallel course. The diploic layer is mostly uniform across the entire occipital bone. At the level of the external occipital protuberance, the diploic layer is thicker than in the rest of the occipital bone. The internal table is also uniform in thickness in most of the occipital squama, including the area of the depression. It is considerably thinner around the area below the sinus bifurcation on the endocranial surface. The transverse slice shows that the external table is variable in its thickness at the level of both the superior and the inferior supranuchal lines. It is at its thickest on the lateral left and right of the depression. In addition, on this slice, the depression is clearly visible as a small indentation in the middle of the nuchal area.

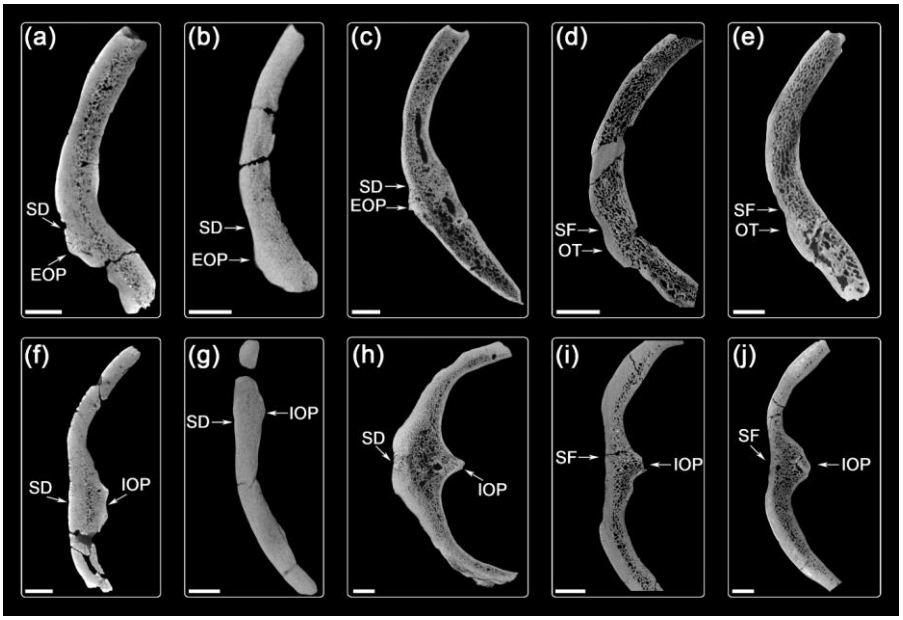

Figure 3. Vertical and transverse slices of Eyasi I, ADU-VP-1/3, Masai 12, La Chapelle-aux-Saints 1, and La Ferrassie 1. Arrows indicate the location of occipital superstructures (scale bars = 0.5 centimeter). (a) Eyasi I vertical slice; (b) ADU-VP-1/3 vertical slice; (c) Masai 12 vertical slice; (d) La Chapelle-aux-Saints 1 vertical slice; (e) La Ferrassie 1 vertical slice; f) Eyasi I transverse slice; (g) ADU-VP-1/3 transverse slice; (h) Masai 12 transverse slice; (i) La Chapelle-aux-Saints 1 transverse slice; (j) La Ferrassie 1 transverse slice. Abbreviations: EOP = External occipital protuberance; IOP = Internal occipital protuberance; SD = Suprainiac depression; SF = Suprainiac fossa; OT = Occipital torus.

3.4. Internal metric analysis

Table 3 summarizes the absolute and relative data of the internal composition of the suprainiac depressions analyzed in this study, which are subsequently compared to data published by Balzeau and Rougier (2010). With regards to Eyasi I, ADU-VP-1/3, and Masai 12, there is a general trend of relatively thicker diploic layers at the level of the suprainiac depression, compared to the thickness of the external and internal tables. This is related to the observation that the outer layer of the external table is influenced by the depression, while the inner layer is not, which reduces the relative contribution of the external table to the total cranial vault thickness in this area. In the area of the occipital structures, such as the external occipital protuberance, the external table is slightly thicker than in the area of the depression. The internal table varies only slightly throughout the occipital bone. It follows the topography of the external table to some extent but variations in thickness are much less pronounced.

The PCA (Figure 4; Supplementary Figure 2), based on the relative contributions of all internal structures of the occipital squama, reveals that Neanderthals and *H. sapiens* are well separated on the second axis, which explains 27.5% of variation. The external table has positive loadings along this axis, indicating that Neanderthals are characterized by relatively low values and little variation in the relative thickness of the external table. In contrast, *H. sapiens* are characterized by a large amount of variation in the external table across the occipital squama. The diploic layer is associated with negative loadings along the first and the second axes, indicating that most Neanderthals show relatively high values and a large amount of variation in the relative thickness of the diploë, while *H. sapiens* show relatively low values for the thickness of the diploic layer. Eyasi I and ADU-VP-1/3 both plot within the convex hull of the *H. sapiens* group along the first two PCs. The projected La Chapelle-aux-Saints 1 and La Ferrassie 1 specimens plot close to the respective specimens from Balzeau and Rougier's (2010) comparative sample, suggesting a low inter-observer error. Moreover, the Holocene Masai 12 specimen plots on the extreme negative end of PC1 due to the extremely high relative contribution of the diploic layer in all areas of the occipital bone, above the maximum range of both Neanderthals and *H. sapiens* (Table 3).

Table 3. Structural composition of the occipital plane in Eyasi I, ADU-VP-1/3, Masai 12, La Chapelle-aux-Saints 1 and La Ferrassie 1 collected in this study. Data on other Neanderthals and *H. sapiens* were obtained from Balzeau and Rougier (2010). Data from Cioclovina obtained from Bosman and Harvati (2019). Data are summarized per group (mean, standard deviation, and range). Abbreviations: DL = Diploic layer; ET = External table; IT = Internal table; sd = standard deviation.

	Area above depression (%)			Area of depression (%)			Center of depression (mm)			Center of depression (%)		
	ET	**DL**	**IT**	**ET**	**DL**	**IT**	**ET**	**DL**	**IT**	**ET**	**DL**	**IT**
Eyasi I	31	50	19	34	48	18	3.1	5.4	1.9	30	52	18
ADU-VP-1/3	35	48	17	32	54	14	2.4	4.4	1.3	30	53	17
Masai 12	17	69	14	21	68	11	2	8.9	1.8	16	70	14
Cioclovina	31	50	19	39	44	17	1.9	3.0	1.0	33	50	17
La Chapelle-aux-Saints 1	27	55	18	28	54	18	2.5	6.4	1.7	24	60	16
La Ferrassie 1	22	64	14	24	62	14	2.3	6.0	1.2	24	63	13
Neanderthals												
Mean	23	57	20	28	52	20	2.5	5.3	2.0	26	52	22
sd	4.7	8.0	3.8	5.3	8.4	4.8	0.3	1.2	0.4	3.3	8.4	5.7
Range	18	41	15	23	39	13	2.1	3.3	1.5	22	39	14
	-	-	-	-	-	-	-	-	-	-	-	-
	32	65	27	37	63	28	2.9	6.9	2.6	32	62	29
H. sapiens												
Mean	30	50	20	39	45	16	4.5	6.4	2.0	35	50	16
sd	4.8	8.0	3.5	8.0	8.6	3.3	1.5	2.0	0.5	4.6	7.7	5.4
Range	23	40	16	31	23	10	3.1	2.5	1.4	30	31	10
	-	-	-	-	-	-	-	-	-	-	-	-
	35	61	26	57	51	20	7.8	8.7	2.8	43	57	28

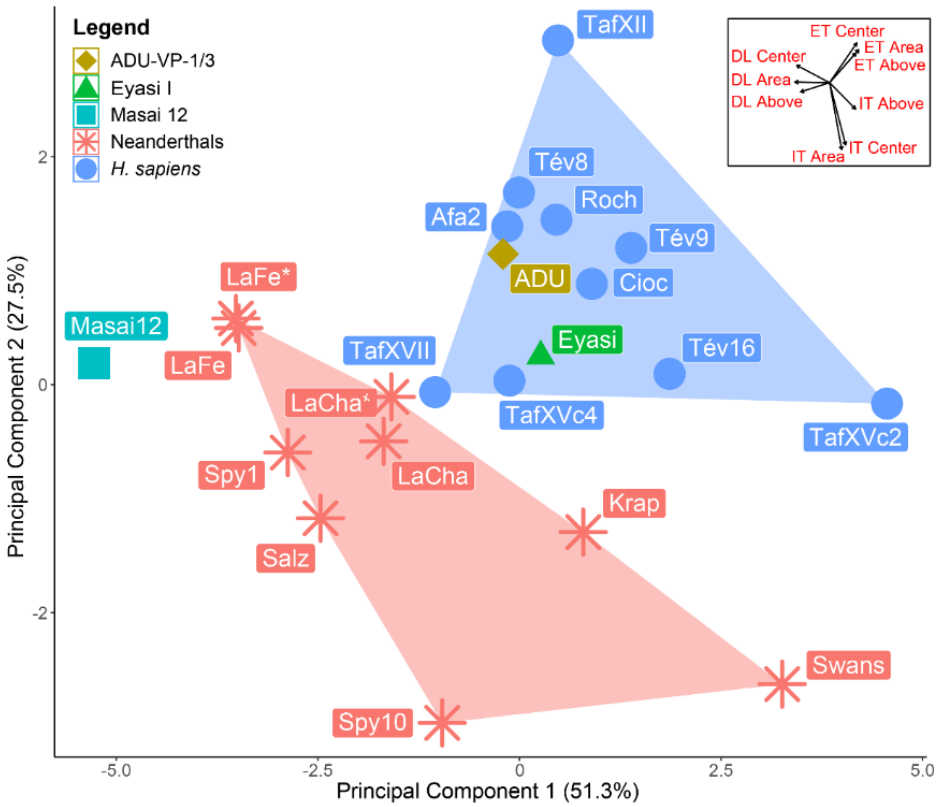

Figure 4. Principal Component Analysis (PCA) on the correlation matrix, showing PC1 (51.3% of total variance) and PC2 (27.5 % of total variance). Data collected in this study (Eyasi I, ADU-VP-1/3, Masai 12, La Chapelle-aux-Saints 1, and La Ferrassie 1) were projected onto the PCA of the comparative data. Black arrows (inset) represent the loadings of all variables, as indicated with red text (DL=diploic layer; ET=external table; IT=internal table) Symbols: Eyasi I = green triangle; ADU-VP-1/3 = gold diamond; Masai 12 = cyan square; Neanderthals = red stars; recent *H. sapiens* = blue circles. Abbreviations: Cioc = Cioclovina; LaCha = La Chapelle-aux-Saints 1; LaCha* = Data on La Chapelle-aux-Saints 1 collected in this manuscript. LaFe = La Ferrassie 1; LaFe* = Data on La Ferrassie 1 collected in this manuscript; Salz = Salzgitter-Lebenstedt 1; Kra = Krapina 5; Swa = Swanscombe; Roch = Rochereil; Tév = Téviec; Afa = Afalou; Taf = Taforalt.

4. Discussion

4.1. Variation in the supranuchal morphology of Eyasi I, ADU-VP-1/3, and Masai 12

As already suggested by Trinkaus (2004), specific traits, such the weak occipital torus and the depression above inion separate Eyasi I from most other African Middle Pleistocene fossils such as Broken Hill (Woodward, 1921), Bodo (Conroy et al., 1978), and Ndutu (Mturi, 1976). The presence of a suprainiac depression is also different from the morphology

of other African early *H. sapiens,* including Ngaloba LH-18 (Day et al., 1980), Omo 2 (Day, 1969), and KNM-ER 3884 (Bräuer et al., 1992). A depression is however present in the Eliye Springs KNM-ES 11693 (Bräuer & Leakey, 1982) and Kebibat (Rabat) 1 (Saban, 1975) specimens. Moreover, the presence of an external occipital protuberance, a possible *H. sapiens* apomorphy (Hublin, 1978b; Lahr, 1996), appears to be rare in the Middle Pleistocene, and has only been reported for only a few other Middle Pleistocene African specimens (including the Ndutu cranium, also from Tanzania; Clarke, 1990). While Trinkaus (2004) considered it to be absent in Eyasi I, we agree with Hublin (1978b) in assessing its presence. We noted that even the Eyasi assemblage itself shows high variability in occipital bone morphology. Bräuer and Mabulla (1996) considered Eyasi II to exhibit a more modern morphology, characterized by weaker angulation between the nuchal and occipital planes. Trinkaus (2004), on the other hand, considered that Eyasi II and IV exhibit a similar occipital torus morphology to Eyasi I.

With respect to the external supranuchal morphologies outlined by Nowaczewska (2011), the depression present in Eyasi I does not fully conform to any of the proposed categories, but is most similar to the third type. Depressions grouped under this type are typically transversely elongated, and are associated with an occipital torus structure which is not bilaterally arched, is poorly expressed laterally, weakly developed, and with obscure upper margins (Nowaczewska, 2011). However, the presence of an external occipital protuberance in Eyasi I, despite its weak expression, does not conform to the third type. While the depression extends slightly into the external occipital protuberance, the inferior border of the depression does not have a marked V-shaped appearance, unlike the typical supranuchal fossae found in other recent *H. sapien*s. Internally, the depression on the Eyasi I cranium contrasts in several ways to what has been described for the Neanderthal state (Balzeau & Rougier, 2010). The outer and inner layers of the diploë, where it interfaces with the external and internal table respectively, have a parallel course, while the outer layer of the external table is influenced by the presence of the depression and shows extensive bone remodeling. When compared to the specimens described by Balzeau and Rougier (2010),

the internal morphology of the occipital bone and depression on Eyasi I bears the greatest resemblance to Téviec 8, a Mesolithic *H. sapiens* individual. In this specimen, the depression is mostly confined above the external occipital protuberance and not solely related to the presence of this structure. The depression is elongated laterally and is located above the medial part of the occipital torus structure. The presence of the depression only influences the outer layer of the external table, which shows pronounced irregularities likely due to bone remodeling, while the thickness of the diploic layer is constant (Balzeau & Rougier, 2010).

As for ADU-VP-1/3, although the inferior limit of its depression is straight, which is similar to the fossa in most Neanderthal crania such as La Chappelle-aux-Saints 1 and Salzgitter-Lebenstedt 1 (Balzeau & Rougier, 2010), the superior nuchal lines in this specimen cannot be compared to a bilaterally arched Neanderthal occipital torus. The external surface displays bony spicules and pits due to bone remodeling, although this does not appear to be as extensive as in the depression on the Eyasi I cranium. With respect to the types of depressions and their related superstructures outlined by Nowaczewska (2011), the depression on ADU-VP-1/3 conforms to either the first or the second type. There are no clear supreme nuchal lines and no distinct occipital torus. Unlike Eyasi I, there is a clearly marked external occipital protuberance. However, its presence in ADU-VP-1/3 does not strictly define the depression, and the depression does not have an obvious inverted triangular shape. Thus, the external morphology of the depression on ADU-VP-1/3 is most similar to the second type of non-supranuchal depressions found on recent *H. sapiens* crania.

As far as can be ascertained from our investigation of the ADU-VP-1/3 CT scans, the internal morphology of the depression on this specimen contrasts in several ways to what has been described for the Neanderthal state, both in terms of its external morphological characteristics, as well as the relative thinning of the external table and the unaffected diploic layer. The depression and the morphology of the other occipital superstructures

resemble those of the terminal Pleistocene Afalou 2 specimen. This individual exhibits a deep depression that is located well above the external occipital protuberance, is not solely restricted by the presence of this structure, and only influences the outer layer of the external table (Balzeau & Rougier, 2010).

The depression of Masai 12 is located opposite to the sagittal sinus bifurcation, a feature that it has in common with the depression on the Manot 1 cranium (Hershkovitz et al., 2015, 2017). The depression is a typical example of the supranuchal (Caspari, 2005), or first type, depression (*sensu* Nowaczewska, 2011). This type has an inferiorly projecting apex that protrudes into the robust external occipital protuberance and is associated with well-developed superior nuchal lines. The internal morphology of this specimen shows an extremely high relative contribution of the diploic layer. However, in the center of the suprainiac depression, only the external table decreases in relative thickness, which is consistent with the pattern described for *H. sapiens* (Balzeau and Rougier, 2010).

In general, the occipital depressions above inion described for the presented sample are variable in their external morphology (Figs. 2 and 3; Table 2). This variability is reflected in our quantitative results. We note that for Eyasi I, our external dimension measurements differ from those previously reported by Trinkaus (2004), likely as a result of the difficulty in delimiting its borders directly on its rugose surface as opposed to our virtual slice protocol. By contrast, measurements of ADU-VP-1/3's depression are similar to those previously reported as a result of its more well-defined borders. We further note that the specimens measured in our study showed varying levels of asymmetry in the distance from the center of the depression to the lateral margins (Supplementary Table 1). As such, we recommend that the inferred total breadth or width measurements for incomplete specimens like ADU-VP-1/3 be treated with caution. Nevertheless, external dimensions of both Eyasi I and ADU-VP-1/3 fall outside of the range for Neanderthal suprainiac fossae reported in the literature (Trinkaus, 2004; Verna et al., 2010). However, some studies (e.g. Lahr, 1996) have shown that there is a strong relationship between cranial dimensions and

non-metric traits. Thus, measurements of external dimensions of suprainiac depressions, by themselves, might not be useful in separating (non)supranuchal depressions in *H. sapiens* from Neanderthal suprainiac fossae. A formal study that incorporates a large sample of all categories of suprainiac depressions (*sensu* Nowaczewska, 2011) with metrical information of cranial size is therefore necessary to elucidate this issue.

Considering the internal quantification of the supranuchal area and the associated PCA (Figure 4), the first principal component is mostly associated with variation in the diploic layer, and shows that this structure is responsible for some of the overlap between the Neanderthal and *H. sapiens* specimens included in this study. This also explains the position of Masai 12, which is characterized by a very low relative contribution of the external table, and a very high relative contribution of the diploic layer. These values fall outside of the range for both Neanderthals and *H. sapiens*. This greatly increased thickness of the diploic layer may be at least partly due to a pathological condition. Bräuer (1983) reported that Masai 12 was likely affected by yaws, due to the presence of caries sica (or scars from osteolytic lesions) on the frontal bone. However, it is unclear to what extent any of the treponemal diseases influence the diploic layer in areas of the crania not presenting any surface osteological lesions. Moreover, caries sica is represented by clear cavities in the internal structures (Hackett, 1976), and the Masai 12 frontal bone only shows some alterations on the external table. We also note that there are no signs of healing and preliminary ascribe the alterations on the Masai 12 frontal bone as taphonomic.

The second component of the PCA is associated with variation in the external and internal tables. While the external table principally separates the Neanderthals and *H. sapiens*, the internal table is responsible for some of the overlap between the two groups, as La Ferrassie 1 plots on the positive end of this axis. This is due to the fact that La Ferrassie 1, like the modern *H. sapiens* in this sample, presents a low value and minor variation in the relative thickness of its internal table. The other Neanderthal specimens included in this sample, on

the other hand, show a relatively higher amount of variation of internal table thickness (Table 3).

While the PCA on all available data separates Neanderthals and *H. sapiens* quite well, PCAs on data subsets corresponding to the three different occipital bone areas (Supplementary Figure 2) elucidate the similarity in principal component scores between several Neanderthal and *H. sapiens* specimens (such as the Neanderthal Swanscombe and Krapina plotting within the range of the *H. sapiens* group on the first principal component). However, it should be noted that these additional PCAs are only based on three variables per individual (external table, diploic layer, and internal table), and thus present a limited picture. Together, these results reconcile previous interpretations of Neanderthal similarities in the suprainiac depression of Eyasi I and ADU-VP-1/3 (e.g. Trinkaus, 2004) with the more nuanced interpretations that describe a difference when considering the surrounding occipital squama that differentiates them from Neanderthals, including the variably present occipital superstructures such as the occipital torus, the superior nuchal lines, cruciform eminence, and the external occipital protuberance.

4.2. Phylogenetic implications

We considered at the outset of this study that if Eyasi I and ADU-VP-1/3's suprainiac depressions were found to be similar to that of Neanderthal fossae, a re-assessment of this feature as a Neanderthal autapomorphic trait would be necessary. Trinkaus (2004, 2005, 2011) had previously considered the form of the suprainiac depressions in these specimens to approximate the Neanderthal condition. In contrast, our results show that both the external and internal morphology of the depressions of Eyasi I and ADU-VP-1/3 and their surrounding area do not exhibit qualitative or quantitative similarities to the Neanderthal condition but resemble *H. sapiens* from the Late Pleistocene and Holocene. Thus, the commonly accepted status of the Neanderthal suprainiac fossa as a derived feature of this lineage is not affected by our findings.

Genetic admixture

Related to the autapomorphic status of the Neanderthal suprainiac fossa are the implications of this study for the discussion centered on the effect of Neanderthal/*H. sapiens* admixture on the skeletal phenotype of hybrid descendants (Frayer, 1992; Smith, 2005). Late Pleistocene Eurasian specimens such as the Cioclovina (Romania) and Xuchang (China) crania, are critical in this regard, as they have been argued to exhibit a suprainiac depression that resembles the Neanderthal state (Li et al., 2017; Soficaru, 2007; Trinkaus, 2007). Cioclovina has been ascertained to possess Neanderthal genetic material, albeit at levels similar to extant non-African populations (Fu et al., 2016). Moreover, a recent re-examination of its supranuchal external and internal morphology found that it is well within the range of modern *H. sapiens* morphology and does not show any Neanderthal-like features (Bosman & Harvati, 2019). The internal structure of the Xuchang 2 occipital bone has been described as following a Neanderthal pattern, with no thinning of the external table (Li et al., 2017). However, a quantitative analysis is needed in order to further assess the supranuchal morphology of this and other Middle-Late Pleistocene fossils exhibiting suprainiac depressions

Moreover, while admixture between Neanderthals and *H. sapiens* is now well-documented for the Late Pleistocene (e.g. Green et al., 2010; Posth et al., 2016), the presence of genetic material from other archaic hominin groups in the Middle Pleistocene could complicate our understanding of the influence of Neanderthal genetic material on the *H. sapiens* phenotype. For example, it has been demonstrated that modern day *H. sapiens* from Oceania, in addition to the Neanderthal genetic component present in all modern non-Africans, have substantial levels of Denisovan ancestry (2-4%; e.g. Reich et al., 2011; Vernot et al., 2016), with lower levels of Denisovan ancestry also likely present in other populations (e.g. Skoglund & Jakobsson, 2011; Qin & Stoneking, 2015). As Denisovan nuchal morphology is currently not known, caution is warranted when using the supranuchal morphology as a potential indicator of gene flow between Neanderthals and *H. sapiens*,

since interbreeding with Denisovan but also other archaic lineages may have also played a role in the expression of the *H. sapiens* phenotype.

Common ancestry

The alternative hypothesis proposed to explain the presence of suprainiac depressions in both Neanderthals and *H. sapiens, i.e.* that this feature was inherited from their common ancestor, is difficult to evaluate with the current evidence. Nowaczewska et al. (2019) have recently argued, based on their analysis of several recent Australian crania, that non-supranuchal depressions in *H. sapiens* that exhibit Neanderthal-like features in their internal morphology are examples of the kind of morphological variability of the supranuchal region occurring in Middle-Late Pleistocene hominins. Our study shows that, while there is clear variability in the expression of supranuchal external morphology, Eyasi I and ADU-VP-1/3 do not exhibit Neanderthal-like affinities in their overall internal occipital morphologies and only minimally in the area of the suprainiac depression. Nevertheless, in order to properly evaluate the hypothesis of common ancestry, we have to consider competing models of modern human origins, as well as the taxonomic status of Middle-Late Pleistocene African hominins with suprainiac depressions.

Certain models of recent human evolution time the divergence of Neanderthals and *H. sapiens* some half a million years ago while others stipulate a deeper divergence in time, closer to a million years ago (reviewed in Rightmire, 2012). Under the first scenario, investigation of Middle Pleistocene specimens from Africa is crucial, as these might represent ancestral variation. Although Eyasi I likely post-dates the lowest boundary of the Neanderthal/*H. sapiens* divergence, if Mehlman's (1987) view of its antiquity to some 375 ka is accepted, it dates close to proposed first appearance of *H. sapiens* morphological traits around 300 kya (Hublin et al., 2017; Richter et al., 2017). However, a robust direct date promises better contextualization and taxonomic attribution of this material. Additionally, there are currently only two other Middle Pleistocene African specimens, Eliye Springs KNM-ES 11693 (Bräuer & Leakey, 1982) and Kebibat (Rabat) 1 (Saban, 1975), which have been argued to possess a depression above inion. In the case of KNM-ES 11693, the

depression is very small and oval in shape, conforming to Nowaczewska's second type common in modern humans, albeit located quite high (20 mm) above inion (Bräuer & Leakey, 1986). Also, it should be taken into consideration that the neurocranial vault of KNM-ES 11693 is likely affected by pathology (Bräuer et al., 2003). In the adolescent Kebibat 1, the suprainiac area is characterized by some porosity but the shape of the fossa is uncertain due to a break in this area (Saban, 1975). Both are quite likely not comparable to the Neanderthal suprainiac fossa (Trinkaus, 2004), although an investigation of the internal morphology is required to confirm this. It should also be noted that these two specimens are poorly dated and can only be broadly placed within the Middle Pleistocene (Bräuer & Leakey, 1986; Millard, 2008; Stearns & Thurber, 1965). As such, we have a limited understanding of the morphological variability in this time period, and even the extent of morphological variability in the suprainiac morphology in modern *H. sapiens* is understudied.

Nevertheless, the common ancestry hypothesis could align with the accretional scheme of Neanderthals. In this scenario, the supranuchal fossa of Late Pleistocene "classic" Neanderthals would have its roots in the so-called "incipient" form present in Middle Pleistocene "pre-Neanderthals" from Europe, including Swanscombe (Marston, 1937), Steinheim (Hublin, 1978a), Reilingen (Dean et al., 1998), and Sima de los Huesos (Arsuaga et al., 1997, 2014). Such "incipient" form would be similar to the condition in pre-modern *H. sapiens* like Eyasi I and possibly other Middle Pleistocene fossils from Africa. If Eyasi I is taken as a representative of a common ancestor of *H. sapiens* and Neanderthals, its suprainiac form would have been variably maintained in Late Pleistocene and Holocene individuals (such as ADU-VP-1/3) along the *H. sapiens* lineage and gradually shifted towards the derived fossa configuration in Late Pleistocene European fossils (such as La Ferrassie 1 and La Chapelle-aux-Saints 1) along the Neanderthal lineage. However, we note that Eyasi I's internal morphology is different from Swanscombe, the only specimen in our comparative sample that is typically considered a pre-Neanderthal (e.g. Dean et al., 1998; Stringer & Hublin, 1999).

Under a human evolution model that places the divergence of Neanderthals and *H. sapiens* deeper in time, testing the common ancestry hypothesis would require an assessment of the internal occipital morphology in specimens assigned to the *erectus/ergaster* taxon. Such specimens have not been reported to possess a clearly defined suprainiac depression that is constrained by an occipital torus, even though some African specimens (e.g. KNM-ER 3733: Leakey, 1976; OH 9: Leakey, 1971; OH 12: Leakey, 1971) exhibit a laterally elongated supratoral sulcus (*sensu* Lahr, 1996). Toward this end, we note that Leakey (1974) has proposed affinities between Eyasi I and OH 12 in general cranial form. However, Neanderthals and *H. sapiens* present an occipital/nuchal torus associated with a depression instead of a supratoral sulcus, and these structures are not similar in external morphology (Lahr, 1996), although a systematic investigation of both the external and internal morphological similarities of these traits has not been performed.

Moreover, recent research suggests that that there were likely multiple *H. sapiens* lineages in Africa, which experienced high levels of population structure, morphological variability and interbreeding (e.g. Gunz et al., 2009; Crevecoeur et al., 2009, 2016; Harvati et al., 2011; Scerri et al., 2014, 2018; Stringer, 2016; Schlebusch et al., 2017). The presence of suprainiac depression in some Middle Pleistocene *H. sapiens* might thus reflect morphological variation that was lost later in time due to this deep population structure and/or the loss of lineages that were originally present but did not contribute substantially to *H. sapiens* evolution, possibly due to isolation, changes in effective population size, and later expansions (see Scerri et al., 2018). These factors will obfuscate the possible effects of common ancestry, as well as archaic and/or recent admixture, on the *H. sapiens* phenotype. As such, further testing of this hypothesis will require a broader analysis of pene-contemporaneous Middle Pleistocene fossils from both Africa and Eurasia, applying the kinds of quantitative analyses used here and those recently proposed by Nowaczewska et al. (2019).

Functional convergence and biomechanics

Understanding the presence and etiology of the distinct morphological features in Neanderthals and *H. sapiens* could also be approached in a biomechanical framework, since both types of depression might serve similar functions in the two lineages (e.g. Caspari, 2005; Lieberman, 1995; Nowaczewska, 2011). In this case, the expression of suprainiac fossae in Neanderthals and suprainiac depressions in *H. sapiens* might be related to similarities in strain induced by the nuchal musculature during ossification and development of the occipital structures (Bräuer et al., 2004; Cartmill & Smith, 2009; Caspari, 2005; Lieberman, 1995; Nowaczewska, 2011; Srivastava, 1992). This is supported by the observation that depressions are often found on modern *H. sapiens* crania with a large convexity of the occipital plane (Nowaczewska, 2011), a trait in which these crania show some similarity with Neanderthals (Arsuaga et al., 1997; Trinkaus & Lemay, 1982). Most of the suprainiac depressions in recent *H. sapiens* were observed in an Australian hunter-gatherer sample, with types one to four occurring in, respectively, 22.2%, 5.6%, 8.3%, and 2.8% of the investigated crania (Nowaczewska, 2011). Australian crania are often characterized by their relatively narrow and elongated shape, coupled with a high degree of metric and non-metric robusticity (*sensu* Lahr, 1996). In cranial phenotypes such as these, a depression theoretically assists in maintaining optimal cranial shape under stress generated by the nuchal musculature (Caspari, 2005; Nowaczewska, 2011). However, this hypothesis should be tested with data on neurocranial shape, as a study on the iniac region in isolation will not be conclusive.

At present, we also have to consider that the diverse hypotheses proposed for the presence of suprainiac depressions in both Neanderthals and *H. sapiens* are not mutually exclusive. For example, Gunz et al. (2019) have recently suggested that the presence of Neanderthal alleles on specific chromosomes in *H. sapiens* is associated with reduced endocranial globularity. It is possible that supranuchal depressions in *H. sapiens* might not be a direct result of the presence of specific Neanderthal alleles responsible for the expression of supranuchal form but rather represent a biomechanical response that helps distribute stress

generated by the nuchal musculature in less globular crania. In this regard, the presence and variation in suprainiac depression can be considered a phenotypic byproduct resulting from changes in overall cranial form

5. Conclusion

This study presented a quantitative investigation of supranuchal depressions in two Middle-Late Pleistocene hominins, which were only quantitatively assessed in most previous studies. The results suggest that the Eyasi I and ADU-VP-1/3 supranuchal depressions are not homologous to the Neanderthal suprainiac fossa but rather resemble the external and internal supranuchal morphology observed in recent modern *H. sapiens*. This implies that, when considering the internal structure of the suprainiac depression and its surrounding occipital squama region, the presence of a superficially similar morphology in Middle - Late Pleistocene African specimens does not negate the commonly accepted derived status for the Neanderthal suprainiac fossa. In a broader context, there is currently no straightforward answer to the question of etiology of the suprainiac fossae in Neanderthals and supranuchal depressions in *H. sapiens*. Several mutually non-exclusive scenarios have been discussed and remain to be tested with further investigation of Middle-Late Pleistocene hominins and recent anatomically modern *H. sapiens*, including a close investigation of the cranial shape of the individuals that express these traits in comparison to individuals that do not. Such data must also be eventually combined with additional relevant information, such as analyses on the biomechanics of the nuchal musculature and possibly even a better understanding of how and to what extent the genotype has played a role during the development and ontogeny of specific anatomical traits. Moreover, the possible effects of early admixture with archaic hominin lineages and population structure should be taken into account, especially when the analyses include recent *H. sapiens* from diverse geographic contexts.

6. Acknowledgements

Support for this research was provided by the German Research Foundation (DFG FOR 2237: Project "Words, Bones, Genes, Tools: Tracking Linguistic, Cultural, and Biological Trajectories of the Human Past"), and the DFG INST 37/706-1 FUGG: Paleoanthropology High Resolution CT Laboratory. KH is supported by the European Research Council (ERC CoG no. 724703). We thank Yonatan Sahle for suggesting the inclusion of ADU-VP-1/3 in this study, facilitating access to this specimen, and for comments on earlier versions of this manuscript. We thank the Middle Awash Project team, as well as the Authority for Research and Conservation of Cultural Heritage of Ethiopia, for access to the ADU-VP-1/3 fossil. In particular, we thank Berhane Asfaw, Yonas Beyene, and Tim White for their hospitality during our visit to the National Museum of Ethiopia and for access to the µCT scan of ADU-VP-1/3. We thank Nicholas Conard, Michael Francken, and Wieland Binczik for assistance with scanning of the Eyasi I and Masai 12 specimens. Lastly, we thank Antoine Balzeau, Dominique Grimaud-Hervé, as well as the curators of the Muséum National d'Histoire naturelle (MNHN) for access to the CT scans of La Chapelle-aux-Saints 1 and La Ferrassie 1.

7. References

Ahern, J. (2006). Non-metric variation in recent humans as a model for understanding Neanderthal-early modern human differences: just how "unique" are Neanderthal unique traits? In K. Harvati & T. Harrison (Eds.), *Neanderthals revisited: New Approaches and Perspectives* (pp. 255-268). Dordrecht: Springer.

Aiello, L. C. (1993). The Fossil Evidence for Modern Human Origins in Africa: A Revised View. *American Anthropologist, 95*(1), 73-96.

Arsuaga, J. L., Martínez, I., Gracia, A., & Lorenzo, C. (1997). The Sima de los Huesos crania (Sierra de Atapuerca, Spain). A comparative study. *Journal of Human Evolution, 33*(2), 219-281.

Arsuaga, J. L., Martínez, I., Arnold, L. J., Aranburu, A., Gracia-Téllez, A., Sharp, W. D., . . . Carbonell, E. (2014). Neandertal roots: Cranial and chronological evidence from Sima de los Huesos. *Science, 344*(6190), 1358-1363.

Balzeau, A., & Rougier, H. (2010). Is the suprainiac fossa a Neandertal autapomorphy? A complementary external and internal investigation. *Journal of Human Evolution, 58*(1), 1-22.

Balzeau, A., & Rougier, H. (2013). New information on the modifications of the Neandertal suprainiac fossa during growth and development and on its etiology. *American Journal of Physical Anthropology, 151*(1), 38-48.

Bosman, A. M., & Harvati, K. (2019). A virtual assessment of the proposed suprainiac fossa on the early modern European calvaria from Cioclovina, Romania. *American Journal of Physical Anthropology, 169*(3).

Boule, M. (1911-1913). l'Homme fossile de La Chapelle-aux-Saints. *Ann. Paléont., 6, 111–172; 7, 21–56, 85–192; 8, 1–70*.

Bouyssonie, A., Bouyssonie, J., & Bardon, L. (1908). Découverte d'un squelette humain moustérien à la Bouffia de la Chapelle-aux-Saints (Corrèze). *L'Anthropologie, 19*, 513-518.

Bräuer, G. (1983). Die menschlichen Skelettfunde des" Later Stone Age" aus der Mumba-Höhle und anderen Lokalitäten nahe des Eyasi-Sees (Tanzania) und ihre Bedeutung für die Populationsdifferenzierung in Ostafrika. In H. Müller-Beck (Ed.), *Die archäologischen und anthropologischen Ergebnisse der Kohl-Larsen-Expeditionen in Nord-Tanzania, 1933–1939* (Vol. 4). Tübingen: Verlag Archaeologica Venatoria.

Bräuer, G. (2012). Middle Pleistocene Diversity in Africa and the Origin of Modern Humans. In J.-J. Hublin & S. P. McPherron (Eds.), *Modern Origins: A North African Perspective* (pp. 221-240). Dordrecht: Springer.

Bräuer, G., & Leakey, R. E. (1986). The ES-11693 cranium from Eliye Springs, West Turkana, Kenya. *Journal of Human Evolution, 15*(4), 289-312.

Bräuer, G., & Mabulla, A. (1996). New hominid fossil from Lake Eyasi, Tanzania. *Anthropologie, 34*(1-2), 47-53.

Bräuer, G., Leakey, R. E., & Mbua, E. (1992). A first report on the ER-3884 cranial remains from Ileret/east Turkana, Kenya. In G. Bräuer & F. H. Smith (Eds.), *Continuity or replacement: Controversies in Homo sapiens evolution* (pp. 111-119). Roterdam: AA Balkema.

Bräuer, G., Groden, C., Delling, G., Kupczik, K., Mbua, E., & Schultz, M. (2003). Pathological alterations in the archaic Homo sapiens cranium from Eliye Springs, Kenya. *American Journal of Physical Anthropology, 120*(2), 200-204.

Bräuer, G., Collard, M., & Stringer, C. (2004). On the reliability of recent tests of the Out of Africa hypothesis for modern human origins. *Anatomical Record, 279A*(2), 701-707.

Capitan, L., & Peyrony, D. (1909). Deux squelettes humains au milieu de foyers de l'époque moustérienne. *Rev. Ecole Anthropol. Paris, 4*, 402-409.

Capitan, L., & Peyrony, D. (1911). Un nouveau squelette humain fossile. *Revue Anthropol.*, 148-150.

Capitan, L., & Peyrony, D. (1912). Trois nouveaux squelettes humains fossiles. *Comptes rendus des séances de l'Académie des Inscriptions et Belles-Lettres, 56*, 449-454.

Cartmill, M., & Smith, F. H. (2009). *The Human Lineage*. Hoboken: Wiley-Blackwell.

Caspari, R. (2005). The suprainiac fossa: the question of homology. *Anthropologie (Brno), 43*(2-3), 229-239.

Clarke, R. J. (1990). The Ndutu cranium and the origin of Homo sapiens. *Journal of Human Evolution, 19*(6), 699-736.

Conroy, G. C., Jolly, C. J., Cramer, D., & Kalb, J. E. (1978). Newly discovered fossil hominid skull from the Afar depression, Ethiopia. *Nature, 276*(5683), 67-70.

Crevecoeur, I., Brooks, A., Ribot, I., Cornelissen, E., & Semal, P. (2016). Late Stone Age human remains from Ishango (Democratic Republic of Congo): New insights on Late Pleistocene modern human diversity in Africa. *Journal of Human Evolution, 96*, 35-57.

Crevecoeur, I., Rougier, H., Grine, F., & Froment, A. (2009). Modern human cranial diversity in the Late Pleistocene of Africa and Eurasia: Evidence from Nazlet Khater, Peştera cu Oase, and Hofmeyr. *American Journal of Physical Anthropology, 140*(2), 347-358.

Curnoe, D. (2011). A 150-Year Conundrum: Cranial Robusticity and Its Bearing on the Origin of Aboriginal Australians. *International Journal of Evolutionary Biology, 2011* (632484).

Day, M. H. (1969). Early *Homo sapiens* Remains from the Omo River Region of South-west Ethiopia: Omo Human Skeletal Remains. *Nature, 222*(5199), 1135-1138.

Day, M. H., Leakey, M. D., & Magori, C. (1980). A new hominid fossil skull (L.H. 18) from the Ngaloba Beds, Laetoli, northern Tanzania. *Nature, 284*(5751), 55-56.

Dean, D., Hublin, J.-J., Holloway, R., & Ziegler, R. (1998). On the phylogenetic position of the pre-Neandertal specimen from Reilingen, Germany. *Journal of Human Evolution, 34*(5), 485-508.

Domínguez-Rodrigo, M., Mabulla, A., Luque, L., Thompson, J. W., Rink, J., Bushozi, P., . . . Alcala, L. (2008). A new archaic *Homo sapiens* fossil from Lake Eyasi, Tanzania. *Journal of Human Evolution, 54*(6), 899-903.

Franciscus, R. G., & Holliday, T. W. (2013). Crossroads of the Old World. In F. H. Smith & J. C. M. Ahern (Eds.), *The Origins of Modern Humans* (pp. 45-88). New York: Wiley-Blackwell.

Frayer, D. W. (1992). The persistence of Neanderthal features in post-Neanderthal Europeans. In G. Bräuer & F. H. Smith (Eds.), *Continuity or Replacement: Controversies in Homo sapiens Evolution* (pp. 179-188). Rotterdam: Balkema.

Fu, Q., Posth, C., Hajdinjak, M., Petr, M., Mallick, S., Fernandes, D., . . . Reich, D. (2016). The genetic history of Ice Age Europe. *Nature, 534*, 200.

Gorjanović-Kramberger, D. (1902). Der paläolithische Mensch und seine Zeitgenossen aus dem Diluvium von Krapina in Kroatien. *Mitt. Anthropol. Gessell. Wien, 32*, 189-216.

Grün, R., & Stringer, C. B. (1991). Electron Spin Resonance Dating and the Evolution of Modern Humans. *Archaeometry, 33*(2), 153-199.

Guérin, G., Frouin, M., Talamo, S., Aldeias, V., Bruxelles, L., Chiotti, L., . . . Turq, A. (2015). A multi-method luminescence dating of the Palaeolithic sequence of La Ferrassie based on new excavations adjacent to the La Ferrassie 1 and 2 skeletons. *J. Archaeol. Sci., 58*(Supplement C), 147-166.

Gunz, P., Tilot, A. K., Wittfeld, K., Teumer, A., Shapland, C. Y., van Erp, T. G. M., . . . Fisher, S. E. (2019). Neandertal Introgression Sheds Light on Modern Human Endocranial Globularity. *Current Biology, 29*(1), 120-127.

Hackett, C. J. (1976). *Diagnostic criteria of syphilis, yaws and treponarid (treponematoses) and of some other diseases in dry bones (for use in osteo-archaeology)*. Berlin: Springer Verlag.

Haile-Selassie, Y., Asfaw, B., & White, T. D. (2004). Hominid cranial remains from upper Pleistocene deposits at Aduma, Middle Awash, Ethiopia. *American Journal of Physical Anthropology, 123*(1), 1-10.

Harvati, K. (2015). Neanderthals and their contemporaries. In W. Henke & I. Tattersall (Eds.), *Handbook of Paleoanthropology* (pp. 2243-2279). New York: Springer.

Harvati, K., Gunz, P., & Grigorescu, D. (2007). Cioclovina (Romania): affinities of an early modern European. *Journal of Human Evolution, 53*(6), 732-746.

Harvati, K., Stringer, C., Grün, R., Aubert, M., Allsworth-Jones, P., & Folorunso, C. A. (2011). The Later Stone Age Calvaria from Iwo Eleru, Nigeria: Morphology and Chronology. *PloS One, 6*(9), e24024.

Harvati, K., Röding, C., Bosman, A.M., Karakostis, F.A., Grün, R., Stringer, C., Karkanas, P., Thompson, N.C., Koutoulidis, V., Moulopoulos, L.A., Gorgoulis, V.G., Kouloukoussa, M., 2019. Apidima Cave fossils provide earliest evidence of Homo sapiens in Eurasia. Nature 571, 500-504.

Hershkovitz, I., Marder, O., Ayalon, A., Bar-Matthews, M., Yasur, G., Boaretto, E., . . . Barzilai, O. (2015). Levantine cranium from Manot Cave (Israel) foreshadows the first European modern humans. *Nature, 520*(7546), 216-219.

Hershkovitz, I., Latimer, B., Barzilai, O., & Marder, O. (2017). Manot 1 calvaria and recent modern human evolution: an anthropological perspective. *Bulletins et Mémoires de la Société d'Anthropologie de Paris, 29*(3), 119-130.

Hublin, J.-J. (1978a). *Le torus occipital transverse et les structures associees: evolution dans le genre homo.* Ph.D. Dissertation, Université Paris VI.

Hublin, J.-J. (1978b). Quelques caractères apomorphes du crâne néandertalien et leur interprétation phylogénique. *Comptes rendus de l'Académie des sciences. Série III, Sciences de la vie., D287*, 923-926.

Hublin, J.-J. (1983). Les superstructures occipitales chez les prédécesseurs d'Homo Erectus en Afrique : quelques remarques sur l'origine du torus occipital transverse. *Bulletins et Mémoires de la Société d'Anthropologie de Paris*, 303-312.

Hublin, J.-J. (1984). The fossil man from Salzgitter-Lebenstedt (FRG) and its place in human evolution during the Pleistocene in Europe. *Zeitschrift für Morphologie und Anthropologie, 75*(1), 45-56.

Hublin, J.-J. (1998). Climatic changes, paleogeography, and the evolution of the Neanderthals. In K. Aoki & O. Bar-Yosef (Eds.), *Neanderthals and modern humans in Western Asia* (pp. 295-310). New York: Plenum Press.

Hublin, J.-J., Ben-Ncer, A., Bailey, S. E., Freidline, S. E., Neubauer, S., Skinner, M. M., . . . Gunz, P. (2017). New fossils from Jebel Irhoud, Morocco and the pan-African origin of Homo sapiens. *Nature, 546*(7657), 289-292.

Klaatsch, H. (1902). Occipitalia und Temporalia der Schädel von Spy verglichen mit denen von Krapina. *Zeitschrift für Ethnologie., 33*, 17.

Klein, R. G. (2009). *The Human Career: Human Biological and Cultural Origins*. Chicago: University of Chicago Press.

Kohl-Larsen, L. (1941). Meine Expedition in Deutsch-Ostafrika (1934–1936 und 1937–1939). *Zeitschrift der Gesellschaft für Erdkunde, 1-4*, 126-144.

Kohl-Larsen, L. (1943). *Auf den Spuren des Vormenschen: Forschungen, Fahrten und Erlebnisse in Deutsch-Ostafrika (Deutsche Afrika-Expedition 1934-1936 und 1937-1939)*. Stuttgart: Strecker und Schröder.

Kramer, A., Crummett, T. L., & Wolpoff, M. H. (2001). Out of Africa and into the Levant: replacement or admixture in Western Asia? *Quaternary International, 75*(1), 51-63.

Kuhlwilm, M., Gronau, I., Hubisz, M. J., de Filippo, C., Prado-Martinez, J., Kircher, M., . . . Castellano, S. (2016). Ancient gene flow from early modern humans into Eastern Neanderthals. *Nature, 530*, 429.

Lahr, M. M. (1994). The Multiregional Model of modern human origins: a reassessment of its morphological basis. *Journal of Human Evolution, 26*(1), 23-56.

Lahr, M. M. (1996). *The evolution of modern human diversity: a study of cranial variation*. Cambridge University Press.

Leakey, L. S. B. (1936). A New Fossil Skull from Eyassi, East Africa: Discovery By A German Expedition. *Nature, 138*, 1082.

Leakey, L. S. B. (1946). Report on a visit to the site of the Eyasi skull found by Dr. Kohl-Larsen. *Journal of the East African Natural History Society, 19*(4), 43.

Leakey, L. S. B. (1974). *By the evidence: memoirs, 1932-1951*. New York: Harcourt Brace Jovanovich.

Leakey, M. D. (1971). *Olduvai Gorge; volume 3, excavations in beds I and II, 1960-1963*. Cambridge [England: University Press.

Leakey, R. E. F. (1976). New hominid fossils from the Koobi Fora formation in Northern Kenya. *Nature, 261*(5561), 574-576.

Li, Z.-Y., Wu, X.-J., Zhou, L.-P., Liu, W., Gao, X., Nian, X.-M., & Trinkaus, E. (2017). Late Pleistocene archaic human crania from Xuchang, China. *Science, 355*(6328), 969-972.

Lieberman, D. E. (1995). Testing hypotheses about recent human evolution from skulls: integrating morphology, function, development, and phylogeny. *Current Anthropology, 36*(2), 159-197.

Lieberman, D. E. (2011). *The Evolution of the Human Head*. Cambridge: Belknap (Harvard University) Press.

Marston, A. T. (1937). The Swanscombe Skull. *The Journal of the Royal Anthropological Institute of Great Britain and Ireland, 67*, 339-406.

Mehlman, M. J. (1984). Archaic *Homo sapiens* at Lake Eyasi, Tanzania: Recent misrepresentations. *Journal of Human Evolution, 13*(6), 487-501.

Mehlman, M. J. (1987). Provenience, age, and association of Archaic *Homo sapiens* crania from Lake Eyasi, Tanzania. *J. Archaeol. Sci., 14*, 133-162.

Mirazón Lahr, M. (2016). The shaping of human diversity: filters, boundaries and transitions. *Philosophical Transactions of the Royal Society of London. Series B: Biological Sciences, 371*(1698).

Mirazón Lahr, M., & Foley, R. A. (2016). Human Evolution in Late Quaternary Eastern Africa. In S. C. Jones & B. A. Stewart (Eds.), *Africa from MIS 6-2: Population Dynamics and Paleoenvironments* (pp. 215-231). Dordrecht: Springer Netherlands.

Mturi, A. A. (1976). New hominid from Lake Ndutu, Tanzania. *Nature, 262*(5568), 484-485.

Nowaczewska, W. (2011). Are *Homo sapiens* nonsupranuchal fossa and neanderthal suprainiac fossa convergent traits? *American Journal of Physical Anthropology, 144*(4), 552-563.

Nowaczewska, W., Binkowski, M., Kubicka, A. M., Piontek, J., & Balzeau, A. (2019). Neandertal-like traits visible in the internal structure of non-supranuchal fossae of some recent Homo sapiens: The problem of their identification in hominins and phylogenetic implications. *PloS One, 14*(3), e0213687.

Protsch, R. (1981). The Eyasi hominids I, II, and III. A new morphological analysis based on a reconstruction, description, and dating of the Eyasi hominids. In R. Protsch (Ed.), *Die*

Archäologischen und Anthropologischen Ergebnisse der Kohl-Larsen-Expeditionen in Nord-Tanzania 1933–1939. Band 3: The palaeoanthropological finds of the Pliocene and Pleistocene (pp. 31-181). Tübingen: Verlag Archaeologica Venatoria.

Posth, C., Renaud, G., Mittnik, A., Drucker, Dorothée G., Rougier, H., Cupillard, C., . . . Krause, J. (2016). Pleistocene Mitochondrial Genomes Suggest a Single Major Dispersal of Non-Africans and a Late Glacial Population Turnover in Europe. *Current Biology, 26*(6), 827-833.

Potts, R., Behrensmeyer, A. K., Faith, J. T., Tryon, C. A., Brooks, A. S., Yellen, J. E., . . . Renaut, R. W. (2018). Environmental dynamics during the onset of the Middle Stone Age in eastern Africa. *Science, 360*(6384), 86-90.

Qin, P., & Stoneking, M. (2015). Denisovan Ancestry in East Eurasian and Native American Populations. *Molecular Biology and Evolution, 32*(10), 2665-2674.

R Core Team (2019). R: A language and environment for statistical computing. R Foundation for Statistical Computing, Vienna, Austria, https://www.R-project.org/.

Rafalski, S., Schröter, P., & Wagner, E. (1978). *Die Funde am Eyasi-Nordostufer.* . Tübingen: Verlag Archaeologica Venatoria, Institut für Urgeschichte der Universität Tübingen.

Reck, H., & Kohl-Larsen, L. (1936). Erster Überblick über die jungdiluvialen Tier- und Menschenfunde Dr. Kohl-Larsens im nordöstlichen Teil des Njarasa-Grabens (Ostafrika). *Geologische Rundschau: Zeitschrift für Allgemeine Geologie, 27*(5), 401-441.

Reeve, W. (1946). Geological report on the site of Dr. Kohl-Larsen's discovery of a fossil human skull, Lake Eyasi, Tanganyika Territory. *Journal of the East African Natural History Society, 19*, 44-50.

Reich, D., Patterson, N., Kircher, M., Delfin, F., Nandineni, Madhusudan R., Pugach, I., . . . Stoneking, M. (2011). Denisova Admixture and the First Modern Human Dispersals into Southeast Asia and Oceania. *The American Journal of Human Genetics, 89*(4), 516-528.

Reyes-Centeno, H., Hubbe, M., Hanihara, T., Stringer, C., & Harvati, K. (2015). Testing modern human out-of-Africa dispersal models and implications for modern human origins. *Journal of Human Evolution, 87*, 95-106.

Richter, D., Grün, R., Joannes-Boyau, R., Steele, T. E., Amani, F., Rué, M., . . . McPherron, S. P. (2017). The age of the hominin fossils from Jebel Irhoud, Morocco, and the origins of the Middle Stone Age. *Nature, 546*(7657), 293-296.

Rightmire, G. P. (2012). The evolution of cranial form in mid-Pleistocene Homo. *South African Journal of Science, 108*, 68-77.

Saban, R. (1975). Les Restes humains de Rabat, Kébibat. *AnnPaléontol (Vert), 61*, 153–207.

Sahle, Y., Reyes-Centeno, H., & Bentz, C. (2018). Modern human origins and dispersal: current state of knowledge and future directions. *Evolutionary Anthropology: Issues, News, and Reviews, 27*, 64-67.

Sahle, Y., Reyes-Centeno, H., & Bentz, C. (2019). *Modern Human Origins and Dispersal*. Tübingen: Kerns Verlag.

Santa Luca, A. P. (1978). A re-examination of presumed Neandertal-like fossils. *Journal of Human Evolution, 7*(7), 619-636.

Scerri, E. M. L., Drake, N. A., Jennings, R., & Groucutt, H. S. (2014). Earliest evidence for the structure of Homo sapiens populations in Africa. *Quaternary Science Reviews, 101*, 207-216.

Scerri, E. M. L., Thomas, M. G., Manica, A., Gunz, P., Stock, J. T., Stringer, C., . . . Rightmire, G. P. (2018). Did our species evolve in subdivided populations across Africa, and why does it matter? *Trends in Ecology & Evolution, 33*(8).

Schlebusch, C. M., Malmström, H., Günther, T., Sjödin, P., Coutinho, A., Edlund, H., . . . Jakobsson, M. (2017). Southern African ancient genomes estimate modern human divergence to 350,000 to 260,000 years ago. *Science, 358*(6363), 652-655.

Schwartz, J. H., & Tattersall, I. (2002). *The Human Fossil Record, Vol. 1: Terminology and Cranial Morphology of Genus Homo (Europe)*. New York: Wiley-Liss.

Schwartz, J. H., & Tattersall, I. (2005a). *The Human Fossil Record. Vol. 2. Craniodental Morphology of Genus Homo (Africa and Asia)*. New York: Wiley-Liss.

Schwartz, J. H., & Tattersall, I. (2005b). The Le Moustier adolescent: A description and interpretation of its craniodental morphology. In H. Ulrich (Ed.), *The Neandertal Adolescent of Le Moustier 1: New Aspects, New Results.* (pp. 95-103). Berlin: Staatlische Museum/Preussischer Kulturbesitz.

Skoglund, P., & Jakobsson, M. (2011). Archaic human ancestry in East Asia. *Proceedings of the National Academy of Sciences, 108*(45), 18301-18306.

Sládek, V. (2000). Hominid evolution in Central Europe during Upper Pleistocene: origin of anatomically modern humans. Ph.D. Dissertation. *Université de Bordeaux I, Bordeaux*.

Smith, F. (1991). The Neandertals: Evolutionary Dead Ends or Ancestors of Modern People? *J. Anthropol. Res., 47*(2), 219-238.

Smith, F., Janković, I., & Karavanić, I. (2005). The assimilation model, modern human origins in Europe, and the extinction of Neandertals. *Quaternary International, 137*(1), 7-19.

Soficaru, A., Doboş, A., & Trinkaus, E. (2006). Early modern humans from the Peştera Muierii, Baia de Fier, Romania. *Proc. Nat. Acad. Sci. U. S. A., 103*(46), 17196-17201.

Soficaru, A., Petrea, C., Doboş, A., & Trinkaus, E. (2007). The human cranium from the Peştera Cioclovina Uscată, Romania: context, age, taphonomy, morphology, and paleopathology. *Current Anthropology, 48*(4), 611-619.

Srivastava, H. C. (1992). Ossification of the membranous portion of the squamous part of the occipital bone in man. *Journal of Anatomy, 180*(Pt 2), 219-224.

Stearns, C. E., & Thurber, D. L. (1965). Th230/U234 dates of late Pleistocene marine fossils from the Mediterranean and Moroccan littorals. *Progress in Oceanography, 4*, 293-305.

Stringer, C. (2000). Eyasi. In E. Delson, I. Tattersall, J. Van Couvering, & A. S. Brooks (Eds.), *Encyclopedia of Human Evolution and Prehistory* (pp. 263). New York: Garland Publishing.

Stringer, C. (2016). The origin and evolution of *Homo sapiens*. *Philosophical Transactions of the Royal Society B: Biological Sciences, 371*(1698).

Stringer, C. B., Hublin, J.-J., & Vandermeersch, B. (1984). The origin of anatomically modern humans in Western Europe. In H. Smith & F. Spencer (Eds.), *The Origins of Modern Humans: a World Survey of the Fossil Evidences* (pp. 51-135). New York: Alan R. Liss.

Suzuki, H. (1970). The skull of the Amud man. In H. Suzuki & F. Takai (Eds.), *The Amud man and his cave site*. Tokyo: University of Tokyo Press.

Tattersall, I., & Schwartz, J. H. (2006). The distinctiveness and systematic context of Homo neanderthalensis. In K. Harvati & T. Harrison (Eds.), *Neanderthals Revisited: New Approaches and Perspectives* (pp. 9-22). Dordrecht: Springer.

Thorne, A. G., & Macumber, P. G. (1972). Discoveries of Late Pleistocene Man at Kow Swamp, Australia. *Nature, 238*, 316.

Tillier, A.-M. (2005). The Tabun C1 Skeleton: A Levantine Neanderthal? *Mitekufat Haeven: Journal of the Israel Prehistoric Society, 35*, 439-450.

Trinkaus, E. (1983). *The Shanidar Neandertals*. New York: Academic Press.

Trinkaus, E. (2004). Eyasi 1 and the suprainiac fossa. *American Journal of Physical Anthropology, 124*(1), 28-32.

Trinkaus, E. (2007). European early modern humans and the fate of the Neandertals. *Proceedings of the National Academy of Sciences, 104*(18), 7367-7372.

Trinkaus, E. (2011). Late Neandertals and Early Modern Humans in Europe, Population Dynamics and Paleobiology. In S. Condemi & G.-C. Weniger (Eds.), *Continuity and Discontinuity in the Peopling of Europe: One Hundred Fifty Years of Neanderthal Study* (pp. 315-329). Dordrecht: Springer.

Verna, C., Hublin, J.-J., Debenath, A., Jelinek, A., & Vandermeersch, B. (2010). Two new hominin cranial fragments from the Mousterian levels at La Quina (Charente, France). *Journal of Human Evolution, 58*(3), 273-278.

Vernot, B., Tucci, S., Kelso, J., Schraiber, J. G., Wolf, A. B., Gittelman, R. M., . . . Akey, J. M. (2016). Excavating Neandertal and Denisovan DNA from the genomes of Melanesian individuals. *Science, 352*(6282), 235-239.

Virchow, R. (1872). Ueber die Methode der wissenschaftlichen Anthropologie. Eine Antwort an Herrn de Quatrefages. *Zeitschrift für Ethnologie, 4*, 300-320.

Wolpoff, M. H., Hawks, J., Frayer, D. W., & Hunley, K. (2001). Modern Human Ancestry at the Peripheries: A Test of the Replacement Theory. *Science, 291*(5502), 293-297.

Woodward, A. S. (1921). A New Cave Man from Rhodesia, South Africa. Nature, 108(2716), 371-372.

Yellen, J., Brooks, A., Helgren, D., Tappen, M., Ambrose, S., Bonnefille, R., . . . Renne, P. (2005). The archaeology of Aduma Middle Stone Age sites in the Awash Valley, Ethiopia. *Paleoanthropology, 10*(2).

8. Supplementary Material

Supplementary Table 1. Measurements of external suprainiac depression surface in millimeters, using the internal surface as a guide (Supplementary Figure 1).

Specimen measured	Total breadth	Left to center	Right to center	Total height	Top to center	Bottom to center
Eyasi I	25.8	12.8	12.9	8.8	4.9	4
ADU-VP-1/3	-	-	17.6	9.0	4.5	4.5
Masai 12	21.8	12.1	8.6	8.7	4.5	4.2
La Chapelle-aux-Saints 1	36.0	19.9	16.1	8.1	4.3	3.8
La Ferrassie 1	32.5	15.9	16.8	9.7	6.9	2.7

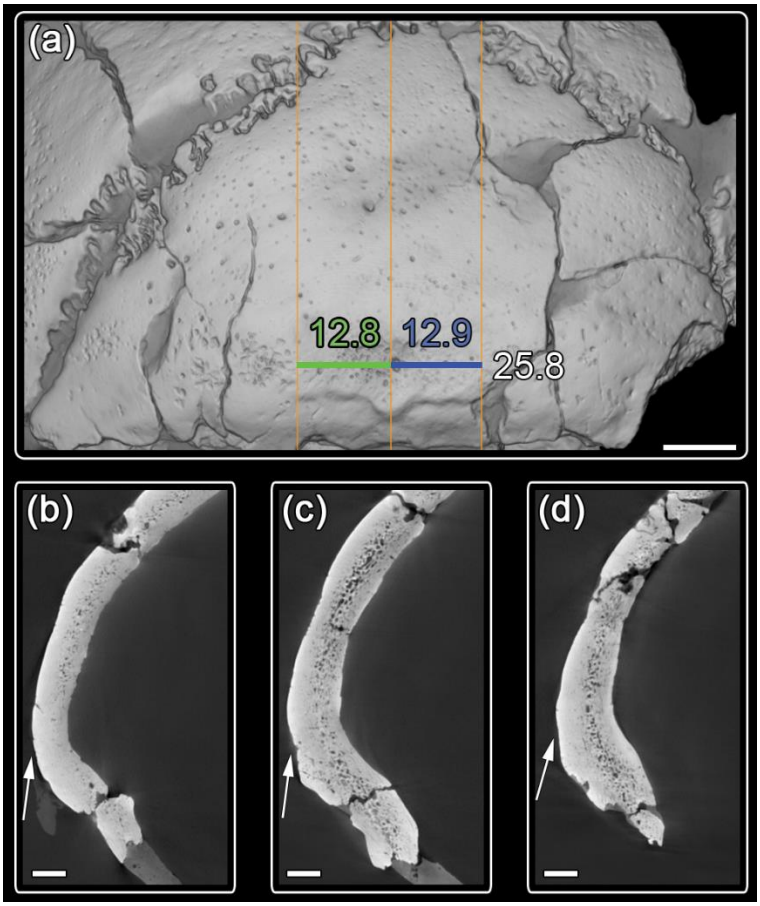

Supplementary Figure 1. Figure detailing the protocol for external measurements, with arrows indicating the supranuchal area (scale bars = 1 cm). (a) Posterior view of Eyasi I occipital bone. Orange lines indicate the position of the maximum left, central, and maximum right slices. The white text represents the singular measurement of the transverse breadth of the suprainiac depression, while the green and blue text and line segments represent the left to center measurement and the right to center measurement, respectively; (b) Lateral view of the maximum left slice; (c) Lateral view of the central slice; (d) Lateral view of the maximum right slice.

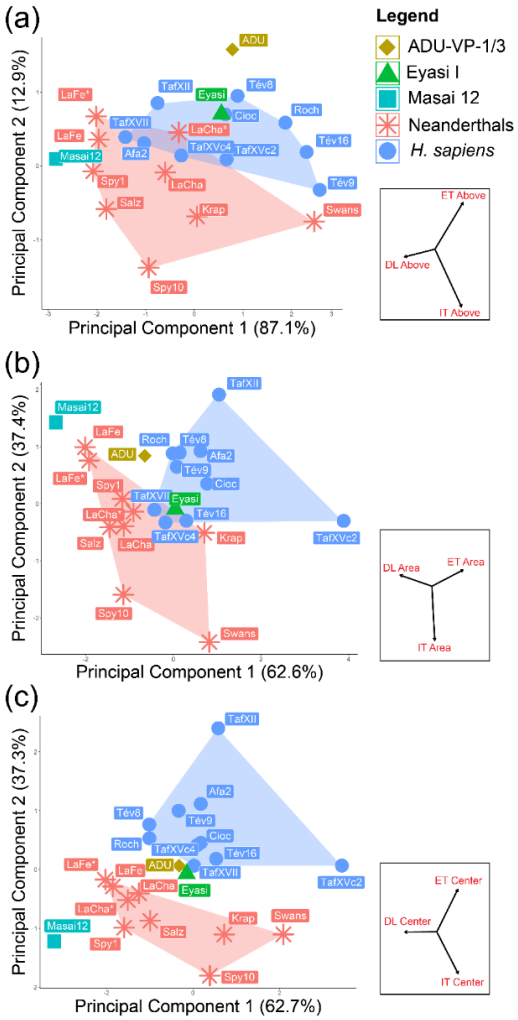

Supplementary Figure 2. Principal Component Analyses on the correlation matrix, showing PC1 and PC2 for each zone, in the same order as indicated in Table 3. (a) Area above the suprainiac depression; (b) area of the depression; (c) center of the depression. Data collected in this study (Eyasi I, ADU-VP-1/3, Masai 12, La Chapelle-aux-Saints 1, and La Ferrassie 1) were projected. Eyasi I = green triangle; ADU-VP-1/3 = gold diamond; Masai 12 = cyan square; Neanderthals = red stars; recent *H. sapiens* = blue circles. There is a similar separation of Neanderthals and *H. sapiens* along the second principal component as in Figure 4 (main text) when considering only the area above the depression, albeit with overlap of one Neanderthal specimen (La Chapelle-aux-Saints 1, as measured in this study and projected) with the convex hull of *H. sapiens*. In addition, Eyasi I plots within the convex hull of *H. sapiens,* while ADU-VP-1/3 is outside of it. When considering only the area of the depression, the separation between Neanderthals and *H. sapiens* is mostly on the first axis. In this case, three modern human specimens (Taforalt XVII c1, Taforalt XV c4, and Téviec 16) overlap with the Neanderthal convex hull, Eyasi I is at the border of it, and ADU-VP-1/3 is outside the convex hull of either the Neanderthal or *H. sapiens* group. Finally, Neanderthals and *H. sapiens* are separated along the second principal component when only the central measurement is considered. There is no overlap between the two groups. Both Eyasi I and ADU-VP-1/3 are outside either convex hull, but closest to that of *H. sapiens.*